The thin green line – a novel lateral flow assay platform for point of care diagnostics

Dissertation

to obtain the academic degree of Doctor of Natural Sciences

- Dr. rer. nat. –

by

Andreas Schielke

born in Wesel

Faculty of Chemistry

Institute for Technical Chemistry I

University of Duisburg-Essen

Essen, 2022

The present thesis was conducted from October 2017 to January 2022 in the group of. Dr. Rehbock at the Institute for Technical Chemistry I (headed by Prof. Dr.-Ing. Stephan Barcikowski) at the University of Duisburg-Essen.

1. Referee: Prof. habil. Dr.-Ing. Stephan Barcikowski

2. Referee: Prof. Dr. Sebastian Schlücker

Chairman: Prof. Dr. Matthias Ropohl

Day of disputation: 08.11.2022

DOI: 10.17185/duepublico/77116
URN: urn:nbn:de:hbz:465-20230404-092210-2

Erklärung

Hiermit versichere ich, dass ich die vorliegende Arbeit mit dem Titel

„The thin green line – a novel lateral flow assay platform for point of care diagnostics“

Selbst verfasst und keine außer den angegebenen Hilfsmitteln und Quellen benutzt habe, und dass die Arbeit in dieser oder ähnlicher Form noch bei keiner anderen Universität eingereicht wurde.

Essen, im Januar 2022

Andreas Schielke

Teilergebnisse (Kapitel 3.2.3) der vorliegenden Arbeit wurden 2021 zur Veröffentlichung angenommen von *ACS* Publications (Bioconjugate Chemistry). Die entsprechende Quelle findet sich im Literaturverzeichnis. Die Aufschlüsselung der Arbeitsteilung der beiden Erstautoren findet sich im Abschnitt Contributions wieder.

I got a bad feeling about this.

Han Solo

Content

List of Abbreviations

Abbreviation	Meaning
ADC	analytical disc centrifuge
ALFA	aptamer lateral flow assay
Ag NP	silver nanoparticles
AgAu NP	silver-gold-alloy nanoparticles
Au NP	gold nanoparticles
BfR	Bundesinstitut für Risikobewertung
CL	control line
DLS	dynamic light scattering
DNA	deoxyribonucleic acid
EDTA	ethylenediaminetetraacetic acid
ELAA	enzyme-linked aptamer assay
ELISA	enzyme-linked immunosorbent assay
EU	European Union
FDA	food and drug administration
FSN	fluorosurfactants
hCG	human chorionic gonadotropin
Ig	immunoglobins
LAL	laser ablation in liquids
LCA	last common ancestor
LFA	lateral flow assay
LNA	locked nucleic acid
MRE	molecular recognition element
MRL	maximal residual limit
N-IR	near infrared
NLS	nucleus localizing sequence
NP	nanoparticle(s)

Abbreviation	Meaning
OtA	ochratoxin A
POC	point of care
RNA	ribonucleic acid
RT-PCR	real time - polymerase chain reaction
SERS	surface enhanced Raman spectroscopy
TBE	Tris, Borate, EDTA
TEM	transmission electron microscopy
TL	test line
UV	ultraviolet
UV-vis	ultraviolet and visible light
Vis	visible light
WHO	World Health Organization

Abstract

Lateral flow assays (LFA) represent one of the most important tools in point-of-care-diagnostics (POC) and therefore play a crucial role in disease control and food safety. However, the underlying technology of LFAs features severe limitations. High limits of detection and the absence of suitable molecular recognition elements (MRE) for small analyte molecules, highly toxic, and non-immunogenous targets limit their field of applications. At the same time the high demand for LFAs calls for sustainable and green solutions to assure the sufficient supply in the future. Here, these problems are tackled by introducing the first LFA system featuring nano-bio-conjugates (NBC) consisting of laser-generated nanoparticles and aptamers. The conjugation and functionality of the NBCs was analyzed via physiochemical methods (spectroscopy, color analysis, LFA functionality testing). Conjugates featuring moderate surface coverages provided the best functionality. The elemental surface composition does affect the functionality of the NBCs, yet they represent robust detection units that operate over a broad range of varying alloy compositions. It was possible to demonstrate NBC functionality und LFA conditions when recovered hexaethylenglycol (HEGL)-spacer-aptamers from previous conjugation processes were used, which represents a great example of improved atom economy. All findings were fused into one functional test system for ampicillin detection. This new type of LFA upholds the high standards of POC-diagnostics, while introducing aspects of green chemistry. These findings might contribute to aptamer-LFAs finding their niche in the vast and growing field of POC-diagnostic tools and help LFAs to take the next steps towards green technology.

1. Introduction and Objectives

Pregnant or not?

Infected or not?

Drinkable or not?

Lateral Flow Assays (LFA), fulfilling the WHO´s assured-criteria, assist people throughout life by giving quick answers to crucial questions [1]. The paper-based test-stripes indicate the presence of a given analyte within a liquid sample within minutes. Since the first commercial test stripe introduction in 1988 [2], the range of test systems detecting various analytes has been steadily expanded. Today, it is possible to detect drugs [3], food hazards [4], antibiotics [5], viruses [6,7], bacteria [8], heavy metals [9], hormones [10], and many more analytes [11,12] within minutes – without the help of expensive analytical equipment. The test principles are robust and can be easily utilized wherever needed, whenever needed, thus, providing qualitative analytics wherever one may go. This flexibility allows these detection systems to operate at the point-of-care (POC). [13]

However, the technology behind the paper-based test stripes is already more than thirty years old. Advancements have been made for almost every component of the LFA system, including its very heart - the nano-bio-conjugate. Typically, LFAs utilize nano-bio-conjugates consisting of antibodies bound to a chemically synthesized noble metal nanoparticle sphere. Antibodies are part of the immune defense of mammals. These protein complexes bind highly specific to antigens of potential infectious cells and viruses. Even though antibodies can tackle a vast selection of antigens, some substances are just not immunogenic. [14] Those substances do not cause any immune response; therefore, no antibodies exist against them. Other substances are just too toxic and kill the organism before an immune response can be successfully executed. Herein lies a perfectly suited field of applications for aptamers. These short, single-stranded DNA/RNA-sequences can be chemically synthesized, bind target molecules with high specificity and represent one of the most interesting ways to improve the existing LFA systems and expand their field of applications. [14] In addition to that, aptamer can be synthesized chemically and do not require host organisms during their production. The state of the art monoclonal antibody generation procedure requires heavily on the utilization of mice [15]. Thus, aptamer synthesis contributes to reduced animal suffering and to the reduced utilization of animals within the pharmaceutical/chemical industry and research. This is a major column of the European Green Deal of which Germany is an valid participant of [16]. Nevertheless, why stop after replacing the antibody with its green counterpart? It is time that the nanoparticles are modernized too.

Laser-ablation in liquids (LAL) has gained considerable attention throughout the years in the field of material science. It allows the green synthesis of highly pure, organic-ligand-free noble metal nanoparticles (NP). In addition to that it represents the only way to generate alloy nanoparticles within a single working step, without any organic precursors, while upholding to the principles of green chemistry [17–19].

The principles of green chemistry were established in the early 1990s [18,20,21]. The twelve principles aim to prevent waste, maximize the incorporation of used materials into the final product, replace hazardous substances whenever possible, be energy efficient, and more [18]. Laser-generated NP have been proven to be more energy efficient in their synthesis than chemical synthesized nanoparticles [22], do not require the utilization of auxiliary reducing agents like e.g. citrate, and bypass the problem of incompletely converted chemical precursors (atom economy) [17]. Regarding the drastically increased demand for LFA systems since the outbreak of SARS-CoV-2 – with 1,200,000,000 units being used so far in the U.S.A. and India only (status: 04.12.2021) [23] – the commandment arises to minimize the production requirements of LFA systems drastically with regard to its energy and material demand. The global crisis will continue to take its toll on mankind regarding human lives, energy, and resources. Green alternatives must be established to existing systems as soon as possible. LAL NP could positively contribute to less resource intense test systems. However, it must be made clear, that one-time test systems will never be green products in regard of green chemistry. But the raw materials for LFA production could be produced in accordance with these high and sustainable standards.

So far, there is no existing commercially available LFA system to our best knowledge utilizing both: aptamers and LAL NP. The combination of both green alternatives to the existing state-of-the-art components and the consecutive development of a proof-of-concept LFA test system represents this work´s focus. The developed test system aims to be an easily modifiable platform for a huge variety of analytes. Its main component, namely the nano-bio-conjugate consisting of LAL Au NP and thiolated aptamers, is carefully developed with optimal target binding efficiency, modifiability, atom economy, waste prevention and energy efficiency in mind. However, there is an significant knowledge deficit how aptamer LAL NP conjugates perform in LFA systems.

Until now, no systematic evaluation has ever been performed on the conjugation of LAL NP with aptamers in the context of LFA applications. Petersen and Barcikowski laid the foundations for the nano-bio-conjugation of LAL nanoparticles [24–26]. Barchanski et al. could build upon these findings with their basic research on the influence of the aptamers design and the functionality of laser-generated Au NP conjugates. [27,28] One aim of this work is to expand the understanding of bioconjugation of LAL Au NP with aptamers. So far, it is unknown how LAL NP change the signal

intensity and LOD of LFA systems. Therefore, conjugates are analyzed concerning their optical properties, ideal concentration, and surface coverage by UV-vis extinction spectroscopy and by color analysis based on digital photos. Conjugates´ functionality is quantified spectroscopically, and via LFA testing. Low limits of detections represent a bottleneck in the development of new LFA test systems [29].

So far, the influence of the surface coverage of conjugates has only been material to assumptions [17]. Walter et al. were able to demonstrate the functionality of *in situ* aptamer conjugated laser-generated gold nanoparticles, thus laying the foundation of this work. [30] Based on this very important finding, this work aims to provide a detailed evaluation of how to achieve a freely adjustable surface coverage to allow the ideal configuration for different analytes. Furthermore, its aim is to systematically link surface coverage and functionality for the first time for aptamer LAL AuNP conjugates. Thus, it seeks to ultimately generating evidence which surface coverage is providing the highest functionality. Different salt-aging techniques are compared and evaluated based on the resulting colloidal stability and functionality. In addition to that, this work aims to provide a better understanding of the influence of the surface composition with respect its elemental composition of the nanoparticle onto the functionality of the respective conjugates. Thus, the transferability from gold to alloy nanoparticles has been examined. Furthermore, this work evaluates the potential of aptamer LAL NP to achieve high atom efficiency and waste prevention by introducing an aptamer recycling process.

A subsequent bibliographic analysis of the existing aptamer-LFA systems, how the newly developed proof-of-concept-LFA contributes to the progress of the field of LFA-based POC diagnostics, and how future test systems can overcome the existing limitations of LFAs. The aim of this study is to analyze if the LOD is the main bottleneck or not.

2. Theoretical Background

The year 2020 has proven itself to be one of the most challenging ones in recent human history. Climate change, political, and social changes and all above the Covid-19 pandemic take their tolls on public life and our society. In early 2019 the healthcare system was craving for fast, cheap, and reliable test systems to tackle the tremendous amounts of testing of possibly Covid-19 infected. At this early stage of the pandemic, the lion´s share of testing was done via real-time-polymerase chain reaction tests (RT-PCR), which is time-consuming and easily misinterpreted [31]. Currently LFAs have taken the helm in our work and everyday life, providing the necessary testing capacity allowing the required safety for personal and professional meetings and events. Nanotechnology is doing its part to fight the virus, coming along with various approaches to prevent infections, destroying virions [32], or even speeding up vaccine development [33]. However, only a small community within the discipline of nanotechnologies tackles the field of fast, easy, and reliable testing via point of care (POC) devices; all above the lateral flow assay (LFA) test system, which began its rise in 1988 with the release of the first commercial pregnancy test.

The need for a reliable POC-diagnostic tool in the current pandemic stresses not only the importance of such technologies but serves as a reminder that there are much more target molecules out there, requiring efficient testing systems. The following sections will mainly focus on lateral flow assays to detect small, highly toxic molecules, like ochratoxin and ampicillin. State-of-the-art compounds will be fused into a novel functional bioconjugate: laser-generated metal nanoparticles (NP) and highly specific binding single-stranded DNA strands, called aptamers.

2.1 Point of care diagnostics

Diagnostic and analytical aid wherever and whenever you need it – point of care diagnostics must keep a great promise. Instrumental analytic chemistry is performing at an undreamed performance capacity with state-of-the-art instruments like HPLC-MS, GCxGC, and many more. Nevertheless, what should one do if there is no high-end analytical laboratory available? What if resources, all above time and money, are strictly limited? Or if one is lost within the wilderness? To survive or to master her/his/their specific environment, one requires analytical devices that can be easily used and can tell with high accuracy if, e.g., one can drink safely from a water supply or if antibiotics are required. In this case,

there is a high demand for point of care devices. The WHO provides strict criteria which must be fulfilled by a device to be considered POC summarized by the ASSURED criteria: affordable, sensitive, specific, user-friendly, robust and rapid, equipment-free, and deliverable (see **Figure 1**). [34]

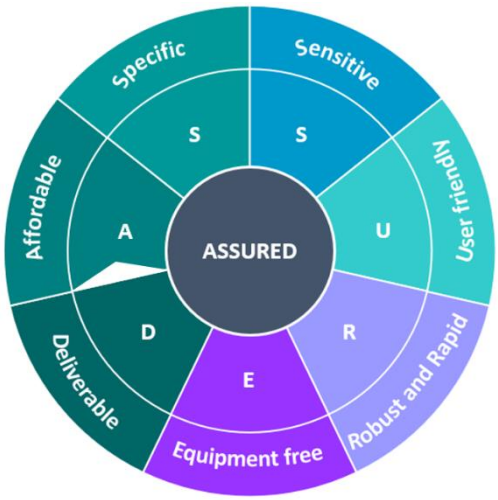

Figure 1: ASSURED criteria according to WHO; based upon the work of Drain et al. [1].

These criteria are designed to "assure" that POC-devices can be efficiently operated in resource-limited areas e.g., in rural areas of developing counties. This concept is already widely applied and more than 40.000 devices have already been developed based on these criteria [34]. They have been designed to cope with a huge variety of analytes, ranging from severe viruses like HIV [1] to bacteria [35] and finally to very small toxic compounds like, e.g. ampicillin [36].

The POC market is steadily growing, and it can be assumed that the demand for POC will steadily increase within years to come. This market´s expected growth is estimated to increase from 23.16 billion $ in 2016 to 36,96 billion $ in 2021. [37]

2.2 Lateral Flow Assays

Without a doubt, the LFA remains the most prominent POC-device since the market introduction of the pregnancy test. Easy to use, cheap, rapid results, low limit of detection (LOD), and a broad spectrum of analytes make the LFA a formidable POC-all-time-champion. However, the recent years featured many new developments like, e.g. multiplex LFAs [38], and the advancing in-silico analysis lead to the development of "lab-on-a-chip"-devices. The classical LFA is facing its technological successors. However, the POC-device´s digitalization will eventually end in their metamorphosis into highly complex and therefore no longer POC-suited devices – thus, the LFA will stay with humanity for years to come.

From a technical point of view, LFAs are simple pads glued on a supported paper matrix. The basic set-up can be modified, e.g., to feature multiple test lines, filters, or additional markers, but the core LFA always follows the same scheme (see **Figure 2**). The sample pad serves as an entry point for the analyte. Here unwanted components of the sample matrix are filtered, and a buffer loaded onto the pad can assure the correct test performance. The sample proceeds through the LFA, wetting the conjugate pad – home of the conjugate, which will ultimately tell if the analyte is present or not. Here, the typical red

line indicating the analytes presence is produced by the accumulation of gold nanoparticles and their respective strong absorbance of green light due to their strong localized surface plasmon resonance (LSPR; since bulk material is of no importance in this work the term SPR will be used likewise, yet usually it would refer to the surface plasmon resonance of bulk material not nano-sized material [39]). [40] Thus, a red line can be seen. The dried and loaded conjugate redisperses, mixes with the sample, and finally enters the nitrocellulose membrane. If we are looking at a sandwich assay, this is also the moment at which the conjugate´s functional molecule binds to the target. Through capillary flow, analyte and target wander towards the waste pad. By doing so, they pass the test-, and control line. The control line binds specifically to unbound conjugate, therefore always generating a positive signal. However, the test line will behave differently based on the type of LFA used. [41]

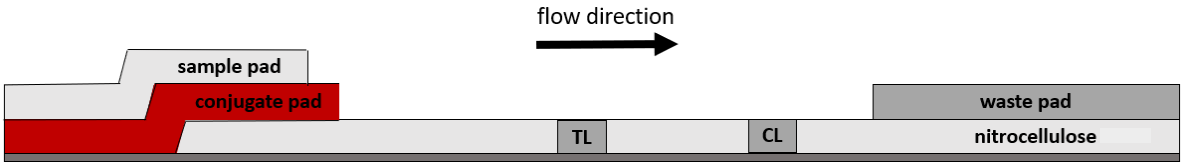

Figure 2: Schematic overview over a standard LFA test system without its protective encasing. TL = test line; CL = control line.

State-of-the-art LFA functionality is achieved by one of two opposing approaches: the sandwich-assay and the competitive assay [13,42] – both providing their own strengths and weaknesses.

The sandwich format (see **Figure 3**) allows the targeting of two distinct docking points of the target, called epitopes or, in the case of aptamers, “aptatopes”, thus guaranteeing a high specificity and sensitivity while keeping the readout simple [43]. One antibody is immobilized on the test line, whereas the second antibody is immobilized onto the nano-bio-conjugate surface. However, not every target offers two simultaneously functioning aptatopes. Especially targets of low molecular weight are unsuitable for the sandwich format. [44] However, high molecular weight targets can also cause hardship for the detection process if they are encountered at low concentrations [45].

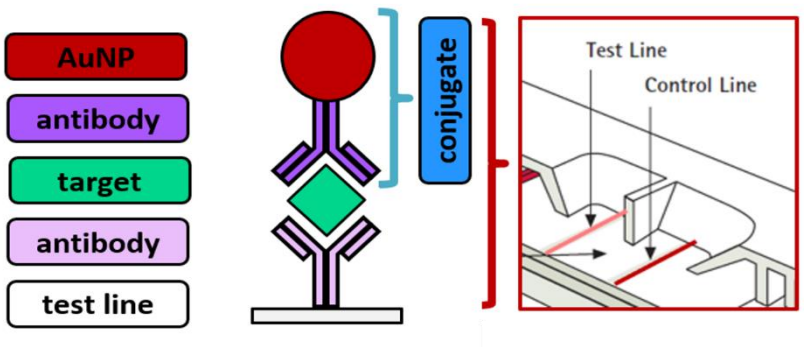

Figure 3: Principle of a "sandwich format" LFA utilizing antibodies. Content of the red box is based on an EMD Millipore information material [41].

It is much easier to detect low molecular weight compounds via the competitive format (see **Figure 4**). Here, the target molecule competes with a label featuring the molecular recognition element (MRE). If the target is present within the sample, it will prevent MRE binding to the immobilized binding agent on the test line (e.g. streptavidin), resulting in a reduced or even vanished test line staining. [34] Depending on the target concentration, a visible readout may be impossible and additional analytical devices are required to allow the correct readout, limiting the POC-advantages.

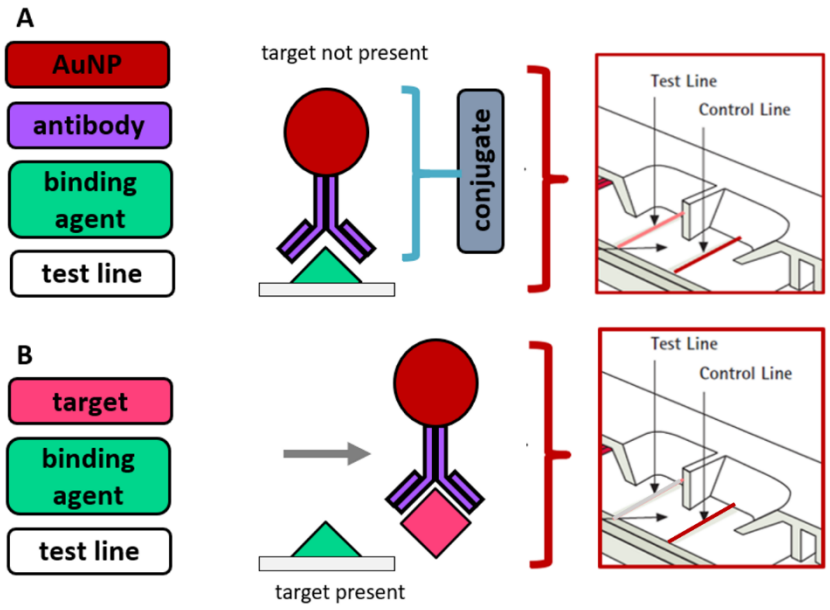

Figure 4: Principle of a "competitive" LFA. Content of the red box is based on an EMD Millipore information material [41]. A) target is not present. Therefore, the nano-bio-conjugate binds to the test line. B) Target analyte is present and binds to the nano-bio-conjugate. The test line shows less to no staining.

However, the very heart of both LFA schemes is always a functional nano-bio-conjugate (NBC). Without this NBC, there is no visible readout. The user sees either the accumulation of the NBC at the test line or the NBC being carried away by the analyte solution. Usually, the NBC consists of a specific-binding

molecule, e.g., an antibody, and a marker. Common marker molecules are fluorophores or noble metal nanoparticles, e.g., gold nanoparticles. There have been extensive studies on how to design and improve such nano-bio-conjugates [28,46]. The following sections will focus on the distinct components of such a conjugate (MRE and marker) and how to generate them.

2.3 Aptamers as Molecular Recognition Elements

Aptamers are short single-stranded DNA or RNA molecules, which fold into a specific 3D-structure, allowing them to bind a certain target with high specificity. The same effect can be achieved by utilizing peptides, which is then called aptatid, but this species of molecules, and RNA-aptamers, will be used in this work but the focus will be on DNA-based aptamers. [47,48] The origin of aptamers dates back to the late 1960s, when it became clear that DNA does not only bear the blueprint to every biological structure, but that it itself can form complex functional structures besides the proposed double helix structure by Watson, Crick, and Wilkins. [49] These first hints were further verified when RNA-molecule´s catalytic activity was proven in the eighties [50]. Nevertheless, why does the functionality of such molecules besides information storage matter? These findings may be only of importance to scientists' interest in the origin of life, the finding of last common ancestors (LCAs), and the way primitive organisms were able to evolve a complex metabolism without the highly specific enzyme tools modern organisms dispose of.

It should take till 1999 until the term "aptamer" came into this world. Ellington and Szostak found RNA motifs that would bind to random targets and thus, called them aptamer. At the same time, Tuerk and Gold developed the systematic evolution of ligands by exponential enrichment (SELEX), which became the state-of-the-art aptamer development process [51]. The RNA aptamers were shortly followed by the DNA aptamers, binding organic dyes specifically [52,53]. Nowadays, the basic SELEX process has undergone several modifications, which lead to improved techniques in aptamer synthesis. Capillary electrophoresis SELEX offers the opportunity to produce aptamers without any need for immobilization on a carrier surface, allowing for maximized target binding ability [54]. Cell SELEX can be used within living cells and enables scientists to generate aptamers against unknown target structures within e.g. pathogens, described by Homann et al. [55]. An auspicious approach for small molecule target detection was presented by Stoltenburg et al. [56], which is based on Nutiu et al.´s findings, that a target sequence can break the hybridization of an aptamer to its complementary oligonucleotide sequence [57]. Stoltenburg used this key finding and adapted the Selex procedure by immobilizing complementary sequences, which were then hybridized to possible aptamer sequences. Therefore, successful binding events would lead to a conformation change within the aptamer and break the DNA duplexes. This method, known as capture SELEX, made it obsolete to bind the target to

a matrix, making possible aptatopes more accessible by reducing steric hindrance. [56] **Figure 5** provides an overview over the SELEX-procedure.

s

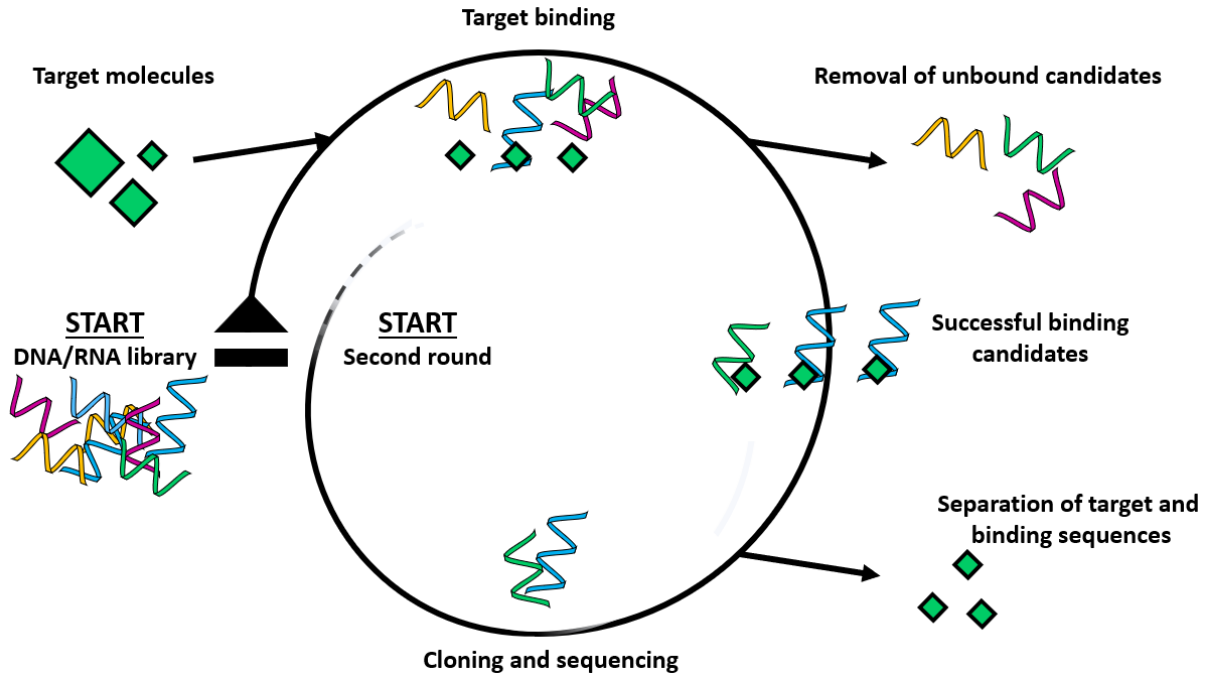

Figure 5: Exemplary Picture of SELEX process based on the scheme published by Stoltenburg et al. [58]

Today there are already over 584 known aptamer sequences (according to the Apta-Index™ by Aptagen, LCC; state 06.11.2020), which can bind specific targets via the induced-fit mechanism, as described for protein substrate interaction [59]. This novel concept of DNA molecules, leads to a huge variety of aptamers as biosensors in many applications [60], including e.g. the detection of cancer [12,61], pathogens [6–8,62–65], biotin [11], mycotoxins [4], aflatoxin [66–68], progesterone [69], vaspin [70,71], pesticides [72], exosomes [73,74], cortisol [10], dopamine [75], cholera toxin [76], thrombin [77,78], drugs [3], metal ions [9,79], and small molecule detection [5,80,81], which are known to be challenging targets, since their small size does not offer many aptatopes. Despite all this progress and advances in aptamer technology, to this moment, the state-of-the-art binding molecule of choice are still antibodies since their production via hybridoma technology is well established and allows for high antibody yields [82].

Antibodies, or immunoglobins (Ig), are proteins that bind with high affinity, specifically to a target via induced fit, just like aptamers [83]. The aforementioned pregnancy test utilizes an antibody that binds specifically to the human chorionic gonadotropin (hCG) hormone, which can be found at an increased

concentration in pregnant women´s urine [84]. The pregnancy test, based on antibody-target-binding, was the first commercially available LFA test-system [85]. Since then, antibodies have become the basic tool of target binding for many different LFA test-systems. All above the IgG antibody class has become the most important antibody class for biosensors [86]. However, antibodies are subject to severe limitations. First of all, they can only be generated for immunogenic substances [87]. Their production is much more expensive than aptamer production [88], and the desired target analyte cannot be too toxic [89]. In addition to that the binding ability of antibodies is limited evolutionary due to their function in the immune system. The half-life of an antigen complex is limited by the endocytosis time. Thus, there exists a natural affinity limitation for antibodies. [90] In this regard, aptamers are superior to their bio-synthetic counterparts. Furthermore, it could also be shown that aptamers offer a comparable if not increased affinity than antibodies [47]. Indeed, aptamer´s advantages can be further pushed by utilizing multivalent systems, as shown by Hianik et al. [91] and Hasegawa et al. [92]. In addition to that, aptamers feature increased stability concerning heat stress compared to antibodies, which allows for easy "reactivation" via heating after a successful binding event, thus recovering the aptamer´s functionality [47].

The functionality of aptamers is based upon their distinct 3-dimensional folding [48]. Double- stranded (ds) DNA can usually be found in a double helix structure due to the interaction of complementary bases leading to hydrogen-hydrogen bonding between adenine and thymine and guanine and cytosine. Single-stranded (ss) oligonucleotides can build up partial helix structures on their own, but they can form a variety of other structures, including e.g. tetrads/quadruplex, or hairpin formations (see **Figure 6**), which are based on correct base pairing and sometimes even on mismatches [93]. Certain aptamers require their respective sub-structure/motif or multiple of them to bind to their target, e.g. the streptavidin binding "miniStrep" aptamer requires a stem-dumbbell folding [94]. Furthermore, the functionality can depend on the correct stacking of flat moieties, complementary molecular shape for effective target binding, and hydrogen bonding [95].

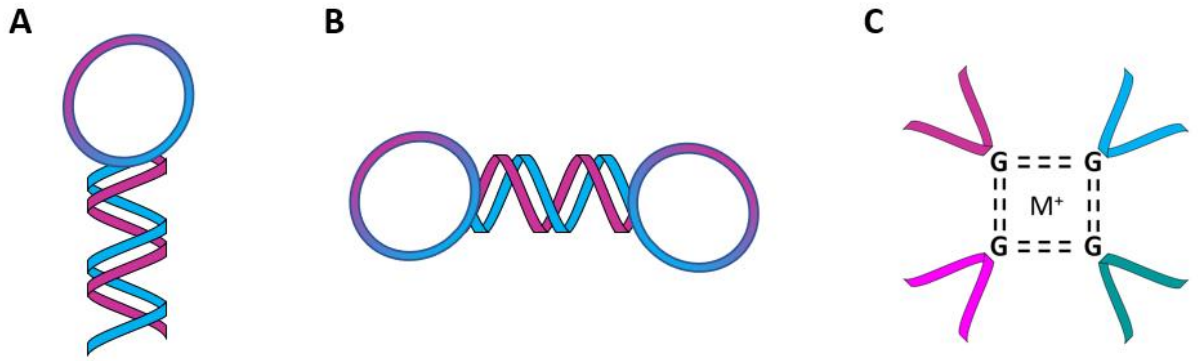

Figure 6: Exemplary DNA/RNA-motifs, that can be found in aptamers. A) hairpin/stem-loop based on [96]; B) stem-dumbbell based on [97]; C) tetrad/G-quadruplex with monovalent metal cation (M^+), based on [98].

The correct aptamer folding depends on several parameters, all above salt concentration, pH-value, and temperature [48]. Magnesium chloride plays a special role in the aptamer folding process, and its concentration plays a crucial role in the final 3D-structure. Butcher et al. were able to demonstrate how the $MgCl_2$ concentration influenced hairpin formation of a ribozyme (functional RNA unit) [99]. It is typically used as a component of the Selex-buffer during aptamer development and widely used as a component of the final binding buffer to allow specific target binding, like e.g. the binding of aminoglycoside antibiotics, which was performed by Nikolaus & Strehlitz in 2014 [100]. In addition to that, aptamers require a certain pH-value to operate – or beyond that to perform highly specialized tasks like drug delivery via pH-control, as was shown for the delivery of daunorubicin to cancer cells via aptamer-gold-nanoparticle conjugates by Taghdisi et al. [101] or the delivery of doxorubicin via aptamer by Zhang et al. [102]. Zhang et al. were able to generate an aptamer-micelle construct for pH-controlled drug release of paclitaxel due to the aptamer changing its conformation in dependence of the pH [103]. Nevertheless, the pH-range, which one can exploit, is limited, and extreme pH values may lead to protonation of the binding site within the aptamer sequence, depurination, or even the total denaturation of the aptamer [104,105], even though some aptamers can recover from such pH changes [106]. Concerning temperature, aptamers are considered more thermostable than their antibody counterparts [42]. However, their functionality is directly linked to the actual temperature and may also require preceding heat treatments, like it was shown e.g. by Tsukakoshi et al. [107]. A heat treatment serves as a restart of the DNA-structure´s folding. Like in PCR, it can be used to break unwanted base pairings and allow aptamers to regain their correct folding [108,109]. However, aptamer functionality in a LFA must be guaranteed even when the aptamer is bound to a surface, i.e. a noble metal nanoparticle surface.

2.4 Nanoparticles in diagnostics

Above all, gold nanoparticles (Au NP), have become indispensable in modern bio diagnostics and therapeutics. They have been a useful tool in this matter for almost 50 years and will most likely remain useful for years to come due to their diverse field of applications [110]. Nanoparticles with additional ligands, like e.g. locked nucleic acid (LNA) [111], DNA [112], RNA [113], peptides [114], antibodies [115], but even without any additional ligands [116] have been used extensively for e.g. imaging cellular uptake, cancer diagnosis and therapy, and gene control. [117]

In the field of POC, especially LFAs, Au NP play a crucial role. Here, most commercial and experimental set-ups utilize Au NP as an agent for the visible readout; compare **Figure 3** and **Figure *4***. All relevant reference systems for this work feature Au NP. The different ochratoxin detection systems utilize a variation of Au NPs. Wang et al. used 20 nm Au NP, whereas Liu et al. used Au NP antibody conjugates [118,119]. In ampicillin detection, the most prominent detection system by Song et al. is based on a colorimetric and fluorescence approach utilizing Au NP, as well [120]. However, there are also test systems that can operate without any Au NP. Alternative set-ups utilize quantum dots [121], silver nanoparticles (Ag NP) [122], titanium dioxide [123], or a combination of Au NP and a silver enhancer [124].

At this moment, it must be stressed that all described test systems and mentioned applications featured chemically synthesized nanoparticles. The chemical synthesis of gold nanoparticles can be performed according to the Frens [125] or Enuston and Turkevich [126] method. The latter being the method of choice for the synthesis of most aforementioned NP. The synthesis is based on reducing chloroauric acid via citrate in an aqueous solution and allows size control of the final conjugate [126]. However, the surface of such nanoparticles is covered with reagents from the synthesis process. Even though citrate may provide additional steric stabilization, it also covers the surface, thus, hindering the later conjugation of functional ligands. La Spina et al. were able to show that at least 3 additional cleaning steps are required to free the covered surface from citrate [127]. Park and Parry could verify that citrate anions bind very strongly to the metal surface and are not replaced by the thiol-groups and thus limit the possible co-adsorbation [128,129]. Citrate´s surface-blocking effect was further demonstrated by Dinkel et al., who compared the surface coverage of NaBr stabilized Au NP with that of citrate stabilized Au NP and a 30 % mass concentration decrease when citrate was on the NP´s surface [130]. An ideal particle for biofunctionalization would have a surface free of any organic ligands, like i.e., laser-generated nanoparticles.

Laser ablation in liquids (LAL) offers an elegant approach to generate ´naked´ particles, free of any organic ligands on their surface, which could actually hinder the successful adherence of functional

ligands to their surface [25]. It represents a combination of top-down and bottom-up synthesis route, which is based on the ablation of macroscopic targets (top-down) and the thereupon following particle generation based on atoms and initial clusters (bottom-up) [131,132]. The ablation can be performed utilizing a laser beam, featuring a wavelength ranging in between ultraviolet (UV) and near-infrared (N-IR) light [133–135], pulse durations ranging from femtoseconds, over pico-, nano-, and milli-seconds, as well as continuous wavelength lasers [136–143].

The interaction of the laser beam and immersed target leads to the generation of a plume on the target´s surface, which consists of ionized and atomic species. Its lifespan varies from tens of ns to µs depending on the surrounding medium and laser parameters. [144,145] Heat transfer leads to the formation of supercritical vapor, which eventually grows into a cavitation bubble. The supercritical vapor encloses an area of liquid matter, where primary particles and nanoclusters are formed through crystallization. Based on molecular dynamic simulations Zhigilei et al. were able to gain insights into the nanoparticle formation during picosecond laser ablation of Ag in water. They could demonstrate via a large scale atomistic simulation, that Ag atoms evaporating from the hot molten metal layer lead to the rapid nucleation of small nanoparticles in the low-density mixing region between the molten metal layer and the surrounding water (< 10 nm) [146] The cavitation bubble undergoes shrinking and expansion until its collapse, which is accompanied by a shockwave and the release of primary (≤ 10 nm) and secondary particles (> 10 nm). Primary particles form via nucleation of the existing atomic matter within the bubble and its consequent growth within the first 3 ns [147,148]. It has been shown that the bubble represents no fix system but represents a highly dynamic, oscillating system. [149–152] Finally, the bubble collapses but leaves persistent micro bubbles behind, which can hinder the further ablation of the target material through shielding effects. This effect is even more drastic in high viscosity liquids. [153]

However, this work will mainly focus on particles produced via nano- and picosecond laser pulses and their respective size distributions, since the diameter of the used nanoparticles plays a crucial role in LFA performance. [154–156] When it comes to picosecond pulse ablation, one major drawback cannot be excluded. Due to the ps-laser ablation process´s nature, there will always be a size fraction of small particles (< 10 nm) present., as described by Shih et al. [146]

Additional works have already been published on possibilities for nanoparticle generation featuring monomodal particle distributions, essential here is the work of Kohsakowski et al., who were able to show that it is possible to separate both size fractions efficiently in a continuous process without interrupting the synthesis [157]. Unfortunately, this procedure allows only to gain the small size fraction continuously, which can be utilized e.g. in catalytic applications [158,159], but not the bigger

size fraction. Thus, post-processing of ps-laser-generated colloids will always be necessary to gain monomodal size distributions. Despite this drawback, laser-generated nanoparticles feature a partially oxidized surface, in the case of gold 3 to 6 %, providing them with the necessary electrostatic repulsion to form stable colloids [160], as well as pH-active hydroxy groups on their surface, providing Au NP with limited buffer capacity [161]. Their surface is readily available for gold-thiol linkage [30], allowing the surface´s easy and rapid functionalization, or putting it more precise, allowing bioconjugation.

In summary, it is possible to generate monomodal, organic-ligand free, laser-generated nanoparticles, featuring diameter within the desired range for LFA applications. The absence of surface-blocking organic-ligands makes them ideal candidates for bioconjugation with functional ligands. At the same time, LAL allows the generation of pure and alloy NP in a single working step.

2.5 Bioconjugation of nanoparticles

Bioconjugation describes the process of linking two or more molecules, of which one at least must be a biomolecule, via covalent bonding. [162] This work focuses mainly on the bioconjugation (or in short: the conjugation) of aptamers onto noble metal nanoparticles, all above Au NP, thus forming nano-bio-conjugates, which have been subject to many studies in recent years [28,46]. There have been many different types of bioconjugates described in the literature, serving very different purposes. Therefore, this section will mainly focus on the conjugation process´s mechanisms, existing state-of-the-art conjugation techniques, and finally, on the conjugation of laser-generated nanoparticles.

How does one achieve conjugation of biomolecules, like DNA, on a noble metal nanoparticle, through covalent binding? Noble metals are known for their rarity, chemical stability, high worth but not for their ability to take part in covalent bonding. Nevertheless, gold and silver have a high affinity towards thiol groups, leading to bonds of high strength (approx. 210 kJ/mol for gold) and therefore almost achieving the strength of a C-C-bond (350 kJ/mol). [163–168] The underlying mechanism of the thiol-gold-linkage has been subject to intense discussions [169]. After an initial physisorption of the thiol onto the gold surface follows a chemisorption which can be divided into the lying down phase formation, nucleation, standing up phase and completion. Different explanations exist how the chemisorption happens. [170] The two most favored mechanisms described in the literature are the saturated and the radical models, which were both discussed by Wang et al. and proposed to be theoretically possible [171]. However, one year before their work, Kankate et al. were able to demonstrate the release of atomic hydrogen during the formation of a thiol-linkage of 4-nitrophenylthiol towards a gold surface providing proof that the proposed mechanism of the radical model does not match the observed products. Therefore, the saturated model (see Reaction 1) must be the most likely mechanism. [172]

Reaction 1 $$R - SH + Au\ (s) \rightarrow R - S - Au + \frac{1}{2}\ H_2$$

In addition to that, Pensa et al. showed that nanoclusters might actually act as ´scavengers´, when it comes to bioconjugation since 79-atom gold nanoclusters can be found, featuring a thiolate protected surface [173]. Thus, stressing the need to reduce the proportion of the unwanted small size fraction on the resulting size distribution of laser-generated colloids. Since aptamers can be easily chemically modified [51,174], adding a thiol-group to an aptamer has become the state- of-the-art modification in nano-bioconjugation [175]. Besides thiol, other groups can also readily adsorb onto the electron-accepting gold surface, namely NH_2, COOH, phosphate, and disulfide bridges (R-S-S-R) [24].

Nevertheless, can one thiol-group alone efficiently bind ligands to an Au NP surface? Since this work´s focus lies on single-stranded DNA aptamers, one must consider the very nature of this special kind of ligand. DNA features a negatively charged phosphate backbone, thus, providing a more negative charge with increasing sequence length. In addition to that, DNA itself can readily adsorb through unspecific binding events onto noble metal surfaces, thus blocking the surface for further gold-thiol-linkages. In this regard, especially adenine bases have a high affinity towards the surface compared to e.g. thymine, which has the lowest affinity towards gold. [175–179] Since Merk et al. stated that the surface of organic-ligand free Au NP themselves exhibit pH-depend negatively charged surface charges [161], three main problems must be overcome: DNA blocking the surface via unspecific binding events, the electrostatic repulsion between negatively charged nanoparticles and the negatively charged phosphate backbones, and the electrostatic repulsion of DNA molecules among each other (see **Figure *7***).

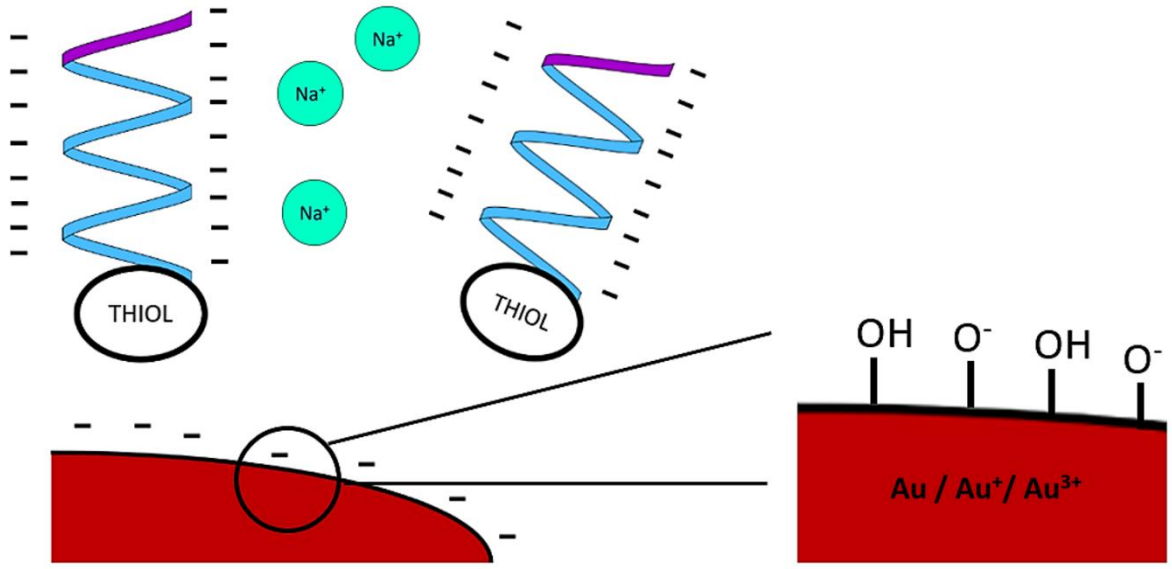

Figure 7: Charge screening via sodium cations between negatively charged phosphate backbones and the partially oxidized nanoparticle surface.

Solving the first problem is just a matter of time, as was shown by Wang et al. since conjugation is always a two-phase process: a first rapid DNA-adsorption leads to the coverage of the nanoparticle surface with a few DNA molecules, who may lie down and block the surface, and the second phase of reorganization, ultimately rearranging the gold-thiol-linkages to allow for maximum surface coverage. [180] Since most conjugation protocols feature a 24 h incubation phase, this problem can be easily avoided. Solving the repulsion problem between NPs and DNA, and in between DNA molecules presents a more challenging problem – but a problem that has been tackled thoroughly. The working group around Chad A. Mirkin provided the lion´s share of experimental work regarding the maximization of DNA-loading on chemically synthesized nanoparticles. "Maximizing DNA loading on a range of gold nanoparticle sizes" by Hurst et al. [175] represents maybe one of the most important publications in the field of nano-bioconjugation. In that work, the negative charge is screened by cations through the stepwise increase of NaCl concentration, known as salt-aging. Until today salt-aging represents the state-of-the-art *ex-situ* conjugation approach and was used to generate the conjugates featured in most aforementioned applications (including but not limited to [36,100,118,119]). The Na^+ cations introduced to the conjugation reaction reduce the Debye-length of the nanoparticles, which is directly linked to reducing the electrostatic repulsion between NP and DNA. In this regard, it must be considered that laser-generated NP are primarily stabilized through their electrostatic repulsion. Thus, reducing the Debye-length too much can cause the agglomeration or even aggregation of the NP. [181] Nevertheless, with higher surface coverage, more steric hindrance and negative charge of the additional phosphate backbones are provided, ultimately leading to improved colloidal stability [182]. Most of the introduced cations end up in the DNA-layer covering the

nanoparticle surface, leading to a 15-times higher cation-concentration in the DNA-layer compared to the surrounding medium. This finding by Kewalramani provides evidence for the actual charge screening cations provide in between the applied DNA, thus allowing DNA-molecules to overcome their electrostatic repulsion among each other. [183] In addition to the introduction of salt aging to the nano-bioconjugate community, the working group around Mirkin elucidated the influence of the nanoparticle´s curvature on their conjugation. Hill et al. could show that smaller nanoparticles allow higher surface coverages than bigger particles concerning their respective radius. This phenomenon is directly linked to the space available in between neighboring, bound DNA strands since with increased curvature, the deflection angle decreases, and the orthogonal, linear orientation of the DNA increases. On the other hand, a 60 nm particle already behaves like a planar surface in ligand conjugation. [184] In addition to that, the design of the DNA ligand must be optimized for conjugation purposes to allow enough distance to the nanoparticle surface and offer sufficient room for the folding. In this regard, spacer sequences are added to the DNA strands, supporting the correct aptamer´s orthogonal orientation [28].

These findings stress the importance of three key parameters in this work: aptamer design, particle size, and surface coverage. Since aptamer function is based upon its distinctive 3D-structure and folding, the provided space is highly relevant when bound to a nanoparticle. Besides salt aging, featuring NaCl, various other approaches have been performed throughout the years. Experiments featuring varying cations concerning their charge density, concluding that smaller, highly charged cations have to be favored above bigger, less charged ones. [175] Besides that conjugation was performed via pH-alteration. Zhang et al. could achieve an instantaneous functionalization of Au NP by pH-reduction to pH 3 [185]. However, such harsh pH conditions can also introduce strand breaking to DNA molecules and may limit its functionality [105]. All these findings provide an excellent understanding of how conjugation of chemically synthesized particles can be achieved and what mechanisms and kinetics these processes are based on. Nevertheless, all these findings have been made for chemically synthesized nanoparticles, featuring a citrate layer on their surface. Thus, the question arises, what is the state-of-the-art in bioconjugation of organic-ligand-free, laser-generated NPs.

It has been more than ten years since the first bioconjugation of laser-generated nanoparticles was described in the literature by Petersen et al. [25]. Thus, offering a novel and fascinating approach: *in-situ* conjugation, meaning the conjugation of particles during their synthesis, not after particle synthesis (*ex-situ*). This initial and bold experiment provided evidence for a faster conjugate synthesis route with higher achievable surface coverages than described in previous milestone publications. The *in-situ* conjugates achieved up to four times higher surface coverages than their *ex-situ* conjugated

counterparts. [24–26] In addition to that it was shown by Walter et al. that *in-situ* miniStrep-aptamer functionalized nano-bio-conjugates still exhibited the desired functionality and were able to bind streptavidin [30]. However, *in-situ* conjugation comes with a drawback once again. Due to ligand-induced size quenching effects, the produced conjugates feature a nanoparticle core only 5.7 ± 3.4 nm in diameter [25], thus making it less attractive regarding POC utilization or even LFA applications. However, Petersen et al. aimed for different applications, ultimately turning their small functionalized nanoparticles into cell-penetrating, drug-delivery units [186]. This concept was adapted in the following years, ultimately leading to a highly specific application of conjugates featuring laser-generated nanoparticles or even agglomerates, like in the work of Krawinkel et al., where peptide-conjugated gold nanoparticle agglomerates achieved intracellular molecule delivery [187]. But nano-bio-conjugates do not only allow molecule delivery but also transfection – the introduction of foreign DNA/RNA into a cell, as it was demonstrated by Gamrad et al. for murine regulatory T cells [188]. In addition to that, laser-generated nano-bio-conjugates were subject to further works related to reproductive biology. Barchanski et al. conjugated sex chromosome-specific moieties as well as cell-penetrating ligands to laser-generated Au NP and were able to demonstrate the non-destructive penetration of spermatozoa in dependency of their respective membrane status [27,189]. Gamrad et al. utilized a similar approach to hybridize DNA/LNA functionalized nano-bioconjugates towards bovine Y-chromosomes [190]. Even though this work focuses on the POC-applications of nano-bio-conjugates, very important findings of these sexting experiments must be stressed. One fundamental rule was described by Gamrad et al., who found out, that the charge of ligands on a nanoparticle surface has to be adjusted so that the total resulting charge of the ligands leads to either a positive or negative zeta-potential [191]. Thus, this work offers a new perception on bioconjugation and the possibilities to introduce cations to the system, but in general a mixture of positively and negatively charged ligands. Furthermore, it was shown by Sajti et al. that it is possible to gain nano-bioconjugates in a continuous flow liquid jet system, which may ultimately serve as template technology for the scale-up of bioconjugation [192,193]. Another auspicious approach to fight Alzheimer's disease was presented by Streich et al., who could show that the laser-generated nanoparticles' organic-ligand free surface can be covered in a controlled manner with functional ligands to utilize multivalency-effects to bind low-affinity ligands and even further to drastically increase the ligands functionality in comparison to the pure, unconjugated ligand [194].

It was shown, how surface coverage may influence the functionality of conjugated ligands on an Au NP. However, LAL nano-bio-conjugates have not been subject to POC applications so far. The next section of this thesis will tackle the analytes that were subsequently chosen to serve as targets for aptamers, conjugated towards laser-generated nanoparticles.

2.6 Target systems

This section will describe in detail the chosen target molecules, their importance to science, human health, and the economy, as well as challenges in detecting them.

2.6.1 Streptavidin

The streptavidin-biotin-bond is considered one of the strongest non-covalent bonds, featuring a dissociation constant (K_D) of only $4*10^{-14}$ over a huge range of pH and temperature values [195]. The streptavidin protein, which can be isolated from Streptomyces avidinii [196], consists of four identical subunits. All these subunits can bind biotin, which is also commonly known as vitamin B7. B7 serves as an activated carbon dioxide carrier, thus playing a major role in the regulating carbohydrate-, fat-, and protein metabolism. [197] The structure of streptavidin was mainly elucidated by Weber et al. [198] and Hendrickson et al. [196]. Today streptavidin-biotin coupling can be found throughout countless immunoassay applications that exploit the strong bonding, making streptavidin an ideal model compound for aptamer applications. Walter et al. were able to demonstrate the streptavidin binding ability of a specifically designed aptamer, called miniStrep aptamer [30], which is based on the streptavidin binding sequence described by Bittker et al. in 2002 [94]. Since the miniStrep aptamer can be easily be displaced by biotin [94], this system makes for a perfect candidate to generate basic insights into the functionality of nano-bioconjugates featuring laser-generated nanoparticles.

2.6.2 Ochratoxin A

Ochratoxin A (OtA) represents a highly toxic contaminant that can be found in various foods and drinks, including but not limited to beer, wine, coffee, wheat, flour, etc. The Bundesinstitut für Risikobewertung (BfR, Germany) and the scientific food commission of the European Union (EU) determined a maximal recommended ochratoxin A uptake of only 0.9 ng per kilogram body weight per day for a male (no data provided for females). Additional uptake could ultimately lead to severe tissue damage of the kidneys and lead to cancer, as was shown in rats and mice. The primary uptake per kilogram body weight per day of this mycotoxin occurs through coffee (0.2 ng/kg product) and up to 0.5 ng/kg through wheat products, with beer contributing 0.2 ng/kg. [199] Its hazardous nature and abundance arouse increased interest in its cost-effective and easy POC –

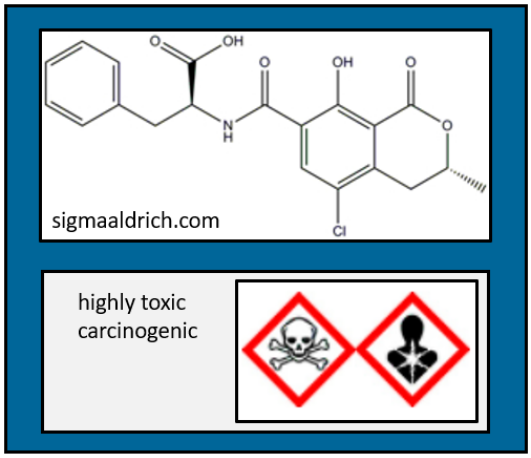

Figure 8: Molecular structure of ochratoxin A and its main hazards, based on safety data sheet by sigmaaldrich.com

detection and finally in the development of various working test formats [118,119,122–124,200–213]. Some working groups developed classical LFA tests, like Anfossi et al., who were able to detect OtA in wine and grape must [200], Moon et al. developed an OtA-LFA for different buffer systems [207], Zhang et al. found a method to detect OtA in corn samples [211], whereas Zhou et al. were able to detect OtA in Astragalus membranaceus [212]. Other groups tried alternative approaches. Cruz-Aguado et al. utilized a combination of affinity columns and aptamers to detect OtA [202], whereas Evtugyn et al. performed experiments with an impedimetric aptasensor [213]. Barhelmebs et al. used an Enzyme-linked Immunosorbent Assay (ELISA)-related format, based on aptamers, which is called Enzyme-linked Aptamer Assay (ELAA), which allowed OtA detection in wine [201]. Furthermore, there are many fluorescence [206] and fluorescence-quenching-based test formats, like the silver-nanoparticle fluorescence quenching assay by Jiang et al. [122] or the titanium dioxide quenching-based test by Sharma et al. [123]. In addition to that, there are some rather unique test systems. Yang et al. utilized unmodified Au NP as indicator for OtA detection [209]. One rather outstanding work has been presented by Lai et al., who were able to mimic ochratoxin for LFA experiments, thus, replacing the highly hazardous substance by a less toxic component [204]. These findings will potentially simplify the work on highly toxic small molecules like OtA in the future and thus accelerate further research.

2.6.3 Ampicillin

Ampicillin represents one of the most commonly encountered antibiotics since it is classified as a broad-band antibiotic and is widely used in molecular biology and agriculture. In general, antibiotics are anti-microbial substances that either kill bacteria or inhibit their cell growth. The structure that is targeted by the antibiotic determines whether it is effective against gram-positive, or -negative cells. Ampicillin belongs to the β-lactam antibiotics, which prevent the peptidoglycan synthesis in gram-positive, and -negative bacteria, thus interfering with their murein-membrane-biosynthesis, making it a broad-band antibiotic. [214] Even though mammalian cells lack a murein-membrane, penicillin like ampicillin, can cause severe side effects in mammals, including humans. The usage of antibiotics leads to residues in the produce, like meat and milk, which can then lead to allergic reactions in humans, including but not limited to seizures and breathing difficulties.

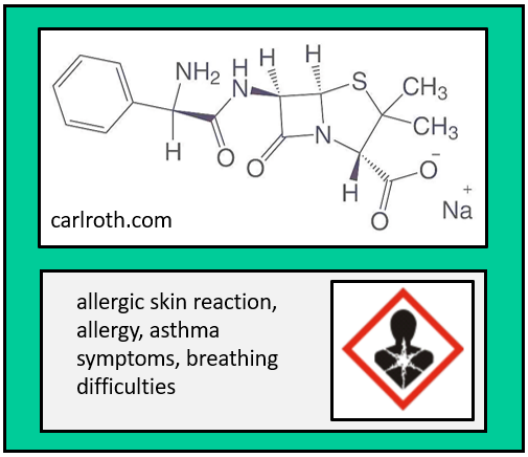

Figure 9: Molecular structure of ampicillin and its main hazards, based on safety data sheet by carlroth.com

Strict residual limits have been determined by major health organizations, like e.g. the Food and Drug Administration (FDA) or Word Health Organization (WHO). [120]

However, the detection of ampicillin is quite challenging. So far, different approaches have been realized to tackle this analyte. Nelis et al. make use of tandem solid-phase extraction to analyze ampicillin in bovine and dog plasma via liquid chromatography [215]. Luo et al. were able to develop a fluorescence detection – liquid chromatography – coupled detection approach for residual ampicillin in animal muscle tissue [216]. Kurittu et al. chose an alternative approach without utilizing liquid chromatography. Their detection of tetracycline residues, like residual ampicillin, was performed by a luminescent *Escherichia coli* strain in raw bovine milk. These genetically modified organisms produce luciferase in the presence of tetracyclines, which leads to measurable bioluminescence, allowing for a detection limit down to 2 ng/mL. [217] However, none of these approaches can be considered POC-suitable. Here, aptamers offer a novel approach in detecting this challenging analyte. Song et al. described different aptamers that are suited to bind ampicillin [120]. Even though Song et al. were able to lay the foundation for future POC-ampicillin detection, Kaiser et al. were able to demonstrate how the ampicillin aptamers suffer from C-reactive-protein cross recognition. Since C-reactive-proteins are linked to inflammatory processes, this cross recognition may exhibit an additional challenge for the correct detection of ampicillin, or if used wisely, could also allow for additional detection approaches. [5]

3. Results and Discussion

The results of this thesis are presented within five main sections and their respective, distinct subchapters. The first division includes nanoparticle generation and characterization, which is followed by section two “bioconjugation”. The third section moves on to the functionality of the generated nano-bioconjugates, whereas section four focuses mainly on the influence of the introduced nano-conjugate modifications on the on lateral-flow-assay´s performance. This experimental section will be completed by the introduction of aptamer recycling and an extensive literature review on how the findings can be evaluated in context with the current state of the art of aptamer-based LFA.

3.1. Nanoparticle characterization

The very heart of every nano-bio-conjugate consists of a nanoparticle. As mentioned above, the nanoparticles serve as detection agents in an LFA. Thus, it is of the highest importance that the nanoparticle´s optical properties meet the high demands of these POC devices. The nanoparticle´s color must provide strong optical contrast to the surrounding nitrocellulose membrane, and vibrant color can be of use to allow the correct visual readout. Here, the strong red color of gold nanoparticles comes in handy since red represents a worldwide, interculturally accepted signal color. At the same time, the nanoparticles must provide sufficient stability to allow their bioconjugation via aging-technique of choice, their immobilization onto a glass fiber pad, as well as the resuspension through contact with the sample matrix, and their journey through the LFA. Another important requirement is the diameter of the nanoparticles and their respective size distribution. As already established, size plays a crucial role in the bioconjugation process. Smaller nanoparticles feature an increased surface curvature, allowing more thiol-groups of DNA-molecules to bind onto the surface. In retrospect, this also means small particle fractions will be conjugated more efficiently than bigger particle fractions – they will “scavenge” the utilized DNA-molecules. Nanoparticles for LFA applications underly a strict diameter limitation since the most frequently used nitrocellulose membranes only allow the passage of nanoparticles of less than 60 nm in diameter [41].

In this work, laser-generated nanoparticles of varying diameters were produced: 10 nm, 30 nm, 40 nm, and 50 nm, of which exemplary colloids are shown in **Figure 10 (A-C)**. More details on the synthesis of the particles can be found in “Material and Methods”; section 8.1.2. The smallest particles were used for basic function assays to allow to elucidate the surface composition´s influence onto the conjugated aptamer-binding ability. Larger particles were used for aptamer bioconjugation, followed by transfer onto glass fiber membranes, nitrocellulose and real LFA runs. Chemically synthesized Au NP of 20 nm in diameter were utilized as a comparison throughout this work.

It is well known in the existing literature that the size of the nanoparticles plays a crucial role for the sensitivity of the LFAs. The spot brightness of the red stained test line is mainly based on the extinction of green light rather than scattering [40,218]. Zhan et al. could demonstrate an increase of sensitivity for larger Au NP [219]. However, the functionalization of large particles is drastically limited by their instability under LFA conditions [40]. Even though the influence of the scattering remains a crucial topic of discussion throughout literature [219], studies show that Au NPs of 30 – 40 nm in diameter should perform best under LFA conditions [155,156], which is supported by the theoretical calculations and experimental data for CTAC-stabilized Au NP of Khlebtsov et al. in 2019. Based on their findings they also conclude that chemically synthesized Au NP should provide less spot brightness on the nitrocellulose membrane due to their broader size distribution. [40] With these works in mind it is to be expected that 30 - 40 nm laser-generated Au NP should represent the best candidate for LFAs, whereas it can be expected that 10 nm Au NP do not provide sufficient extinction cross section while larger particles should face stability problems.

The raw colloids, directly after LAL-synthesis, featured broad and multimodal size distributions. As mentioned above, this phenomenon is well known for laser-ablated nanoparticles featuring diameters above 10 nm [150,220,221] and has been thoroughly investigated by Shih et al. for picosecond laser ablation [146]. The size separation via centrifugation to gain Au NP smaller 10 nm has been established by Gamrad et al. and used in several studies [187,189–191]. Furthermore, it has been already shown by Kohsakowski et al. that continuous centrifugation can be utilized to scale-up the production volume of this particular size fraction beyond a scale required for this work [157]. A unified centrifugation protocol (see **Figure *72***) was established in this work to generate nanoparticles, featuring a diameter of 30 nm, 40 nm and 50 nm, with moderate reproducibility (batch to batch variation of desired mean diameter per colloid batch of ± 1.5 STD). In this regard, the most important finding was the necessity of an initial incubation step of 24 h before the colloid´s centrifugation to allow rapid-barrierless coalescence, which has been discovered to happen for laser-generated platinum nanoparticles [222]. This forced coalescence has been described by Ziefuß et al. for the generation of laser-generated NP, featuring a diameter of 54 nm [223], and was adopted in this work to generate monomodal gold colloids of the desired diameters. The established centrifugation procedure allowed to increase the ratio of the desired size fraction even further, as shown in **Figure 10 D**. (Centrifuge protocol; see chapter 8.1.2)

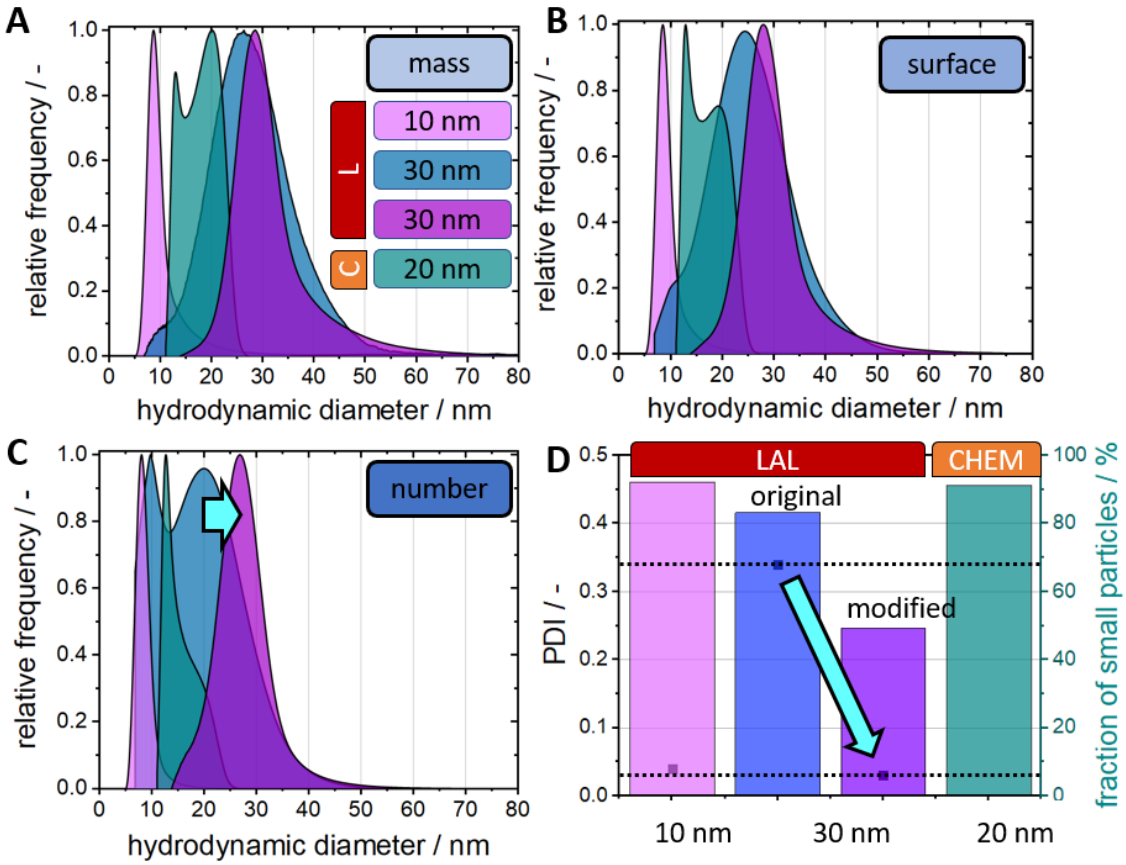

Figure 10: Size distribution for laser-generated colloids (L/LAL) and chemically synthesized NP (CHEM) weighted by mass (A), surface (B), and number (C). Two 30 nm colloids are shown: blue represents the initial centrifuge protocol (original), whereas dark purple represents the modified centrifuge protocol which has been established throughout this work (modified). Section D compares the PDI of the different LAL colloids and shows the fraction of particles smaller than the respective desired diameter. A PDI above 0.3 indicates a polydisperse distribution, whereas a PDI value < 0.3 indicates a monodisperse sample. No PDI has been provided for the chemically synthesized particles, since no legitimate fit-function could be fitted onto the raw distribution.

Here, the size distribution of LAL colloids (10 nm, 30 nm) and chemically synthesized Au NP by Fassisi GmbH are shown. The distributions are presented with their respective weighting by mass, surface, and number. Each weighting stresses a different aspect of the samples. Mass and surface weighting reveal a strong bimodal distribution of the chemically synthesized nanoparticles, whereas the number-weighted distribution reveals, that the main fraction of particles exhibits a hydrodynamic diameter of only 12.8 nm instead of the desired 20 nm. In fact, the unwanted fraction of smaller particles makes up to 92.26 % within this colloid. Here, it has to be expected, that these particle fraction will ultimately scavenge DNA molecules due to its high specific surface, which would be in accordance to the observations of Hill et al. for small particles [184]. In addition to that the 12.8 nm fraction will

contribute less effective to the required spot brightness of the test line due to its low extinction cross section. [218]

The 10 nm LAL nanoparticles exhibit a strict monodisperse distribution as described by Gamrad et al. [187,189–191]. However, the centrifugation procedure for larger particles had to be drastically improved. Initial colloids featured more than 80 % smaller, unwanted particles and exhibited PDI values above 0.3, making them polydisperse. The optimized centrifuge protocol (**Figure *72***) lead to narrow, monodisperse distribution, thus eliminating unwanted scavenging by small particles. However, at this point, the improved size distribution of the laser generated nanoparticles is achieved throughout a higher workload in centrifugation steps. The optical properties of the generated colloids were analyzed via UV-vis extinction spectroscopy (see **Figure 11**).

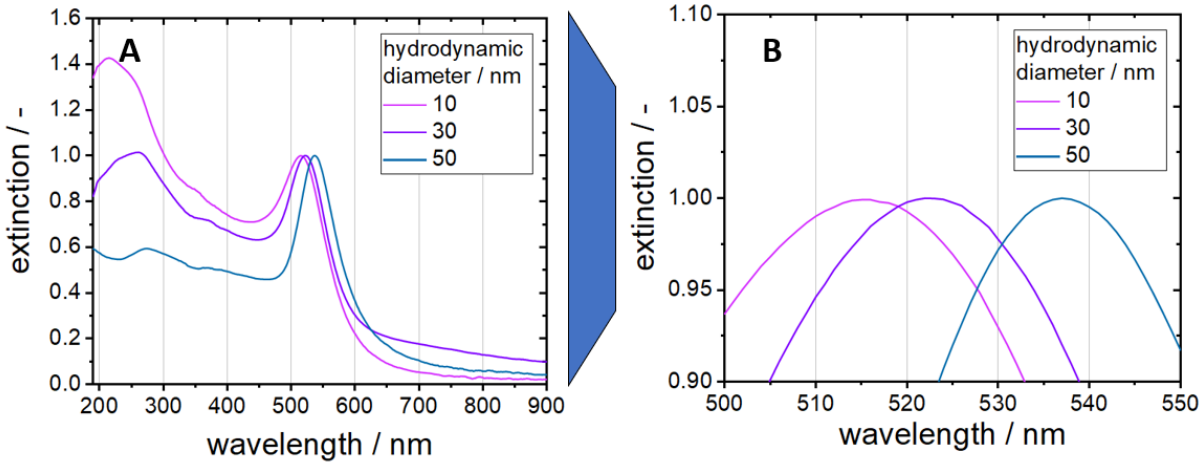

Figure 11: UV-vis extinction spectra of laser-generated monomodal Au NP colloids. A) entire spectrum normalized to 1 at the respective SPR-peak. B) Zoom into the SPR peak top region.

The observed red-shift of the SPR peaks for increasing diameters is as expected for Au NP [40]. All produced colloids feature a strong SPR peak, which makes them to potential labels. However, due to the specific requirements and the best yield of monomodal, stable, LFA-suited 30 nm Au NP became the standard LAL Au NP throughout this work. This is in good accordance to the ideal NP diameter of 30 to 40 nm proposed by Safenkova et al. in 2010 [224].

3.2 Bioconjugation of Au NP with thiolated Aptamers

Nano-bio-conjugates represent a versatile tool in diagnostics and therapeutics. Many bioconjugation protocols have been established and published since the first salt-aging procedure was published in 2006 [175]. Despite the procedure being widely used all out through the literature, only little research has been conducted on the simplification and acceleration of this time-consuming process. Above all, one must mention the alternative protocol by Zhang et al., which is based on controlling the conjugate batch´s pH instead of utilizing metal cations [185]. However, even less research has been performed in the matter of the ideal conjugation process regarding conjugate stability and functionality. This section focuses on the optimization of the conjugation process of ´naked´ model nanoparticles. The absence of any foreign organic ligands allows for a precise tuning and characterization of the ligand-corona composition and the exclusion of any side effects caused by the organic ligand shell from the chemical nanoparticle generation process. These findings show that ligand-free nanoparticles allow exact precise surface coverage adjustment at sufficient stability, allowing for high surface coverages with functional ligands.

The works of Hill et al. [184] and Petersen & Barcikowski [25] both represent milestones in the field of bioconjugation. For the first time, the influence of the particle's curvatures on the bioconjugation process was shown. Whereas, the introduction of the *in-situ* conjugation procedure, which combines the nanoparticle generation and their conjugation in one step, allowed for the first time to save valuable work hours and allowed for higher surface coverages in comparison to conjugates produced via the established *ex-situ* salt-aging. This work aims to combine the best out of both approaches. Since *in-situ* conjugation always leads to very small particles (< 10 nm; see **Figure 12**), this technique was not included in this thesis. However, the conjugation of laser-generated nanoparticles > 10 nm has not been subject to systematic research. The main advantage lies within the organic ligand-free surface. During the chemical synthesis, remaining reactants, like e.g., citrate, blocks the surface and prevents functional ligand conjugation. This may lead to additional cleaning steps, as was shown by La Spina et al. [127]. *Ex-situ* conjugation represents a reliable, yet not totally understood process that allows for precise surface coverage adjustment.

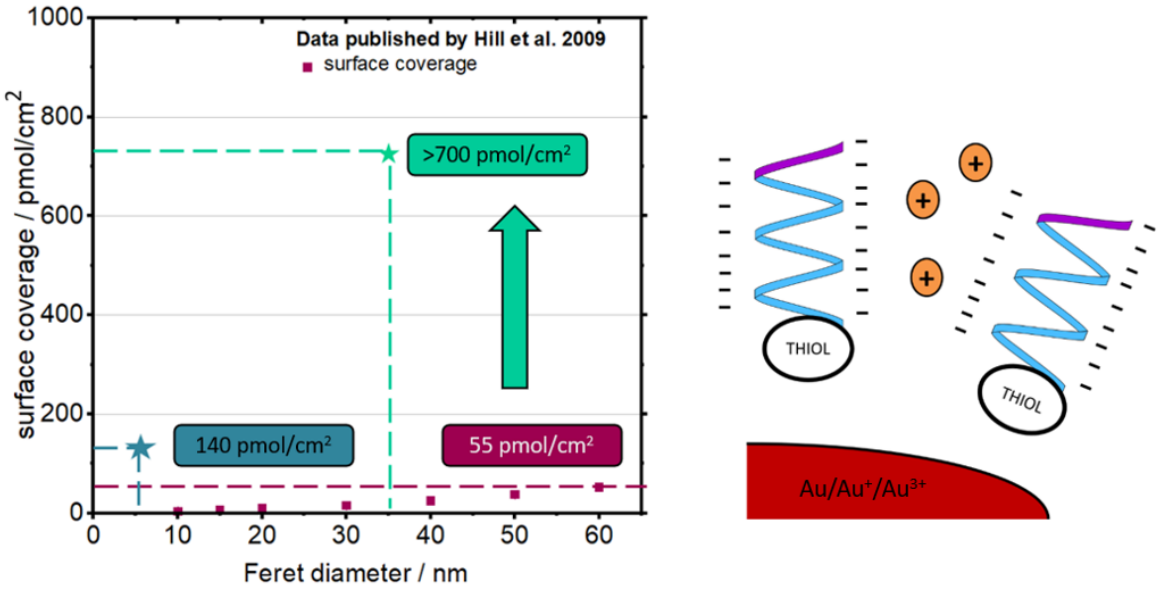

Figure 12: Bioconjugation of Au NP throughout literature; blue represents the highest achieved surface coverage by Petersen & Barcikowski via *in-situ* conjugation [25]; purple represents the surface coverages achieved for varying particle sizes by Hill et al. [184]; turquoise represents the highest achieved surface coverage via *ex-situ* conjugation throughout this work.

The shown ferret diameter range was chosen since the main field of application addressed in this work focuses on LFAs, which generally feature particles between 20 and 60 nm. The presented high surface coverage above 700 pmol/cm^2 (determined by supernatant analysis as described in section 8.2) represents an exceptionally high surface coverage that exceeds by far any surface coverages described in the literature to our best knowledge. Nevertheless, the focus of this work was not to increase the surface coverage by adjusting the *ex-situ* conjugation process of chemical NPs for laser-generated NPs, but also to succeed in their functionality. It must be mentioned that the ideal surface coverage of the state-of-the-art nano-bio-conjugates in LFAs, consisting of antibodies conjugated to chemically synthesized Au NP, is known to be very low. Liu et al. were able to determine a optimal ratio of 30:1 antibody to nanoparticle ratio for their respective test system [225]. Findings of Byzova and Safenkova support this findings [226]. However, as Zherdev and Dzantiev stated in their review on the matter of lower LODs for LFAs, it might not be possible to simply transfer insights from one test systems to another one. [227] The results presented in this work differ even more from the already published data in that regard, that laser-generated Au NP and aptamers are introduced. Therefore, it is of high scientific interest to evaluate the ideal surface coverage for this test system, since it has not been demonstrated in the existing literature to our best knowledge.

To provide a better understanding of the conjugation of laser-generated NP not only NaCl, but also $MgCl_2$, and $CaCl_2$ were utilized for the salt aging process. Since the cations of these salts are responsible for the charge screening between the negative nanoparticle surface and the DNA strands, as well as

charge screening in between DNA strands themselves, **Figure 13** provides a schematic overview of the ion diameter of the tested species and their respective charge density concerning their diameter.

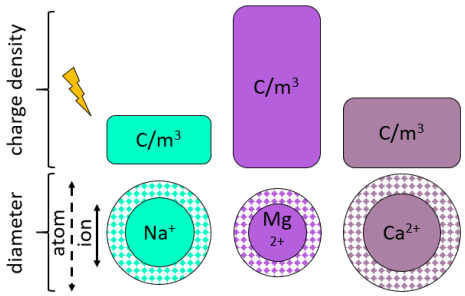

Figure 13: Cations used for salt-aging and their respective ion radius (full color) and atom radius (checked) and their respective charge density in C/m^3.

Based on this initial situation, the Schulze-Hardy rule and the observations described by Hurst et al. [175], one would expect that all cations allow for an effective charge screening. However, due to magnesium and calcium providing two times positively charged cations, they should provide more efficient charge screening. Furthermore, due to its small ion radius, magnesium cations feature a very high charge density of $1,2 * 10^{49}$ C/m^3, whereas sodium and calcium only reach 30 %, respectively 42 % of this charge density. Since the cation concentration within the DNA shell around the particle can excel the 15-fold of the cation concentration in the bulk solution, one must expect that magnesium chloride should provide the highest conjugation efficiency, respectively the highest surface coverage of the three tested salts, followed by calcium chloride and finally sodium chloride. Concerning stability, one would expect in return the opposite order: sodium chloride should induce the least electrostatic destabilization of the colloidal particles, whereas colloids conjugated by salt-aging via calcium chloride should be less stable. Magnesium chloride is expected to induce certain agglomeration/aggregation, based on the finding that laser-generated NP mainly depend on their electrostatic stability, as was highlighted by Pfeiffer et al. [182]. **Figure 14** shows the experimental results of conjugation experiments featuring the same 40 nm Au NP colloid at a constant concentration, the OtA-aptamer at constant concentration, and ionic strength adjusted salts.

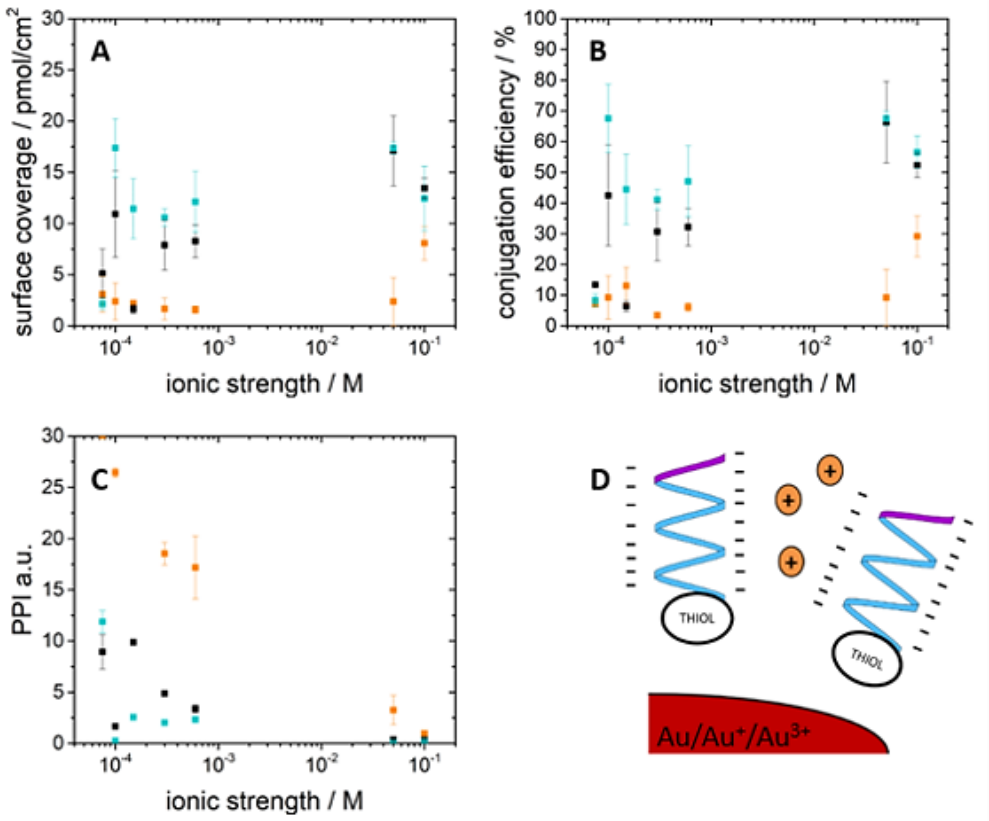

Figure 14: Salt-Aging of 20 nm Au NP with NaCl, $MgCl_2$, $CaCl_2$. A) surface coverage; B) conjugation efficiency; C) PPI; D) schematic overview.

As expected, the achieved surface coverages, respectively conjugation efficiencies raise with increasing ionic strength. Throughout the entire tested range of varying ionic strength, calcium chloride provides the highest surface coverages together with magnesium chloride at high ionic strength above 0.1 M. As expected, sodium chloride provided the lowest conjugation efficiency (A), hence the lowest surface coverages (B). The colloidal stability of the generated colloids was estimated using the primary particle index (PPI), which was introduced by Merk et al. to describe the colloidal stability indirectly with regard to the portion of aggregates and agglomerates of laser-generated nanoparticles via UV-vis extinction spectroscopically analysis [161]. It must be stressed that the conjugation of laser-generated nanoparticles directly influences the UV-vis extinction spectra since DNA is UV-vis sensible and accounts for strong extinction at 260 nm, thus influencing the interband absorbance of gold nanoparticles. However, it can be used as a first glance at the colloidal stability of nano-bio-conjugates since the PPI represents the interband absorbance ratio at 380 nm and the agglomeration/aggregation signal at 800 nm, which is independent of the DNA UV-vis signal. Therefore, PPI values of conjugates may be shifted towards more stable, higher PPI values, due to an increased absorbance at 380 nm caused by DNA but are still able to indicate a lack of stability. In the following paragraphs, a more suitable approach using visible readout-based stability evaluation of nano-bio-conjugates will be presented.

Here, the PPI remains the highest for sodium chloride for almost the entire tested range of ionic strength, as was expected. However, the PPI for magnesium chloride aged conjugates exceeds the PPI for calcium chloride aged conjugates almost throughout the entire tested range. At first glance, this contradicts the assumptions made earlier. However, even though the system has already been simplified by excluding any interactions between synthesis-dependent surface-bound organic ligands on the particle surfaces, e.g., citrate, with the added DNA molecules, one must consider the high complexity of a nanoparticle – thiolated DNA single strand – system. Single-stranded DNA molecules, especially aptamers, can form complex three-dimensional structures depending on the sequence, the temperature, and the ionic environment. Here, only the utilized cations were changed. To fully understand the interactions of aptamers, cations, and nanoparticles it is necessary to analyse conjugate stability and surface coverage/conjugation efficiency as one phenomenon instead as two unrelated phenomena. One must consider the influence different cations may have onto DNA-folding, hybridization, and binding ability.

It is known that some aptamers require magnesium ions for their target binding ability, like e.g. tetracycline or streptomycin binding [228–230]. Magnesium ions support the formation of kissing complex formations in RNA [231–233] – which means they can stabilize hairpin – hairpin – interactions between two different strands. If two strands bound to different nanoparticles undergo kissing complex formation, this will lead to approximation of the particles and ultimately lead to agglomeration and aggregation. Yet, magnesium chloride leads to higher PPI values than calcium chloride. Therefore, it must also introduce stability increasing interactions. Linked aptamers on the same nanoparticle may form larger aptamer complexes, which may ultimately block the nanoparticle surface for further aptamer adsorption via gold-thiol-interaction but may provide increased steric stabilization. This would explain why $MgCl_2$ conjugates feature lower surface coverages, but higher PPI values than $CaCl_2$ conjugates.

Ducongé et al. were able to provide evidence that magnesium-supported interactions ultimately lead to an increased inter-backbone distance of RNA molecules [234]. Larger phosphate – phosphate – distance translates to less electrostatic repulsion between DNA-strands, as was suggested by molecular dynamics by Beaurain et al. in 2003 [235]. Since RNA-aptamers and DNA-aptamers share many properties, which Ducongé and Toulmé showed in 1999 [236], one can conclude that such a magnesium ion-induced hairpin – hairpin interaction is also most likely to happen for DNA-aptamers featuring hairpin formations. These findings support the observed lower conjugation efficiency for $MgCl_2$ in comparison to $CaCl_2$.

The described OtA aptamer features multiple sides for hairpin formation, as shown by using the OligoAnalyzer 3.1 tool (see **Figure 15**). Furthermore, the complementary oligonucleotide, required for utilizing the aptamer in an LFA application, features a hairpin formation as well. Thus, the functionality of the OtA detection system could be negatively affected in presence of Mg^{2+}.

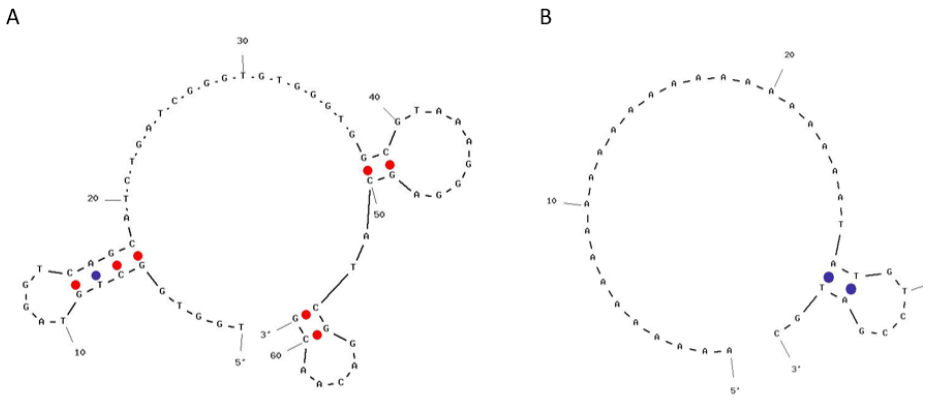

Figure 15: Predicted structures for the OtA aptamer (A) and its complementary oligonucleotide (B) via OligoAnalyzer 3.1; Hairpin formations are marked via dots (red dot = C/G bond; blue dot = A/T bond).

Just like magnesium ions, calcium ions are known to be required for target binding of some aptamers. However, the cations are most likely required close to the actual target binding sites and less for the support and folding of the aptamer structure itself [237,238]. Sodium ions are known to interact and to introduce conformational switches within g-quadruplex conformations, as was shown by Smestad et al. [239]. Since the in-silico analysis of the OtA aptamer does not indicate the presence of a g-quadruplex conformation, an effect of the sodium concentration on the resulting OtA aptamer conformation seems unlikely.

In summary, the observed conjugation efficiency and resulting conjugate stability of the utilized salts during salt aging differed from the expected ones. Based on their charge, respectively charge density, it was expected magnesium chloride would provide the highest conjugation efficiency and surface coverages, followed by calcium chloride and finally sodium chloride. Concerning the resulting conjugate stability, the opposite order was expected. However, the results indicate that the highest conjugation efficiency was achieved using calcium chloride, followed by magnesium chloride and sodium chloride (compare **Figure 16**).

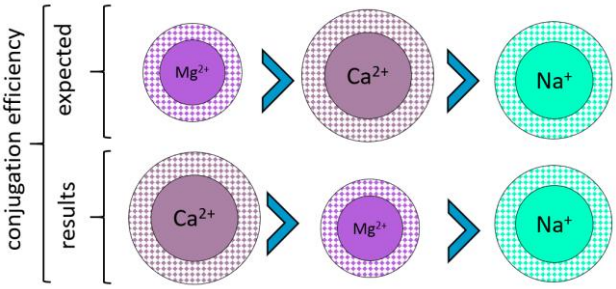

Figure 16: Conjugation efficiency; expectations vs. results.

This finding is supported by the above-mentioned influence of the utilized salt onto the three-dimensional DNA structures. Mg^{2+} provides the highest charge density, therefore, should lead to the highest conjugation efficiencies and surface coverages. However, since Mg^{2+} supports hairpin – hairpin interactions, it may lead to surface blocking inter-strand aptamer complexes, blocking the surface leading to a reduced surface coverage and conjugation efficiency, while providing improved colloidal stability in comparison to calcium chloride. Calcium chloride does not introduce structures featuring high steric hindrance, thus, providing higher conjugation efficiencies and less colloidal stability. The monovalent sodium cation acts as expected in this regard but may also have a significantly different behavior if the analyzed aptamer structure exhibits g-quadruplex formations. The resulting conjugate´s observed stability also differs from the expectations, solely based on the charge density of the utilized salts (see **Figure 17**).

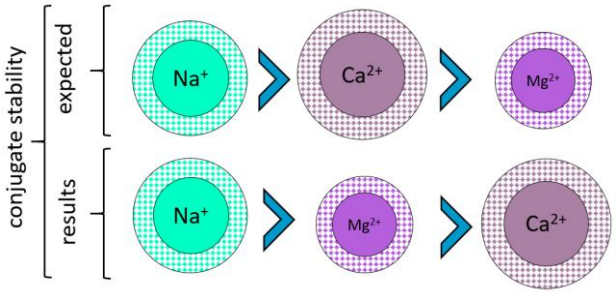

Figure 17*:* Conjugate stability; expectations vs. results.

Here, it was expected that monovalent cations would cause the least reduction of the resulting conjugate stability due to the Schulze-Hardy rule. The results support that suggestion. However, despite their higher charge density, Mg^{2+} cations lead to more stable conjugates than Ca^{2+} cations, shown in detail in **Figure 18**, where a PPI of at least 10 is considered moderately stable. Even with the bare eye, samples´ noticeable color shifts can be observed for all tested salts. However, samples treated with calcium chloride turned purple and precipitated within hours, making them unsuitable for further LFA applications. Thus, calcium chloride was excluded from further experiments.

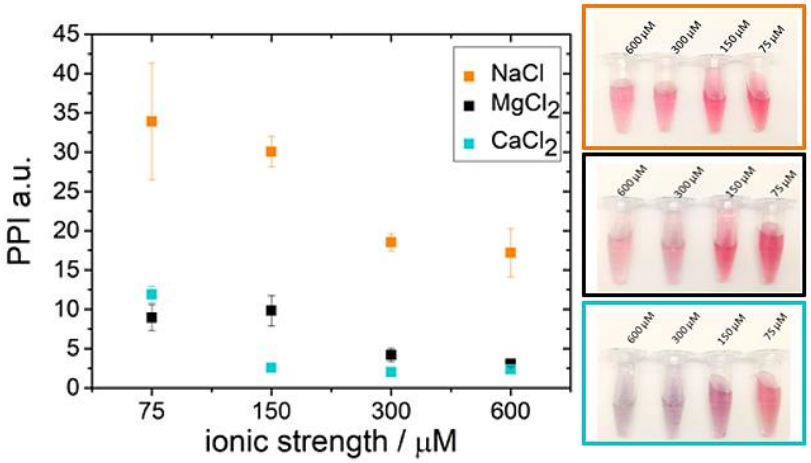

Figure 18: PPI at varying ionic strengths of NaCl, $MgCl_2$, and $CaCl_2$. Exemplary pictures of the conjugates are shown.

The introduction of additional inter-strand-interactions through Mg^{2+} may lead to an improved steric stabilization of the generated conjugates, which counteracts their higher charge screening ability. Future work could be conducted in this regard to find out what kind of aptamer-aptamer-interactions take place on the surface of a conjugate produced via $MgCl_2$ salt aging. Raman spectroscopy could represent a suitable tool to observe such inter-strand-interactions.

These findings represent the first time the utilized salt´s influence during aptamer-conjugation has been studied for laser-generated nanoparticles. The findings are interesting in that regard that predictions solely based on simplified electrostatic interactions are not suitable for the planning of a conjugation process but also require advanced knowledge in molecular biology and DNA-structures to allow for precise predictions in conjugate analysis and development. The experimental data strongly suggest that the aptamer structure, especially its functional subunits, must be considered to find the most suitable salt-aging technique for optimal surface coverage and stability. Another aptamer sequence may ultimately lead to different results if it features different substructures. Therefore, conjugation protocols cannot serve as general guidelines or even as a recipe for bioconjugation but must be adjusted and specifically designed for each aptamer test system to guarantee its ideal surface coverage for optimal function. Chapter 4.1.3 will go more into detail on the correlation of surface coverage and resulting function in form of target binding ability.

3.2.1 Conjugation via pH-aging

The generation of nano-bio-conjugates is a tedious and time-consuming process. The entire process, including pre-incubation, salt-aging, separation of conjugates and unbound DNA molecules, and finally, the redispersion, takes up to three days. It is no wonder that there have been approaches to reduce the incubation periods and the number of work steps required in the process chain from raw materials to the final nano-bio-conjugate. At the same time, securing the stability of the resulting conjugate and

its function remains a challenging task. In 2006, a conjugation protocol featuring fluorosurfactants (Zonyl FSN) was published by Zu and Gao, which allowed the generation of stable conjugates within 2 h. [240] Since fluorosurfactants are known to be cytotoxic, their application in the biomedical field is limited. However, it has not been elucidated if they would interfere negatively with the functionality of aptamer-LFA-systems. One milestone work on the matter of rapid conjugation, by Zhang et al. was published in 2012, where they could demonstrate that chemically synthesized nanoparticles could be readily functionalized within DNA within minutes. Furthermore, they could overcome the well-known difficulties of the conjugation of larger particles. [185] Shortly after that, the same working group also published a similar work about the successful functionalization of silver nanoparticles – an even more challenging task. [241] Later on, Zhang et al. expanded their publication portfolio to pH-assisted conjugation of larger Au NP. [242] In summary, their work concludes that the usage of excess DNA, like required for the typical salt aging procedures [175], can be avoided via the pH-assisted conjugation protocol. Thus, their work provides an alternative, resources saving conjugate synthesis route, which could push the field of nano-bio-conjugation more towards green chemistry. Since all works in this regard were performed on chemically-synthesized nanoparticles, it is interesting to examine the transferability of the described procedures to laser-generated nanoparticles with LFA relevant diameters. Since their surface is free of any organic ligands, like i.e., citrate, it has never been shown before how solely electrostatically stabilized nanoparticles behave at this condition. Yet, the complexity of a system consisting of LAL NP covered with aptamers has always to be considered.

The results of initial experiments of a pH assisted conjugation are shown in **Figure 19**. The negative control featured only DNA and Au NP without any addition of salts or pH changes – staying at neutral pH during the entire incubation time of the experiment. The samples conjugated via “pH-aging” underwent a 3 min pH change towards pH 3 with HCl before being neutralized again with OH. The conventional salt-aging samples were adjusted to pH 3 before the salt aging procedure and afterwards neutralized. As expected, the negative control showed only minimal conjugation efficiency. Due to the strong attraction of the thiol-linker towards the gold surface, an initial surface coverage occurs, but without additional charge screening, further DNA strands fail to adhere to the surface.

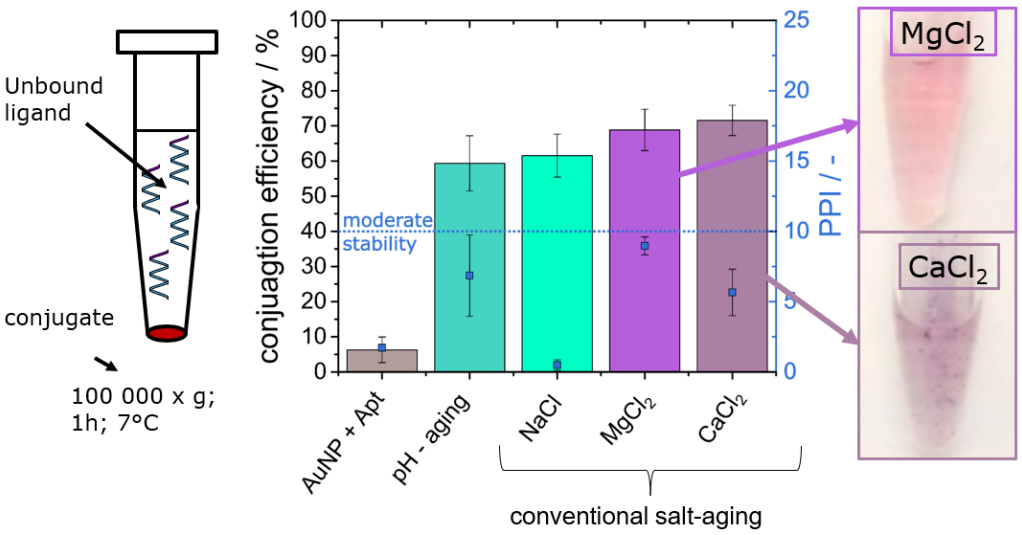

Figure 19: Salt-aging vs pH-aging. 20 nm Au NP were conjugated with OtA aptamer (0.1 µM).

The pH-aging attempt leads to remarkable high conjugation efficiencies, easily reaching up to 60 %, only exceeded when additional salts were utilized. These samples were further evaluated for colloidal stability via PPI. It is remarkable that once again, calcium chloride fails to produce moderately stable conjugates. However, sodium chloride aged conjugates also drastically lose stability and precipitate within hours after the conjugation procedure. Regarding the conjugate stability, all approaches failed to generate conjugates of moderate stability – only magnesium chloride aged conjugates feature in-comparison increased stability. Once again, this could be connected to the support of hairpin-hairpin interactions, which may provide steric hindrance on the particle surface, thus preventing the conjugates 'aggregation. One crucial aspect that must be considered when working with purely electrostatically stabilized nanoparticles is that the isoelectric point marks the least stable state of the particles, where attractive forces between particles overpower the electrostatic repulsion. The isoelectric point of laser-generated nanoparticles lies at a pH of 2.5 [182]. In this regard, the pH-assisted conjugation process may allow the increased absorption of DNA molecules in the first phase of conjugation [180,242], but since the particles are almost at isoelectric conditions, their initial stability is too drastically reduced to fully recover after the incubation. A more detailed experimental series was conducted, where the pH of different conjugate batches was adjusted respectively from 7 (neutral) to 3 (acidic). The results are shown in **Figure 20**. Two different gold concentrations were used to exclude colloid concentration linked stability effects since it was stated by Gamrad et al. that lower colloid concentration might prevent agglomeration and aggregation due to the increased ligand to NP ratio. [191]

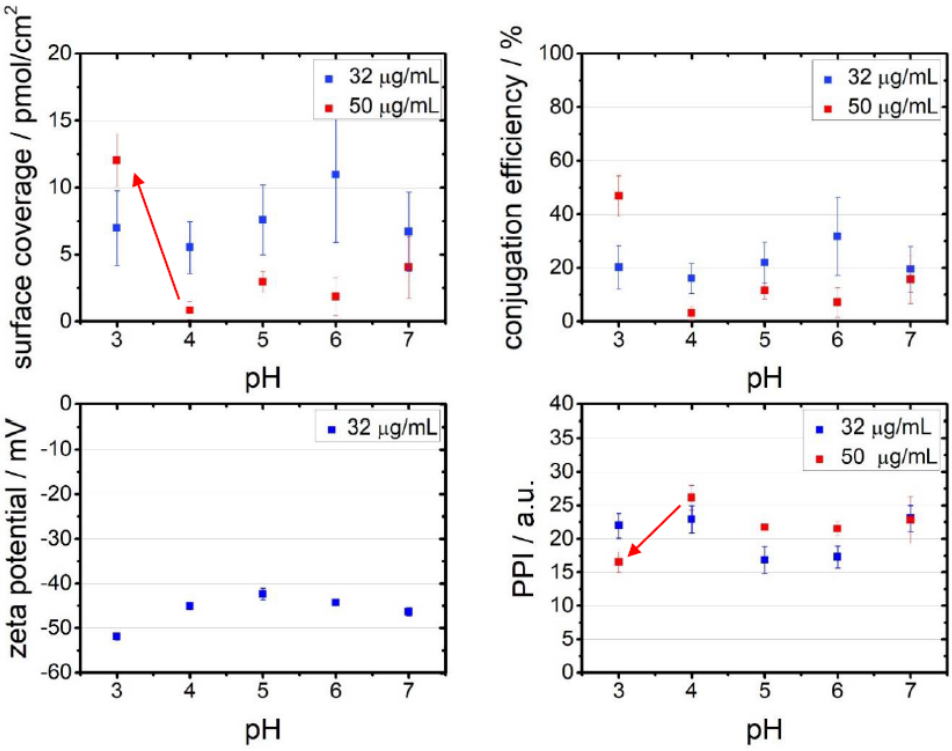

Figure 20: pH-aging of 20 nm Au NP with 0.1 µM OtA-aptamer. A) surface coverage; B) conjugation efficiency; C) zeta potential; D) PPI.

Only minimal conjugation efficiency was observed at pH 7 for both colloid concentrations. Over the entire tested pH range, no batches are exceeding 40 % conjugation efficiency, except for 50 µg/ml Au NP at pH 3. Expressed in surface coverage (A), one notices a drastic increase in the number of bound ligands only at that acidic pH of 3 and low colloid concentration. The parallel conjugation batches featuring lower colloid concentration do not show any significant trend yet depict higher conjugation efficiencies, which seems counter-intuitive since effectively less surface is available for Au-thiol-bonding. The higher ligand to nanoparticle ratio seems to counteract the observed pH effect since the particles in lower concentrated colloids feature in general a higher ligand/NP surface ratio, which should drastically increase the demand for positive charge carriers as a charge screening agent. However, these observations raise exciting questions. If higher ligand to nanoparticle ratios counteract the pH-assisted conjugation procedure, what is mainly affected by the pH reduction: ligands or nanoparticle surface? The initial adsorption of thiolated ligands is always controlled by the thermodynamically favorable gold-thiol-binding [172,180]. Any conjugation above that must be supported by charge screening. Charge screening can occur between the negatively charged NP surface and the DNA, as well in between the added DNA strands, respectively their negatively charged phosphate backbones. At pH 3, the Au NP are close to their isoelectric point. Hence, there is almost no negative surface charge left to prevent the approximation of unbound aptamer molecules towards the NP surface. At the same time, due to the pH´s logarithmic character, there are 10 times more H^+ -

cations available for an effective charge screening. Nevertheless, we only see a significant increase in conjugation efficiency for the higher concentrated Au NP colloid, featuring statistically fewer DNA strands per particle on average and at the same time more surface. If the NP´s negative surface charge was the main obstacle preventing an increased surface coverage, both colloid concentrations should provide the same drastic increase in conjugation efficiency at pH 3. However, the lower concentrated colloid´s conjugation efficiency remains only at half the level than its higher concentrated counterpart. Thus, surface charge screening can be excluded as a phenomenon. Instead, the H^+ cations seem to influence the DNA strands primarily. It is known that the phosphate group of the phosphate backbone possesses a pK_a of 12.32. The DNA bases have different pK_a values, ranging from 3.33 (G), 4.15 (A), 4.45 (C), to 9.7 (T). In this regard, phosphate represents the weakest acid. In the presence of a strong acid like HCl (pK_a = -6.2), phosphate will most likely be protonated – its charge vanishes, higher conjugation efficiencies can be achieved.

Once again, these simple observations are hard to explain by purely chemical considerations. It could be possible that once again, the three-dimensional aptamer conformation has a massive impact on conjugation behavior. The sole protonation of the phosphate backbone might even lead to strand breaking [185]. Thus, rendering the aptamer useless. Despite that, it is still noticeable that the conjugation efficiency jump was only observed for high Au NP concentration. This interesting phenomenon leads to an interesting follow-up question, which should be addressed by future work to elucidate the influence of the pH on the conjugation process. However, since the provided aptamers in this project were a strictly limited resource, no sufficiently stable conjugates were produced via pH-aging, and the risk of altering, breaking, or destroying the aptamer was too high. No further experiments in this regard were conducted. However, it remains an interesting topic for future work.

3.2.2 Peptide-Aging – Higher surface coverages without increased salinity

Until now, nano-bio-conjugates featuring laser-generated gold nanoparticles have undergone the same conjugate synthesis route, as has been described in the literature for chemically-synthesized particles. So far, only the slow salt-aging at moderate salinity generated sufficiently stable conjugates to allow for further proceeding towards application in LFA test systems. In this regard, the conducted experiments lead to the conclusion that high charge density, like provided by H^+ or Mg^{2+}, of the charge screening agent leads to a faster conjugation procedure with high surface coverage, respectively high conjugation efficiency. However, the DNA ligands fail to provide enough steric hindrance to allow the generated conjugates´ stability on their own. This leads to the question, what happens if one utilizes a highly charged yet bigger charge screening agent. In this regard, the CWR_5 – peptide was utilized to bioconjugate pure gold nanoparticles with the OtA aptamer. Peptide and aptamer were mixed, co-incubated for 24 h, and subsequently added to the colloid. No additional salt-aging steps were performed. **Figure 21** provides a comparison of conventional salt-aging (A) and peptide-aging (B).

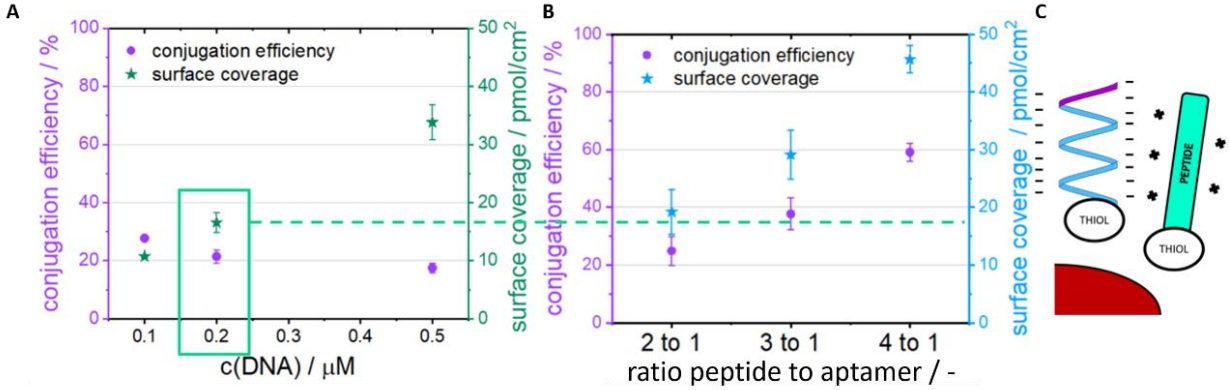

Figure 21: Salt-aging vs. peptide-aging featuring 30 nm Au NP, CWR_5-peptide mixed with OtA aptamer (0.2 µM). A) salt-aging; B) peptide-aging; C) schematic overview. The dashed line indicates the achieved level of surface coverage for a standard salt-aging conjugation procedure featuring 0.2 µM DNA

With increasing DNA concentration during salt-aging conjugation, an increasing resulting surface coverage can be observed, whereas the conjugation efficiency drops. This observation follows the trends observed by Petersen et al. for the conjugation of laser-generated particles with single-stranded DNA molecules. [24,25] However, if a constant DNA concentration of 0.2 µM is combined with varying amounts of the peptide, the conjugation efficiency can be drastically increased. A 2:1 – ratio of peptide to aptamer increases the conjugation efficiency only slightly, yet at a 3:1 ratio, it already exceeds the conventional salt-aging method concerning conjugation efficiency, surface coverage, as well as reduced the workload for the experimenter. The ratio of 4:1 even exceeds the results gained by salt-aging at high excess DNA (0.5 µM). The conjugation efficiency easily reaches up to 60 %, which has not been achieved for particles of 30 nm in diameter with either salt-aging or pH-aging.

Nevertheless, this method too comes with a drawback. Once again, the generated conjugates do not provide sufficient stability despite an excellent surface coverage (see **Figure 22**). In this regard, the shorter complementary oligonucleotide was tested to see how the shorter strand length would react to the peptide aging. In this regard, the complementary oligonucleotide differs significantly from the aptamer since it has no distinct three-dimensional structure, which is required for target binding but instead features a random sequence-based structure.

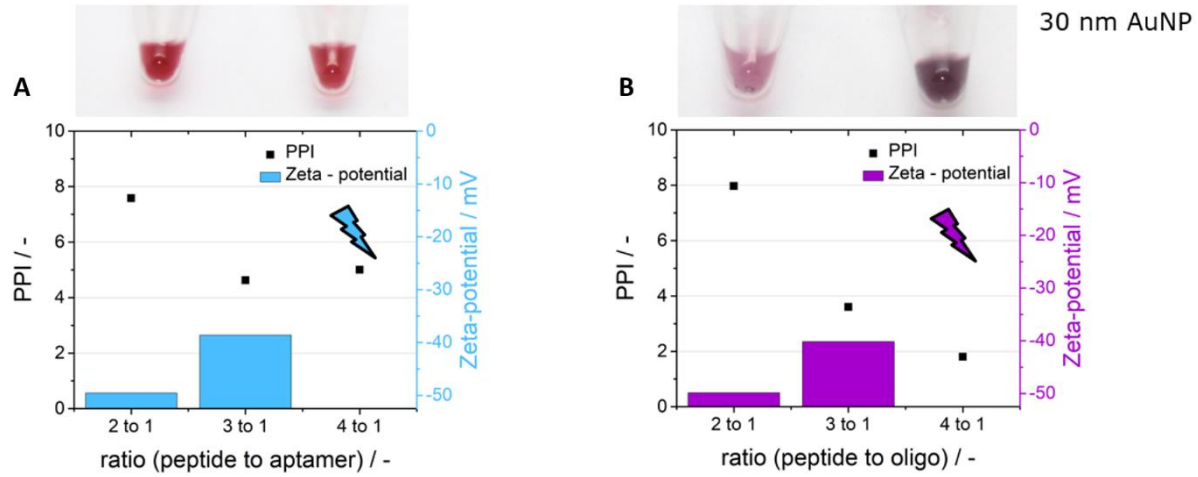

Figure 22: Peptide aging of 30 nm Au NP. A) featuring the OtA aptamer; B) featuring the complementary oligonucleotide.

The PPI of all tested conjugates did not exceed a value of 8 (10 = moderate stability). However, the peptide´s presence may directly hinder the already limited validity of this stability indicator for pure colloids due to its extinction maximum of around 280 nm. Due to that, the zeta-potential was involved in the analysis as well. Typical conjugates after salt-aging feature a zeta-potential of – 40 mV to – 50 mV, depending on the number of bound ligands, in accordance with the work of Gamrad et al. [191] Here, the zeta-potential drastically changes with an increased peptide to DNA ratio for both the aptamer, as well as the oligonucleotide. This effect has been expected in accordance with the existing literature. However, a zeta potential of - 40 is still considered stable, but the respective samples precipitated within hours. Samples featuring the highest peptide to DNA ratio did already precipitate during the measurement, making it impossible to determine their zeta-potential. Once again, DNA conformation should be considered as well. Samples precipitating despite a strongly negative zeta-potential imply that the cationic peptide may have led to bridging events between DNA-strands of different nanoparticles, leading to a reduced interparticle distance and resulting in the final precipitation of the aggregates. A similar phenomenon was actually exploited for the generation of nanoparticle-peptide-agglomerates, utilized for drug-delivery into a living cell, by Krawinkel et al. [187]. It was expected that the 61 base long aptamers, respectively the 37 base long oligonucleotides, would provide sufficient negative charge to counteract such peptide-assisted bridging events.

However, both systems failed to provide sufficient stability. Future experiments could be conducted to elucidate if such an inter-conjugate-agglomeration can be detected via ADC or ultracentrifugation. Since the peptide-aged conjugates´ stability was below the required stability for LFA applications, this remains out of the scope of this work. Furthermore, future work could answer the question if the peptide interferes with the aptamer´s target binding substructure, respectively rendering it useless. In-silico simulations may be the key to find a suitable peptide for the respective aptamer of interest while the length of both biomolecules as well as their 3D orientation would need to be considered. The elimination of manual working steps during the peptide-aging, and the conjugation efficiency of the process, are a welcome advantage but ultimately obsolete if the conjugates lack stability and function.

3.2.3 Varying the surface composition of nanoparticles

Influence of Gold/Silver Ratio in Ablative Nanoparticles on Their Interaction with Aptamers and Functionality of the Obtained Conjugates

Frederic Stein*, Andreas Schielke*, Stephan Barcikowski, Christoph Rehbock

Technical Chemistry I, University of Duisburg-Essen and Center for Nanointegration Duisburg-Essen (CENIDE), Universitätsstr. 7, 45141 Essen, Germany

*both authors contributed equally

Keywords: laser-generated particles, alloy particles, nano-bio-conjugates, aptamers, LAL, AgAu

Reprinted (adapted) with permission from Stein, Schielke, Barcikowski, Rehbock; *Bioconjugate Chem.* 2021, 32, 11, 2439–2446 (DOI: 10.1021/acs.bioconjchem.1c00468); Copyright {2021} American Chemical Society [243]

Abstract

Nano-bio-conjugates, featuring noble metal gold-silver alloy nanoparticles, represent a versatile tool in diagnostics and therapeutics due to their plasmonic and antimicrobial properties tunable by the particle's gold molar fraction. However, little is known about how the binding of thiolated biomolecules to noble metal nanoparticles is influenced by the fraction of gold and silver atoms on the nanoparticle's surface and to which extend this would affect the functionality of the conjugated biomolecules. In this work, we generated gold-silver alloy nanoparticles with average diameters of 7-8 nm using the modern, surfactant-free laser ablation in liquids (LAL) synthesis approach. We conjugated them with thiolated miniStrep aptamer ligands at well-controlled aptamer-to-nanoparticle surface area ratios with maxima between 12 -27 pmol aptamer/cm^2 particle surface area. The results revealed a clear correlation between surface coverage and the nanoparticles' nominal gold/silver ratio, with maximum coverage reached for gold-rich alloys and a pronounced maximum for silver-rich alloys. However, the conjugates' functionality, evaluated by binding of streptavidin, was surprisingly robust and hardly affected by the nominal composition. However, 1.5 times higher surface coverage was needed to obtain maximum functionality in the silver-rich conjugates. Based on these results, it may be concluded that the nominal composition of gold-silver alloy nano-bio-conjugates is freely tunable without a pronounced impact on the attached ligands' functionality, a finding highly relevant for the flexible design of nano-bio-conjugates for future biomedical applications. This study's results may facilitate the design of alloy nano-bio-conjugates for future applications in therapeutics and diagnostics.

Introduction

The synthesis and application of nano-bio-conjugates based on noble metals, especially gold, have been intensively studied in the past [28,244]. A nano-bio-conjugate combines a nanoparticle 'core' with a defined organic ligand shell, usually composed of functional biomolecules. In particular, conjugates featuring synthetic oligonucleotides have been frequently studied and are used for multiple applications, above all diagnostic and therapeutic purposes [245,246]. In this field, aptamers have been established as specifically designed oligonucleotides, prone to bind specific targets [247,248]. In contrast to conventional antibody systems, aptamers can be more easily modified, are available for non-immunogenic and highly toxic compounds, and provide low batch to batch variations [249,250].

When it comes to the nanoparticles used as cores for a nano-bio-conjugate, various aspects must be considered for choosing the most suitable ones. Firstly, different noble metal nanoparticles provide different optical properties. The intense red color and remarkable surface-plasmon-resonance (SPR) peak of the biocompatible gold nanoparticles (Au NP) and gold nanorods makes them ideal candidates for diagnostic [251,252] and therapeutic approaches like lateral flow assays [253], cancer therapy [254], and thermo-optical therapy [255]. Simultaneously, silver nanoparticles (Ag NP) are known for their antimicrobial and plasmonic properties, the latter being even stronger than those of gold. However, Ag NP show lower long-time chemical stability compared to Au NP [256]. Furthermore, Ag NP tend to release toxic silver ions, effectively killing host cells as well as bacteria [257,258]. Monometallic nanoparticles and alloys of those elements have been used in nano-bio-conjugates for many applications, e.g., heavy metal ion detection [259,260] or sensing of cells [261,262]. The idea behind the utilization of alloys is to combine the desired properties of two elements, designing multi-functional chimera nanoparticles. Gold-Silver-alloy nanoparticles are particularly interesting in this context as their optical [263], antimicrobial [264], and cytotoxic [265] properties can be tuned with the nominal gold molar fraction [266].

In addition to that, thiol linkers, which are widely used to bind functional molecules to noble metal particles, exhibit high affinities towards both gold and silver surfaces [163,165]. Exact values for the binding affinities and energies differ significantly in the literature but are generally speaking in the same range for gold and silver, with slightly higher values for gold [166–168,267]. Nonetheless, even minor differences in affinities may influence the binding of thiolated biomolecules on gold-silver alloy surfaces. This could affect the resulting surface coverage of the nano-bio-conjugates and their target binding ability since a variation in surface coverage may also lead to changes in the functionality, in this case, the functional binding of the respective target. The reason for this originates from the innate structure of an aptamer-sequence. An aptamer molecule will only target its respective target if it is folded in the desired way [268] and targeting sequences are sterically available to the target molecule.

This is a function of the surface coverage. If the surface coverage is too high, the negatively charged phosphate backbones of the DNA will repel each other and thus unfold and stretch the sequence, which will inhibit target binding. On the other hand, at low surface coverage, the aptamers will assume a lying-down confirmation with strong interaction between the nucleic bases and the gold surface, affecting the aptamer conformation and impair binding [177,269]. Based on this, we can assume that optimal binding occurs at an intermediate surface coverage.

A thiol-group alone is not sufficient to guarantee adequate surface coverage of the nanoparticles since the negative charges of the DNA phosphate-backbones will repel each other – limiting the maximal surface coverage [270]. This problem has to be overcome by a charge screening procedure known as salt aging [175]. By increasing the cation or even the H^+ concentration, the negative charge of the phosphate backbone of the DNA can be efficiently screened [242]. The positive charge carriers will then accumulate between the DNA strands as 'cation clouds' [183] so that the biomolecules will stretch away from the surface and allow the formation of sub-monolayers.

Although gold and silver form an ideal solid solution in bulk, AgAu nanoparticles' synthesis by different preparation routes can produce profoundly different alloy nanoparticles. These typical synthesis routes include flame-spray pyrolysis [271], chemical vapor deposition [272], biological reduction [273], and the chemical reduction method of the most commonly used precursors $HAuCl_4$ and $AgNO_3$ [274]. All synthesis routes based on the co-reduction of precursors suffer from several disadvantages, primarily the differences between reduction potentials of gold and silver, which leads to a faster reduction of the more noble gold before the silver leading to the formation of nanoparticles with a gold-rich core and silver-rich shell. [275,276]. Another disadvantage is that stabilizing ligands or capping agents must be used in chemical synthesis to ensure constant particle sizes, blocking the active particle surface and obstruct the aptamer's conjugation to the nanoparticle. To overcome the disadvantages of traditional nanoparticle synthesis routes, laser ablation in liquids (LAL) is used in this study to produce the AgAu alloy nanoparticles of varying molar fractions [277]. This method commonly results in ultra-pure, spherical nanoparticles. Previous works produced AgAu alloy nanoparticles by LAL and achieved an ideal solid solution FCC crystal structure with homogeneous elemental distribution on a single particle level with reproducible particle sizes [277,278]. Hence, alloys of both metals can be synthesized in every ratio due to their complete miscibility. Note that LAL has been shown to be a well scalable, continuous colloid synthesis method [279], yielding ~8 g/h nanoparticles at optimized focusing and beam guidance [280].

One problem of LAL in the past was that the ablated nanoparticles showed significant heterogeneities when certain materials and pure water were used. However, in recent years, there has been a

significant process in the size control of laser fabricated nanoparticles, especially of noble metals[281]. Ion and pH-induced size quenching [161,182,282] and centrifugal purification [283] allows to obtain monomodal and monodisperse nanoparticle colloids.

Multiple studies on nanoparticles synthesized by LAL also showed that the resulting particle size can be controlled well in the low nanometer scale and is very reproducible [17,282].

In its purest form, LAL consists of a pulsed laser beam focused on a target immersed in a liquid that leads to a heating of both target and liquid and photoionization of the target surface. A plasma plume forms [17], and initial nanoparticles are already expected to form a few nanoseconds after the laser pulse hits the target. This plume subsequently expands to a cavitation bubble in whose vapor the nanoparticles form [284]. Nanoparticles are released after the collapse of the oscillating cavitation bubble [146]. LAL has been shown to produce ligand-free, solid-solution alloy nanoparticles of the same composition as the target [281], at least when fully miscible elements like Ag and Au are used, as well as nanosecond pulses that reheat and homogenize the ablation plume [285].

So far, many works focus on pure gold nanoparticle conjugates [30,186,226,286,287]. However, AgAu alloy nanoparticles are rarely used in conjugates, and their conjugation behavior has, to date, not been studied systematically. Hence, vital information correlating core composition and final functionality are still missing. As alloy compositions for our study, we chose a very gold-rich composition (Ag_1Au_9), a primarily silver-rich composition (Ag_7Au_3) with high expected antibacterial properties [264], and a very silver-rich composition (Ag_9Au_1) as the other extreme. Pure silver was not tested because of its high instability and lacking reproducibility when produced via LAL without stabilizing ligands. [288]

As the conjugation process is primarily surface-driven, we used surface-area-normalized colloids for our study. [184]. This approach deviates from commonly applied mass-based dosing but is vital for comparing particles with varying density and slightly deviating size distributions. For example, Ag_9Ag_1 NPs, in contrast to Au NP controls, would have a 1.7 times higher surface area when used at equal mass. This would introduce unnecessary systematic errors into the experimental design, which we avoided by using surface-normalized concentrations.

As a model oligonucleotide ligand, we used the miniStrep aptamer, as described by Walter and colleagues, since it was specially designed to bind streptavidin [30]. The miniStrep aptamer readily binds to one of streptavidin's four biotin-binding sites but can be readily displaced by streptavidin's preferred target biotin as the streptavidin-biotin bond is one of the most robust key-and-lock bindings between biomolecules [289]. Thus, the miniStrep – Streptavidin system constitutes a sound model system for the read-out of conjugate functionality. The functionality of this test system after in situ

conjugation was demonstrated in a previous work [30]. However, the addition of ligands during the ablation process ultimately alters the resulting particle diameter and, therefore, the resulting curvature. Curvature plays a crucial role in the loading of nanoparticles[184], if one wants to maximize the functionality of conjugates. The tested particles should feature comparable diameters, which can be assured by utilizing the ex-situ conjugation procedure, as described in previous works[175]. Furthermore, pronounced photo-induced conjugate degradation found during in-situ conjugation can be avoided using ex-situ two-step conjugation [290]. This method also allows superior control of the surface coverage, utilization of lower aptamer concentrations, and better transferability to other research conducted with chemically-generated nanoparticles.

Results and Discussion

Since gold represents the standard particle for diagnostical applications [46,291], and the conjugation of pure gold nanoparticle (Au NP) synthesized via LAL has been the subject of various studies [26,28,186,292], it was chosen as the reference system. The three other alloy samples featured a high silver molar fraction (Ag_9Au_1), a moderate silver molar fraction (Ag_7Au_3), and a low silver molar fraction (Ag_3Au_7). Their molar fraction was previously analyzed via TEM/EDX on a single particle level [277].

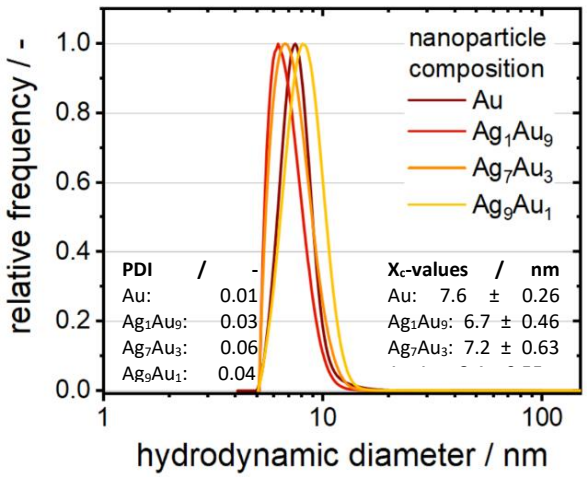

Figure 23: Mass-weighted size distribution of LAL-prepared Au and AgAu alloy NP after centrifugation measured by ADC. PDI is the polydispersity index of the distributions and x_c values are mean values derived from a log-normal fitting of the distributions.

Since LAL represents an ideal way to produce nanoparticles free of organic ligands on their surface [17], we can exclude any influence of surfactants on the conjugation process and the resulting conjugates' functionality. All samples were adjusted to a total applied surface-concentration of 7.4 cm^2/ml after determining the hydrodynamic particle size distribution via analytical disc centrifuge and concentration determination by UV-Vis (see **Figure 23**). The laser-generated colloids with four different gold molar fractions had a similar size distribution of 7-8 nm mean diameter and a PDI between 0.01 to 0.06,

indicating monodispersity (see **Figure 24**). TEM measurements showed that the particles are spherical (see **Figure S 3**).In addition to that, it has already been shown multiple times that nanoparticles from LAL are predominantly spherical and show a homogenous elemental distribution of Ag and Au in the bulk[277] and on the surface near volume [293], verified via extensive TEM, XAF, and XPS measurements.

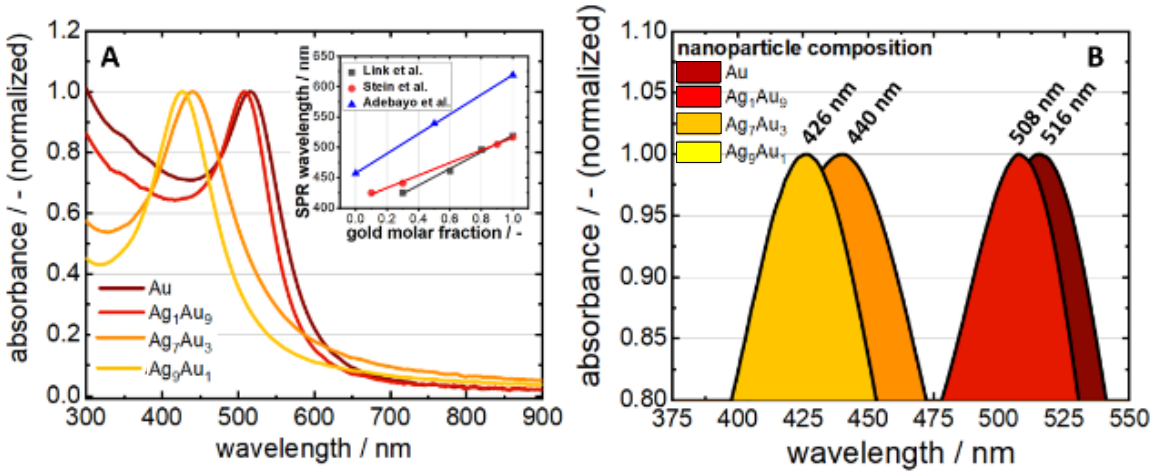

Figure 24: A UV/Vis extinction spectra of prepared LAL-NP of different gold molar fraction; the insert shows the SPR peak positions of this work (red) and those previously described for chemically synthesized particles by Link et al. (dark grey) [21] and biological synthesized particles by Adebayo et al. (blue) [71] **B** Zoom onto the SPR-peak positions of the shown nanoparticle compositions.

Besides minimal differences in the size distributions, the particles feature very different optical properties, as seen via UV-Vis spectroscopy (see **Figure 24**). The surface plasmon resonance (SPR) peak is located at 426 nm for Ag_9Au_1 at 440 nm (Ag_7Au_3), at 508 nm (Ag_1Au_9), and at 516 nm for pure Au NP. An increasing gold molar fraction should generally lead to an almost linear red-shift of the SPR-peak [263]. The insert in Figure 1 shows the SPR peak positions from AgAu NP synthesized by LAL in this work compared to chemical and 'biological' reduction values taken from literature [263,294]. One can directly see that the positions of the SPR peaks are highly dependent on the synthesis method. A significant contribution to these optical responses can be attributed to the state of the nanoparticle surfaces. Nanoparticles produced by chemical or biological reduction need to be stabilized with ligands, altering the particle's vicinity refractive index compared to a bare surface [166,167].

Additionally, the medium surrounding the nanoparticles, their size, shape, and even interparticle distance shift their optical properties [168]. As seen by Abedayo et al. [294], the red-shift of the lines is consistent with the presence of surface ligands, resulting in an increased refractive index and a red-shift of the SPR. The missing red-shift of the particles synthesized by Link et al. can be dedicated to multiple reasons. Link et al. used much smaller ligands and concentrations during nanoparticle production compared to Abedayo et al. Furthermore, the particle sizes and shapes are closer to those used in this study. These factors have a significant impact on the position of the SPR. Nevertheless, the

linear red-shift of the SPR-peak in dependence of the GMF can be observed in our samples, which is in good agreement with previous studies [263,294].

All colloids were subsequently conjugated with varying amounts of miniStrep-Aptamer. Due to the same applied nanoparticle size and surface, curvature effects can be excluded [287]. The resulting surface coverage (see **Figure 25**) is solely based on the affinity of the thiol-group of the miniStrep-Aptamer towards the exposed, ligand-free nanoparticle surface. It is known that gold surfaces strongly attract the thiol group, but similar reactions, even though with a lower affinity, were also reported for silver surfaces [165,295]. However, the underlying nature of the gold/silver-sulfur bond remains unenlightened [169]. Kankate et al. found evidence for an adsorption mechanism, including the release of atomic hydrogen [172]. Pakari et al. showed that the binding energy between gold and thiol groups is lowered by alloying it with silver, whereas those between silver and thiol groups will be increased. They also concluded that the attractive forces between thiol-groups and silver are increased when silver atoms are substituted with gold atoms [267]. Note that biomolecules that adsorb to nanoparticle surfaces tend to follow a Freundlich isotherm [296]. The reference Au NP system shows a typical shallow saturation of its surface coverage with an increasing concentration of applied DNA [292]. The samples featuring a low and moderate silver molecular fraction follow almost the Au NP reference system trend, whereas the silver-rich sample reaches its maximum surface coverage of 20 pmol/cm^2 already at 0.2 µM applied DNA surpassing all three other samples. However, when more DNA is introduced, the achieved surface coverage is slightly reduced. This may be linked to a leaching effect of the utilized disulfide bridge of the miniStrep aptamer since it is known that thiosulfates can leach metallic silver [297]. The redox potential of silver nanoparticles is a function of the diameter, which reaches values of -0.1 V when the diameter is below 10 nm compared to the bulk values [298]. To that it is highly probable that thiols and disulfides can oxidize these species [299]. Thus, applied thiolated DNA may bind to ionic silver instead of silver-rich alloy nanoparticles, forming dissolved silver complex compounds leading to the observed reduced surface coverage. Accordingly, all samples except Ag_9Au_1 exhibit Freundlich adsorption behavior. However, the leaching of ions may also affect the composition of the particle surface. For the laser-fabricated nanoparticles, we have done extensive examinations on the surface composition of our particles and indeed discovered that surface and bulk composition deviate [293]. Furthermore, we recently observed the extent to which gold-silver nanoparticles leach and are restructured upon dissolution [80], but to what extent ligands influence this phenomenon is subject to ongoing studies in our group.

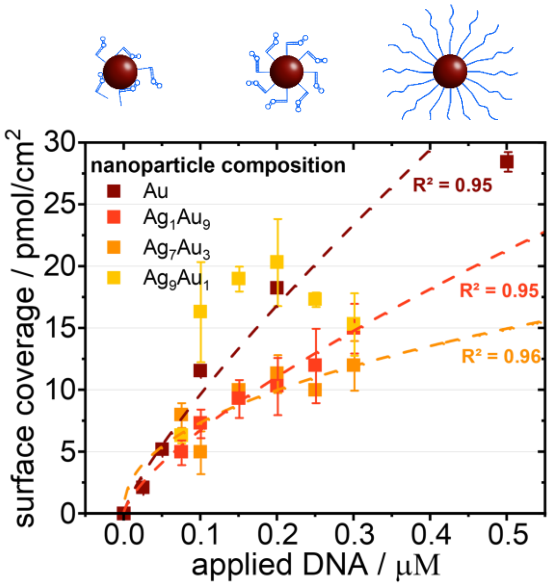

Figure 25: Reached surface coverage of the tested AgAu compositions compared with the pure Au NP depending on the used DNA concentration during the conjugation process. Dashed lines represent a Freundlich-Fit, which was not suitable for Ag9Au1

In the next step, the prepared conjugates were tested for their functionality, evaluated by their ability to bind streptavidin (see **Figure S 7**). It is expected that the conjugates' maximum functionality is linked to their surface coverage; however, there has to be a surface coverage of maximal functionality. Too many aptamer ligands on the surface would introduce steric hindrance for further target binding due to impaired functional folding of the aptamer [17]. In this context, it should be noted that the measured trends in Figure S 7 suffer from a limited tested range and high error bars, so that an actual maximum was only observable for the Au control. For the other compositions, we solely determined the point of maximum functionality for comparison, even though the trend was not clear. The reference Au system reaches its highest functionality at a surface coverage of around 6.2 ± 0.2 pmol/cm^2, Ag_1Au_9 at 8.8 ± 1.1 pmol/cm^2, and Ag_7Au_3 at 9 ± 1.7 pmol/cm^2. Concerning the large error bars, we could find no significant differences between these samples. These three AgAu alloy samples exhibit a robust functionality affected by the surface composition in a minimal matter. Only at a high silver molar-fraction of 90 % (Ag_9Au_1) an effect of the surface composition can be seen. Here, the highest functionality is achieved at a surface coverage of 17.3 ± 2.7 pmol/cm^2, exceeding the ideal surface coverages of the other AgAu alloy samples by up to 70 %.

Before the reasons for the different observed functionalities will be discussed, only the highest average functionality of all systems will be compared in more detail (see **Figure 26**). The average functionalities of the different alloy nanoconjugates and the gold reference nanoconjugate only differ slightly between 60 pmol/cm^2 and 70 pmol/cm^2 of bound streptavidin. These values refer to a surface coverage ratio of about 4-8 streptavidin molecules per aptamer, which indicates multilayer binding.

Remarkably, the ideal surface coverage of the silver-rich alloy-aptamer-conjugate exceeds the ideal surface coverage of the other samples by a factor of ~1.5. Thus, the ideal surface coverage strongly depends on the surface's molecular fraction, while the total maximum functionality of all tested systems stays almost constant. Therefore, conjugates featuring alloy particles show a very robust functionality, but finding the ideal surface coverage for varying elemental compositions must be considered.

There are many possible reasons for the observed reduced streptavidin binding efficiency of the silver-rich alloy-aptamer-conjugate. The interaction of noble metals and their respective ions and DNA occurs mainly between bases and metal, not phosphate backbone and metal [269]. The miniStrep aptamer features 20 thymine bases – ten of them aligned to form a poly-T-spacer. Thymine exhibits a strong affinity for noble gold surfaces but almost none towards silver surfaces [177,300]. This affinity may lead to a flattening of the aptamer onto the gold or gold-rich nanoparticle surface, which hinders further adsorption of thiol-linked aptamers, as was previously described for single-stranded DNA

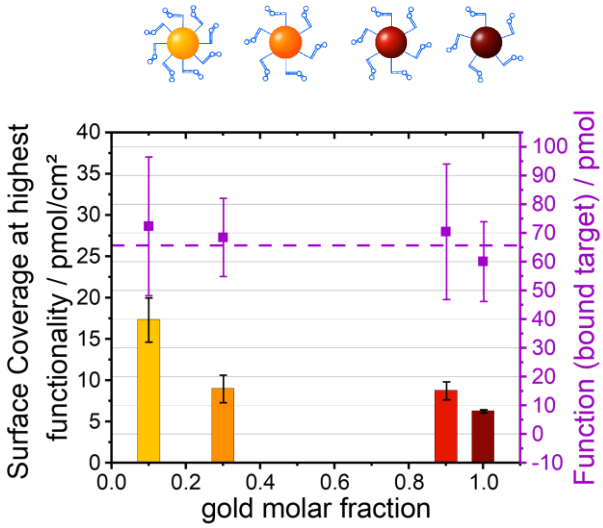

Figure 26: Reached average maximal functionality (bound streptavidin) of the different gold molar fractions compared to the respective aptamer surface coverage, featuring the maximal functionality. Dashed line provides guidance to the eye.

molecule adsorption onto laser ablated Au NP [28]. A higher biomolecule concentration would be required to switch the nano-bioconjugate from side-on to end-on binding, as we have already shown for laser-generated Au conjugates [292].

On the other hand, thymine shows almost no affinity towards silver; the aptamer will more likely bind with just the thiol group. Therefore, this leads to either a lower surface coverage or non-functional side-on-binding of aptamer molecules to gold-rich and pure-gold particles compared to silver-rich ones. One would expect that lower surface coverage comes hand in hand with lower functionality.

However, it is the most silver-rich alloy conjugate exhibiting the lowest function to surface coverage ratio.

Furthermore, it was shown via small-angle X-ray scattering that the average cation concentration in the DNA shell of a conjugate is drastically increased compared to the bulk solution concentration [183], leading to the assumption that released silver ions will be primarily found in the DNA shell of the conjugates. Those silver cations could then induce the hairpin-formation of the aptamer [301]. Since the miniStrep aptamer's function is based on a stem-dumbbell structure [94], additional hairpin structures may affect and reduce the functionality of bound aptamers on the alloy nanoparticle surface. This could explain the higher surface coverages needed for silver-rich conjugates to achieve the same functionality as gold-rich conjugates, especially for Ag_9Au_1. However, it should be noted that thiolated ligands are known to etch noble metal nanoparticles surfaces, and hence cross effects from alterations in surface composition upon bioconjugation cannot be entirely excluded.

Conclusion

In summary, one can say that all tested surface-normalized conjugates, featuring laser-generated NP of varying gold molar fraction, exhibited good streptavidin binding functionality. The maximal achievable functionality of all tested alloy- and the pure Au NP conjugates reached a comparable level of 65-70 % of bound streptavidin. Therefore, the functionality of the conjugates is independent of the gold molar fraction, making this alloy series test system highly robust. Hence, adding silver to a gold nanoparticle gives access to additional functionality (plasmonics, antimicrobial activity), and, on the other hand, the binding functionality suffers no adverse effect on the ligands. This is a surprising finding, particularly as the binding affinity between gold and silver and thiolated ligands is different.

Nonetheless, there were element-correlated differences in the conjugation process. The above-mentioned highest binding efficiency was reached at significantly different surface coverage, with maximum efficiency for pure gold and a higher requirement of bound ligand per measured aptamer functionality for silver-rich alloys. This could be explained by possible leaching of the silver surface via the thiolated biomolecules, which leads to a higher fraction of unbound ligands. Thus, it has to be considered that the elemental composition of the nanoparticle might limit the maximum achievable surface coverage. Furthermore, silver cations can introduce hairpin formation within the aptamer, which may affect its functionality. When designing conjugates for biomedical applications, such high silver-content AgAu alloy conjugates should be avoided as additional ligand utilization per particle could be an important economic factor, particularly when highly specialized and expensive custom-made aptamers are needed. For future works, the addition of a poly-thymine spacer between the nanoparticle binding thiol-group and the folding sequence will help to facilitate the formation of a

functional conjugate as thymine holds the lowest affinity of all four nucleobases. Furthermore, using fluorophore labels in the aptamer sequence could allow a more sensitive surface coverage read-out compared to the pure UV/Vis measurement done in this study by using well-established fluorescence assay [302]. This approach would also allow the utilization of replacement assays with biotin.

Experimental

Particle Synthesis

Gold and gold-silver alloy nanoparticles were synthesized via LAL of respective pure gold and gold-silver metal sheets (Au, $Ag_{10}Au_{90}$, $Ag_{70}Au_{30}$, and $Ag_{90}Au_{10}$), all with 0.5 mm thickness, 99.99 % purity (Institute for noble metal and metal chemistry, Schwäbisch–Gmünd, Germany) in a self-constructed PTFE batch-chamber with a total volume of 30 ml. The process was conducted using a highly dilute electrolyte in Milli-Q water (0.1 mM NaCl) for electrostatic stabilization and size quenching [161,182,282]. The chamber was continuously stirred to remove the created nanoparticles from the ablation site to reduce shielding effects and minimize reirradiation. All particles were synthesized using an ns pulsed laser (Nd-YAG, Rofin Powerline E) with a wavelength of 1064 nm and a fluence of 23.5 J/cm². The laser pulses were focused onto the target in the batch-chamber with an f-theta lens (f = 100 mm) and scanned on the target via a galvanometric scanner system (Scanlab, SCANcube10) in a spiral pattern with a diameter of 6 mm. The ablation was carried out for 10 min for each composition. The pulsed laser ablation in liquids of gold and gold/silver alloy nanoparticles produces completely spherical nanoparticles. Silver/Gold alloy nanoparticles are known to form an ideal solid-solution structure [277].

To exclude size effects and separate large agglomerates or aggregates, all produced colloids were size-separated in a centrifugation step after synthesis. Only the particle fraction smaller than 10 nm was used for further experiments. Around 80 % of the total nanoparticle mass is typically larger than 10 nm and is either discarded or used for other projects if applicable. For this purpose, the colloids were filled in 8.9 ml OptiSeal tubes from Beckmann Coulter and spun at 30,000 g for 17 min at a temperature of 7 °C in an ultra-centrifuge (Optima MAX-XP, Beckman Coulter). Afterward, the supernatant, which contains the particle fraction smaller than 10 nm, was carefully transferred and used for all further experiments. Size separation by centrifugation is a well-established method to exclude certain particle sizes from the laser-generated colloidal nanoparticles [283]. The nanoparticles do not agglomerate because of their electrostatic stabilization due to the added electrolyte during the ablation process [282].

Conjugation

Each colloid was diluted to a surface area of 7.4 cm^2/ml in an aqueous solution, determined as specified in the supporting information. The colloids were consecutively mixed with a working aptamer solution of the miniStrep aptamer as used by Walter et al.[30] (TCT GTG AGA CGA CGC ACC GGT CGC AGG TTT TGT CTC ACA G -T10-(CH2)3-S-S-(CH2)6OH, see ***Figure S 6*** for folding and structure; working concentration 10 µM, the Biospring GmbH, Frankfurt, Germany). The solutions were then mixed thoroughly and incubated for 10 min on ice. The concentration of $MgCl_2$ was increased to 200 µM within three steps to perform the salt aging. Between each salt aging step, the samples were allowed to incubate for 10 min. Afterward, samples were incubated at 4 °C overnight. Excess unbound aptamers were removed via centrifugation (1180 g at 7 °C for 1 h), followed by one more centrifugation of the resuspended conjugate (1180 g at 7 °C for 1 h). The supernatant containing unbound DNA was further centrifuged via ultracentrifuge to guarantee the absence of any nanoconjugate (100,000 g at 7 °C for 1 h) and analyzed as specified below. Surface coverage and conjugation efficiency were calculated by quantifying the concentration of unbound ligands in the supernatant via UV-Vis extinction spectroscopy. A calibration curve correlating known concentrations of the aptamer with UV absorbance at 260 nm is depicted in **Figure S 4**.

Functionality Assay

The conjugates' streptavidin-binding ability was tested by mixing the two times centrifuged conjugates with 25 µg/ml streptavidin solution. The samples were incubated overnight at 4 °C and again centrifuged (100,000 g at 7 °C for 1 h). Thus, conjugates with bound streptavidin were separated from the supernatant containing the unbound streptavidin. The supernatant was then analyzed via UV-vis extinction spectroscopy to determine the amount of unbound streptavidin (see **Figure S 5**). No BSA-blocking solution was used since the conjugate was analyzed in its colloidal state and not surface-bound like e.g., in an ELISA assay. In addition to that, BSA might have interfered with the aptamers folding on the surface and thus, might have altered the optimal surface coverage if not prevent the successful target binding.

Characterization

For all colloids, mass concentrations were determined gravimetrically by weighting the ablated targets before and after particle synthesis using a microbalance (Precisa XT 220A) and by UV-Vis extinction spectroscopy after centrifugation. UV-Vis-spectra were recorded in a range from 190-900 nm in a quartz glass cuvette with 10 mm path length and a total volume of 1.5 ml using a Thermo Scientific Evolution 201 photometer. Calibration curves were used to correlate the absorbance at the surface plasmon resonance (SPR) peak (see **Figure S 1** for the non-normalized spectra) with known mass concentrations for each sample. The position of the SPR peak in UV-Vis extinction spectra depends on

the particle composition and follows a linear red-shift with increasing gold molar fraction. Hence, individual mass-extinction calibration curves were generated and applied for each particle composition (see **Figure S 2**). Furthermore, UV-vis-spectroscopy was also performed to calculate the DNA concentration in each conjugate supernatant by measuring the absorption at 260 nm for the DNA and at 280 nm for the protein, again based on a calibration for the used DNA/Protein-sequences (see Figure S 4). We checked each time if the supernatant was nanoparticle free by measuring the whole spectrum from 190 – 900 nm. When there was no SPR-peak visible, the supernatant was deemed nanoparticle/conjugate-free.

Size characterizations were done with an analytical disc centrifuge (ADC, DC 24000 from CPS instruments) at 24000 RPM, which measures the attenuation of an incident laser beam with a wavelength of 405 nm against a D(+)-sucrose density gradient in a sample volume of 0.1 ml. The obtained mass-weighted and number-weighted size distributions represent spheres with equal sedimentation characteristics and were subsequently used together with the calculated mass-concentrations to determine the overall surface-concentration in cm^2/ml of each colloid. Details on this procedure can be found in the Supporting Information.

Acknowledgment

We want to express our gratitude to Jurij Jakobi for the performance of the TEM imaging featured in this work. Laser ablation of Ag-Au alloy nanoparticles was funded by the Deutsche Forschungs Gemeinschaft (DFG) (Project number: BA 3580/24-1).

Supporting Information is available

The Supporting Information contains raw data as the original UV/Vis spectra, calibration curves for the mass concentration determination of the colloids, calibration curves to calculate the aptamer and protein concentrations in the supernatants, and exemplary TEM micrographs. In addition to that, they also explain the protocols we used to calculate the total surface area of our colloids and the conjugation protocol we used in this study. At least, we also show some more information on the aptamer sequence and additional results for the conjugation experiments.

Supporting information are available online:
https://pubs.acs.org/doi/10.1021/acs.bioconjchem.1c00468 (last access: 19.01.2022).

All cross-references of this chapter regarding supporting information refer to the supporting information, that can be found under the respective link.

3.2.4 Impact of additional stabilization ligands during conjugation

So far, the main challenge in utilizing laser-generated NP instead of chemically synthesized ones has been the insufficient conjugate stability. Without their surface covered in citrate, the nanoparticles fail to evade agglomeration and finally aggregation. The post-conjugation addition of citrate to LAL-nano-bio-conjugates did fail to counter this effect. Thus, citrate alternatives have been chosen and added to the conjugate's batches prior to or post conjugation. The first stabilizers tested were chosen based on their ability to provide a steric hindrance. Bovine serum albumin (BSA) has been utilized throughout the literature and stabilizes even agglomerating nanoparticles [187]. However, it has been described to bind ochratoxin A – making it an inappropriate candidate for developing an aptamer-based OtA detection device. [303] Instead, polyethyleneglycol (PEG) and mercaptoundecanicacid (MuA) were chosen stabilizers. Both ligands were featured in the existing literature on nano-bio-conjugates. [304–306] The chosen nanoparticles were conjugated with OtA aptamer, and the resulting conjugates consequently mixed with the stabilizer to guarantee optimal surface coverage with the functional molecule. The results can be seen in **Figure 27**.

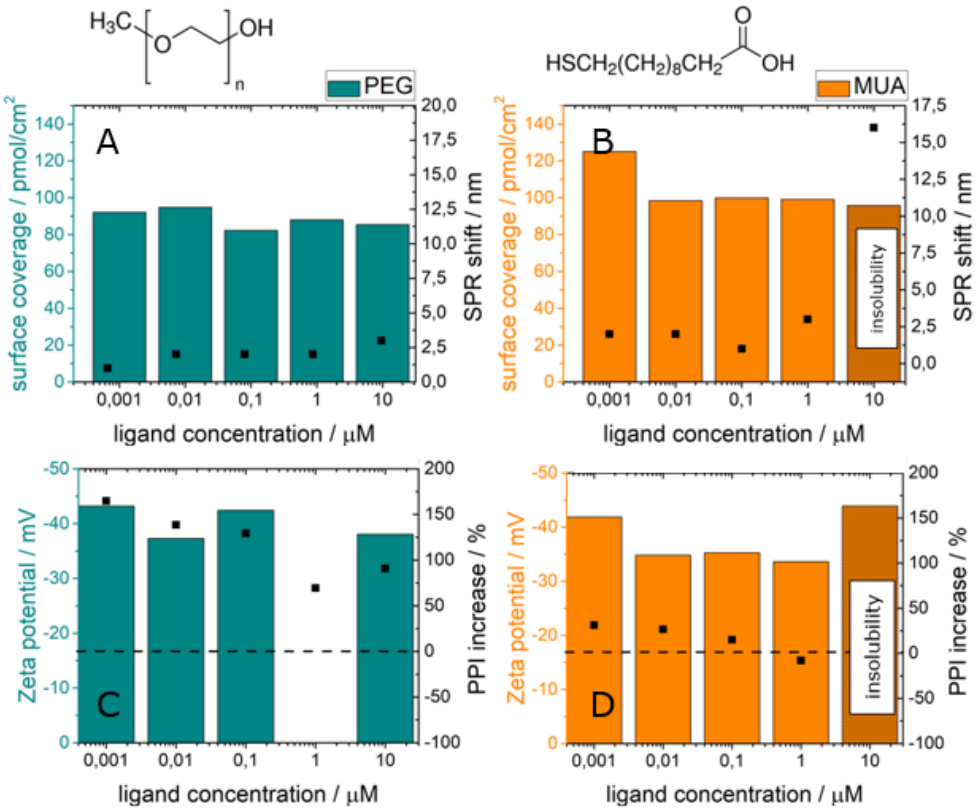

Figure 27: Conjugation of 50 nm Au NP via salt-aging in presence of sterical stabilizers. A) surface coverage featuring PEG; B) surface coverage featuring MUA; C) zeta potential featuring PEG; D) zeta potential featuring MUA. Measurements represent one-time-measurements.

The measurements were performed as serial of one-time measurements. Therefore, the data must be examined with care. Yet, they can be used as first measure if an improvement was achieved. First, one should compare the achieved surface coverages for both ligands. It is noticeable that an increasing concentration of PEG and MUA does not seem to influence the maximal achievable surface coverage. There is a drastic increase at minimal MUA concentration, but this could be a statistical outlier. Thus, it is possible to introduce a steric hindrance ligand while retaining the desired aptamer surface coverage. However, the stability has only been increased for those conjugates featuring PEG. The zeta potential remains almost stable around - 40 mV, whereas the PPI increased to more than 150 % of samples conjugated without PEG. Nevertheless, an increased PEG concentration does not necessarily lead to increased stability. This may be attributed to excess PEG building up a multilayer around the conjugate particles. Therefore, once the conjugate has been encapsulated in a PEG matrix, no further stability increase can be expected. In contrast to that, an increased MUA concentration ultimately leads to the sample´s agglomeration and aggregation. This phenomenon may be based on hydrogen bonding between different MUA molecules on separate nanoparticles. Thus, high concentrations of MUA lead to the observed interconnection and agglomeration of the particles. With that in mind, PEG 350 seems to be the most suitable stabilizer. However, functional assays in the LFA format indicated unspecific binding events towards the test line when PEG was utilized for conjugate stability.

3.2.5 Resuspension buffer – the solution to the stability crisis?

The nano-bio-conjugate generation procedure features many steps and a multitude of parameters within each step that must be adjusted carefully to guarantee optimal stability and functionality. The resulting conjugate must withstand the loading onto the glass fiber, the subsequent drying procedure, and finally the redispersion into the sample buffer while still being able to bind the desired target molecule. Until now, the conjugation procedure was optimized for laser-generated NP by comparing different charge screening agents, the influence of the pH on the conjugation procedure, and the conjugate stability. In addition to that, alternatives to salt-aging were analyzed, as well as the utilization of stabilizing ligands. Despite the important findings that were made this way, LAL-Au NP containing conjugates lack the robustness of their chemical-synthesized containing counterparts. In this chapter, the resuspension process will be subject to a systematic evaluation. It will be examined whether the resuspension buffer´s choice influences the resulting conjugate stability or if it can be even enhanced by adding surfactants and compatible solutes subsequently.

So far, the resuspension of conjugates after the separation from unbound DNA took place in pure MilliQ-water. However, many samples precipitated within hours after resuspension. In a first attempt, four different basic approaches of resuspension were compared: 1. Pure MilliQ-water; 2. TRIS-buffer (15 mM, pH 8); 3. BSA (1 mg/mL). BSA should provide the best sterical hindrance, yet it could also lead

to unexpected and unwanted unspecific interactions with the utilized aptamer sequence. TRIS-buffer has previously been used during the conjugation procedure and leads to the highest observed stability and survival rate. Trehalose belongs to the family of compatible solutes. Compatible solutes are organic molecules of low molecular weight that can be accumulated within the cell without interfering with the cell´s metabolism supporting the cell to survive stress conditions [307]. They stabilize proteins, DNA, and cell membranes and keep them functional under stress conditions like heat, cold, drought, high salt concentrations, as well as high and low pH values [308]. Compatible solutes can be assigned to the following groups of organic molecules: sugars, amino acids, polyols, and their respective derivatives [309]. Naturally occurring trehalose is a non-reducing disaccharide, made of two glucose units linked together via an α,α-1,1-glycoside linkage [310]. It protects proteins from heat [311], denaturation during freezing and drought [312] and cells/organisms from oxidative stress [313], and the consequences of drought [314], and it stabilizes lipid bilayers [308]. In addition to that, trehalose is utilized for various industrial applications, protecting of enzymes during drying processes [315] and the dehydration of unstable biomolecules, like antibodies for storage purposes [316,317]. Furthermore, trehalose can be found in everyday products, like deodorants to reduce human odors and as a food additive, due to its stabilizing function [318]. This research was included to see whether a compatible solute would affect the conjugation procedure itself and could improve the conjugate´s drying behavior. The subsequent **Figure 28** shows the four different samples right after resuspension.

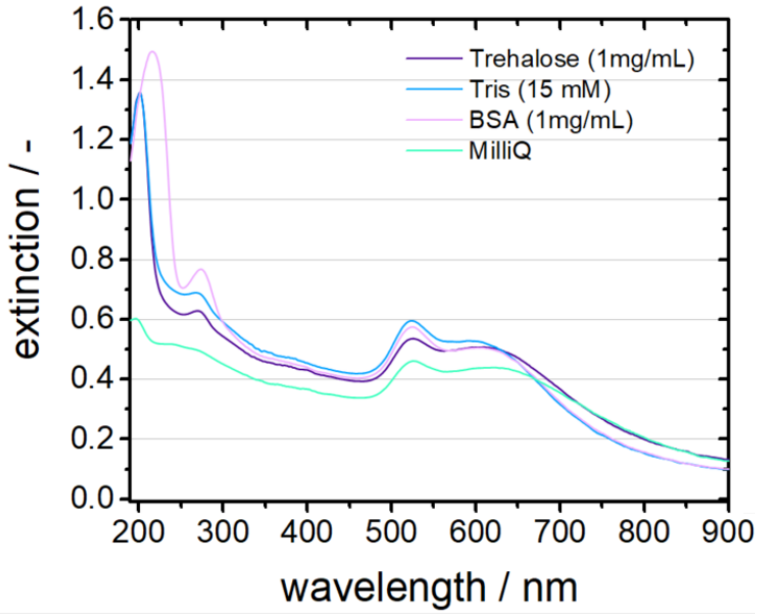

Figure 28: Comparison of different resuspension solutions after the final centrifugation step to separate conjugates and unbound DNA molecules via UV-ext. spectroscopy.

All four approaches featured an increase in their extinction from 600 nm to 700 nm, indicating agglomeration and aggregation. Thus, neither pH, compatible solute, nor steric ligand could stabilize the generated conjugates on their own. Because of these findings, additional approaches were tested. The aptamer- volume to Au NP-volume ratio was adjusted to 1:9. The resulting conjugates were redispersed using either MilliQ or MilliQ plus varying amounts of Tween20. The UV-vis extinction spectra are shown in **Figure 29**.

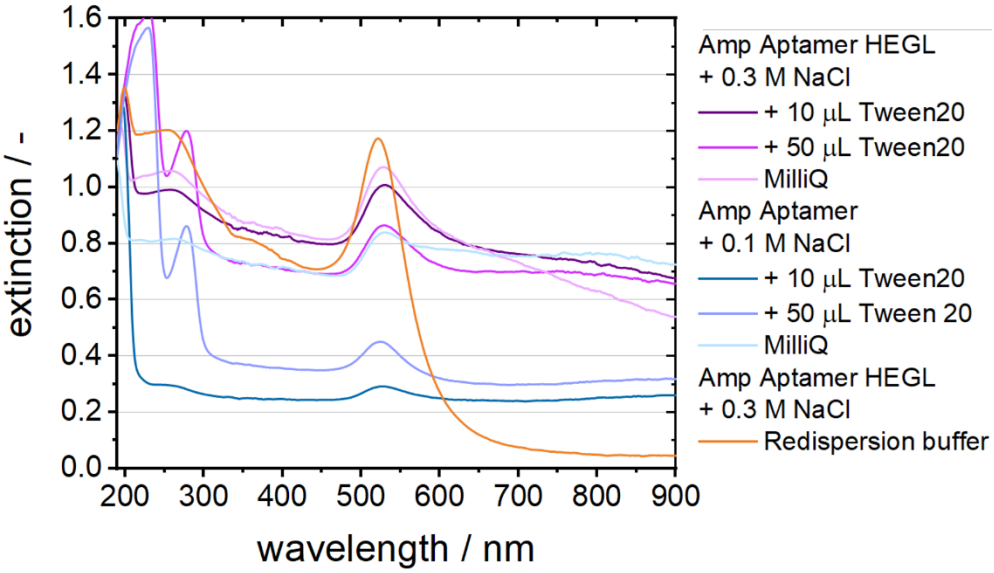

Figure 29: Conjugates featuring the Amp aptamer plus HEGL spacer (#183408), redispersed in MilliQ water, featuring varying amounts of Tween20. VS. conjugates featuring the Amp aptamer (# not available), redispersed in MilliQ water, featuring varying amounts of Tween20 VS conjugate redispersed in redispersion buffer (0.01 M PBS, 0.5% PEG250, 2% saccharose, 0.1 % Tween20; according to Song et al. [319])

The addition of Tween20 reduces the loss of conjugate during the separation of unbound ligands. However, the modified redispersion buffer described by Song et al. [36] provided a much more stable redispersed conjugate. It consists of 0.01 M PBS, 0.5% PEG250, 2% saccharose, 0.1 % Tween20. PBS buffer features a buffer range from 5.4 to 7.4. It has been established throughout literature and will be discussed in detail in section 4.2.2. “The ideal buffer”. The other constituents fulfill different roles in stabilizing the conjugate. PEG250 provides steric hindrance, thus contributing to the conjugate´s stability [304,305]. Saccharose serves as drying agent analogous to trehalose [320]. Tween is known to contribute to the stabilization of colloidal chemically synthesized Au NP by preventing unwanted adsorption of screening agents onto the particle´s surface [306].

This buffer will be used as a standard redispersion buffer for future experiments. The salt-aging for conjugates featuring the aptamer + HEGL spacer could be performed until a salt concentration of 0.3 M NaCl was reached. Conjugates featuring aptamer without the spacer did not “survive” salt-aging above 0.1 M NaCl. The ampicillin aptamer, including the HEGL spacer, will be the main aptamer for further testing.

With three of the most prominently featured steric stabilizers out of the way, a more suitable stabilization way was chosen in form of the resuspension buffer. The experiments on isolated conjugates allowed to gain insights on the correct handling and preparation of this very important part of the LFA test system. However, it also became clear how minuscule it is to analyze it behavior without considering it functionality on LFA test stripes. Thus, the following chapter provides detailed information on the preparation of LFA test stripes and the application of the LAL NP-aptamer-conjugates.

3.2.6 Rating of bioconjugation strategies – summary

Several nano-bio-conjugation techniques, as well as auxiliary agents like stabilizing agents, buffers and pad-preparation techniques have been applied featuring laser-generated Au NP. This section aims to provide an overview over the pros and cons of the applied techniques and their impact on the nano-bio-conjugate stability and functionality.

Regarding the nano-bio-conjugation process, different conjugation techniques have been established throughout literature. However, only salt-aging proofed itself reliable enough for nano-bio-conjugates featuring aptamers and laser-generated Au NP with respect to conjugate stability and functionality. Choosing the correct charge screening agent can support the correct aptamer folding if the stability threshold of the respective nanoparticles is not exceeded.

Nano-bio-conjugation is a robust process and varying noble metal nanoparticles can be utilized in this regard. The color of Ag NP makes them unsuited as conjugate for LFA applications, yet they exhibit the desired binding ability. Future work could feature other alloys, like e.g., gold-platinum alloy nanoparticles to utilize their strong, contrast rich color for LFA applications.

Additional stabilizing agents and buffers can greatly improve the nano-bio-conjugates stability. However, stabilizers and buffers must be carefully chosen to exclude unwanted side effects like reduced stability or unspecific binding events. Buffers are cheap and the correct choice has proven to improve the conjugates stability the most. The results of section 4.2 and its subchapters are shown in **Table 1**.

Table 1: Overview over different approaches of nano-bio-conjugation

Approach	Technique	Pros	Cons
conjugation techniques	salt-aging	cheap charge screening agents, freely adjustable surface coverage, correct charge screening agent can support correct DNA folding	excess DNA required, limited stability threshold, long incubation time cations may interfere with aptamer folding (lower specifity)
	pH-aging	fast conjugations, high surface coverages	excess DNA required, low pH may damage DNA (strand breaking), insufficient conjugate stability
	peptide-aging	very high surface coverages and conjugation efficiencies	long preparation time (co-incubation peptide and aptamers), peptides may interfere with correct DNA folding, insufficient conjugate stability
nanoparticle	surface composition	highly robust system, nanoparticle surface composition can be adjusted freely without loosing functionality: pure Au NP – alloy NP– Ag NP	ideal surface coverage depends on respective nanoparticle surface composition (higher surface coverages may be necessary to achieve the same function)
additives and buffers	stabilizing agents	drastically increase nano-bio-conjugate stability,	possible interference with LFA (unspecific binding events), possible interference with DNA folding → *in-silico* analysis may be required prior to choosing the correct stabilizer
	resuspension buffer	cheap, supports correct folding of DNA, supports correct drying of conjugate on LFA	none

3.3. LFA development

3.3.1 Salt aging – influence on drying behavior

The results from chapter 4.2 stress how important choosing the charge screening aging is for the success of the conjugation and the resulting conjugate stability. However, results presented in this section mainly focus on the PPI a measure of conjugate stability in the colloidal state. The PPI was established by Merk et al. [161] to establish a measure of stability for pure laser-generated noble metal colloids. However, the ligands introduced during the conjugation procedure influence the UV-vis extinction spectrum providing the 380 nm and 800 nm values for PPI calculation. Thus, an alternative approach had to be introduced to not only estimate but to quantify conjugate stability in the liquid colloidal state, as well the dried state on the conjugate pad. Finding the most stable conjugate is of uppermost importance since the LFA application demands such a robust nano-bio-conjugate. Only stable conjugates will perform as desired on LFA test systems. [41] Here, a visual readout system was established, which allows for conjugate stability evaluation and quantification of the conjugate drying behavior on glass fiber – the state-of-the-art conjugate pad material.

First, the experimental throughput had to be increased to allow the testing of more parameters and drastically reduce the amount of required aptamer. The 96-well-plate test format was established in this regard and the test volume reduced from 1 mL to 0.200 mL. Based on the findings described in section 4.2, $CaCl_2$ was excluded from these experiments. A first test run was performed, utilizing varying amounts of aptamer (0.125 µM – 1.000 µM; top to down) and varying concentrations of charge screening agents (0 M – 2 M). Due to the Schulze-Hardy-Rule, the dilution of the $MgCl_2$ experiment was adjusted (see **Figure 30**).

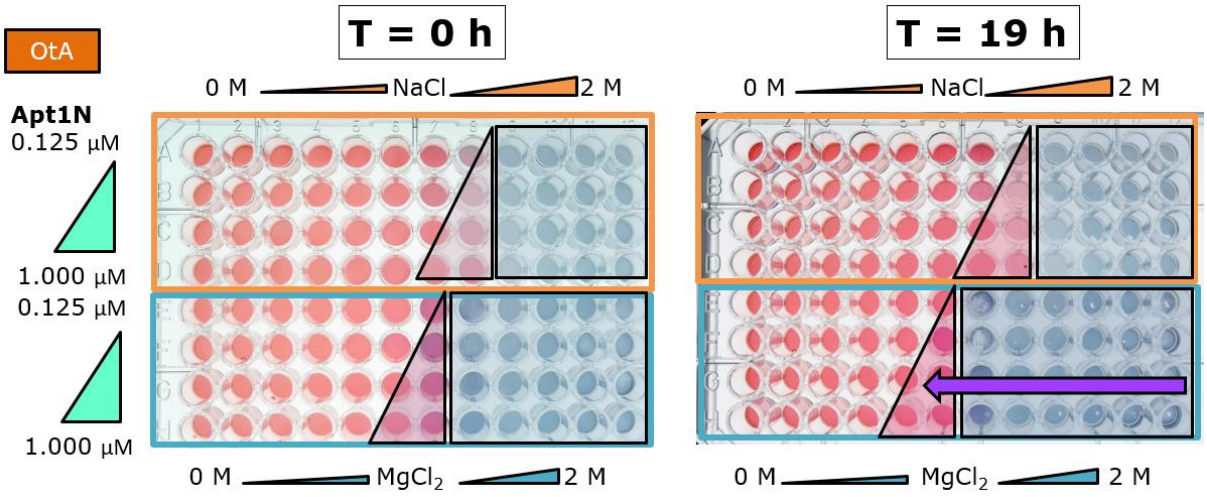

Figure 30: 96-well-plate conjugation of 30 nm Au NP featuring OtA aptamer. The plates are shown directly after the salt-aging procedure (T = 0 h) and after the overnight (ON) incubation (T = 19 h).

Directly after adding the salt, a color change could be observed for all samples featuring 600 – 700 µM NaCl and 125 – 250 µM $MgCl_2$. The strong and desired red turns purple. Samples featuring higher salt concentration turn bluish-purple and precipitate within minutes. After 19 hours, there are no visible changes for the NaCl-aged samples, yet, the $MgCl_2$ – aged samples that showed a minor color shift, turned purple and precipitation could be observed. This purely visible approach was subsequently transformed into an R/G/B-coded data set.

R/G/B represents an additive color code system that allows separation of millions of colors. It was chosen since R/G/B analysis can be easily done at high throughput for digital images, and its resemblance to the human vision, which is based on the addition of color signals of receptors for red, green, and blue light. With this in mind, a formula was developed to quantify the reddishness of a conjugate sample. Here, gold nanoparticles of 30 nm in diameter should provide a strong red color. Ultimately the rapid-red formula was introduced and utilized to analyze the conjugate stability. **Figure 31** depicts the analysis routine and formula.

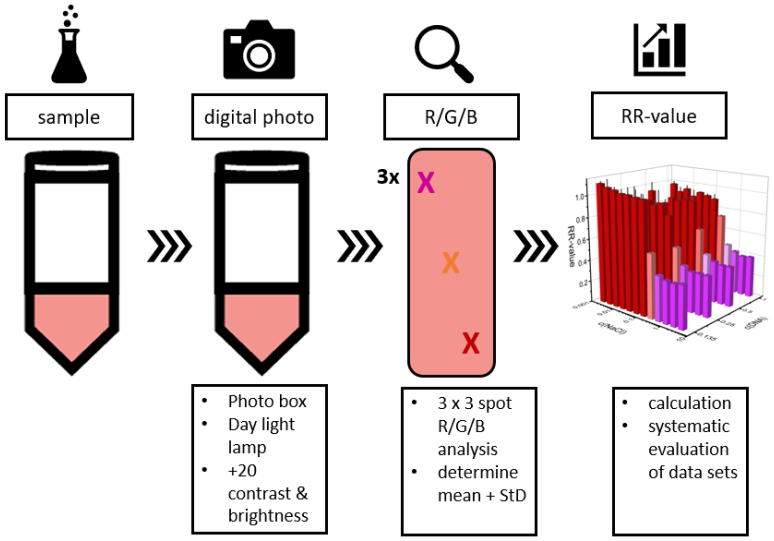

Figure 31: From sample to RR-value. Schematic step-by-step-overview.

The rapid red formula puts the R, G, and B value into relation with each other, like shown in formula 1.

$$\textbf{\textit{Formula 1}}: \qquad RR = \frac{R}{G + B + 1}$$

Thus, the data set for every well is reduced to three measurements, which can be used to give an average value with its corresponding standard deviation. Due to its very nature, the rapid red value spans a range from 0 to 1.8 (compare **Figure 32**).

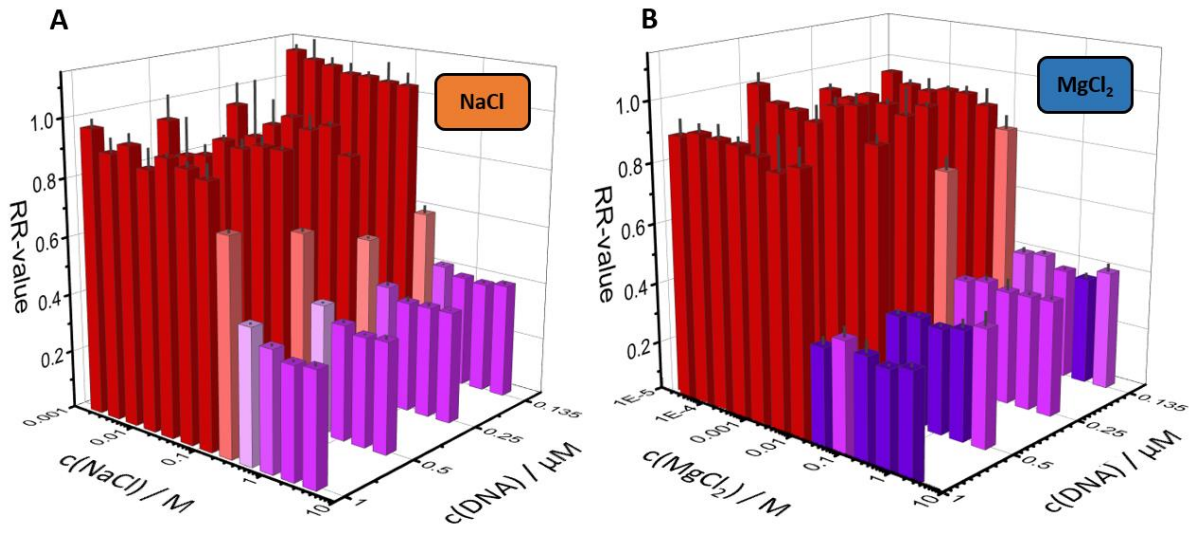

Figure 32: Rapid red of 96-well-plate shown in **Figure 30**.

The comparison of RR-values right after conjugation and after 19 h of incubation leads to the finding that all samples that featured a RR-value of at least 1 did not fall, whereas samples exhibiting RR-values

above 0.9 did change from the status “most stable” to “transition”. For subsequent experiments, the aim was to reach at least an RR-value of 1 for the generated conjugates. However, this threshold is only reliable for liquid conjugate samples within their respective wells. If the conjugate is transferred onto glass fiber or the final LFA-test strip, it is still possible to determine the RR-value, yet the material´s opaqueness may alter the RR-value to significantly lower values (see **Figure 33**).

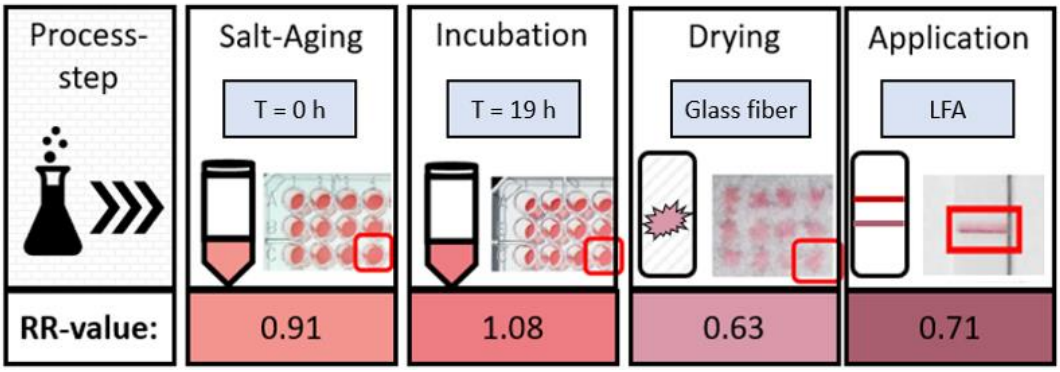

Figure 33: RR-value for different materials with varying opaqueness.

It is noticeable that the RR-value of stable samples was not constant during the 19 h incubation but increased, as can be seen in **Figure 33**; exemplary sample C4. This change could be linked to the successful conjugation procedure. Wang et al. described that a much slower conjugation step follows the fast-initial conjugation step. The ligand-free surface offers enough room for a fracture of the applied thiolated ligands to adsorb without resistance, according to the observed conjugation efficiencies (less than 10 %). Hence, if this initial conjugation step is over, the surface is covered with negatively charged ligands. The second phase consists of the charge screening agents allowing the residual unbound ligands to find their way through the already attached ligands rearranging the thiol-linkages so that it can be maximized which takes up to at least 5 hours. [180] The conjugation of additional ligands is indicated by an SPR-peak-shift, as described by Walter et al. in 2010. [30] Here, the method can detect the SPR-peak-shift linked to the successful conjugation, which an increasing RR-value indicates after 19 hours.

However, as soon as the sample is transferred to glass fiber, the RR-value drops significantly, only to rise again when transferred onto an LFA-test line. This opaqueness-dependent RR-value drop makes the RR-method less attractive for the analysis and quantification of the staining of glass fiber and determining the successful staining of the test line. Future experiments will have to be performed to find the correct material/opaqueness-dependence of the RR-value and the suitable thresholds for each tested material. Nevertheless, this is beyond the scope of this work. However, it must be stressed that the RR-method allowed choosing one sample out of 96, based on empirically determined data, which could be successfully transferred onto glass fiber and subsequently onto a lateral-flow-assay, providing

the desired staining of the test line. According with the handbook by EMD Millipore, the most stable sample was also the one best suited to be used as nano-bio-conjugate on an LFA-test strip. [41] In this regard, this method adds up to the green chemistry character of this LFA-development. Since it introduces a way to reduce the number of required materials while reducing the number of samples that must be tested for a systematic evaluation drastically. Thus, this method will be encountered throughout this thesis whenever conjugate stability of nano-bio-conjugates featuring laser-generated gold nanoparticles has to be evaluated.

The same methodology was utilized to examine the alternative approach towards an OtA detecting nano-bio-conjugate, which would not feature the aptamer, but its complementary conjugate. However, it was already noticeable that the generated oligo-conjugates did not reach the desired stability as their aptamer-bearing counterparts (compare **Figure 34**).

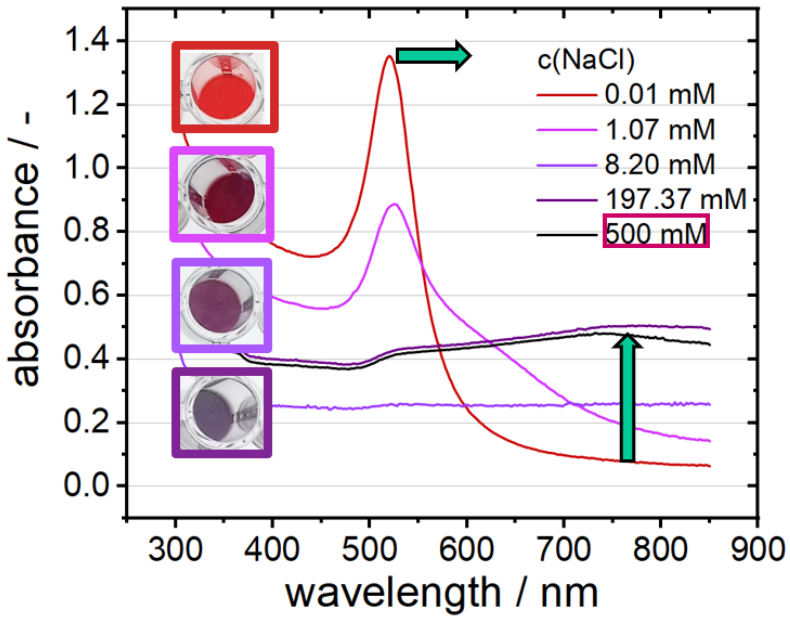

Figure 34: Conjugation of laser-generated Au NP with complementary oligonucleotide for competitive assay formats with varying sodium chloride concentrations (0.01 mM – 500 mM). Samples were analyzed via the TECAN Spark 20 M multimode microplate reader. Pictures of samples were made according to the photo documentation protocol described in section 8.2.2.

According to Hurst et al., optimal surface coverage can be achieved by salt-aging up to a concentration of 0.7 M NaCl. [175] Here, the tested conjugates´ total precipitation could be observed already at a concentration of 8.20 mM NaCl. Two things must be considered when it comes to generating nano-bio-conjugates featuring thiolated DNA-molecules. First, the steric hindrance provided by the much shorter oligonucleotide (37 bases) is expected to be much less than the steric hindrance of the 61 bases long aptamer. Second, the oligonucleotide is not designed in such a manner that a complex 3D-structure is formed. The conjugates were only considered stable at deficient salt concentration, which would only allow for very low surface coverages – not suited for LFA applications. For future work, it could be of interest to study more intensely the alternative nano-bio-conjugate, featuring the

complementary oligonucleotide. However, optimizing the oligonucleotide conjugation procedure was too time-, and resource-consuming.

3.3.2 The ideal buffer

It was previously shown how the pH could influence the conjugation procedure and the resulting conjugate stability. However, this systematic evaluation lacks a detailed analysis of the influence of the pH on the generated conjugates´ functionality. In addition to that, a detailed analysis is missing if the pH itself is the main parameter for the aptamer-nano-bio-conjugate function or if the chosen buffer itself influences the function. This chapter combines intense literature research on the most prominently used buffer in the field of nano-bio-conjugation and a systematic experimental comparison of the two best-suited buffer systems in combination with LAL-NP. Buffers were mainly chosen due to the achieved LODs of the described LFA-test-systems. Later on, it will be discussed why the LOD might not be the ideal parameter to evaluate LFA-effective-ness, but for now, it allows to narrow down the buffers for the experimental part of this chapter based on empirical data.

If one works its way through the state-of-the-art literature on aptamer-nano-bio-conjugates in diagnostics, it is apparent that all applications feature a buffer system. Utilizing a buffer is a standard procedure when working with biomolecules to guarantee constant pH conditions. The main buffers used in 30 publications are shown in **Figure 35**. The most frequent buffer is the phosphate-buffered-saline (PBS) solution. This complex-forming buffer releases protons in the presence of metal ions and binds divalent cations. Its buffer range spans from pH 5.8 to 7.5. [321] It must be mentioned that PBS buffers usually contain $MgCl_2$. Yang et al., Barthelmebs et al., and Zhang et al. used 1 mM $MgCl_2$ in their respective PBS buffer. [201,209,211] It was previously shown that the conjugate stability of conjugates featuring LAL-generated NP was significantly reduced when $MgCl_2$ concentrations above 0.2 mM were reached. The second most-frequently-used buffer is Tris(hydroxymethyl)aminomethane (TRIS). It features a buffer range of pH 7 to 9, which is strongly temperature-dependent. It was previously used as a SELEX-buffer to generate the miniStrep aptamer by Bittker et al. [94]. TRIS is commonly used for physiological applications yet is limited due to its relatively high pH-range. [321] The remaining buffers on this list feature MES, carbonate, HCl/citrate, and phosphate citrate. Since no pure-LFA-application utilized those buffers, these buffers were excluded from the experimental part of this work. However, it might

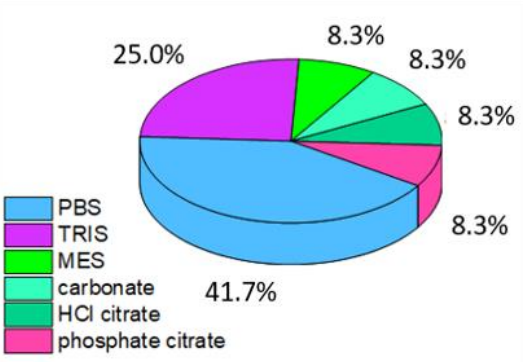

Figure 35: Buffers utilized for OtA detection throughout literature.

be of interest to get an overview of the aforementioned buffers and the respective pH-values of the analyzed samples (compare **Figure 36**).

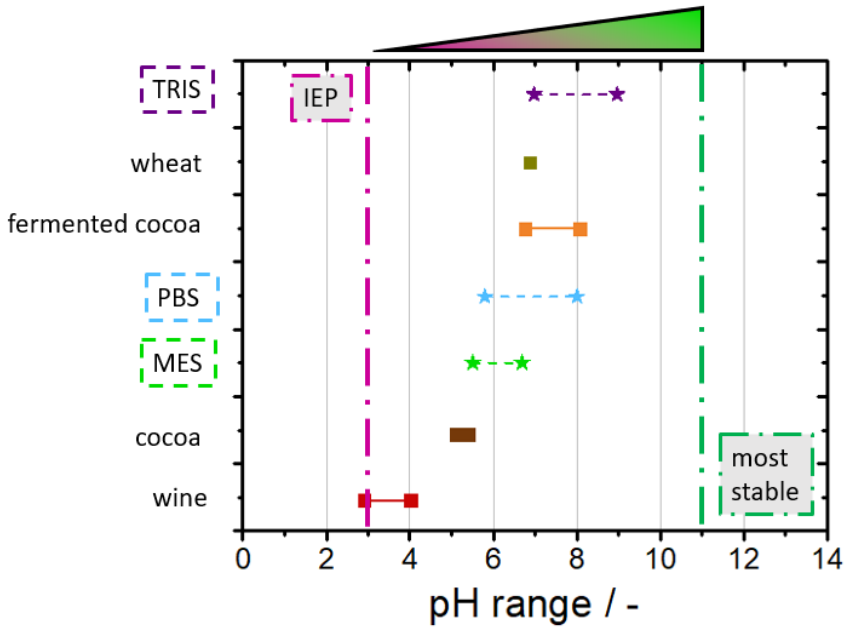

Figure 36: Visualization of samples and their respective pH ranges (continuous lines), as well as the most used buffers in literature and their respective buffer range (dashed lines). The isoelectric point of gold nanoparticles is shown in pink, the pH at which Au NP are most stable is marked in green. Both values were extracted from Merk et al. [161].

As can be seen, the pH-range of the most prominently used buffers covers a weak-acidic to the weak-basic range. However, samples like wine or cocoa, which feature a strongly acidic pH, might require buffer systems, featuring a broader pH-range, as well as an improved buffer capacity. Due to its technical limitations, an LFA-test-stripe can only provide a limited buffer capacity, and samples featuring low pH values might just render the buffer useless. Here, PBS buffer provides the broadest pH-range, leading to significant overlap with samples like fermented cocoa or wheat. Only MES buffer provides buffer capacity at lower pH values, making it an interesting solution to acidic samples. Nevertheless, the ultimate question remains which buffer system provides the best LOD results. Different approaches from the literature were compared to answer this question (**Figure 37**).

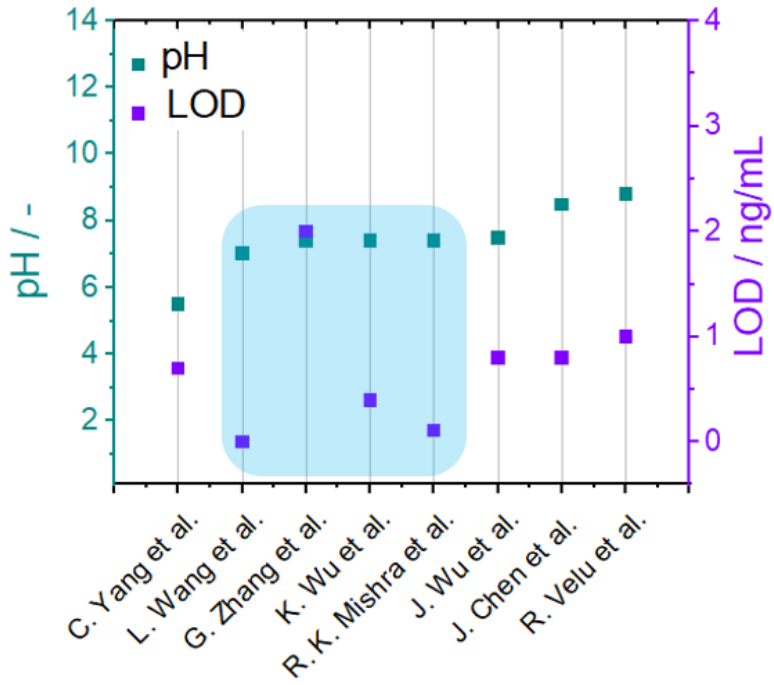

Figure 37: Comparison of the pH conditions of the respective test systems and their limit of detection (LOD) in ng/mL.

Here, eight different OtA – detection devices are compared. The three lowest LODs were achieved at a pH of around 7.5. [118,123,322] Nevertheless, a clear statement if this pH-value represents the optimum for OtA detection remains unclear since all three publications feature different detection-techniques. Mishra et al. utilized titanium dioxide nanoparticles as an aptasensing platform [123], Wu et al. utilized a fluorescence-based biosensor with subsequent signal enhancement via RNase H [322], whereas Wang et al. established a traditional LFA-test system supported by a test reader [118]. Despite the three presented systems differing significantly in their technical approaches, it remains of interest that TRIS-buffer and MES-buffer could achieve comparable LODs at the same pH. The data of Zhang et al. were determined for ochratoxin extracted out of solid corn samples; hence the limit of detection might be affected by the extraction of the analyte [211]. However, the data indicate that the chosen buffer is of secondary importance if the pH is adjusted correctly. However, different approaches were used to generate the data. In this work, nano-bio-conjugates were prepared in either PBS -, or TRIS – buffer while all other parameters were kept constant. The results are shown in **Figure 38**.

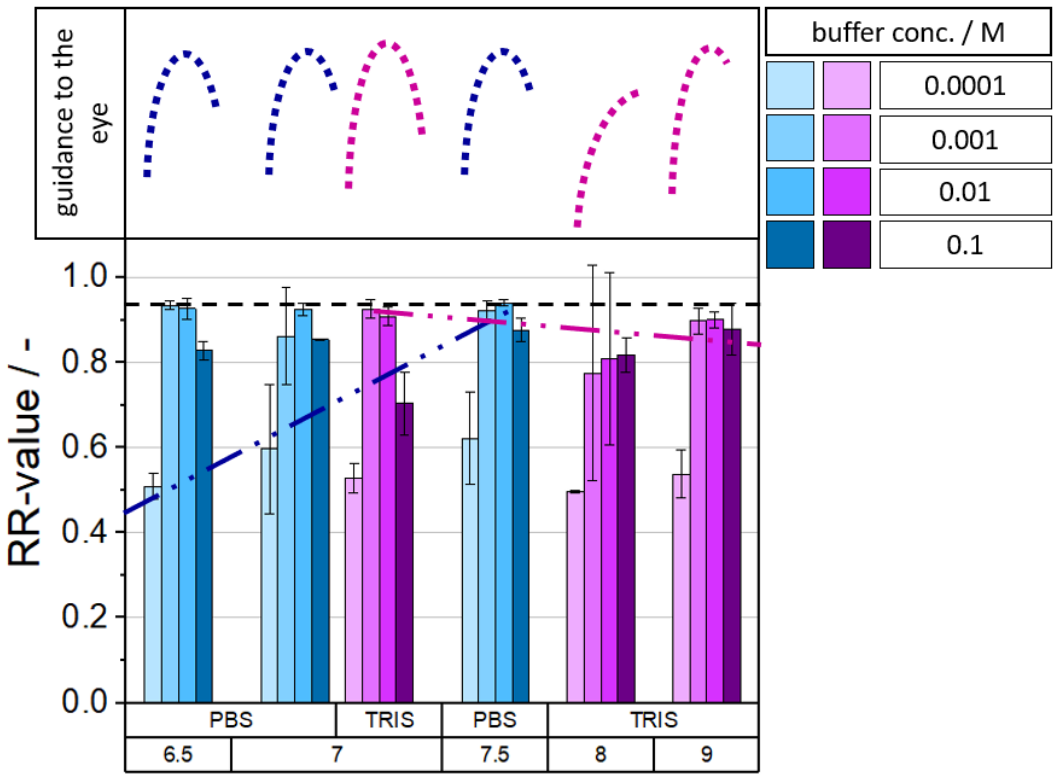

Figure 38: Influence of the pH on the generated conjugates´ stability, featuring 30 nm laser-generated Au NP and HEGL-4x-Amp-aptamer (0.2 µM). The respective tests were performed in the microplate format (200 µl total volume per well), and the buffer concentrations were adjusted from 0.0001 to 0.1 concerning the main buffer component. Buffers were adjusted with HCl to the respective pH values (6.5 to 9). It has to be noted that PBS and TRIS feature different pH ranges, which is the main reason both buffers are compared in an overlapping range rather than at the same pH values.

Interestingly, the lowest (0.0001 M) and highest (0.1 M) tested buffer concentration for both buffer systems lead to the least stable conjugates, which did not exceed RR-values of 0.8. This was to be expected since buffer capacity depends on the buffer´s concentration. The buffer capacity is minimal at its lowest concentration; thus, it cannot provide sufficient protection from unfavorable pH conditions. At maximum concentration the salinity of the utilized buffer leads to charge screening in between the colloidal nanoparticles and destabilizes them.

Especially, conjugates featuring PBS failed to exceed RR-values of 0.6. Eleven samples reached RR-values of 0.9, indicating mediocre stability. All samples featured either 0.001 M or 0.01 M buffer solution. Since standard deviations overlap, it is impossible to give an absolute answer which buffer is superior. However, it was possible to generate stable conjugates over the entire tested pH-range. The reason for the differences in conjugate stability, especially for the overlapping pH-values, must be caused by the buffers´ chemical properties. As mentioned, PBS represents an anionic buffer, featuring a considerable amount of salt (1x PBS = 137 mM NaCl + 2.7 mM KCl + 12 mM phosphate). Though, the isotonic solution may contribute to additional charge screening, destabilizing the generated conjugates. In comparison to that, TRIS features an amino group that is readily available to adsorb to

the nanoparticle surface. However, this could ultimately lead to hydrogen-bridge-formation between conjugate-particles at neutral pH, which is with accordance to the highest stability at pH 8. To allow a final statement on the ideal conjugate stability, the samples´ total survival rate was compared. The survival rate does only consider how many samples did not precipitate within a definite amount of time (here one week) in ratio to the samples that precipitated. The results are shown in **Figure 39**. The PBS-treated samples` survival rate remains below 45 %, whereas TRIS-treated samples showed a survival rate of up to 50%. However, this data must be considered with caution since TRIS samples were adjusted to pH-values of 8 and 9. It is well known that Au NP are most stable in alkaline pH. [182] However, the same trend for liquid colloid samples was observed for dried conjugates on glass fiber membranes (see **Figure 40**).

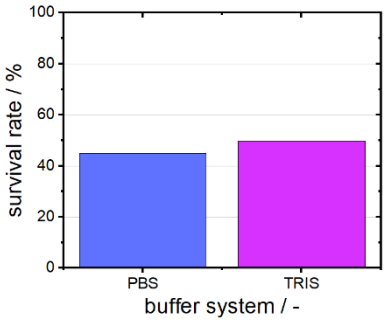

Figure 39: Survival rate of conjugates exposed to PBS or TRIS buffer.

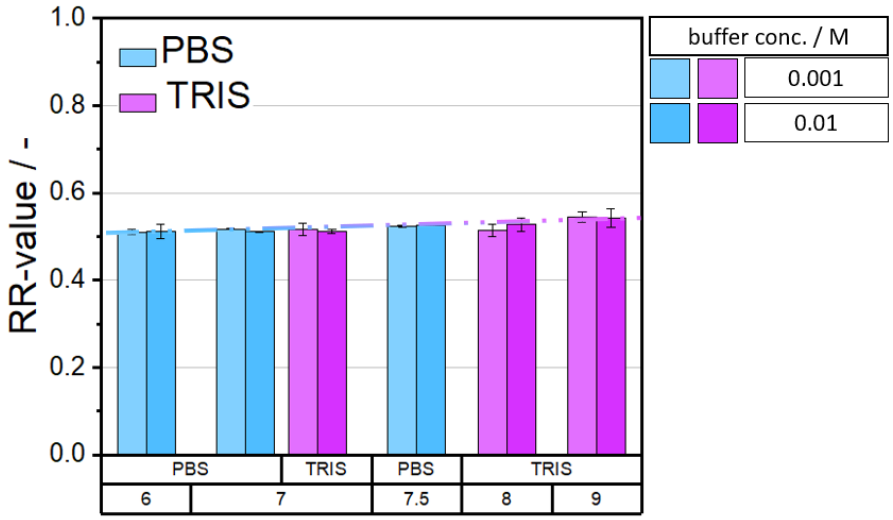

Figure 40: Observed RR-values for conjugate samples dried on glass fiber (2h, 40°C, 10 µL of conjugate).

In conclusion, nano-bio-conjugates featuring laser-generated nanoparticles show pH-dependent stability. Just like for the pure nanoparticles, aptamer-conjugated LAL NP exhibit their optimal stability at alkaline pH. They can be utilized in established buffer-systems that have been previously used for nano-bio-conjugates, featuring chemically synthesized particles. Here, the results indicate that TRIS buffer may ultimately lead to more stable conjugates. However, the sample´s pH may make it necessary to switch towards PBS or MES buffer if required. This chapter adds to the total understanding of the stability and intelligent design of nano-bio-conjugates and significantly improving the conjugate stability, which is of uppermost importance for functionality. However, the final decision on which buffer system to use should always be made with the target molecule, sample volume, buffer capacity,

range, and colloidal stability in mind. It is impossible to provide one clear rule for all imaginable applications of nano-bio-conjugates in the vast field of LFA-applications.

3.3.3 Conjugate pad preparation

The conjugate pad needs to be pre-treated to allow for a stable, redispersable conjugate. This procedure has not been evaluated and optimized for conjugates featuring LAL NP. Zhou et al. used 0.01 M PBS buffer at pH 7.4 [212]. This buffer was utilized to wash the Fassisi glass fiber, and finally the treated glass fiber was dried at 37°C. The washing buffer was analyzed via UV-vis after every washing step, and its pH was determined (see **Figure 41**).

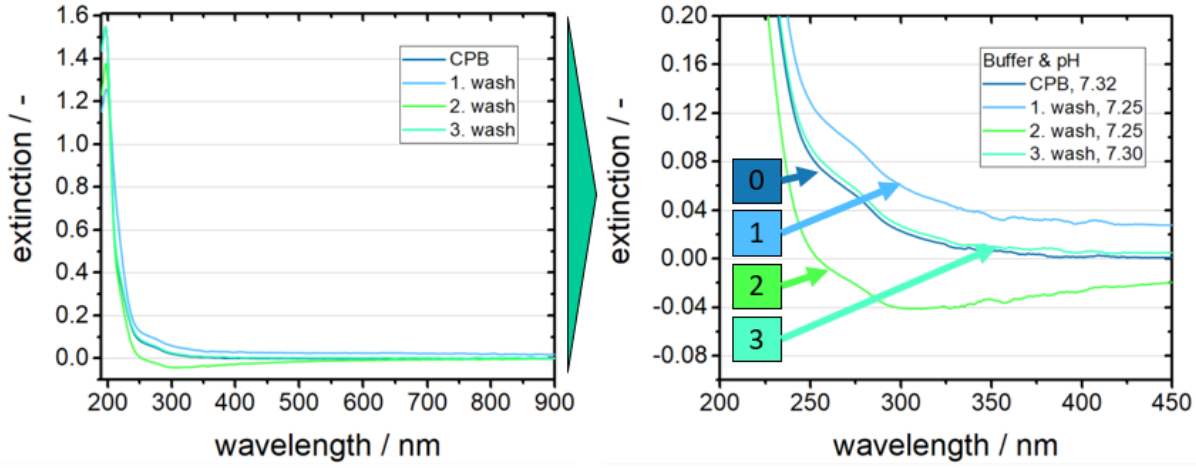

Figure 41: Fassisi glass fiber was cleaned with conjugate pad buffer, described by Yang et al. [212]. The fiber sheets were cleaned 4 times for 1 h. After every cleaning step, the buffer was analyzed via UV-VIS, and the pH was determined.

The pH value showed only minor variations between the washing steps. However, the UV-vis measurements revealed huge deviations. The third washing buffer resembles the reference sample very closely. Thus, it was decided that 3 washing steps should be applied to the glass fiber, before the drying. Small aliquots of 4xHEGL-Amp-aptamer-Au NP-conjugates were pipetted onto the washed glass fiber to see whether the applied conjugate would provide sufficient staining or vanish (see. **Figure 42**).

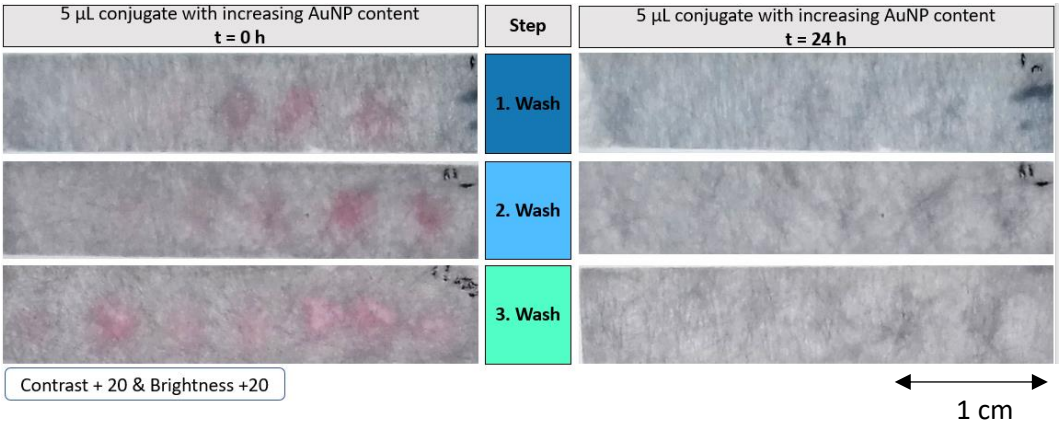

Figure 42: Influence of washing of the glass fiber onto the drying behavior of conjugate. The conjugates with increasing Au NP content (from left to right). 5 µL of the respective conjugates were applied via pipette, and the glass fiber photographed directly after application and after 24 h incubation.

The washing and preparation of the glass fiber did not improve the drying behavior significantly. The experiment was repeated using three conjugate pad buffers to exclude pH effects, featuring pH 7.5, 8.0 and 8.5 (see **Figure 43**). As a consequence of **Figure 41**, the washing was performed 3 times, before the conjugate pad could dry.

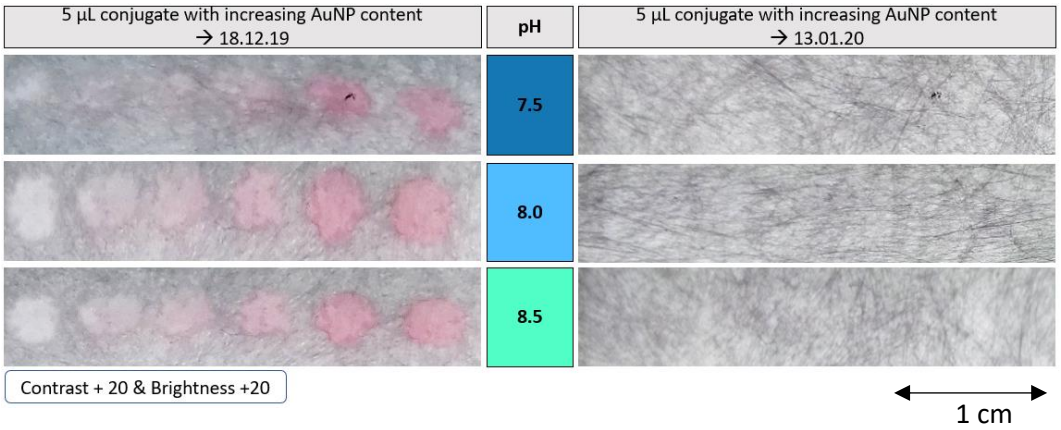

Figure 43: Influence of different pH values during washing of the glass fiber onto the drying behavior of conjugate. The conjugates with increasing Au NP content (from left to right). 5 µL of the respective conjugates were applied via pipette, and the glass fiber photographed directly after application and after 24 h incubation.

No tested pH value provided a successful loading of the conjugate pad. Therefore, the utilized conjugates were further analyzed to exclude the possibility of insufficient DNA surface coverage (see **Figure 44**).

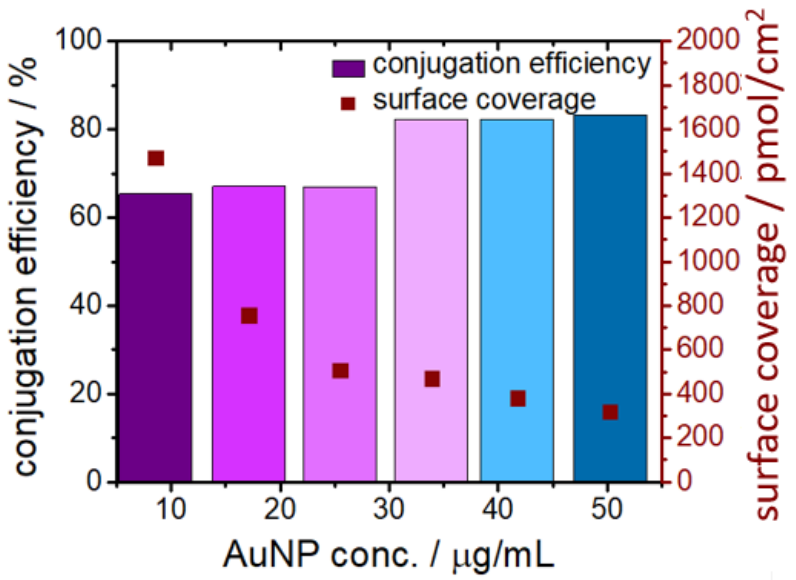

Figure 44: Conjugation of Au NP of increasing colloidal concentration with Amp aptamer with HEGL spacer (#183408)

The conjugate with the lowest Au NP concentration features the highest surface coverage, whereas the conjugate with the highest Au NP concentration features the lowest surface coverage. However, all samples feature a DNA surface coverage above the determined minimal surface coverage of 155 pmol/cm^2, previously determined for the OtA-aptamer system. Samples that included an Au NP concentration above 20 µg/mL, provided a strong pink to red color (see **Figure 45**).

Figure 45: Color of the utilized conjugates for glass fiber loading. Samples were photographed using a Huawei Y6 (2019).

Despite the strong color of the colloid, no red marks were left on the pre-treated glass fiber. The conjugates were further analyzed via UV-VIS (see **Figure 46**).

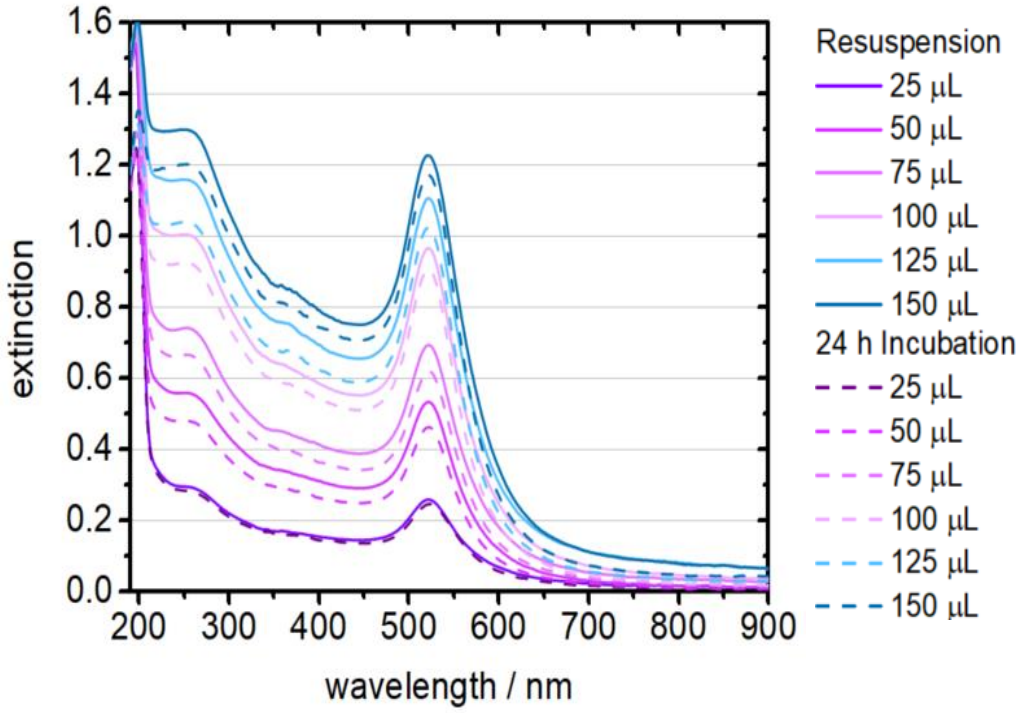

Figure 46*:* UV-VIS extinction spectra of conjugates, featuring an increasing gold concentration from lowest (1; 9 µg/mL) to highest (6; 50 µg/mL)). The conjugates were analyzed before separation from excess DNA (Pre Centri), after separation from excess DNA, and resuspension in resuspension buffer (Resusp) after 24 h incubation.

The strongest signal in the area 700 to 900 nm, which is linked to agglomeration/aggregation, was measured for the conjugate featuring the highest Au NP concentration, see **Figure 47**.

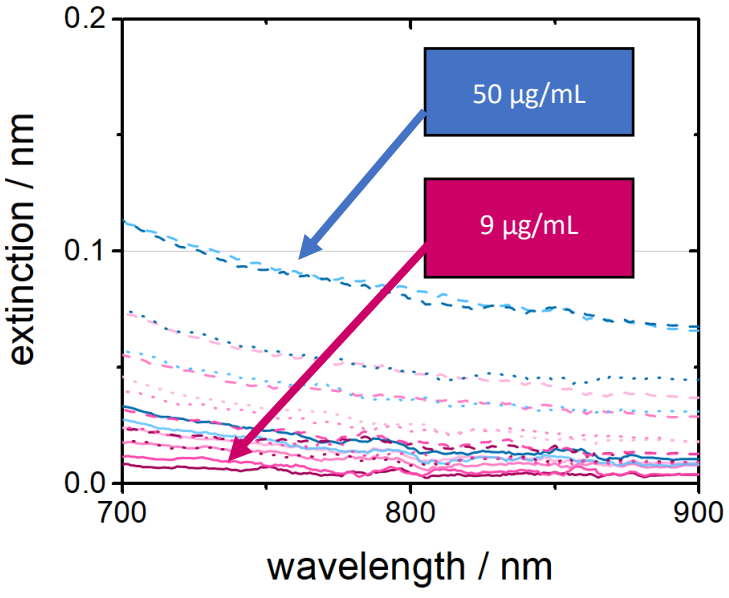

Figure 47: Extinction of conjugates featuring varying Au NP concentration between 700 nm and 900 nm.

However, all tested samples feature a strong SPR peak, whereas the observed agglomeration remains very low. Thus, it can be said that the conjugates feature sufficient DNA load and are stable after resuspension, yet do not survive on glass fiber used by Fassisi, even without being sprayed via bio dispenser. These findings lead to the conclusions that the conjugate concentration should always exceed a certain threshold concentration (see **Figure 49**), since surface coverage alone does not guarantee its stability on the glass fiber. However, the stability can pe positively influenced if redispersion buffer is used. Trehalose and BSA failed to stabilize the conjugate sufficiently. However, experience from the literature suggests the positive effects of saccharose on the conjugate stability during the drying process. [212] If the conjugates are not the reason behind the vanishing of the conjugate on the conjugate pad, it may be necessary to discuss the influence of the glass fiber onto the conjugate, as well as the chosen impregnation mechanism.

Glass fiber is a silica based material, which is not only used as conjugate pad material, but also in many applications, including but not limited to 3D-printing [323], light and data transfer [324], or as composite with polymers (fiber-reinforced polymer; FRP) [325]. One of the most crucial steps during the generation of glass fibers is the sizing of the fibers, which refers to a protective coating with e.g. organic molecules. The utilized sizing agents are responsible for the final properties of the resulting fibers and can influence their hydrophobicity/hydrophilicity. [326] In addition to that the 3-dimensional structure of glass fiber accounts already for a signal loss of up to 90% of the applied nano-bio-conjugates. Only those nano-bio-conjugates can be seen on the test line that are located in the upper layers of the fiber and not hidden in the deeper layers. [41] A possible reason for the vanishing could be an unwanted hydrophobic interaction between the colloid and the glass fiber of the conjugate pad. However, this seems unlikely since the Fassisi glass fiber has been designed for impregnation with water-based colloids. Another important factor in glass fiber coating remains the interaction of so-called nanofillers with the fibers and their respective surface molecules. The nano-bio-conjugate can be seen as such an nanofiller, as described in detail by Mahmood et al. [327]. The application via airbrush and subsequent anchoring of a nanofiller via attractive interactions onto the glass fiber substrate may represent the state-of-the-art technique in the field of LFAs, yet it may lead to the agglomeration of the nano-bioconjugates [328]. This might be the main reason why the application of the nano-bio-conjugates via bio dispenser failed. As observed in chapter 4.2, aptamer might not provide sufficient steric hindrance to allow the conjugates to withstand such high-pressure conditions. Due to that, immersion was chosen as main impregnation mechanism of the conjugate pad. This technique is known to cause drying artefacts. Yet, the total vanishing of an applied colloid has never been demonstrated in the existing literature.

However, one more additional experiment was conducted to see if the nano-bio-conjugates´ application onto the glass fiber was causing trouble. Based on information from EMD Millipore (booklet "What you should know before you specify a membrane for your next assay") the conjugate pad was washed at pH 7.5 and incubated directly within the respective colloids featured in **Figure 46** via immersion. R/G/B values were used as measure of color quantification. https://www.rapidtables.com/web/color/RGB_Color.html provides further information on RGB color codes and was used as reference (last visit: 03.01.2022).

The resulting staining of the conjugate pads is shown in **Figure 48**.

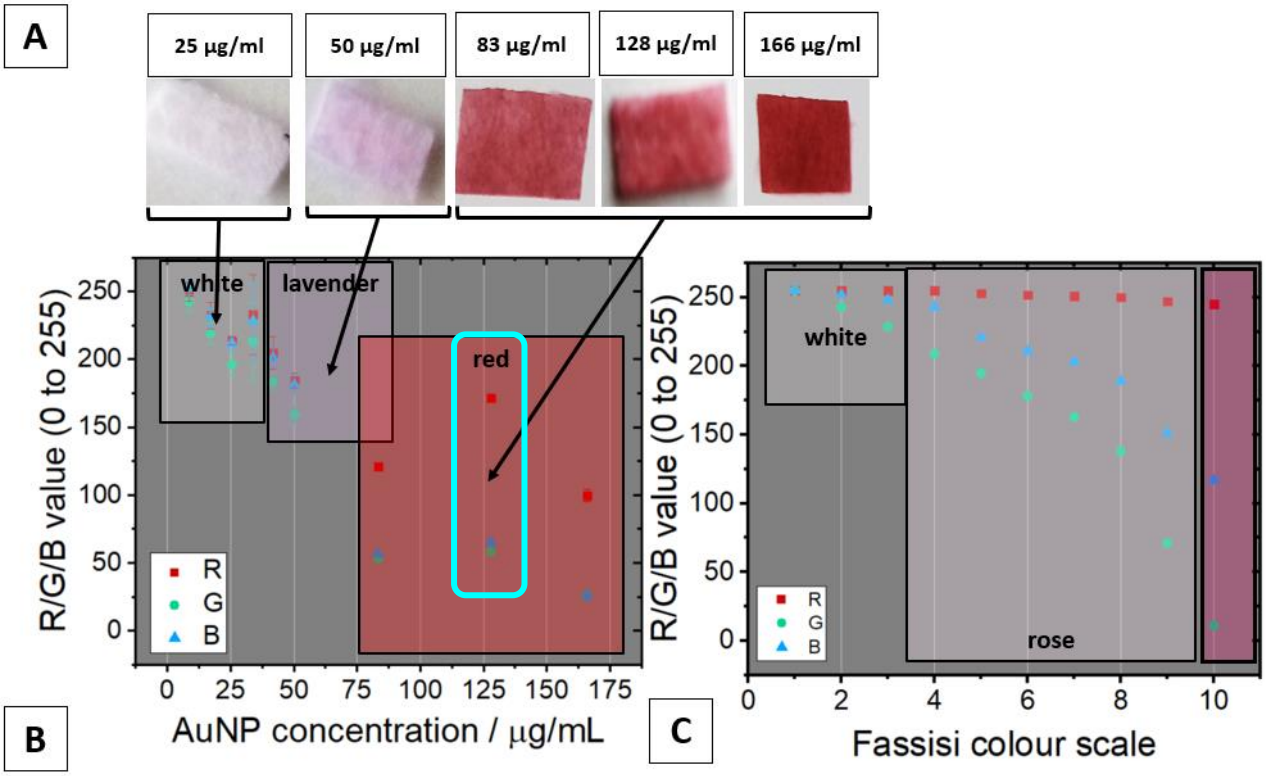

Figure 48: A) Conjugate pads (3x washed at pH 7.5) incubated with conjugates at a varying concentration of Au NP. **B)** resulting colors in RGB values. All conjugates featured the 4x HEGL ampicillin aptamer except for the one marked via the cyan box; it features a miniStrep conjugate. **C)** Fassisi color scale (10 equals the best color possible) transformed into RGB values for comparison. RGB values for the different colors were determined via PowerPoint. Brightness and contrast of all images were increased by 20.

No tested conjugate featuring the Ampicillin aptamer and an Au NP concentration of up to 50 µg/mL provided sufficient staining of the conjugate pad. However, the staining of the conjugate pads remained even for 2 days. To see whether an increase in the Au NP concentration could even improve this effect, a conjugate featuring 10 µM miniStrep – Aptamer and 128 µg/mL 30 nm Au NP was used as an incubation medium for a glass fiber conjugate pad. The miniStrep-Aptamer was chosen for this experiment since this kind of test requires huge amounts of aptamer and the supply of HEGL-Amp-aptamer (#183408) was limited in the project. It could be shown that this conjugate provided a strong red staining of the conjugate – a strong indication, that this conjugate pad will be of

use in LFAs and a sufficient amount of nano-bioconjugates will be available for the staining of the test line. Based on this approach, further conjugate pads were prepared, featuring HEGL-Amp-aptamer-conjugate at an Au NP-conc. of 83 µg/mL and 166 µg/mL. Both samples provided strong red staining of the conjugate pad. However, the strong color changed after a few hours of incubation (see **Figure 49**).

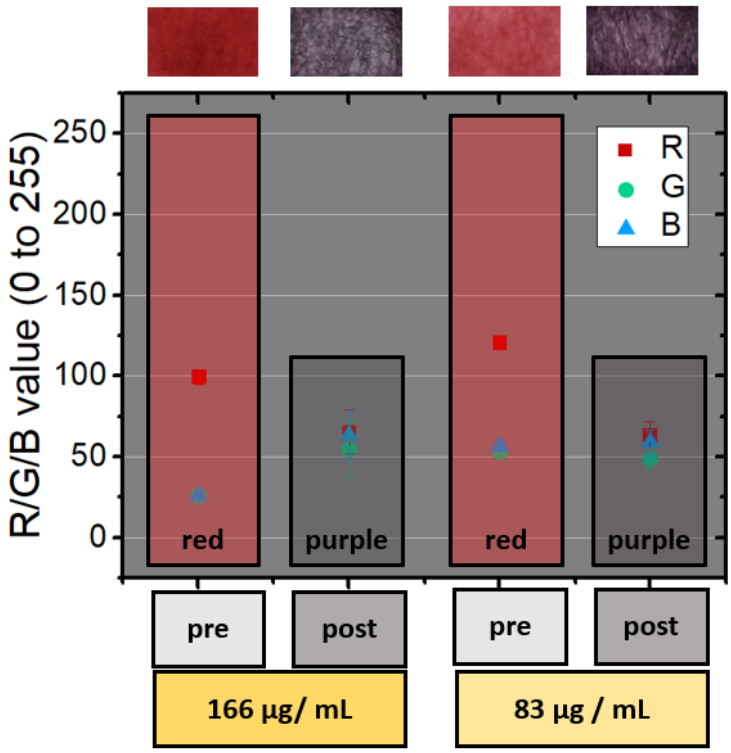

Figure 49: Conjugate pads prepared via dipping technique as described by EMD Millipore were photographed directly after the dipping process (**pre**) and after 1 h of drying at 37°C (**post**). Results are provided for conjugate featuring 166 µg/mL Au NP and 83 µg/mL Au NP.

Thus, further experiments were performed to optimize the drying process of the conjugate. Saccharose was applied in larger quantities and the temperature during the drying process was increased to 40°C. Analogue to the dehybridization of randomly bound and self-hybridized DNA strands via heat treatment (HT; 95°C) before polymerase chain reaction (PCR). This pre-treatment was also utilized to pre-treat the ampicillin solution before conjugating. Conjugation was performed as usual (final concentration: 0.3 M NaCl) and the conjugates transferred onto glass fiber and dried for two hours at 40°C (see **Figure 50**).

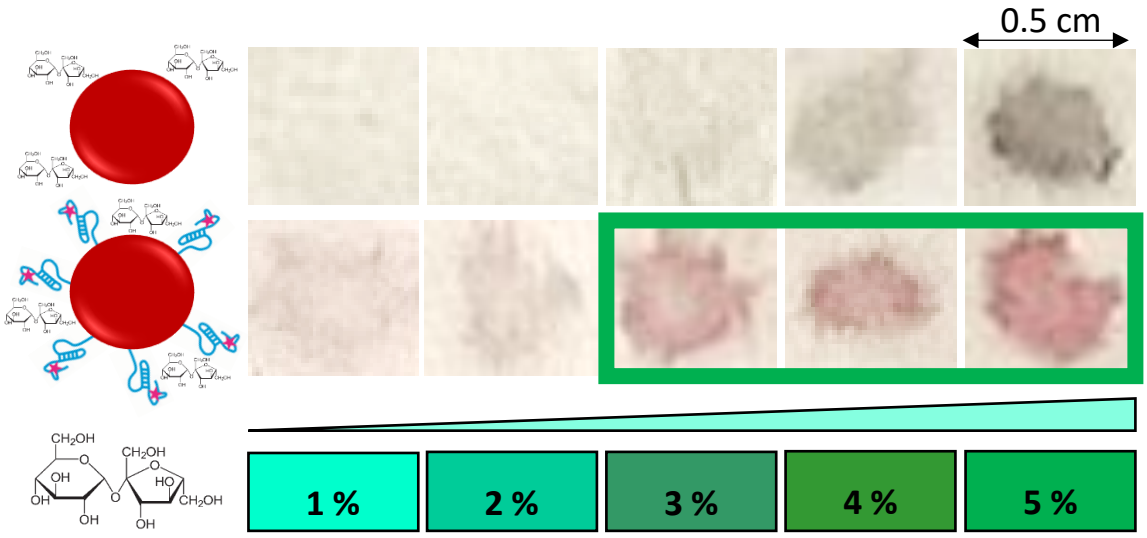

Figure 50*:* Pure nanoparticles in saccharose solution (top row) vs. aptamer-np-conjugates in saccharose solution (lower row)

As can be seen, the conjugates treated with 3 wt% saccharose showed only limited color change, due to the drying process, whereas samples treated with 5 wt% saccharose did not lose their strong reddish color. The resulting colors were quantified via RGB analysis (see **Figure 51**).

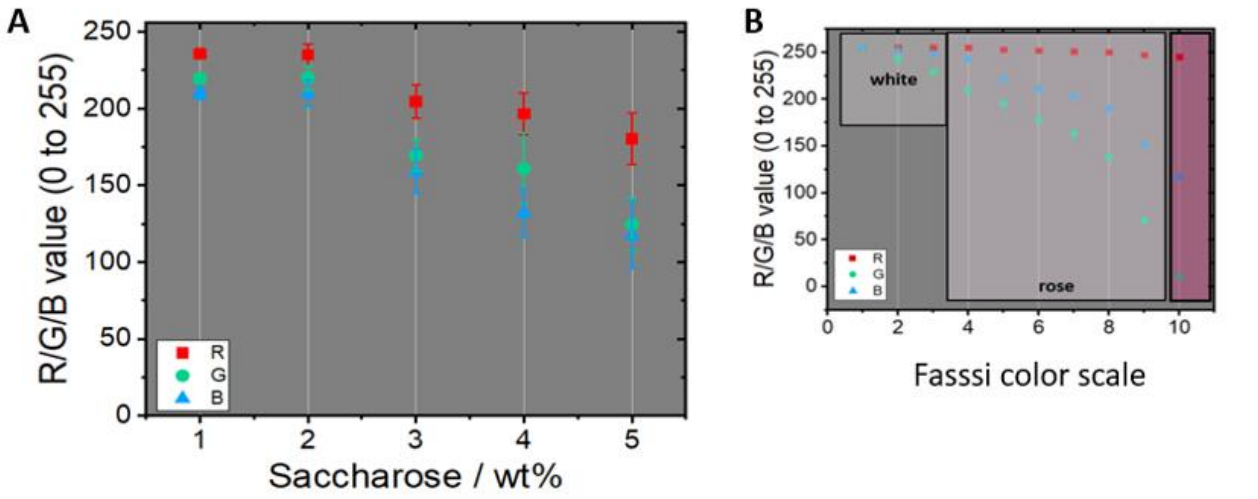

Figure 51: RGB analysis of loaded glass fibre after addition of 5 µL conjugate (heat treated at 98°C for 5 min) featuring different weight percentages of saccharose. (A) Fassisi color scale for comparison (1; worst to 10; best result).

Due to the overall appearance (RGB, which was chosen instead of the introduced RR-value to allow for better comparability with the established Fassisi color scale, and UV-Vis analysis) 5 wt% saccharose were used for all following experiments. When tested on streptavidin-labeled test stripes, the conjugates were able to generate a clear test line staining.

Within this subchapter, it could be shown why the initial application of the conjugate onto the glass fiber might have failed and lead to the vanishing of the stable nano-bio-conjugates. Incubation of conjugate pads with conjugates require at least an Au NP concentration above 50 µg/mL. The conjugate pad´s incubation within the conjugate seems to be the suitable technique to apply conjugate onto the glass fiber. The conjugate pad must be washed 3 times before the incubation procedure. The ideal pH must be analyzed for every test system individually. The existence of a threshold concentration, required for the successful preparation of the conjugate pad, leads to the assumption, that only a small fraction of the conjugate can anchor in such a manner onto the glass fiber, that it can be redispersed again. The dark, purplish spots which can been seen in e.g., **Figure 42**, might indicate the agglomeration and aggregation of conjugates within in the glass fiber. Agglomeration leads to an increased extinction of red light, which typically can be seen as purple color. Only if excess conjugate is presented, successful anchoring events can take place and sufficient conjugates are available for redispersion and target binding.

3.3.4 Lateral Flow Assay Functionality Readout

In addition to the optimization of the LFA and its conjugate pad a different approach was experimentally tested, see **Figure 52**. This approach is a modification of the LFA presented by Zhou et al. [212].

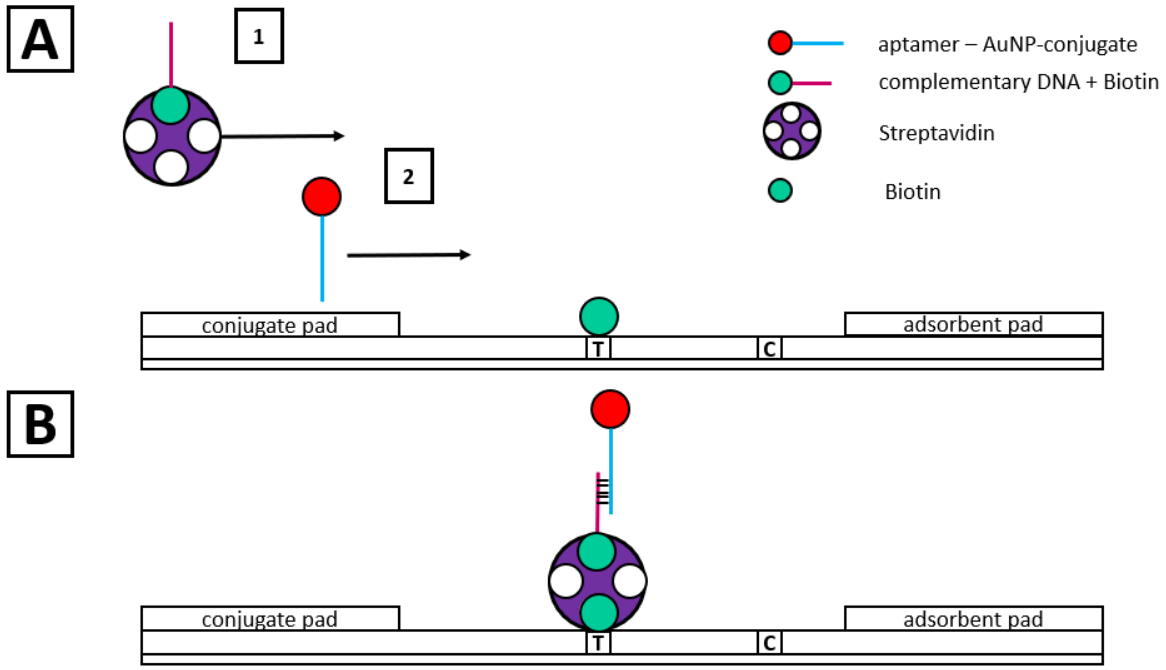

Figure 52: A) Biotin-labelled (test line) nitrocellulose membrane. 1) binding of streptavidin – biotin labelled complementary oligonucleotide probe to biotin on test line. 2) Hybridization of aptamer – Au NP conjugate to DNA probe. B) resulting construct on stained test line. T = test line; C = control line.

A biotin – labeled complementary oligonucleotide is coincubated with streptavidin. This probe is then linked to the test-line of the test tripe via biotin-streptavidin binding. After washing off unbound streptavidin-biotin-DNA probe, the aptamer-Au NP conjugate is given onto the test tripe and binds to the DNA – probe onto the test line, thus, generating a red staining.

However, the red stain is hardly visible with the naked eye and ever harder to detect after digital post-processing, compare **Figure 53**. The amount of streptavidin (from 1 µM to 0.1 µM) was decreased for follow-up experiments; to see whether sterically hindrance disturbs the successful binding of conjugate onto the test line.

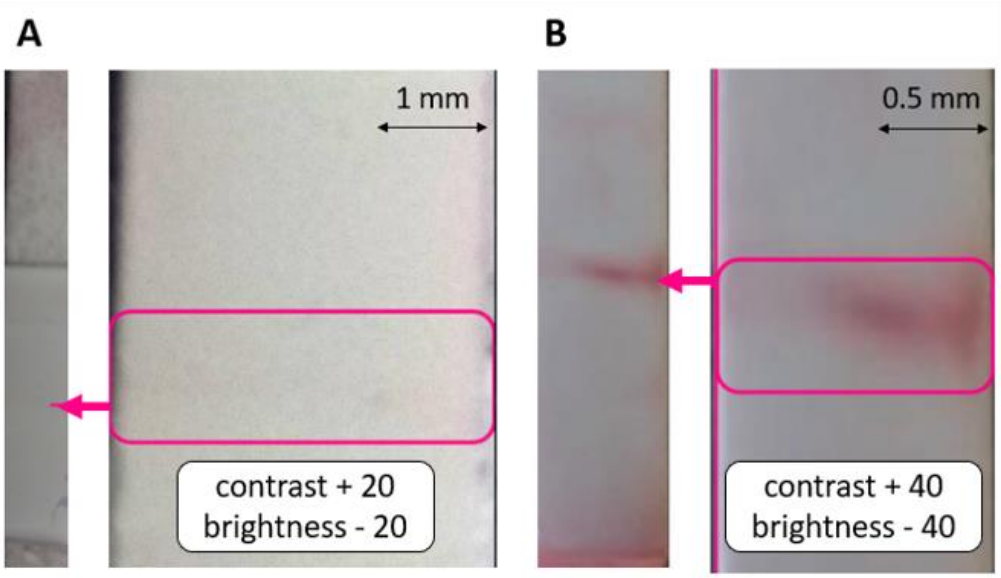

Figure 53: A) Microcoat LFA after treatment with DNA-probe (0.2 µmol) and aptamer – 30 nm Au NP – addition. A weak staining of test line is visible with the bare eye. **B)** Microcoat LFA after treatment with DNA-probe (0.01 µmol) and aptamer – Au NP – addition. A strong staining of the test line is visible.

This successful test stripe served as proof of concept and was further optimized as can be seen later in **Figure 56**. The bad quality of the test line result can be explained by the long storage time of the LFAs, two low humidity during the running process and the complexity of the construct (biotin – streptavidin – biotin-oligo – aptamer-NP-conjugate). The biotin-test line was furthermore replaced by a streptavidin-labeled test line to allow for a direct binding of the DNA probe.

3.3.5 Ampicillin-Test-System – combining all advances to design a working POC device

The main findings described in this work focus on the functionalization of laser-generated gold nanoparticles with aptamer sequences to either bind ochratoxin A or streptavidin. Only limited data have been shown regarding the ampicillin test system so far. However, due to the thesis´ main focus, which is mainly driven by the design of a marketable LFA test system, and its advances in the design of an ampicillin aptamer, the ampicillin test system became the main candidate for the design of a marketable application. The following chapter represents a transfer of ideas and improvements made for the basic test systems towards this main system. Hence, this chapter builds upon the experiments described earlier. Samples were conjugated with the ampicillin aptamer, which had been previously described by Song et al. [36]. In contrast to the work of Song et al. the aptamer sequence was elongated and a 4x hexaethylenglycol (HEGL), respectively an 8x HEGL-Spacer, was added. HEGL is typically used as a terminator for DNA polymerases in molecular biology [58]. Here, it serves as uncharged spacer sequence. Thus, it provides steric distance between the folded aptamer and the nanoparticle surface,

without the requirement for additional charge screening agent, who would decrease the resulting conjugate stability. The spacer sequence is required to allow for optimal folding as was shown in studies by Barchanski et al. [28]. Typical spacer sequences consist of adenine or thymine sequences, which are added to the aptamer [30], yet they can bind unspecific to the Au NP surface and cause the aptamer to lose its function [177]. Due to its uncharged nature, it is most unlikely that HEGL spacer sequences will introduce such unwanted binding events to the nanoparticle surface.

Two aptamers were compared to each other: one featuring the 4x HEGL spacer and the other featuring 8x HEGL spacer (see **Figure 54**).

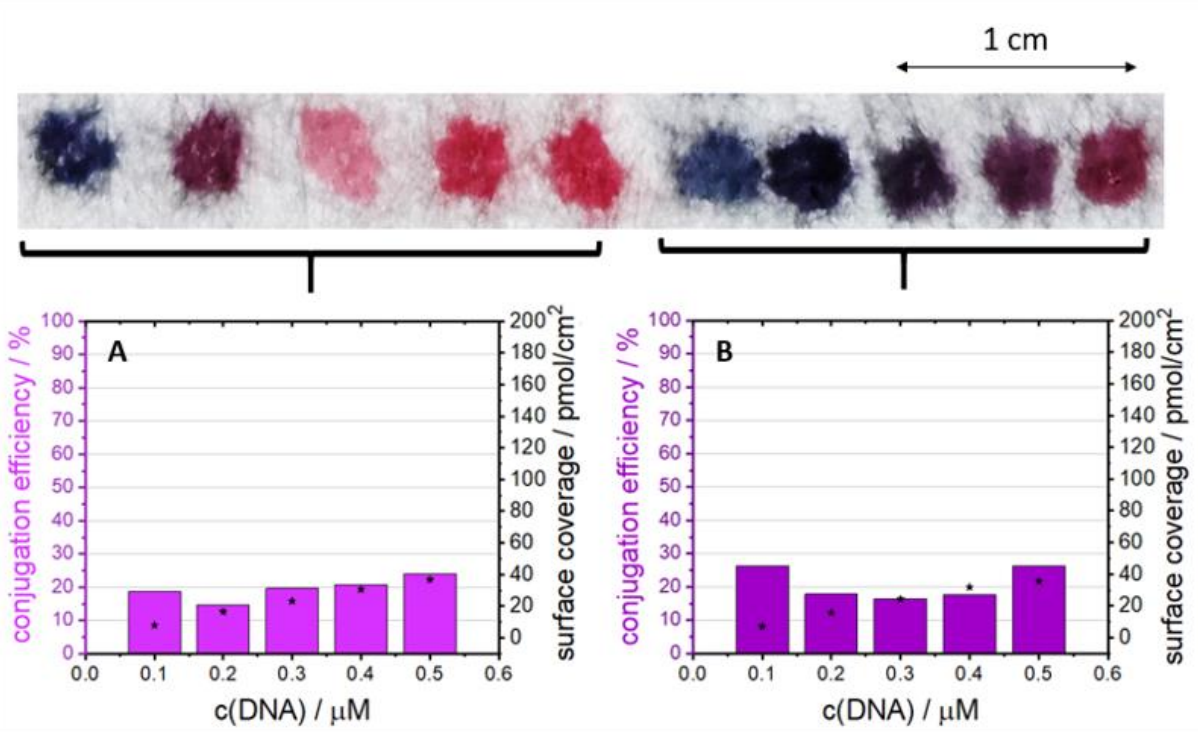

Figure 54: Initial low-surface-coverage conjugations of the Amp-4x-HEGL aptamer (A) and Amp-8x-HEGL aptamer (B) onto 30 nm LAL-Au NP.

The spacer length does not influence the conjugation behavior drastically. Both approaches lead to almost the same surface coverage at maximal applied DNA concentration of 0.5 µM. However, the stability differs significantly, especially when transferred onto glass fiber. All samples featuring the 8x HEGL-spacer turned purple/bluish, whereas the highest tested DNA concentration for the 4x HEGL-spacer aptamer remained reddish, which is a strong indicator for conjugate stability. Due to the cost-intensive 8 x HEGL spacer and the reduced conjugate stability, this approach was discarded. Future work could be conducted on the question what HEGL-spacer length is optimal for this specific aptamer. However, this question is beyond the scope of this work. Since the highest utilized DNA concentration leads to improved conjugate stability the test range was extended up to 3.0 µM aptamer concentration (see **Figure 55**).

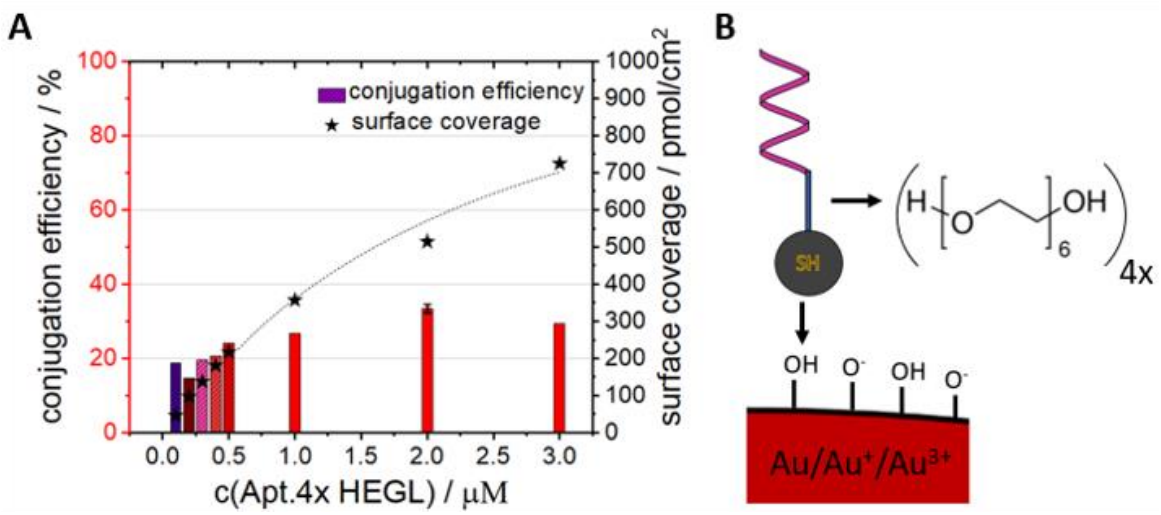

Figure 55: Conjugation of 30 nm Au NP with Amp-4xHEGL-aptamer. Conjugation from 1.0 µM aptamer concentration on were performed in triplicates. Dashed line provides guidance to the eye. (A) Schematic scheme of aptamer during nano-bio-conjugation including its 4x HEGL spacer (formula by Sigma Aldrich; B)

In accordance with the literature on the conjugation of laser-generated nanoparticles with thiolated, single-stranded DNA molecules, the generated surface coverages increased with increasing DNA concentration. However, a saturation at DNA excess concentration can be seen. [292]. Interestingly the conjugation efficiency remains relatively constant between 20 % to 30%. Typically, the conjugation efficiency drops drastically at higher DNA concentrations since bound DNA blocks the surface for further conjugation of DNA molecules [25,175,292]. It is known for PEG to support the loading of the nanoparticle´s surface by guiding the thiolated DNA molecules to the surface, while suppressing the charge repulsion of already attached DNA strands. [329] Based on the observations it can be concluded that the HEGL spacer might as well allow for more effective transfer of thiolated DNA strands after the initial attachment phase. Yet, the question if the HEGL spacer interferes with the ampicillin aptamer´s functionality remains unanswered. It has been described by Bosco et al. that a HEGL spacer can positively influence the aptamers´ functionality [330]. This effect is mainly explained by the ability of uncharged ligands like e.g. PEG to avoid unwanted binding events through steric hindrance [331,332]. Nevertheless, the influence of the HEGL spacer on the conjugation procedure and its influence on aptamer functionality lacks an intense study. The results shown in this work indicate that the replacement of negatively charged phosphate backbone bearing DNA with the 4x HEGL spacer allows excess DNA to slip through the initial DNA monolayer more easily, thus improving the conjugation efficiency. Ultimately, this leads to high surface coverages of above 700 pmol/cm^2 at moderate aptamer resource input. Hence, the aptamer improvement contributes once again to the green chemistry approach of nano-bio-conjugation, which serves as a common motive throughout this work.

Future work will have to focus to understand the full influence of the HEGL-spacer system on the conjugation behavior of laser-generated nanoparticles. Since it was possible to generate stable and glass fiber-compatible conjugates, this basic research remains an interesting challenge for the future. Within the scope of this work, the ideal conjugation procedure for ampicillin carrying nano-bio-conjugates was found. The 30 nm LAL-Au NP were subsequently conjugated with 2.0 µM 4x HEGL-Amp-aptamer. The conjugates were subsequently heat-treated at 95°C for 5 min in accordance to Song et al. [36], coincubated with the DNA-probe, transferred onto glass fiber via dipping (data not shown), dried at 40°C for 2 h and finally redispersed via binding buffer onto the Microcoat test strips. The resulting LFA runs are shown in **Figure 56**.

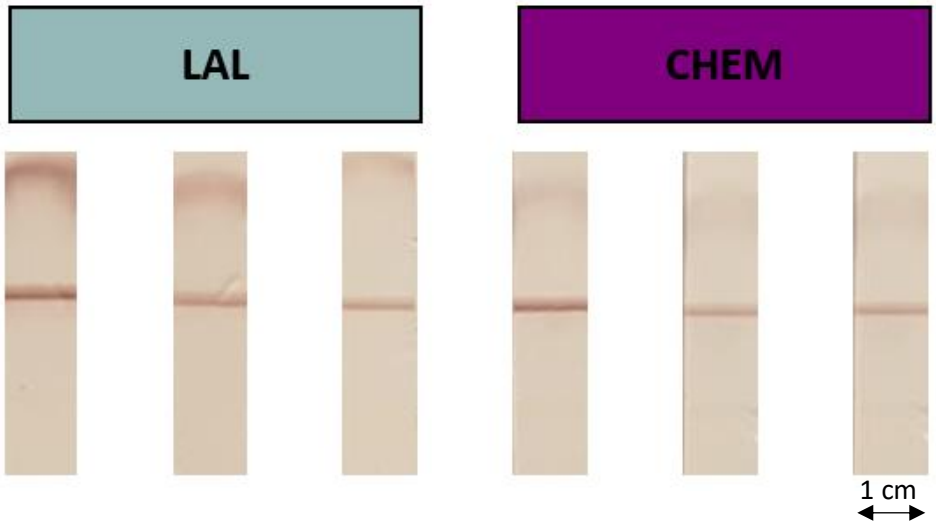

Figure 56: Triplicates of streptavidin-labeled LFAs featuring LAL-nano-bio-conjugates (left) and Fassisi-nano-bio-conjugates (same DNA concentration applied throughout conjugation).

After intensive testing and based on the optimization procedures presented in the previous paragraph, an ideal pre-treatment, conjugation process, lateral-flow-assay-preparation, composition, and its optimal running conditions can be presented (see **Figure 57**).

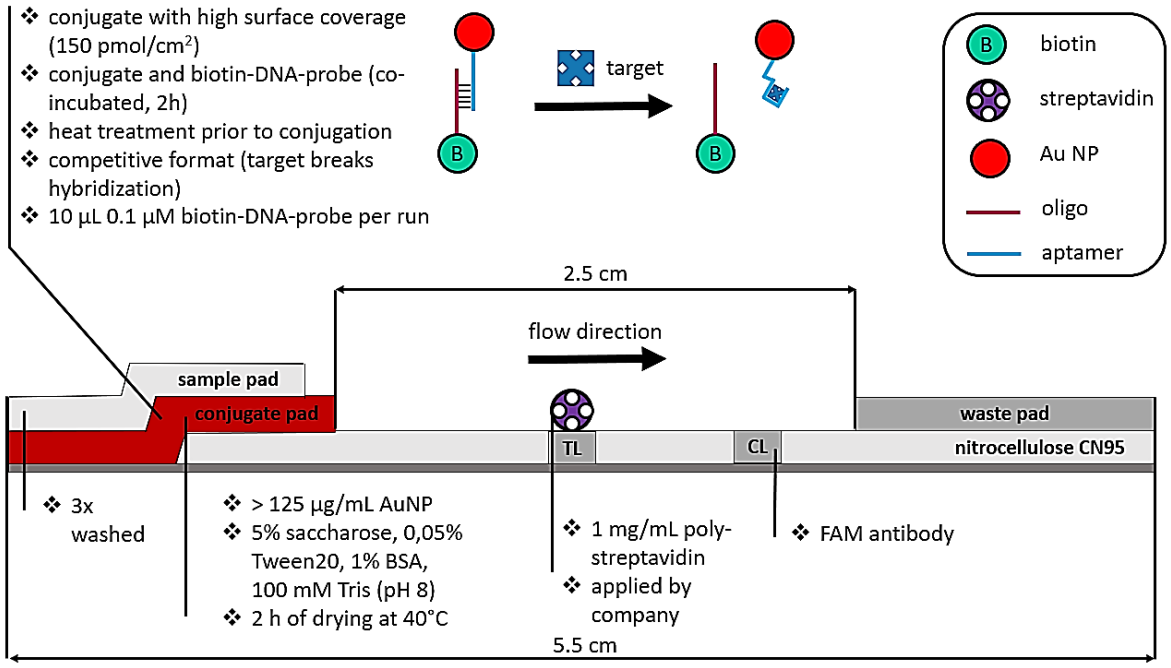

Figure 57: Schematic overview over an optimized LAL-Au NP – aptamer – LFA system; competitive assay for the detection of ampicillin

The transferability of insights regarding the conjugation behavior of aptamers onto laser-generated NP and the conjugate stability towards the ampicillin test systems indicates that this LFA system can serve as general platform for all LFA-systems featuring laser-generated NP in combination with aptamers. In-silico analysis, detailed information about the properties of the target molecule and its specific aptamer concerning pH optimum and ideal surface coverage, can be utilized to expand the field of application of this simple POC-device massively. Nevertheless, differences have been found for every researched aptamer. Due to the unique nature of its specific three-dimensional folding, each aptamer is expected to act differently. However, since the generation of a visible readout of this test device is purely based on the biotin-streptavidin binding platform technology, it can be expected that it can be easily adjusted for other analytes. However, its very design as competitive assay, makes it more suitable for small analyte molecules. Ultimately the ampicillin – system was able to generate a positive test result for the 4xHEGL-Amp-aptamer – LAL Au NP – conjugate. The upper most important change so far was the immobilization of the complementary oligonucleotide via biotin – streptavidin linkage onto the nitrocellulose membrane as described by Zhou et al. [212]

3.4. Recycling Aptamers – An approach towards atom economy

The price advantage of aptamers over antibodies should not lead to the false conclusion that aptamers are cheap and readily available materials. Based on data provided by AptaGen, LLC, the average aptamer costs 238 ± 123 €/g, depending on its sequence length and its respective modifications (C6-spacer, thiol-modification, PEG-spacer, fluorescence label, etc.). So far, the method of choice in the matter of conjugation of DNA to noble metal nanoparticles remains the utilization of excess DNA in combination with subsequent salt-aging. As shown throughout literature for chemically synthesized nanoparticles, as well as above shown for laser-generated particles, the conjugation efficiency drops with increasing DNA concentration. Laser-generated nanoparticles provide a cost-effective and energetical preferable alternative to their chemically-synthesized counterparts. Thus, they represent an asset in the field of green chemistry. In conclusion its only logical to transfer this advantage into the field of nano bioconjugates. Excess utilization of DNA strictly contradicts the credo of atom economy, which represents one major pillar of the principles of green chemistry. Therefore, this section introduces an approach on aptamer recycling – which can be easily adapted by researchers in the field of nano-bioconjugates featuring aptamers. It will be subsequently discussed if and how the presented techniques can be scaled-up towards pilot plant scale. However, the focus remains on the laboratory scale.

The UV-vis extinction spectroscopy quantification of unbound ligands in the supernatant after centrifugal separation of the generated nano-bioconjugates and unbound aptamer ligands remains the state-of-the-art technique in the field of bioconjugation to determine their surface coverage. It was demonstrated by Petersen and Barcikowski that it does not lead to significantly different results like the previously described method of ligand exchange via DTT – a precise yet destructive method. Thus, the supernatant-analysis-approach does not only provide reliable data on the surface coverage but also allows the subsequent utilization of the generated conjugate in follow-up experiments. [25] **Figure 58** shows supernatants of two subsequently performed conjugations processes – both featuring the modified OtA aptamer (Apt1N) featuring an improved spacer sequence.

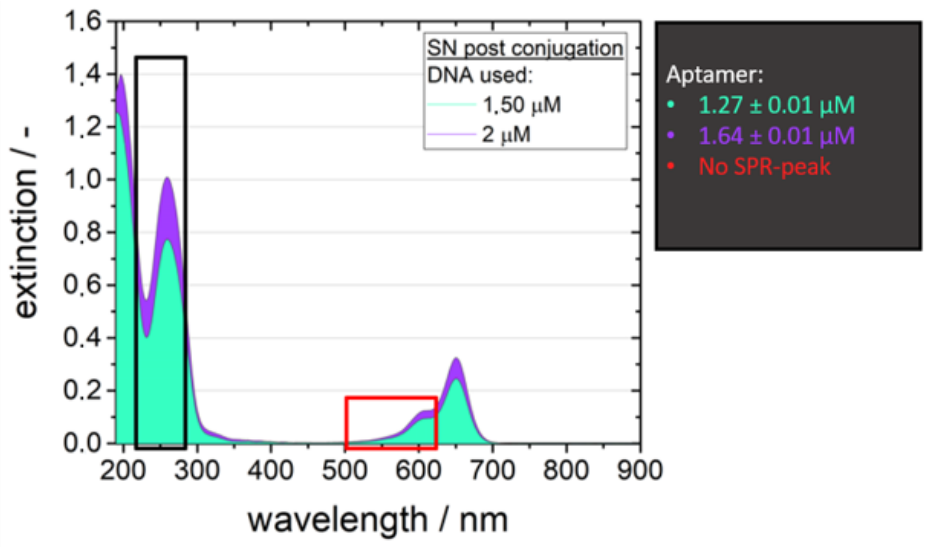

Figure 58: UV-vis extinction spectra of unbound ligands, retrieved after a conjugation procedure via ultracentrifugation (100.000 g, 1 h, 7°C). Black box marks the DNA-typical strong extinction at 260 nm, whereas the red box marks the possible SPR extinction of nanoparticles. The peak in this area can be attributed to the Cy5-label of the utilized aptamer.

The first conjugation (purple) featured 2 µM aptamer as starting concentration. The aptamer was taken directly from its manufacturer`s vile and had never been used in previous experiments. Since an excess amount of DNA was utilized, high concentration of unbound DNA was detected in the supernatant resulting from the conjugate purification procedure. The supernatant did not show any significant signal indicating the presence of residual Au NP, yet a strong extinction can be observed at 260 nm and at around 650 nm. The 260 nm signal can be assigned to the DNA extinction maximum, whereas the peak at 650 can be assigned to the Cy5-fluorescence label of the DNA. Furthermore, the presence of any interfering organic ligands can be excluded, since the generation of laser-generated nanoparticles does not introduce any unwanted organic ligands into the conjugate system. The recovered aptamer was subsequently used for a second conjugation. All parameters, like Au NP concentration, salt aging procedure, incubation time were kept constant, however the maximal used DNA concentration had to be readjusted to 1.5 µM since too much DNA had been bound to the nanoparticles during the first conjugation. Here, future work could also include the concentration of previously utilized aptamers via speed-vac-centrifugation or membrane-based processes to provide ideal conditions for comparability. However, the question rises how the ´recycling´ process influences the generated conjugates in their stability and functionality. **Figure 59** shows UV-Vis extinction spectra of a conjugate with fresh aptamer and two conjugates featuring the same subsequently recycled aptamer. The negative control (Au NP + recycled aptamer) was performed without salt-aging procedure, whereas the recycling conjugate was adjusted to the same salt concentration as the original conjugate.

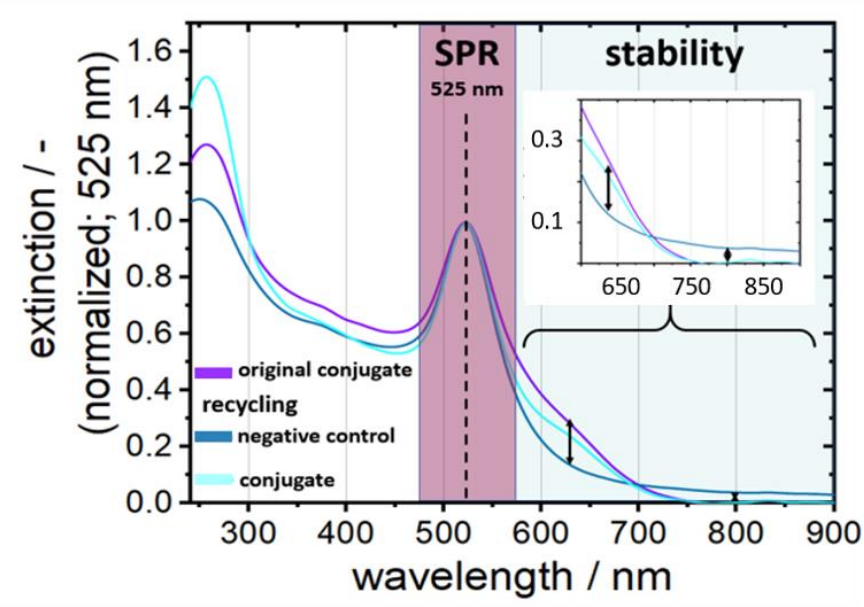

Figure 59: UV-vis extinction spectrum of three conjugates as proof of concept for a lab-scale aptamer recycling procedure. The term "original" refers to the utilization of aptamers, which had not previously been used in experiments, whereas the term recycled refers to aptamers, which were isolated as unbound ligands subsequently to a conjugation procedure and were exposed to the salt-aging process

No notable differences in the SPR-shift for all three conjugation approaches were observed, indicating a successful aptamer-functionalization of all samples. However, the ´double´ salt-aged sample precipitated within a few hours. Only the original conjugate and the negative control remained stable. If one looks at the conjugation efficiency, the double salt aged sample provided a 19 % increase of conjugation efficiency. This can be explained by the accumulation of Mg^{2+} cations in approximation to the negatively charged DNA strands, in accordance to observations of Kewalramani et al in 2013 [183]. The already accumulated Mg^{2+} cations add up with the added second load of Mg^{2+} cations to an increased total Mg^{2+} cations concentration, thus, leading to an increased surface coverage and conjugation efficiency. However, due to the resulting high charge screening screen charging activity, as well as the introduction to inter-strand-interactions between different conjugate particles, this might ultimately lead to the conjugate destabilization and its aggregation.

Ultimately laser-generated nanoparticles were conjugated with ampicillin aptamer and tested under the conditions described in **Figure 57**. The residual, unbound DNA was subsequently utilized for a second conjugation procedure of the respective colloids. However, the second conjugation procedures were performed via salt-aging with NaCl (up to a final concentration of 0.3 M), as well as, without any salt-aging (negative control). The performance of the original conjugates, featuring fresh aptamer, as wells as, conjugates featuring recycled aptamer are shown in **Figure 60**.

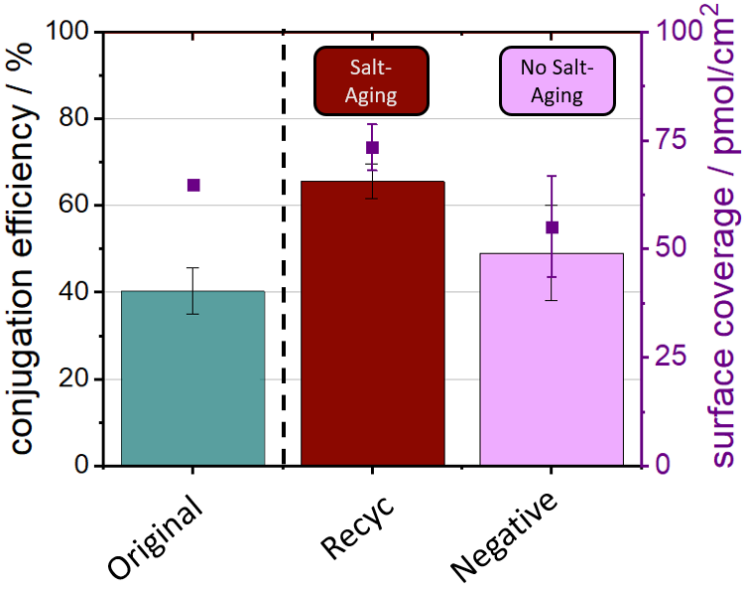

Figure 60: Conjugation of 30 nm Au NP with Amp aptamer (Starting concentration 2 µM) and the respective Recycling (Recyc) conjugate. Negative controls did not undergo the salt-aging procedure. The conjugations were performed in triplicates. Original = fresh aptamer; Recyc = recovered aptamer + salt-aging; Negative = recovered aptamer without salt-aging.

The general conjugation efficiency is lower for the Ampicillin test-system, leading only to a total usage of 79.4 % of the originally introduced aptamer in comparison to the OtA aptamer, but the nature of the Amp aptamer, makes it impossible to perform the highly efficient salt-aging procedure via $MgCl_2$ addition. However, the second conjugation procedure lead to an increased conjugation efficiency and therefore to higher surface coverage, which is once again in accordance to observations of Kewalramani et al in 2013 [183]. Interestingly, the negative control without any additional salt added, still provides an increased conjugation efficiency and a surface coverage of comparable to the original conjugate. This finding opens interesting optimization approaches to adjust the conjugate to the desired surface coverage with minor working steps.

Finally, the functionality of the Amp aptamer test system was evaluated using an original conjugate, one salt-aged with retrieved, previously used aptamer (Recyc), and one without salt-aging, but previously used aptamer (Negative). The results are shown in **Figure 61 A**.

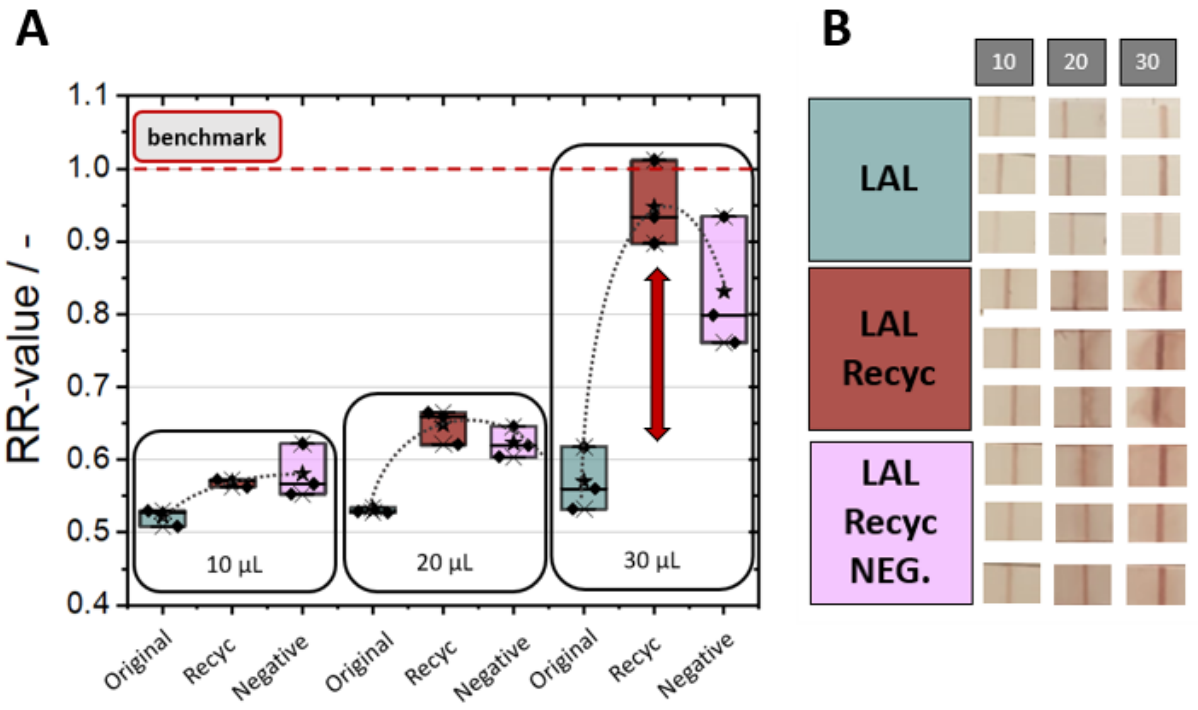

Figure 61*:* A) Conjugation of Au NP with fresh and recycled aptamers. Negative controls lack the additional salt-aging procedure. B) LFAs featuring LAL-conjugate (fresh aptamer), LAL Recyc (featuring recycled aptamer), LAL Recyc NEG. (featuring recycled aptamer without second salt-aging.). Grey boxes indicate the applied conjugate volume in µL.

Three different volumes of the respective conjugates were applied onto the LFA-system (10 µL, 20 µL, and 30 µL). The RR-value was chosen as main value for functionality evaluation via color signal quantification, since LFAs must provide a strong red color. Deviations in color are always linked to instability and a lack of function for colloids feature pure noble metal nanoparticles, whereas a strong red indicates the desired state at the test line. As mentioned in chapter 5 “LFA optimization”, the RR-value represents a fast and easily accessible evaluation method for conjugate stability and was used to evaluate the test line of LFAs. The originally conjugated LAL-NP exhibited a RR-value below 0.55 when bound to the test line. It must be mentioned that the opaqueness of the nitrocellulose does interfere with the evaluation of the RR-value, however, there is no significant difference in the behavior of LAL NP for either 10 µL, 20 µL, or 30 µL. The staining of the test line becomes more reddish (**Figure *61 B***).

However, the average RR-values of the tested samples does not exceed the value of 0.6. A drastically increase of reddishness can be seen for the recycled samples throughout all tested volumes. In general, the negative samples – lacking the second salt-aging procedure – exhibited reduced RR-values in comparison to the twice aged samples. Hence the higher surface coverage achieved for the twice-aged

samples seems to provide improved binding towards the test line. Yet it is interesting, that the achieved color remains still better than for the original conjugates. Hence, the recycled aptamer features already cations in between it strands, which allow for an improved second conjugation procedure, which was to be expected on the findings of Kewalramani et al., who could show, that the cation concentration in between DNA strands exceeds the cation concentration in the bulk solution. [183] Aptamers participating in the first conjugation procedure, without successfully binding to the Au NP surface, did attracted counter ions of the first salt-aging. During the second conjugation procedure, the bound cations provided the required charge screening for a successful conjugation in the recycling run. The observed improved functionality of the two-times aged conjugates is in accordance with the very findings first described by Hurst et al.; higher salt concentration leads to higher surface coverages. [175] The higher surface coverages seem to lead to better functionality in the end. The optimal surface coverage of this particular system has yet to be found and remains a topic for future work. However, it has to be considered that very high surface coverages with e.g. antibodies are known to reduce the sensitivity of the test system in the end as was shown by Urusov et al. [333]. This effect might also be encountered for recycled aptamer conjugates and must be taken into consideration for future experiments. Another challenge might be the additional charge screening due to the higher salt concentration in between the aptamer strands, causing a decrease in colloidal stability. Future work needs to be conducted on how to further improve the colloidal stability of the conjugates.

However, with a new conjugation protocol at hand, the question arises, if it is possible to quantify the advantage of the recycling procedure. Here, multiple aspects must be taken into consideration. First, one must understand the total cost of a conjugate batch in the lab scale. The following calculations were made under the assumptions that a 1 ml conjugate batch would be prepared, leading to a final volume of approx. 100 µL ready-to-use-conjugate after the centrifugal clean-up procedure. This 100 µL could be used in batches of 10 µL on a total of 10 LFAs (96-well-plate preparation). Thus, allowing to analyze 3 different settings for one experimental parameter (e.g. ideal label concentration, ideal surface coverage, etc.). One test stripe out of ten would serve as reserve to repeat a failed test-run, as can be strongly recommended for experiments with LFAs after intense experimental work in this field. All these assumptions allow it to combine the expected costs for the lab scale into one single number: price per tested parameter (€). One may wish to improve the experimental data by increased repetitions or testing more variations of the same parameter, but for an initial evaluation it might be sufficient to test just three expressions per parameter (e.g. low, mediocre, and high surface coverage).

Based on the calculations and experiments of Jendrzej et al., it can be calculated, that the gold colloid contributes only minimal to the cost a conjugate with less than a percent, here equal to 0.07 euro cent per 1 mL conjugate. [22] Material costs for LFAs, like e.g. nitrocellulose, Whatman paper, as well as

plastic cardboard as support in addition to the small production scale for lab conditions leads to costs of 2.5 € per test stripe (based on test stripes ordered from Microcoat Biotechnologie GmbH) . However, the aptamer represents the lion´s share with up to $ 1 - $ 4 (0.82 € - 3.29 €; state of the art June 2021) per microgram (data taken from Aptagen, LLC). So far, the experimental data of this work coincidence with the literature on aptamer-based LFA systems, indicating that high DNA concentrations are required for the successful functionalization of nanoparticles and their subsequent usage in LFAs. [123,205,209,211] The amount of required DNA as well as the information on its price lead to the finding, that the aptamer makes up to 90 % of the total cost of a lab-scale aptamer-based LFA test (compare **Figure 62 A**).

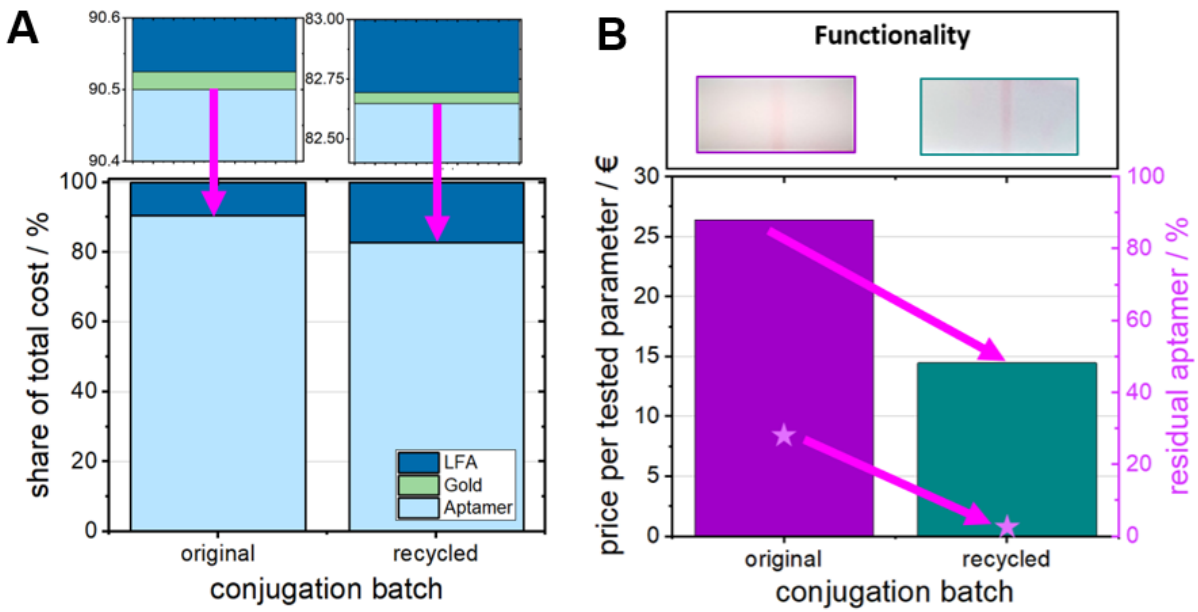

Figure 62: A) Share of total cost of a 1 mL conjugate batch featuring laser-generated Au NP conjugated with aptamer. The term "original" refers to the utilization of aptamers, which had not previously been used in experiments, whereas the term recycled refers to aptamers, which were isolated as unbound ligands subsequently to an conjugation procedure and were exposed to the salt-aging process. B) Price per tested parameter (referring to a 1.0 mL conjugate batch used in 10 subsequent LFA test runs at lab scale; working hours not included, only material costs). Residual aptamer refers to the amount of unbound DNA ligands after the second conjugation procedure in comparison to the originally applied DNA concentration. Fassisi test stripes with complementary oligonucleotide (0.001 mM) loaded test line were used.

If the unbound aptamer can be returned and once again be utilized in subsequent conjugation procedures, a shift in the total cost can be observed. The aptamer will only account for 82.6 % of the total cost. In concrete numbers the price for a statistically usable data acquisition (here = 10 measurements per parameter, based on 100 µL conjugate volume per well of a 96-well-plaze), drops from 26.38 € to 14.44 € for the lab-scale (compare **Figure 62 B**). At this stage it is hard to estimate the total amount of money that could be saved on pilot plant or even industrial plant scale since prices for the required materials strongly vary over time and in dependence on the purchased quantities. Typically, lab-scale represents the highest cost/unit price. Thus, the saving margin for larger scale

production is expected to drop less in comparison when aptamer recycling is introduced. Nevertheless, the aptamer represents the most valuable part of this production process. Thus, significant savings are to be expected in addition to contributing to green chemistry.

However, saving money and resources is only meaningful if the function of the generated conjugates can be guaranteed, for both the original and recycled aptamer. Here both, the original conjugate, and the negative control, lacking the second salt-aging procedure, still were able to bind to the utilized test line on an LFA test, providing a strong red signal. The residual unbound aptamer after the second conjugation was below 2 % of the original amount of DNA utilized. Thus, a 98 % total usage of the utilized aptamer, while upholding its function was achieved. These finding represent a first step towards a green chemistry nano-bioconjugate with maximal achievable atom economy.

In conclusion, it is possible to regain unbound aptamer ligands after the conjugation procedure via salt-aging. The recycled aptamers are readily available to be used in subsequent conjugation experiments, leading to functional conjugates, again. The procedure described here is suitable for lab-scale experiments and may be adapted for the pilot plant scale. It was possible to reduce the costs per tested parameter by 45 %, which may be even greater in the industrial scale. At the same time the atom economy could be improved towards 98 % regarding the utilized aptamer. Through the combination of green LAL-Au NP and a highly atom efficient conjugation procedure this work represents an important step towards green chemistry POC applications.

3.5 ASSURED criteria linked ranking of aptamer-based test systems for ochratoxin A and ampicillin detection

The demand for easy-to-use point of care diagnostic tools has drastically increased also due to the ongoing Covid-19 pandemic. Even though antibody-based LFA-test-systems remain the main answer to this high demand, aptamer-LFAs are an emerging field in point-of-care (POC) diagnostics. Assay formats using aptamers as detection units have been developed against multiple targets e.g., heavy metals, low molecular weight targets and food contaminants, though most of these systems have not yet been developed beyond the lab-scale and are not available on the free market. Even though aptamers represent a green alternative to the established antibodies and are particularly suitable for the detection of low molecular weight and non-immunogenic targets, systematic problems seem to prevent them from replacing their biological predecessors. This study introduces a quantitative evaluation of exemplary aptamer-based test systems in accordance with the ASSURED criteria by the WHO for the exemplary analytes ampicillin and ochratoxin A, which are of high relevance in food safety. It was found that aptamer-based LFAs systems perform on a wide working range above the requirements regarding the limit of detection (LOD) and specificity, yet require advanced analytical equipment for detection and evaluation, which decreases their suitability as POC diagnostic tools. Yet, the analyzed aptamer test systems could not significantly outperform their antibody counterparts concerning sensitivity and specificity. Hence, a potential replacement of antibodies with aptamers in such already established test systems seems less likely. The findings stress the need for a reorientation of the field of aptamer-based LFAs. New aptamer-LFAs must find their niche as either pure POC devices for the detection of non-immunogenic targets where no antibody alternatives exist, or as highly specific aptamer-based analytical test system. With this purpose-orientated separation in mind, aptamers could lead to significant improvements in both fields: POC-diagnostics and advanced analytical chemistry.

Introduction

Point-of-care testing plays a crucial role in pathogen control [334–337], food safety [338–340] and medical diagnostics [341]. Lateral flow assays represent one of the most important POC-diagnostic tools. Within recent years, aptamers were introduced as alternative to the state-of-the-art antibody capture agents of established LFAs [342–344]. Aptamers represent a green alternative to antibodies, and can be designed to bind non-immunogenic and highly toxic targets, can be more easily modified, and provide low batch to batch variations [249]. Aptamer-based test systems cover simple dipstick assays [345,346], dual recognition assays [347,348], fluorescence based assays [349], classical colorimetric approaches [350], magnetic aptasensors [351], as well as LFAs with computational

readout options [352,353]. United in the usage of aptamers as recognition elements, the units of detection vary from noble metal nanoparticles to quantum dots [354]. The readout strategies of LFAs cover manual readout based on eye-vision, mobile phone readout [355] or even advanced analytical techniques like surface enhanced Raman scattering. [356] This work will provide a bibliometric overview over aptamer-based LFA systems and introduce a rating system for the exemplary small molecule analytes ochratoxin A (OtA) and ampicillin (amp).

Ochratoxin A (OtA) represents a highly toxic compound that can cause severe damage to human organs and can be found in many everyday products, including coffee, beer, wine and grain [357]. Its hazardous nature and abundance have stimulated an increased interest in its cost-effective and easy POC – detection, which makes it an ideal model system for a critical and systematic comparison of its different detection systems. Several ochratoxin detecting POC devices were identified through literature research [118,119,122–124,200–202,204–213,340]. Ten of those represent a lateral flow assay test [118,119,122,124,200,204,207,208,211,212]. Only four test systems feature the Ochratoxin A aptamer (see **Figure 63**) in its original or modified form [118,123,205,211].

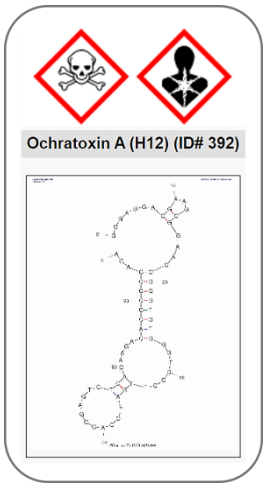

Figure 63: Apta Index info sheet regarding ochratoxin A (status 17.01.2022), information based on Barthelmebs et al. [201]

The β-lactam ampicillin represents one of the most commonly used antibiotics in modern diary industry and intensive livestock farming [358]. Its overuse does not only lead to its accumulation in milk and meat[359,360], but also hinders the production of cheese and yoghurt, since those products rely on living bacteria in their production line [361]. Ultimately, the excessive usage of ampicillin will lead to bacterial resistance rendering it useless. Besides that ampicillin can cause severe type I hypersensitivity reactions in humans, which is the main reason why it is so important to guarantee that the allowed maximum residual levels are not exceeded at all times. [358] Several commercially available test systems for ampicillin have been introduced in the past years [362–364] as well as a wide array of different biosensors [365–367]. This work focusses on 10 chosen ampicillin test systems; four featuring aptamers [5,36,368,369], five featuring antibodies [370–374] and one featuring a penicillin-binding protein [375]. The ampicillin aptamer published by Song et al. is shown in **Figure 64**.

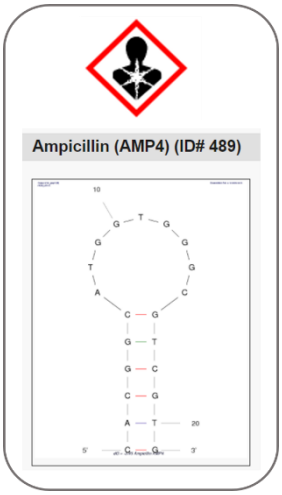

Figure 64: Apta Index info sheet regarding ampicillin (status 17.01.2022), information based on Song et al. [18].

Bibliometric Overview and introduction of an LFA rating system

This section represents an overview of existing aptamer-based point-of-care diagnostic tools, with a strong focus on LFAs. Even though many reviews regarding aptamer-based biosensors and POC-diagnostic tools exist [4,44,64,376–392], so far most of them focus on providing a comprehensive overview over the field itself and mostly just reproduce the content of the corresponding publications but lack a critical and systematic evaluation of the listed test systems. The aim of this review will be to establish a basic concept of a test system evaluation that may lead to a systematic understanding of the problems, limitations but also perspectives of an aptamer-based LFA. Thus, this review differs from its predecessors in that regard that it deliberately focuses its scope on exemplary analytes and provides an in-depth critical comparison of the tested formats. Hence, it will not only point out general strengths and weaknesses, but instead this evaluation will serve as a guide to identify if aptamer-LFAs are superior to the existing antibody-LFAs or not. Based on this, its main aim is to identify possible deadlocks, niches, and the unique features of aptamer-LFAs.

The data set of this collection is mainly based on Web of Science listed publications and the Apta Index of Aptagen, LLC. The Apta Index lists more than 526 aptamers (status 23.06.2021). A systematic study of lateral flow test systems using aptamers on Web of Science (advanced search, "TS=(aptamer* AND lateral flow)" plus "TS=(aptamer* AND LFA*); all years, all databases lead to a total of 193 relevant publications; 38 of those originating from 2021 and six originating from 2022 (status 17.01.2022). The research areas covered by these publications are shown in **Figure *65***.

Figure 65: Visualization of research areas based on a Web of Science advanced search ("TS=(aptamer* AND lateral flow)"; search was conduct on 17.01.2022.

As one notices, the utilization of aptamers for LFAs covers a broad selection of different fields. Of cause, fields like chemistry analytical (107), nanoscience and nanotechnology (42) are represented. Nevertheless, it is notable that application-based fields like e.g. food science technology (26), toxicology (5) are represented as they cover the main advantages of aptamers: the targeting of small, highly toxic, non-immunogenic substances [357]. Just like the numbers of publications regarding aptamers increased over time, exceeding the 250 publications per year in 2012 already [392], the number of publications regarding aptamer-based lateral flow assays has been increasing over the past years (see **Figure 66 A**). However, compared to the total number of publications in the field of aptamers, which peaked at 2330 publications in 2020, the field of aptamer-LFAs makes up only a small fraction in this regard (compare **Figure 66 B**).

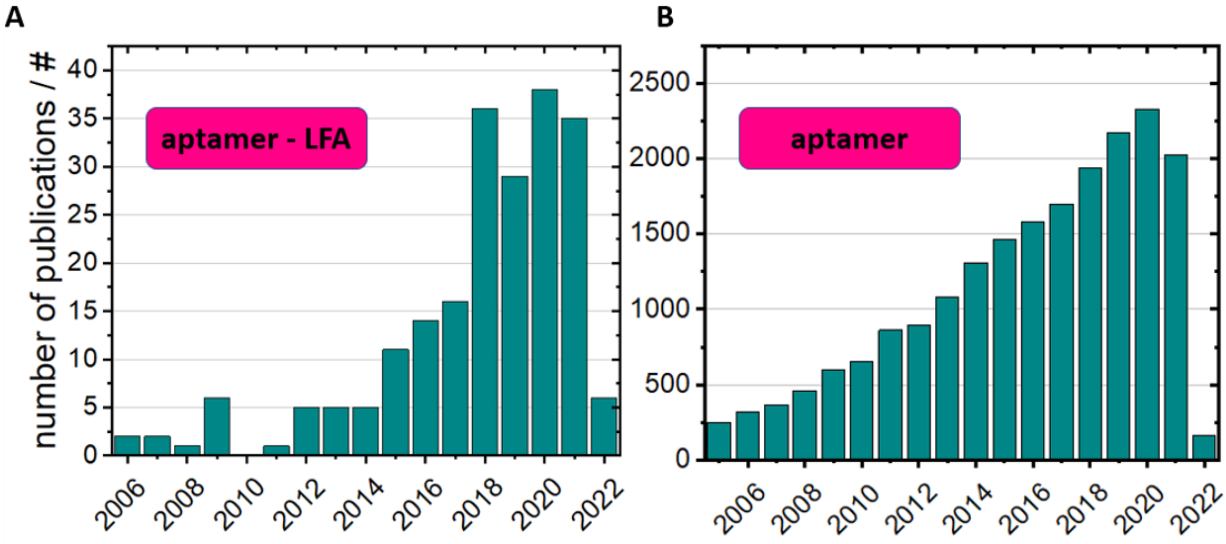

Figure 66: A) Number of publications regarding Aptamer-LFAs according to Web of Science research (All databases; timespan: all years; topic search). B) Number of publications regarding aptamers according to Web of Science research (All databases; timespan: all years; topic search). The figure represents search results from 17.01.2022.

However, highly cited reviews in this field still consider aptamer-LFAs a promising technology, like e.g. Zherdev and Dzantiev [227], Chen et al. [249], Jauset-Rubio et al. [393], and Dhiman et al. [394]. Considering the broad distribution of research areas (compare **Figure *65***) as well as the huge variety of target analytes of the most recent test systems it seems likely that the field diversifies more and more, leading to isolated publications on highly specific applications with low impact factor. In the year 2020 alone, more than 18 different target compounds including but not limited to E. coli [395], food contaminants [396], malaria [397], and C-reactive protein [398] were described in the corresponding published scientific studies. However, despite the broad research approaches with focus on so many possible targets for aptamer-LFAs, to our knowledge, not a single commercially available aptamer-LFA

test system has been marketed to date. Thus, the question arises whether the current path of the aptamer-LFA community is feasible and if the field will profit from it in the long run. To further address these questions, two exemplary test systems, namely ampicillin and ochratoxin, will be evaluated and critically analyzed in this work, focusing on the advantages and disadvantages of the available test systems in comparison to antibody-based LFAs, technical advances reported and, potential for commercialization. The gained insights will be further used to elucidate where the field of aptamer-LFAs has the most potential for growth and transfer to commercialized applications.

In this work will also provide a basic, yet expandable, evaluation system for published test systems based on quantifiable categories, including POC applicability (POC), limit of detection (LOD), specifity and binding ability (SBA), and its Working Range (WR), to provide a reliable evaluation scheme, that allows the direct comparison of systems featuring different LFA approaches, aptamers, etc. Every parameter will be evaluated using marks from 1 (test system fails to work under required conditions) to 5 (test systems exceeds its requirements). **Table *2*** highlights the meaning of every possible score, for every parameter and further explanations are given in the following sections. The parameters were chosen to highlight the most important features of the test systems without losing the original WHO Assured criteria (see **Figure 67**).

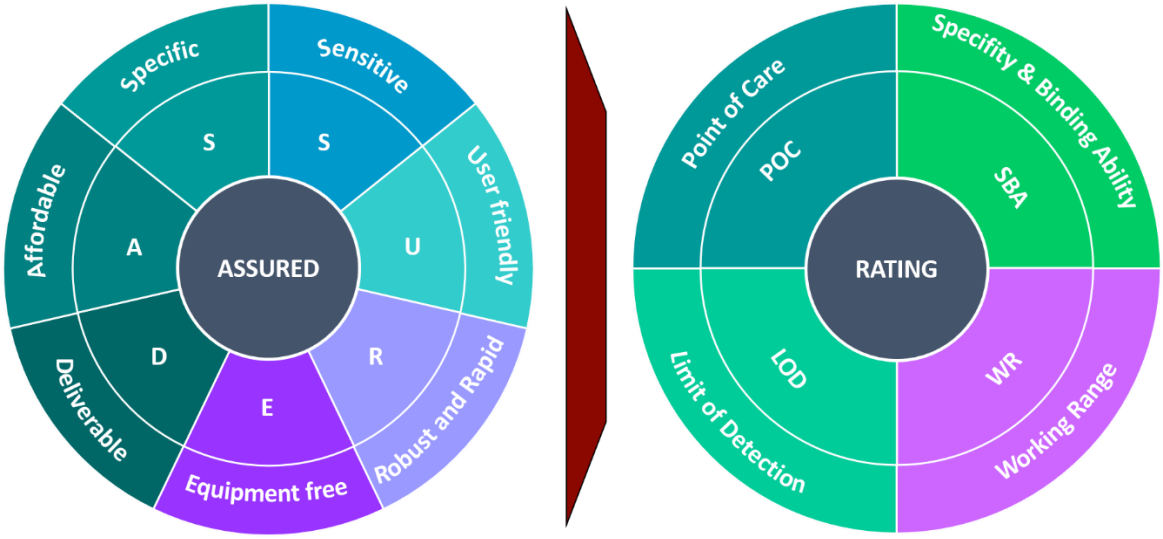

Figure 67: Condensation of the seven-column ASSURED criteria into a four-column rating system for LFA tests.

POC (Point of Care): Each LFA system represents a point-of-care diagnostic tool. The main idea of POC stands for a low-cost analytical tool, which can be used by any non-trained person [357]. Every additional equipment needed to perform the test or to evaluate its outcome drastically reduces the usability as a POC diagnostic tool. An LFA´s usability in POC terms is partially lost, in case either additional equipment (e.g., reader, fluorescence spectrometer, etc.), or intensive training are needed

(e.g., pipetting, incubation at certain temperatures, etc.). The worst case is represented by a scenario where no LFA is available for an analyte and only advanced analytical instruments can be utilized.

LOD (Limit of Detection): The LOD represents the lowest concentration of a desired analyte that still can be detected (DIN 32645). Here, in the evaluation of the test systems we generally consider the lowest LOD as best. Regarding ochratoxin, the maximal residual limit (MRL) is meant to be 2 µg/kg [123]. According to the Bundesinstitut für Risikobewertung (BfR) an average German consumes up to 0.9 ng/kg bodyweight per day (evaluation from 2018). The concentration of OtA in the blood stream lies between 0.18 and 1.8 µg/L (also BfR). [199] Here, every test system providing enough sensitivity to measure the OtA concentration of blood is considered to perform below its required LOD and is rated as 5 out of 5 points. Regarding ampicillin, the MRL is meant to be 50 µg/kg for muscles, fat, liver, and kidney [358]. However, the achieved LOD of commercial test systems is as low as 2 – 5 µg/kg for milk [362–364]. Based on the assumption that 1 L milk = 1.02 kg [399] and the legal MRL of 4 µg/kg for milk in the European Union [400], an LOD of 4.08 ng/mL was rated 5 out of 5 points.

SBA (Specificity and Binding Ability): The specificity represents the true identified negatives. Whereas the binding ability of an aptamer or antibody quantifies its ability to bind to a certain target. Both parameters are combined into a single rating parameter. The specificity and binding ability are used to evaluate if a test system does also provide positive results for substances similar or unsimilar to the target analyte. Positive results for structural similar analytes (like e.g. Ochratoxin B, or amoxicillin) are rated superior over positive results for analytes lacking such structural similarities. The worst case occurs, when a test shows a positive test result for totally unspecific binding events.

WR (Working Range): The WR covers a relatively broad field of aspects of a test. First, the pH working area of the utilized aptamer/antibody and the conjugate must overlap, or the test will fail to provide any results. If there is a diagnostic window available, tests, which can perform with real samples are the best ones. If an LFA does only function with analytical grade analytes and ideal buffer solutions its working range is considered less wide and its rating drops. If the sample must undergo intensive pre-treatment, before it can run on the test stripe (e.g., pH-adjustment), its rating is further reduced.

Table 2: Parameters for test system evaluation, based on a point system ranging from 1 (not sufficient) to 5 (requirement exceeded)

	1	2	3	4	5
POC	Analytical lab equipment required (HPLC-MS, Raman spectroscopy etc.)	Other approaches, training needed (e.g., well plate handling)	LFA + Fluorescence/ Pre-treatment/ Spectrometer/ SERS	LFA + Reader, mobile device	Ready to use LFA; visible readout
LOD	No LOD	Ten-fold above requirement	Above requirement	requirement fulfilled	requirement exceeded
SBA	Cross reactivity against LFA compartments or no data regarding cross reactivity	Cross reactivity against multiple targets	Cross reactivity against different target composition (e.g., peptides)	cross reactivity only against similar targets	No cross reactivity to < 10 % cross reactivity
WR	No overlap	Sample matrix can inhibit test functionality	Functionality in testing solution (analytical grade target in buffer)	Sample pre-treatment required to allow successful detection	Full functionality in provided test matrix (incl. spiked samples)

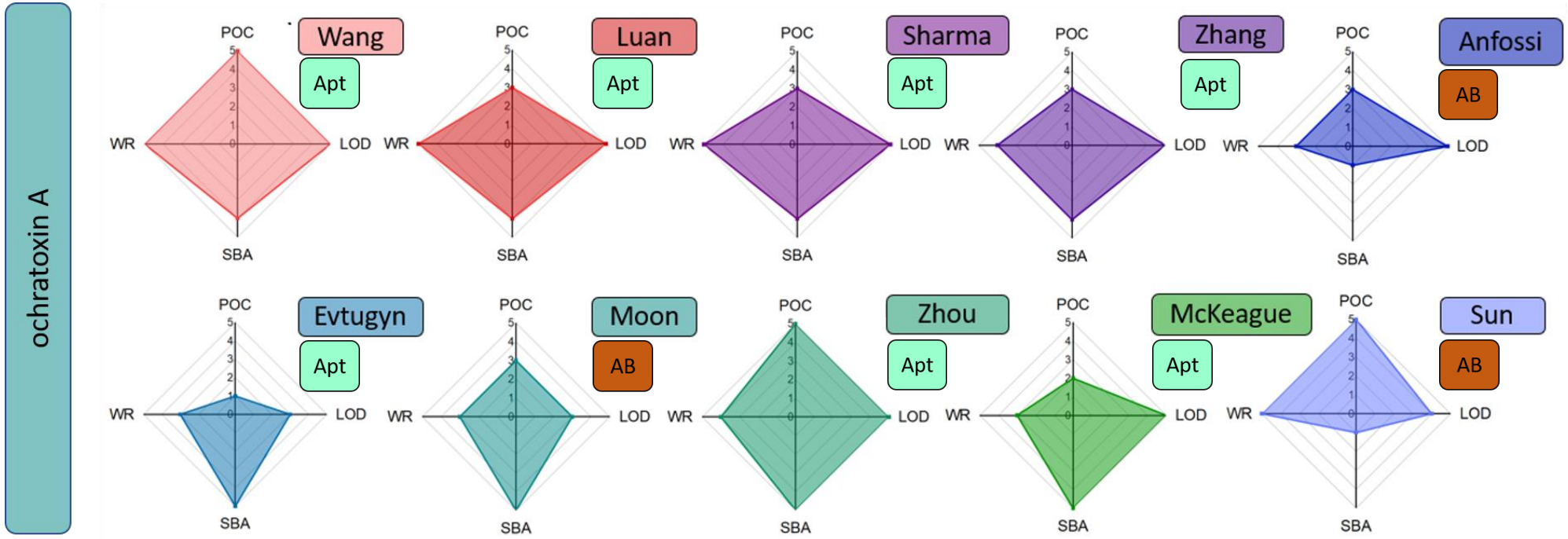

Figure 68: Systematic evaluation of ochratoxin A detecting test systems with respect to POC, LOD, SBA, and WR of the respective test system. The scores range from 1 (not sufficient) to 5 (excellent). The chosen test systems were published by Wang et al. [118], Luan et al. [205], Sharma et al. [123], Zhang et al. [211], Anfossi et al. [124], Evtugyn et al. [213], Moon et al. [207], Zhou et al. [212], McKeague et al. [206], Sun et al. [208].

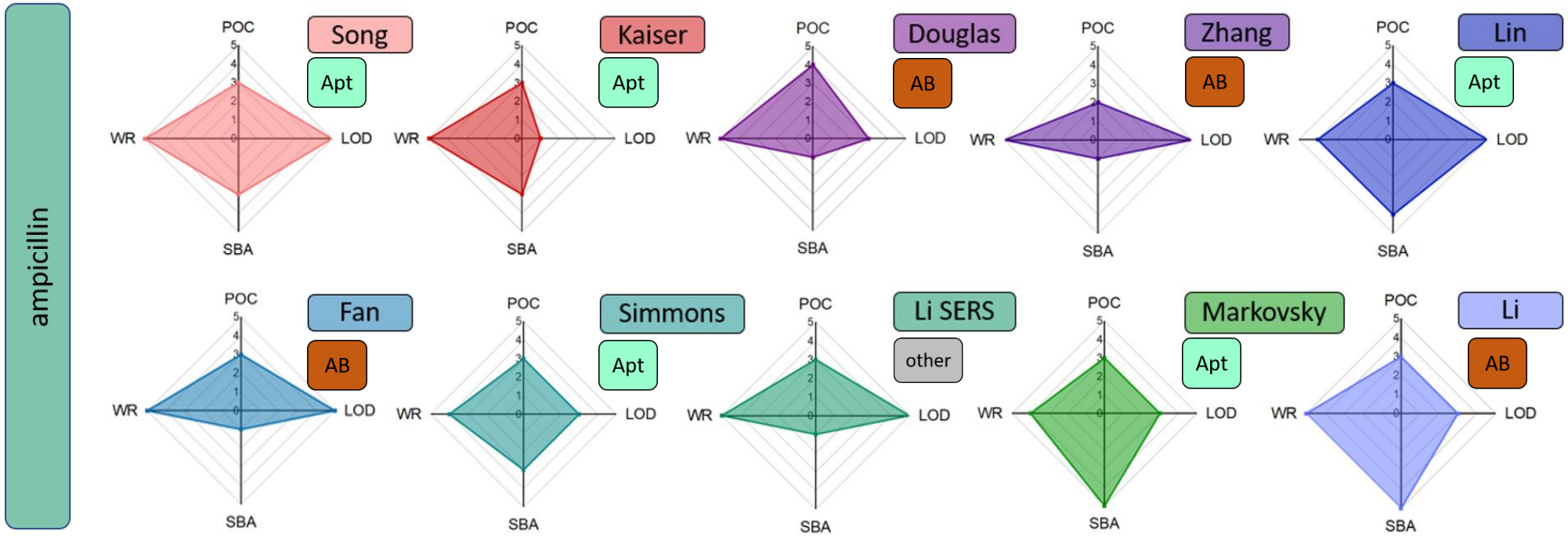

Figure 69: Systematic evaluation of ampicillin detecting test systems with respect to POC, LOD, SBA, and WR of the respective test system. The scores range from 1 (not sufficient) to 5 (excellent). The chosen test systems were published by Song et al. [36], Kaiser et al. [5], Douglas et al. [371], Zhang et al. [374], Lin et al. [368], Fan et al. [373], Simmons et al. [369], Li et al. [370], Markovsky et al. [372], Li et al. [375].

Limit of Detection

It is noticeable that evaluated aptamer-based test systems were able to reach LOD-ratings of up to 5 for the detection of OtA and ampicillin. This is actually in accordance to the expected high sensitivity of aptamers [123]. Yet, the established antibody-based test systems did also provide several LOD-ratings of 5. Even though the evaluated test systems for two specific analytes represent only a small selection of the available publications, it must be noted, that aptamers do not provide significantly lower LODs than antibody-based systems in accordance with a rating based on real MRLs. This statement is valid for the food contaminants OtA and ampicillin, however it might not be valid for virus detection in medical test systems, which may deserve a review on their own. In this regard the true potential of aptamer-based LFAs does not lie in the POC-detection of analytes if antibodies are available for the same targets. Either aptamers can offer drastically reduced LODs in comparison to antibodies, which would allow them to serve as additional tool in modern analytical chemistry, or they can be used to detect non-immunogenic target in POC applications. This statement is further supported by the findings of Khlebtsov et al., who stated that the particle diameter actually plays a much more crucial role in the sensitivity of LFA systems than the actual molecular recognition element (MRR), since the particle diameter does influence the LOD with $d^{-3.1}$. [40] Thus, the minimal achievable LOD depends on the marker not the MRE, limiting LFAs to function in the µg/mL range. In conclusion, the aptamer-LFA test systems fail to succeed over antibody-based LFAs with respect to lower LODs, since both molecular MREs can detect their respective analyte at desirable LODs for POC-diagnostics. The most potential of aptamers lies therefore in the possibility to detect non-immunogenic target molecules. Despite this advantage being mentioned in many reviews and articles, to our knowledge, there is no existing aptamer-LFA targeting a non-immunogenic target molecule. In addition to that another drawback of the hunt for lower LODs was demonstrated by Khlebtsov et al., who could calculate how many nano-bio-conjugates would be bound by one single target molecule to the test line at given LODs of published works. An exemplary antibody-test system analyzed by them would have featured a ratio of one analyte molecule binding 4 nano-bio-conjugates to allow the observed low LOD. [40,401]. Its impossible for a single target molecule to bind to so many conjugates, which indicates that systematic errors were made by determining the LOD. Thus, their work highlights systematic problems and dangers originating from the unconstructive striving for lower LODs for POC systems.

Specifity and binding ability

Interestingly, the aptamer-based test system for ampicillin detection by Kaiser et al. featured the highest LOD of 18.5 µg/mL, respectively 1850 mg/mL in real milk samples, of all evaluated test systems [5]. Here, it must be stressed, that the authors of this work did not aim to provide a test system featuring the lowest LOD possible but did utilize an aptamer´s cross reactivity against a different target, which was found due to in-silico analysis. This work should be understood as a fundamental step into a new generation of aptamer-based test systems instead as an unsuccessful test system. However, the cross reactivity described by Kaiser for the aptamer used by Song et al. [36], which was also used by Simmons et al. [369], actually highlights a systematic problem of the evaluation of the specifity and binding ability, when different test systems are compared. At this moment the rating system for the specificity has major flaws in correctly evaluating the range of analytes that were tested with the presented LFA as well as cross reactivities, that were found in other works or through in-silico analysis. Some publications test more possible analytes than others and may reveal in this effort cross reactivities that were never expected, like Wang et al., who tested the LFA also positive for zearalenone, a different mycotoxin [118]. Since all presented paper by Wang et al. [118], Luan et al. [205], Sharma et al. [123], and Zhang et al. [211] feature the same aptamer (with different modifications) it cannot be fully excluded, that all LFAs feature this unspecific binding event and their specificity rating would have to be adjusted to a lower rating. In this regard, future publications should always include specificity assays featuring the most relevant similar analyte molecules. At this moment it is not possible to determine if aptamers are superior, equal, or inferior to antibodies regarding their specificity. Here, a systematic problem of LFA evaluation is elucidated: if specificity is not tested thoroughly in all relevant works on the topic it is not comparable and therefore cannot be used as an argument for the ongoing establishment of aptamer-based LFAs on the market.

Point of care

Regarding POC characteristics, the evaluations differ drastically for ampicillin and ochratoxin A. Wang et al. [118] and Zhou et al. [212] were able to provide aptamer-based Ota-detecting LFAs that fulfill all requirements of the POC-diagnostics, yet an antibody-based LFA by Sun et al. [208] was also able to score five out of five points with regard to its POC-characteristics. Regarding this particular analyte, no clear advantage can be seen when using aptamers or antibodies. Both MREs can serve as MRE in POCs diagnostic tools. However, no evaluated test system for ampicillin was able to score five out of five points with regard to it POC-characteristics - independent from the used MRE. Actually, the highest score was achieved by Douglas et al. [371] utilizing an antibody-based test system. It is known that

low-molecular weight analytes are harder to detect than those featuring higher molecular weight. [44] Ampicillin exhibits a molar weight of 349.41 g/mol, whereas ochratoxin A exhibits a molecular weight of 403.82 g/mol. Based on the scores shown in **Figure 69** it can be seen that both, aptamer and antibody based systems fail to detect the low-molecular weight analyte ampicillin without utilizing advanced analytical equipment, fluorescence measurements, etc. thus leading to the assumption, that aptamer-LFAs are not superior to antibody-LFAs in regard to their POC characteristics.

Working Range

Most of the evaluated test stripes showed functionality for OtA-spiked samples, like e.g. wine as well as functionality for ampicillin containing urine and milk samples. The working range of the shown test systems is therefore consistently considered to be above average. Aptamer-based LFAs proof to be robust detection devices just as antibody-based ones, that can operate under real conditions, which is in accordance to the ASSURED criteria.

However, this does not mean that more complex test systems are rendered obsolete. Throughout literature research, there have been exemplary systems, that allowed the detection of highly specific analytes or phenomena. For example, Keller et al. were able to distinguish isotopologues of cytokines via an LFA. [356] Even though this particular LFA does not feature aptamers, as recognition elements, it demonstrates the true potential of an LFA system in combination with more complex readout strategy. Another very important example of an experimental LFA set-up is given by the immunoglobin antibody (IgE) and penicillin-binding protein of Staphylococcus aureus (PBP2a) detection via viral nanoparticles by Adhikari et al. [402]. This LFA system can detect 0.13 µg/mL IgE, which represents an approx. 100 x lower limit of detection provided by state-of-the-art test systems. The quantification of the test stripe can be performed via a flatbed color scanner and freeware, making it an interesting approach for future aptamer-LFA-detection systems. Especially since this approach combines both low LOD and POC nature. Aptamer-based test systems can also profit from SERS-technology as was shown by Li et al. [370], who were able to achieve an LOD of $1*10^{-4}$ ng/ml for ampicillin in milk-powder based samples. As mentioned above, such low LODs may not be of high relevance for POC applications since the MRLs for the chosen analytes lies in the $1*10^{0}$ – $1*10^{1}$ ng/mL range. However, the fusion of the LFA format, aptamers, and SERS could provide an interesting perspective for highly specific analytical applications.

The niche of aptamer-LFA-test systems

The findings of the evaluation of the ampicillin and ochratoxin A test systems are presented as cumulative scores in **Figure 70 A** discussion of average POC, LOD, SBA, and WR scores is avoided, since the evaluated test systems represent only samples within the large field of ampicillin and OtA test systems and may be subject to outliers like the LOD scoring of 1 by Kaiser et al. [5] as mentioned earlier. Yet, critical conclusions regarding the role of aptamer-LFAs can be made. It must be noted that the highest cumulative scores were achieved by aptamer-LFAs for both analytes. Only the antibody-based ampicillin test system by Li et al. [375] was able to score the same total score of 16. However, none of the highest scoring OtA aptamer-LFAs were transformed into a commercially available application, despite its publication in 2011 like in the case of Wang et al. [118].

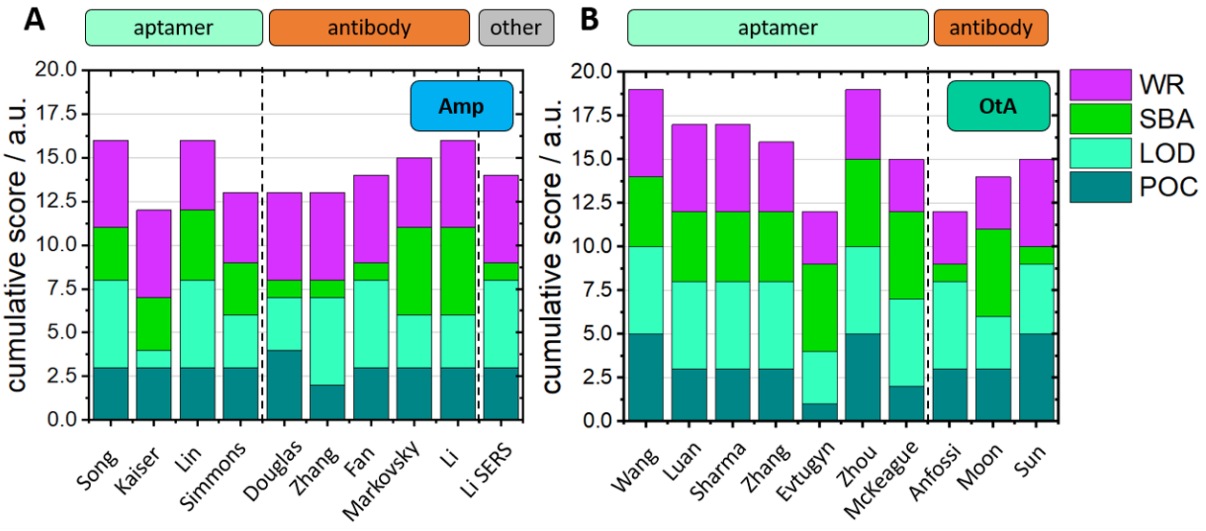

Figure 70: Systematic overview of the total cumulative score of every evaluated test system for A) ampicillin (amp) and B) ochratoxin A (OtA). 20 represents the maximal achievable score.

So, the question arises, what limits the utilization of aptamer-LFAs under real economic conditions. It was shown, that aptamer-LFAs can keep up to antibody-LFAs regarding POC, LOD, SBA, and WR and even best their immune-counterparts. However, they are not offering superior advantages over the existing commercially available test systems. The scoring system established in this work however, stresses possible niches for aptamer-LFAs:

1. aptamer-LFA test systems fulfilling a highly specific purpose, thus representing an ideal addition to the catalogue of state-of-the-art analytical devices

2. aptamer-LFA test systems targeting non-immunogenic targets, while upholding the ASSURED criteria of POC-diagnostic tools

It is appealing to achieve the best out of both approaches, since further improvements in LOD do not improve aptamer LFAs in general if the already achieved LODs are below relevant analyte concentrations, like e.g., the MRL. The arms race towards lower LODs, while ignoring specifity issues and POC requirements of LFA-test systems represents a possible deadlock for the field of aptamer-LFAs. However, if an aptamer-LFA can provide the analytical means to detect an analyte under conditions where antibodies fail, or if it is able to provide additional information through the application of additional analytical equipment like e.g., SERS, it might contribute to the establishment of aptamer-LFAs beyond publications and under real market conditions. The other niche is represented by POC-suitable aptamer-LFAs for non-immunogenic targets. While staying true to the POC-diagnostics, the aptamer-LFAs can evade rivalry with established analytical techniques, whereas the non-immunogenic targets prevent immuno-based test systems to compete with it. Furthermore, the potential for aptamer recycling [add citation of Recyc-paper] may represent the missing extra step for aptamer-LFAs to enter the ranks of established POC tools.

Conclusion

Even though many reviews regarding aptamer-based biosensors and POC-diagnostic tools exist, so far most of them only focus on providing a general overview over the field itself and lack a critical and systematic evaluation of the listed test systems. It was possible to establish a basic concept of an aptamer-LFA evaluation that may lead to a systematic understanding of the problems, limitations but also perspectives of an aptamer-based LFA. It is based on the ASSURED criteria to guarantee that the presented ratings consider real-life conditions in the field of POC-diagnostics. LFA systems featuring aptamers as well as antibodies were analyzed and rated with respect to their respective POC, LOD, SBA, and WR. It could be shown that aptamer-based systems did score the highest results for both observed test systems. Yet, no commercially available aptamer test system exists.

So far, it is noticeable, that aptamer-LFAs do not lack sensitivity for analytes if their molecular weight is high enough but feature major drawbacks in their POC-suitability and specificity. In this regard they share many drawbacks with the established antibody-based test systems. Advances in this regard may push aptamers as biosensors much more than the current run for lower LODs. In addition to that, specificity is only tested arbitrarily throughout different reference, thus, hindering a systematic evaluation of the specificity of aptamer-based LFAs, which may ultimately conceal either this strength or weakness. A common-testing-procedure needs to be established to validate if aptamer-based tests exhibit an increased specificity in comparison to their antibody-based tests or not. To rival existing antibody-based test systems, aptamer-LFAs fail to provide superior properties regarding the ASSURED criteria, as represented by the SBA, LOD, POC, WR parameters. Here a possible niche could be the focus on non-immunogenic targets to justify the development costs of new POC suited aptamer-LFA

systems. However, POC-suitability must not be the main course of aptamer-LFA systems. If they can expand the existing catalogue of analytical devises and allow the detection, quantification and understanding of complex analytes and samples. In the end, the development of novel aptamer-based test systems needs to start with the question what purpose the test is going to serve and what requirements must be fulfilled regarding its POC nature and analytical capabilities.

4. Summary

Point of care diagnostic tools, like lateral flow assays, represent an easy-to-use, cheap and fast method of detection for medical diagnosis, food safety, disease prevention, and drug controls. Despite their large field of applications, the basic principle of the most used LFAs has not changed much since their commercial introduction more than 30 years ago. However, advances in material sciences and biotechnology have been made, that could improve the functionality, availability, and enhance the field of applications of LFAs drastically. On one hand, aptamers represent an emerging class of specifically binding agents, that represent a green alternative to the established antibodies used in state-of-the-art LFAs. Aptamers are chemically synthesized DNA or RNA molecules and can target non-immunogenic and highly toxic substances. Furthermore, they are suited for the detection of small analytes like antibiotics, which play a crucial role in food safety. In addition to aptamers, LFAs can also profit from developments in the field of applied material sciences. Laser-generated noble metal nanoparticles represent an organic-ligand free and green alternative to the state-of-the-art chemically synthesized nanoparticles just in most available LFAs. The combination of both, aptamers and LAL NP, offers unique chances to further improve LFAs and to expand the understanding of how nano-bio-conjugation works.

The generation of functional nano-bioconjugates, featuring monomodal LAL Au NP, was systematically studied by varying the charge density and ionic strength of the utilized charge screening agents. Charge screening is required since the negatively charged phosphate backbone of the DNA aptamers will prevent further functionalization of the Au NP after the successful initial binding of a small fraction of the thiolated DNA. In this regard, sodium chloride, magnesium chloride and calcium chloride were tested in varying concentrations. It was shown that the divalent cations did lead to increased conjugation efficiencies, respectively surface coverages, but failed to generate stable conjugates. However, a stability threshold could be determined for sodium chloride and magnesium chloride, leading ultimately to functional conjugates. The salt-aging via magnesium chloride offers an interesting approach since, the workload per conjugation could be drastically decreased and certain aptamer structures require magnesium chloride anyways to fold properly. Interestingly the observed data was not as expected and did not follow the expected trends based on charge density. Especially the

properties of conjugates prepared via calcium chloride seem to suggest that the 3-dimensional structure of the respective aptamers is massively influenced by the utilized cation, leading to unwanted DNA-inter-particle-hybridization and ultimately to agglomeration and aggregation.

Alternatively, to salt-aging, pH-aging and peptide aging were tested on LAL Au NP. The conjugation through pH changing was previously introduced by Zhang et al. [185] and for the first time adapted for the conjugation of LAL Au NP. Here, it was possible to achieve high conjugation efficiencies and surface coverages, but despite high zeta-potentials, the generated conjugates agglomerated and precipitated within hours. The results stress, that the pH does not only change the three-dimensional structure of the aptamer but can also leads to protonation of the phosphate backbone. The highest achieved surface coverages were generated via peptide aging. Short cationic peptides have been used throughout literature to serve as cell penetrating agents, drug carriers and to conjugate LAL Au NP. [187,189,191] This work represents the first time short cationic peptide are used purely as charge screening agent. However, despite surface coverages exceeding all other tested variants, the conjugates lacked sufficient stability to be further analyzed. Future work is required to elucidate if intelligent peptide design can be introduced to avoid the conjugate agglomeration while upholding the conjugate´s functionality.

The investigation of the conjugation behavior of LAL-generated particles was expanded to LAL AgAu alloy particles. In this regard surface-normalized colloids of different nanoparticle compositions were conjugated with miniStrep-aptamer. This way it was possible to elucidate the conjugation behavior purely based on the differences in the surface composition of the pure Au NP, Au_9Ag_1, Au_3Au_7, and Au_1Ag_9 nanoparticles. It was shown that the maximal functionality of all tested conjugates reached comparable levels of 65 % - 70 %, making this test system highly robust. However, the conjugation processes differed significantly in their respective efficiency and the resulting surface coverages. The maximal functional surface coverage depends on the nanoparticle composition, with pure Au NP providing the lowest surface coverage at its highest functionality. These finding can be explained either by the release of silver ions by alloy particles leading to the formation of unwanted DNA formations, or by leaching of the silver rich surfaces in presence of thiolated molecules, leading to higher fractions of unbound ligands. This is the first time, surface-normalized, ultrapure alloy nanoparticles with varying compositions are directly compared with regard to their bound aptamer functionality.

The stability of the generated LAL nano-bio-conjugates has been one of the major challenges throughout this work. Since mercaptoundecanic acid (MuA) and polyethylenglycol (PEG) have been described in literature to stabilize nano-bio-conjugates, they have been added *ex-situ* subsequently to the conjugation with OtA aptamer. The maximal achievable surface coverage was not influenced by

the steric hindering ligands, yet only PEG increased the stability of the conjugates. MUA introduces hydrogen bonding in between conjugates, thus leading to agglomeration. Unfortunately PEG lead to unspecific binding of the conjugate onto the LFA test line and the exploration of steric hindering stabilizers was ultimately stopped in favor of alternative approaches.

The introduction of an easy and fast conjugate stability analysis via RGB analysis of digital images of samples allowed to systematically evaluate conjugate stability. The rapid-red technique takes the RGB coded color signal of the sample into account and transforms it into a single value (RR-value). Through the systematic comparison of the conjugation of LAL Au NP with sodium chloride and magnesium chloride it was possible to establish a stability threshold. Conjugates reaching RR-ratings of at least 1 were considered stable. The RR-value can also be used to evaluate conjugate stability after its immobilization onto glass fiber (conjugate pad) as well as the reddishness of the final test line. Here, the opaqueness of the material can drastically influence the RR-value. Therefore, it only allows comparability of samples within the same matrix. In addition to that it is limited to the color palette of Au NP. External colors (like e.g., green, blue, orange) can lead to misleading RR-values.

This technique was further used to analyze the optimal buffer system for LAL Au NP featuring nano-bio-conjugates. It was shown that the pH was of higher importance than the utilized buffer system for conjugate stability. Furthermore, it was found, that conjugate stability on glass fiber could only be guaranteed if colloidal concentration, surface coverage, drying temperature, and compatible solutes at 3 %wt – 5%wt. were adjusted properly. Ultimately the LFA design was changed to a biotin-streptavidin-bridging competitive format, which represent a LAL-based adaptation of a LFA design previously described by Zhou et al. for detecting OtA. [212] Here it was modified to serve as prove of concept for an LAL Au NP featuring aptamer LFA (ALFA), detecting the small analyte ampicillin.

At this stage, the utilized Amp aptamer (CT-spacer) was replaced with an Amp aptamer featuring a 4 x HEGL spacer. HEGL spacer have been described to positively influence aptamer functionality [330], yet their use in nano-bio-conjugation of Au NP has not been studied systematically. It could be shown that the achievable surface coverages for this particular aptamer were exceptionally high, while providing the desired functionality on LFA tests. The spacer lacks the unspecific interaction of nucleotide spacers with the nanoparticle gold surface, does not feature any negative charges and seems to promote an increased conjugation efficiency. Thus, HEGL spacer represent a thrilling alternative to the existing spacer sequences used in the field of aptamer nano-bio-conjugates and offers large potential for improving already existing systems.

A high demand for LFAs requires precise and economic resource management. Atom economy represent one of the major principles of green chemistry and represents the key discipline in producing cheap point-of-care diagnostics tools, since the aptamer represents the most expensive component of the entire test system. Here, atom economy could be achieved by retrieving unbound ligands of prior conjugation procedures and using them for subsequent conjugations. It could not only be shown that it is possible to generate functional conjugates via a second salt-aging but also without second salt-aging. Furthermore, conjugates generated by adding recycled aptamer performed better than those generated by adding fresh aptamer. In the end it was not only possible to achieve atom economy despite the usage of excess DNA but to provide new and improved conjugation procedure. This aspect is of the upper most interest for future research in the field of nano-bio-conjugates.

At last, the field of nano-bio-conjugates was evaluated critically with respect to the aforementioned "ASSURED" criteria. These criteria were condensed into a rating matrix, used to analyze existing aptamer LFAs. The rating covers the working range of the system (pH range, spiked samples, pure analytes in buffer solution, real samples), the POC nature of the test system (additional equipment/training/analytical devices required), as well as specificity and limit of detection (LOD). Every parameter is rated from 1 (not sufficient) to 5 (requirement exceeded). The detection of ochratoxin A served as exemplary test system, since it is of high relevance for food safety and has a large impact on human health. The rating system showed, that aptamer LFAs feature LODs above the requirements for ochratoxin A but not for ampicillin detection. However, this excellent ochratoxin A detection comes often at cost of extra equipment or training. The POC aspect is often underrepresented. In addition to that the testing of specificity lacks a systematic universal approach. Thus, it is impossible to evaluate if aptamer LFAs outperform state of the art antibody LFAs with respect to their specificity. Nevertheless, examples were found, that justified the existing of highly complex LFA systems. If a test system fulfills a highly specific purpose and can add to the existing range of analytical devices, it can free itself from any POC-related restrictions. The success of aptamer-based LFAs lies either in their superiority with regard to POC diagnostic of non-immunogenic targets, by their highly specific purpose, or economic favorability via aptamer-recycling.

In summary, it was possible to establish a robust-functioning platform for LFA systems combining ´recyclable´ aptamers and green-synthesized, laser-generated nanoparticles of varying surface compositions, which can detect small molecular weight targets by utilizing a HEGL-spacer bearing aptamer. Thus, this work contributes to the development of novel, green POC-detection systems.

5. Outlook

Throughout this work it was possible to establish a proof-of-concept, functional competitive LFA based on nano-bioconjugates featuring laser-generated Au NP for the detection of the small molecule analyte ampicillin. This basic test stripe system represents an ideal starting point for the development of other LFA systems. Due to the biotin-streptavidin bridging, it is not necessary to change the LFA itself. Only the utilized aptamer and complementary oligonucleotide carrying a biotin residue must be exchanged. With such a flexible test at hand, the initially investigated ochratoxin A test system could be easily revisited and adapted.

A core aspect of this work focused on the generation of functional nano-bio-conjugates. It was possible to improve the nanoparticle colloid generation with respect to the size distribution. However, the upscaling the synthesis of large, monomodal NP via LAL remains a challenging task. The initial steps have been made by Streubel et al. by introducing the continuous multigram nanoparticle synthesis by high-power, high-repetition-rate ultrafast LAL in 2016. [279] This advanced LAL technique allows for productivities of up to 4 g/h and today even 8.3 g/h [280]. This approach could be combined with the size separation by continuous bowl centrifugation as described by Kohsakowski et al. [157] for an improved particle generation. Another interesting approach for future experiments would be the usage of a compact class laser system, since Dittrich et al. found out, that such a laser-system features the highest ablation efficiency. [403] A tabletop device would be able to generate colloids of different materials whenever needed, making it an ideal device for the lab-scale development. However, the development of new centrifuge protocols for all required particle sizes is a time-consuming process and far beyond the scale of this work.

This work features a systematic evaluation of the conjugation of LAL Au NP with aptamers. Different salt-aging techniques and charge screening agents were analyzed regarding their applied concentration, incubation times, and the influence of their charge density on the conjugation. Here, the established salt-aging technique, originally introduced by Hurst et al. [175] remains the method of choice after finding the ideal maximum NaCl concentration of 0.3 M NaCl for the conjugation of 30 nm LAL Au NP. Further testing of different salt-aging procedures does not seem to be very promising regarding the achievable functionality, stability, or atom efficiency. However, the conjugation via short cationic peptides seems to be a thrilling alternative approach if future work leads to more stable conjugates. Here, additional surfactants and stabilizers could lead to more efficient, less work intense conjugation procedures. However, the influence of the cationic peptides onto the conjugate functionality and possible cross reactivities will have to be elucidated carefully.

The recycling of aptamer solutions and their further use remains one of the most interesting fields of study for future work. So far, it could be shown that conjugates bearing recycled aptamers do not only retain their functionality on LFAs but seem to perform even better. More basic research needs to be conducted on this matter. SAXS measurements could show how the cation distribution changes within the DNA-monolayer surrounding the particle, whereas fluorescence spectroscopy of recycled conjugates featuring fluorescence markers could provide valuable information on the state of DNA folding. This way the conjugation procedure could be significantly improved while upholding maximum atom economy in accordance with the principles of green chemistry.

Another promising outlook for future work is given by the utilization of alloy nanoparticles. LAL does not only allow the generation of organic-ligand free nanoparticles, but also the generation of ultrapure alloy nanoparticles. It was possible to prepare functional nano-bio-conjugates featuring different metal nanoparticle cores (Au, Ag_1Au_9, Ag_7Au_3, Ag_9Au_1) and to determine the ideal surface coverage for the respective systems. Future work could deal with alloy nanoparticle suitable for LFAs like platinum-gold or magnetic iron-gold nanoparticles. The broad field of applications for alloy nanoparticles opens many interesting approached towards new and experimental detection units.

6. References

[1] Drain PK, Hyle EP, Noubary F, Freedberg KA, Wilson D, Bishai WR et al. Diagnostic point-of-care tests in resource-limited settings. The Lancet Infectious Diseases 2014;14(3):239–49. https://doi.org/10.1016/S1473-3099(13)70250-0.

[2] Leavitt SA. A. A Thin Blue Line: The History of the Pregnancy Test Kits; Available from: https://history.nih.gov/display/history/Pregnancy+Test+Timeline.

[3] Wang L, McCord B. A four-channel paper microfluidic device with gold nanoparticles and aptamers for seized drugs. Anal Biochem 2020;595:113619. https://doi.org/10.1016/j.ab.2020.113619.

[4] Agriopoulou S, Stamatelopoulou E, Varzakas T. Advances in Analysis and Detection of Major Mycotoxins in Foods. Foods 2020;9(4). https://doi.org/10.3390/foods9040518.

[5] Kaiser L, Weisser J, Kohl M, Deigner H-P. Small molecule detection with aptamer based lateral flow assays: Applying aptamer-C-reactive protein cross-recognition for ampicillin detection. Sci Rep 2018;8(1):5628. https://doi.org/10.1038/s41598-018-23963-6.

[6] Kim SH, Lee J, Lee BH, Song C-S, Gu MB. Specific detection of avian influenza H5N2 whole virus particles on lateral flow strips using a pair of sandwich-type aptamers. Biosens Bioelectron 2019;134:123–9. https://doi.org/10.1016/j.bios.2019.03.061.

[7] Liu J, Qin Q, Zhang X, Li C, Yu Y, Huang X et al. Development of a Novel Lateral Flow Biosensor Combined With Aptamer-Based Isolation: Application for Rapid Detection of Grouper Nervous Necrosis Virus. Front Microbiol 2020;11:886. https://doi.org/10.3389/fmicb.2020.00886.

[8] Lu C, Gao X, Chen Y, Ren J, Liu C. Aptamer-Based Lateral Flow Test Strip for the Simultaneous Detection of Salmonella typhimurium Escherichia coli O157:H7 and Staphylococcus aureus. Analytical Letters 2020;53(4):646–59. https://doi.org/10.1080/00032719.2019.1663528.

[9] Wang D, Ge C, Lv K, Zou Q, Liu Q, Liu L et al. A simple lateral flow biosensor for rapid detection of lead(ii) ions based on G-quadruplex structure-switching. Chem Commun (Camb) 2018;54(97):13718–21. https://doi.org/10.1039/c8cc06810k.

[10] Dalirirad S, Steckl AJ. Aptamer-based lateral flow assay for point of care cortisol detection in sweat. Sensors and Actuators B: Chemical 2019;283:79–86. https://doi.org/10.1016/j.snb.2018.11.161.

[11] Lin W-Z, Chen Y-H, Liang C-K, Liu C-C, Hou S-Y. A competitive immunoassay for biotin detection using magnetic beads and gold nanoparticle probes. Food Chem 2019;271:440–4. https://doi.org/10.1016/j.foodchem.2018.07.152.

[12] Kiplagat A, Martin DR, Onani MO, Meyer M. Aptamer-conjugated magnetic nanoparticles for the efficient capture of cancer biomarker proteins. Journal of Magnetism and Magnetic Materials 2020;497:166063. https://doi.org/10.1016/j.jmmm.2019.166063.

[13] Koczula KM, Gallotta A. Lateral flow assays. Essays Biochem 2016;60(1):111–20. https://doi.org/10.1042/EBC20150012.

[14] Dhiman A, Kalra P, Bansal V, Bruno JG, Sharma TK. Aptamer-based point-of-care diagnostic platforms. Sensors and Actuators B: Chemical 2017;246:535–53. https://doi.org/10.1016/j.snb.2017.02.060.

[15] National Academies Press (US). Monoclonal Antibody Production. Washington (DC); 1999.

[16] European Comission. MITTEILUNG DER KOMMISSION AN DAS EUROPÄISCHE PARLAMENT, DEN EUROPÄISCHEN RAT, DEN RAT, DEN EUROPÄISCHEN WIRTSCHAFTS- UND SOZIALAUSSCHUSS UND DEN AUSSCHUSS DER REGIONEN: Der europäische Grüne Deal 2019.

[17] Zhang D, Gökce B, Barcikowski S. Laser Synthesis and Processing of Colloids: Fundamentals and Applications. Chem Rev 2017;117(5):3990–4103. https://doi.org/10.1021/acs.chemrev.6b00468.

[18] Anastas P, Eghbali N. Green chemistry: principles and practice. Chem Soc Rev 2010;39(1):301–12. https://doi.org/10.1039/B918763B.

[19] Amendola V, Meneghetti M. Laser ablation synthesis in solution and size manipulation of noble metal nanoparticles. Phys Chem Chem Phys 2009;11(20):3805–21. https://doi.org/10.1039/B900654K.

[20] Clark J. Forum. Green Chem. 1999;1(1):G1. https://doi.org/10.1039/gc9900g1.

[21] Anastas PT, Warner JC. Green chemistry: Theory and practice. 1st ed. Oxford: Oxford University Press; 2000.

[22] Jendrzej S, Gökce B, Epple M, Barcikowski S. How Size Determines the Value of Gold: Economic Aspects of Wet Chemical and Laser-Based Metal Colloid Synthesis. Chemphyschem 2017:1012–9. https://doi.org/10.1002/cphc.201601139.

[23] Our World in Data. Full list of total tests for covid 19; Available from: https://ourworldindata.org/grapher/full-list-total-tests-for-covid-19?tab=table.

[24] Petersen S, Barcikowski S. In Situ Bioconjugation: Single Step Approach to Tailored Nanoparticle-Bioconjugates by Ultrashort Pulsed Laser Ablation. Adv. Funct. Mater. 2009;19(8):1167–72. https://doi.org/10.1002/adfm.200801526.

[25] Petersen S, Barcikowski S. Conjugation Efficiency of Laser-Based Bioconjugation of Gold Nanoparticles with Nucleic Acids. J. Phys. Chem. C 2009;113(46):19830–5. https://doi.org/10.1021/jp905962f.

[26] Petersen S, Jakobi J, Barcikowski S. In situ bioconjugation—Novel laser based approach to pure nanoparticle-conjugates. Applied Surface Science 2009;255(10):5435–8. https://doi.org/10.1016/j.apsusc.2008.08.064.

[27] Barchanski A, Taylor U, Klein S, Petersen S, Rath D, Barcikowski S. Golden Perspective: Application of Laser-Generated Gold Nanoparticle Conjugates in Reproductive Biology. Reproduction in Domestic Animals 2011;46. https://doi.org/10.1111/j.1439-0531.2011.01844.x.

[28] Barchanski A, Hashimoto N, Petersen S, Sajti CL, Barcikowski S. Impact of spacer and strand length on oligonucleotide conjugation to the surface of ligand-free laser-generated gold nanoparticles. Bioconjug Chem 2012;23(5):908–15. https://doi.org/10.1021/bc200462b.

[29] Porras JC, Bernuz M, Marfa J, Pallares-Rusiñol A, Martí M, Pividori MI. Comparative Study of Gold and Carbon Nanoparticles in Nucleic Acid Lateral Flow Assay. Nanomaterials (Basel) 2021;11(3). https://doi.org/10.3390/nano11030741.

[30] Walter JG, Petersen S, Stahl F, Scheper T, Barcikowski S. Laser ablation-based one-step generation and bio-functionalization of gold nanoparticles conjugated with aptamers. J Nanobiotechnology 2010;8:21. https://doi.org/10.1186/1477-3155-8-21.

[31] Han MS, Byun J-H, Cho Y, Rim JH. RT-PCR for SARS-CoV-2: quantitative versus qualitative. The Lancet Infectious Diseases 2020. https://doi.org/10.1016/S1473-3099(20)30424-2.

[32] Joe YH, Park DH, Hwang J. Evaluation of Ag nanoparticle coated air filter against aerosolized virus: Anti-viral efficiency with dust loading. J Hazard Mater 2016;301:547–53. https://doi.org/10.1016/j.jhazmat.2015.09.017.

[33] Weiss C, Carriere M, Fusco L, Capua I, Regla-Nava JA, Pasquali M et al. Toward Nanotechnology-Enabled Approaches against the COVID-19 Pandemic. ACS Nano 2020;14(6):6383–406. https://doi.org/10.1021/acsnano.0c03697.

[34] Kosack CS, Page A-L, Klatser PR. A guide to aid the selection of diagnostic tests. Bull World Health Organ 2017;95(9):639–45. https://doi.org/10.2471/BLT.16.187468.

[35] Ngom B, Guo Y, Wang X, Bi D. Development and application of lateral flow test strip technology for detection of infectious agents and chemical contaminants: a review. Anal Bioanal Chem 2010;397(3):1113–35. https://doi.org/10.1007/s00216-010-3661-4.

[36] Song K-M, Cho M, Jo H, Min K, Jeon SH, Kim T et al. Gold nanoparticle-based colorimetric detection of kanamycin using a DNA aptamer. Anal Biochem 2011;415(2):175–81. https://doi.org/10.1016/j.ab.2011.04.007.

[37] Vashist SK. Point-of-Care Diagnostics: Recent Advances and Trends. Biosensors (Basel) 2017;7(4). https://doi.org/10.3390/bios7040062.

[38] Anfossi L, Di Nardo F, Cavalera S, Giovannoli C, Baggiani C. Multiplex Lateral Flow Immunoassay: An Overview of Strategies towards High-throughput Point-of-Need Testing. Biosensors (Basel) 2018;9(1). https://doi.org/10.3390/bios9010002.

[39] Schlücker S. Surface-enhanced Raman spectroscopy: concepts and chemical applications. Angew Chem Int Ed Engl 2014;53(19):4756–95. https://doi.org/10.1002/anie.201205748.

[40] Khlebtsov BN, Tumskiy RS, Burov AM, Pylaev TE, Khlebtsov NG. Quantifying the Numbers of Gold Nanoparticles in the Test Zone of Lateral Flow Immunoassay Strips. ACS Appl. Nano Mater. 2019;2(8):5020–8. https://doi.org/10.1021/acsanm.9b00956.

[41] EMD MILLIPORE. Rapid Lateral Flow Test Strips: Consideration of Product Development. emdmillipore.com/offices;2013.

[42] Reid R, Chatterjee B, Das SJ, Ghosh S, Sharma TK. Application of aptamers as molecular recognition elements in lateral flow assays. Anal Biochem 2020;593:113574. https://doi.org/10.1016/j.ab.2020.113574.

[43] Posthuma-Trumpie GA, Korf J, van Amerongen A. Lateral flow (immuno)assay: Its strengths, weaknesses, opportunities and threats. A literature survey. Anal Bioanal Chem 2009;393(2):569–82. https://doi.org/10.1007/s00216-008-2287-2.

[44] Schüling T, Eilers A, Scheper T, Walter J. Aptamer-based lateral flow assays. AIMS Bioengineering 2018;5(2):78–102. https://doi.org/10.3934/bioeng.2018.2.78.

[45] McCauley TG, Hamaguchi N, Stanton M. Aptamer-based biosensor arrays for detection and quantification of biological macromolecules. Anal Biochem 2003;319(2):244–50. https://doi.org/10.1016/s0003-2697(03)00297-5.

[46] Daniel M-C, Astruc D. Gold nanoparticles: assembly, supramolecular chemistry, quantum-size-related properties, and applications toward biology, catalysis, and nanotechnology. Chem Rev 2004;104(1):293–346. https://doi.org/10.1021/cr030698+.

[47] Jayasena SD. Aptamers: An emerging class of molecules that rival antibodies in diagnostics. Clin Chem 1999;45(9):1628–50.

[48] Klussmann S. The Aptamer Handbook. Wiley; 2006.

[49] Battersby TR, Ang DN, Burgstaller P, Jurczyk SC, Bowser MT, Buchanan DD et al. Quantitative analysis of receptors for adenosine nucleotides obtained via in vitro selection from a library incorporating a cationic nucleotide analog. J Am Chem Soc 1999;121(42):9781–9. https://doi.org/10.1021/ja9816436.

[50] Cech TR. Ribozymes, the first 20 years. Biochem Soc Trans 2002;30(Pt 6):1162–6. https://doi.org/10.1042/bst0301162.

[51] Tuerk C, Gold L. Systematic evolution of ligands by exponential enrichment: RNA ligands to bacteriophage T4 DNA polymerase. Science 1990;249(4968):505–10. https://doi.org/10.1126/science.2200121.

[52] Ellington AD, Szostak JW. Selection in vitro of single-stranded DNA molecules that fold into specific ligand-binding structures. Nature 1992;355(6363):850–2. https://doi.org/10.1038/355850a0.

[53] Bock LC, Griffin LC, Latham JA, Vermaas EH, Toole JJ. Selection of single-stranded DNA molecules that bind and inhibit human thrombin. Nature 1992;355(6360):564–6. https://doi.org/10.1038/355564a0.

[54] Mendonsa SD, Bowser MT. In vitro evolution of functional DNA using capillary electrophoresis. J Am Chem Soc 2004;126(1):20–1. https://doi.org/10.1021/ja037832s.

[55] Homann M, Göringer HU. Combinatorial selection of high affinity RNA ligands to live African trypanosomes. Nucleic Acids Res 1999;27(9):2006–14. https://doi.org/10.1093/nar/27.9.2006.

[56] Stoltenburg R, Nikolaus N, Strehlitz B. Capture-SELEX: Selection of DNA Aptamers for Aminoglycoside Antibiotics. J Anal Methods Chem 2012;2012:415697. https://doi.org/10.1155/2012/415697.

[57] Nutiu R, Li Y. In vitro selection of structure-switching signaling aptamers. Angew Chem Int Ed Engl 2005;44(7):1061–5. https://doi.org/10.1002/anie.200461848.

[58] Stoltenburg R, Reinemann C, Strehlitz B. SELEX--a (r)evolutionary method to generate high-affinity nucleic acid ligands. Biomol Eng 2007;24(4):381–403. https://doi.org/10.1016/j.bioeng.2007.06.001.

[59] Munzar JD, Ng A, Corrado M, Juncker D. Complementary oligonucleotides regulate induced fit ligand binding in duplexed aptamers. Chem Sci 2017;8(3):2251–6. https://doi.org/10.1039/c6sc03993f.

[60] Lakhin AV, Tarantul VZ, Gening LV. Aptamers: Problems, solutions and prospects. Acta Naturae 2013;5(4):34–43.

[61] Tripathi P, Sachan M, Nara S. Novel ssDNA Ligand Against Ovarian Cancer Biomarker CA125 With Promising Diagnostic Potential. Front Chem 2020;8:400. https://doi.org/10.3389/fchem.2020.00400.

[62] Kang J, Yeom G, Jang H, Oh J, Park C-J, Kim M-G. Development of Replication Protein A-Conjugated Gold Nanoparticles for Highly Sensitive Detection of Disease Biomarkers. Anal Chem 2019;91(15):10001–7. https://doi.org/10.1021/acs.analchem.9b01827.

[63] Kwon J, Narayan C, Kim C, Han MJ, Kim M, Jang SK. Development of a Subtype-Specific Diagnostic System for Influenza Virus H3N2 Using a Novel Virus-Based Systematic Evolution of Ligands by Exponential Enrichment (Viro-SELEX). j biomed nanotechnol 2019;15(7):1609–21. https://doi.org/10.1166/jbn.2019.2789.

[64] Paniel N, Noguer T. Detection of Salmonella in Food Matrices, from Conventional Methods to Recent Aptamer-Sensing Technologies. Foods 2019;8(9). https://doi.org/10.3390/foods8090371.

[65] Tasbasi BB, Guner BC, Sudagidan M, Ucak S, Kavruk M, Ozalp VC. Label-free lateral flow assay for Listeria monocytogenes by aptamer-gated release of signal molecules. Anal Biochem 2019;587:113449. https://doi.org/10.1016/j.ab.2019.113449.

[66] Guo X, Wen F, Qiao Q, Zheng N, Saive M, Fauconnier M-L et al. A Novel Graphene Oxide-Based Aptasensor for Amplified Fluorescent Detection of Aflatoxin M1 in Milk Powder. Sensors (Basel) 2019;19(18). https://doi.org/10.3390/s19183840.

[67] Zhao Z, Wang H, Zhai W, Feng X, Fan X, Chen A et al. A Lateral Flow Strip Based on a Truncated Aptamer-Complementary Strand for Detection of Type-B Aflatoxins in Nuts and Dried Figs. Toxins (Basel) 2020;12(2). https://doi.org/10.3390/toxins12020136.

[68] Delmulle BS, Saeger SMDG de, Sibanda L, Barna-Vetro I, van Peteghem CH. Development of an immunoassay-based lateral flow dipstick for the rapid detection of aflatoxin B1 in pig feed. J Agric Food Chem 2005;53(9):3364–8. https://doi.org/10.1021/jf0404804.

[69] Alnajrani MN, Alsager OA. Lateral flow aptasensor for progesterone: Competitive target recognition and displacement of short complementary sequences. Anal Biochem 2019;587:113461. https://doi.org/10.1016/j.ab.2019.113461.

[70] Ahmad Raston NH, Nguyen V-T, Gu MB. A new lateral flow strip assay (LFSA) using a pair of aptamers for the detection of Vaspin. Biosens Bioelectron 2017;93:21–5. https://doi.org/10.1016/j.bios.2016.11.061.

[71] Ali M, Sajid M, Khalid MAU, Kim SW, Lim JH, Huh D et al. A fluorescent lateral flow biosensor for the quantitative detection of Vaspin using upconverting nanoparticles. Spectrochim Acta A Mol Biomol Spectrosc 2020;226:117610. https://doi.org/10.1016/j.saa.2019.117610.

[72] Cheng N, Song Y, Fu Q, Du D, Luo Y, Wang Y et al. Aptasensor based on fluorophore-quencher nano-pair and smartphone spectrum reader for on-site quantification of multi-pesticides. Biosens Bioelectron 2018;117:75–83. https://doi.org/10.1016/j.bios.2018.06.002.

[73] Cheng N, Song Y, Shi Q, Du D, Liu D, Luo Y et al. Au@Pd Nanopopcorn and Aptamer Nanoflower Assisted Lateral Flow Strip for Thermal Detection of Exosomes. Anal Chem 2019;91(21):13986–93. https://doi.org/10.1021/acs.analchem.9b03562.

[74] Yu Q, Zhao Q, Wang S, Zhao S, Zhang S, Yin Y et al. Development of a lateral flow aptamer assay strip for facile identification of theranostic exosomes isolated from human lung carcinoma cells. Anal Biochem 2020;594:113591. https://doi.org/10.1016/j.ab.2020.113591.

[75] Dalirirad S, Steckl AJ. Lateral flow assay using aptamer-based sensing for on-site detection of dopamine in urine. Anal Biochem 2020;596:113637. https://doi.org/10.1016/j.ab.2020.113637.

[76] Frohnmeyer E, Tuschel N, Sitz T, Hermann C, Dahl GT, Schulz F et al. Aptamer lateral flow assays for rapid and sensitive detection of cholera toxin. Analyst 2019;144(5):1840–9. https://doi.org/10.1039/C8AN01616J.

[77] Gao Y, Zhu Z, Xi X, Cao T, Wen W, Zhang X et al. An aptamer-based hook-effect-recognizable three-line lateral flow biosensor for rapid detection of thrombin. Biosens Bioelectron 2019;133:177–82. https://doi.org/10.1016/j.bios.2019.03.036.

[78] Liu G, Gurung AS, Qiu W. Lateral Flow Aptasensor for Simultaneous Detection of Platelet-Derived Growth Factor-BB (PDGF-BB) and Thrombin. Molecules 2019;24(4). https://doi.org/10.3390/molecules24040756.

[79] Wang Y, Wang L, Zhang C, Liu F. A lateral flow assay for copper(II) utilizing catalytic and stem-loop based signal amplification. Mikrochim Acta 2019;186(2):82. https://doi.org/10.1007/s00604-018-3197-4.

[80] Alsager OA, Kumar S, Hodgkiss JM. Lateral Flow Aptasensor for Small Molecule Targets Exploiting Adsorption and Desorption Interactions on Gold Nanoparticles. Anal Chem 2017;89(14):7416–24. https://doi.org/10.1021/acs.analchem.7b00906.

[81] Ou Y, Jin X, Liu J, Tian Y, Zhou N. Visual detection of kanamycin with DNA-functionalized gold nanoparticles probe in aptamer-based strip biosensor. Anal Biochem 2019;587:113432. https://doi.org/10.1016/j.ab.2019.113432.

[82] National Research Council (US) Committee on Methods of Producing MonoclonalAntibodies. Summary of Advantages and Disadvantages of In Vitro and In Vivo Methods. In:

MonoclonalAntibodies, National Research Council Committee on Methods of Producing, editor. Monoclonal Antibody Production. National Academies Press (US); 1999.

[83] Crivianu-Gaita V, Thompson M. Immobilization of Fab' fragments onto substrate surfaces: A survey of methods and applications. Biosens Bioelectron 2015;70:167–80. https://doi.org/10.1016/j.bios.2015.03.032.

[84] Nepomnaschy PA, Weinberg CR, Wilcox AJ, Baird DD. Urinary hCG patterns during the week following implantation. Hum Reprod 2008;23(2):271–7. https://doi.org/10.1093/humrep/dem397.

[85] Encyclopedia of analytical chemistry. Chichester: Wiley; 2011.

[86] Crivianu-Gaita V, Thompson M. Aptamers, antibody scFv, and antibody Fab' fragments: An overview and comparison of three of the most versatile biosensor biorecognition elements. Biosens Bioelectron 2016;85:32–45. https://doi.org/10.1016/j.bios.2016.04.091.

[87] Bouchard PR, Hutabarat RM, Thompson KM. Discovery and development of therapeutic aptamers. Annu Rev Pharmacol Toxicol 2010;50:237–57. https://doi.org/10.1146/annurev.pharmtox.010909.105547.

[88] Kulbachinskiy AV. Methods for selection of aptamers to protein targets. Biochemistry (Mosc) 2007;72(13):1505–18. https://doi.org/10.1134/S000629790713007X.

[89] Walter J-G, Stahl F, Scheper T. Aptamers as affinity ligands for downstream processing. Eng. Life Sci. 2012;12(5):496–506. https://doi.org/10.1002/elsc.201100197.

[90] Batista FD, Neuberger MS. Affinity Dependence of the B Cell Response to Antigen: A Threshold, a Ceiling, and the Importance of Off-Rate. Immunity 1998;8(6):751–9. https://doi.org/10.1016/S1074-7613(00)80580-4.

[91] Hianik T, Porfireva A, Grman I, Evtugyn G. Aptabodies - new type of artificial receptors for detection proteins. Protein Pept Lett 2008;15(8):799–805. https://doi.org/10.2174/092986608785203656.

[92] Hasegawa H, Taira K-I, Sode K, Ikebukuro K. Improvement of Aptamer Affinity by Dimerization. Sensors (Basel) 2008;8(2):1090–8. https://doi.org/10.3390/s8021090.

[93] Lin CH, Patei DJ. Structural basis of DNA folding and recognition in an AMP-DNA aptamer complex: distinct architectures but common recognition motifs for DNA and RNA aptamers complexed to AMP. Chemistry & Biology 1997;4(11):817–32. https://doi.org/10.1016/S1074-5521(97)90115-0.

[94] Bittker JA, Le BV, Liu DR. Nucleic acid evolution and minimization by nonhomologous random recombination. Nat Biotechnol 2002;20(10):1024–9. https://doi.org/10.1038/nbt736.

[95] Hermann T, Patel DJ. Adaptive recognition by nucleic acid aptamers. Science 2000;287(5454):820–5. https://doi.org/10.1126/science.287.5454.820.

[96] Svoboda P, Cara AD. Hairpin RNA: a secondary structure of primary importance. Cell. Mol. Life Sci. 2006;63(7-8):901–8. https://doi.org/10.1007/s00018-005-5558-5.

[97] Wang H-Y, Ma J-L, Yin B-C, Ye B-C. Nicotinamide adenine dinucleotide detection based on silver nanoclusters stabilized by a dumbbell-shaped probe. Analyst 2017;142(10):1765–71. https://doi.org/10.1039/C7AN00293A.

[98] Roxo C, Kotkowiak W, Pasternak A. G-Quadruplex-Forming Aptamers-Characteristics, Applications, and Perspectives. Molecules 2019;24(20). https://doi.org/10.3390/molecules24203781.

[99] Butcher SE, Burke JM. Structure-mapping of the hairpin ribozyme. Magnesium-dependent folding and evidence for tertiary interactions within the ribozyme-substrate complex. J Mol Biol 1994;244(1):52–63. https://doi.org/10.1006/jmbi.1994.1703.

[100] Nikolaus N, Strehlitz B. DNA-Aptamers Binding Aminoglycoside Antibiotics. Sensors (Basel) 2014;14(2):3737–55. https://doi.org/10.3390/s140203737.

[101] Taghdisi SM, Danesh NM, Lavaee P, Emrani AS, Hassanabad KY, Ramezani M et al. Double targeting, controlled release and reversible delivery of daunorubicin to cancer cells by polyvalent aptamers-modified gold nanoparticles. Mater Sci Eng C Mater Biol Appl 2016;61:753–61. https://doi.org/10.1016/j.msec.2016.01.009.

[102] Zhang R, Wang S-B, Wu W-G, Kankala RK, Chen A-Z, Liu Y-G et al. Co-delivery of doxorubicin and AS1411 aptamer by poly(ethylene glycol)-poly(β-amino esters) polymeric micelles for targeted cancer therapy. J Nanopart Res 2017;19(6). https://doi.org/10.1007/s11051-017-3913-8.

[103] Zhang J, Chen R, Fang X, Chen F, Wang Y, Chen M. Nucleolin targeting AS1411 aptamer modified pH-sensitive micelles for enhanced delivery and antitumor efficacy of paclitaxel. Nano Res. 2015;8(1):201–18. https://doi.org/10.1007/s12274-014-0619-4.

[104] Belleperche M, DeRosa MC. pH-Control in Aptamer-Based Diagnostics, Therapeutics, and Analytical Applications. Pharmaceuticals (Basel) 2018;11(3). https://doi.org/10.3390/ph11030080.

[105] An R, Jia Y, Wan B, Zhang Y, Dong P, Li J et al. Non-enzymatic depurination of nucleic acids: factors and mechanisms. PLoS ONE 2014;9(12):e115950. https://doi.org/10.1371/journal.pone.0115950.

[106] Huang P-JJ, Kempaiah R, Liu J. Synergistic pH effect for reversible shuttling aptamer-based biosensors between graphene oxide and target molecules. J. Mater. Chem. 2011;21(25):8991. https://doi.org/10.1039/C1JM11702E.

[107] Tsukakoshi K, Ikuta Y, Abe K, Yoshida W, Iida K, Ma Y et al. Structural regulation by a G-quadruplex ligand increases binding abilities of G-quadruplex-forming aptamers. Chem Commun (Camb) 2016;52(85):12646–9. https://doi.org/10.1039/c6cc07552e.

[108] Tombelli S, Mascini M, Turner A. Improved procedures for immobilisation of oligonucleotides on gold-coated piezoelectric quartz crystals. Biosensors and Bioelectronics 2002;17(11-12):929–36. https://doi.org/10.1016/S0956-5663(02)00084-2.

[109] Frense D, Kang S, Schieke K, Reich P, Barthel A, Pliquett U et al. Label-free impedimetric biosensor for thrombin using the thrombin-binding aptamer as receptor. J. Phys.: Conf. Ser. 2013;434:12091. https://doi.org/10.1088/1742-6596/434/1/012091.

[110] Page Faulk W, Malcolm Taylor G. Communication to the editors. Immunochemistry 1971;8(11):1081–3. https://doi.org/10.1016/0019-2791(71)90496-4.

[111] Seferos DS, Giljohann DA, Rosi NL, Mirkin CA. Locked nucleic acid-nanoparticle conjugates. Chembiochem 2007;8(11):1230–2. https://doi.org/10.1002/cbic.200700262.

[112] Rosi NL, Giljohann DA, Thaxton CS, Lytton-Jean AKR, Han MS, Mirkin CA. Oligonucleotide-modified gold nanoparticles for intracellular gene regulation. Science 2006;312(5776):1027–30. https://doi.org/10.1126/science.1125559.

[113] Giljohann DA, Seferos DS, Prigodich AE, Patel PC, Mirkin CA. Gene regulation with polyvalent siRNA-nanoparticle conjugates. J Am Chem Soc 2009;131(6):2072–3. https://doi.org/10.1021/ja808719p.

[114] Tkachenko AG, Xie H, Liu Y, Coleman D, Ryan J, Glomm WR et al. Cellular trajectories of peptide-modified gold particle complexes: comparison of nuclear localization signals and

peptide transduction domains. Bioconjug Chem 2004;15(3):482–90. https://doi.org/10.1021/bc034189q.

[115] Nitin N, Javier DJ, Richards-Kortum R. Oligonucleotide-coated metallic nanoparticles as a flexible platform for molecular imaging agents. Bioconjug Chem 2007;18(6):2090–6. https://doi.org/10.1021/bc0701242.

[116] Li Li, Li B, Qi Y, Jin Y. Label-free aptamer-based colorimetric detection of mercury ions in aqueous media using unmodified gold nanoparticles as colorimetric probe. Anal Bioanal Chem 2009;393(8):2051–7. https://doi.org/10.1007/s00216-009-2640-0.

[117] Giljohann DA, Seferos DS, Daniel WL, Massich MD, Patel PC, Mirkin CA. Gold nanoparticles for biology and medicine. Angew Chem Int Ed Engl 2010;49(19):3280–94. https://doi.org/10.1002/anie.200904359.

[118] Wang L, Ma W, Chen W, Liu L, Ma W, Zhu Y et al. An aptamer-based chromatographic strip assay for sensitive toxin semi-quantitative detection. Biosens Bioelectron 2011;26(6):3059–62. https://doi.org/10.1016/j.bios.2010.11.040.

[119] Liu L, Xu L, Suryoprabowo S, Song S, Kuang H. Development of an immunochromatographic test strip for the detection of ochratoxin A in red wine. Food and Agricultural Immunology 2017:1–11. https://doi.org/10.1080/09540105.2017.1401043.

[120] Song K-M, Jeong E, Jeon W, Cho M, Ban C. Aptasensor for ampicillin using gold nanoparticle based dual fluorescence-colorimetric methods. Anal Bioanal Chem 2012;402(6):2153–61. https://doi.org/10.1007/s00216-011-5662-3.

[121] Wang L, Chen W, Ma W, Liu L, Ma W, Zhao Y et al. Fluorescent strip sensor for rapid determination of toxins. Chem Commun (Camb) 2011;47(5):1574–6. https://doi.org/10.1039/c0cc04032k.

[122] Jiang H, Li X, Xiong Y, Pei K, Nie L, Xiong Y. Silver Nanoparticle-Based Fluorescence-Quenching Lateral Flow Immunoassay for Sensitive Detection of Ochratoxin A in Grape Juice and Wine. Toxins (Basel) 2017;9(3). https://doi.org/10.3390/toxins9030083.

[123] Sharma A, Hayat A, Mishra RK, Catanante G, Bhand S, Marty JL. Titanium Dioxide Nanoparticles (TiO_2) Quenching Based Aptasensing Platform: Application to Ochratoxin A Detection. Toxins (Basel) 2015;7(9):3771–84. https://doi.org/10.3390/toxins7093771.

[124] Anfossi L, Di Nardo F, Giovannoli C, Passini C, Baggiani C. Increased sensitivity of lateral flow immunoassay for ochratoxin A through silver enhancement. Anal Bioanal Chem 2013;405(30):9859–67. https://doi.org/10.1007/s00216-013-7428-6.

[125] FRENS G. Controlled Nucleation for the Regulation of the Particle Size in Monodisperse Gold Suspensions. Nature Physical Science 1973;241(105):20–2. https://doi.org/10.1038/physci241020a0.

[126] Enustun BV, Turkevich J. J Am Chem Soc 1963;85(21):3317–28. https://doi.org/10.1021/ja00904a001.

[127] La Spina R, Spampinato V, Gilliland D, Ojea-Jimenez I, Ceccone G. Influence of different cleaning processes on the surface chemistry of gold nanoparticles. Biointerphases 2017;12(3):31003. https://doi.org/10.1116/1.4994286.

[128] Park J-W, Shumaker-Parry JS. Strong resistance of citrate anions on metal nanoparticles to desorption under thiol functionalization. ACS Nano 2015;9(2):1665–82. https://doi.org/10.1021/nn506379m.

[129] Park J-W, Shumaker-Parry JS. Structural study of citrate layers on gold nanoparticles: Role of intermolecular interactions in stabilizing nanoparticles. J Am Chem Soc 2014;136(5):1907–21. https://doi.org/10.1021/ja4097384.

[130] Dinkel R, Jakobi J, Ziefuß AR, Barcikowski S, Braunschweig B, Peukert W. Role of Citrate and NaBr at the Surface of Colloidal Gold Nanoparticles during Functionalization. J. Phys. Chem. C 2018;122(48):27383–91. https://doi.org/10.1021/acs.jpcc.8b07897.

[131] Dell'Aglio M, Gaudiuso R, Pascale O de, Giacomo A de. Mechanisms and processes of pulsed laser ablation in liquids during nanoparticle production. Applied Surface Science 2015;348:4–9. https://doi.org/10.1016/j.apsusc.2015.01.082.

[132] Tamura A, Matsumoto A, Fukami K, Nishi N, Sakka T. Simultaneous observation of nascent plasma and bubble induced by laser ablation in water with various pulse durations. Journal of Applied Physics 2015;117(17):173304. https://doi.org/10.1063/1.4919729.

[133] Yan Z, Bao R, Huang Y, Caruso AN, Qadri SB, Dinu CZ et al. Excimer Laser Production, Assembly, Sintering, and Fragmentation of Novel Fullerene-like Permalloy Particles in Liquid. J. Phys. Chem. C 2010;114(9):3869–73. https://doi.org/10.1021/jp911566a.

[134] Giusti A, Giorgetti E, Laza S, Marsili P, Giammanco F. Multiphoton Fragmentation of PAMAM G5-Capped Gold Nanoparticles Induced by Picosecond Laser Irradiation at 532 nm. J. Phys. Chem. C 2007;111(41):14984–91. https://doi.org/10.1021/jp072611k.

[135] Vaccaro L, Sciortino L, Messina F, Buscarino G, Agnello S, Cannas M. Luminescent silicon nanocrystals produced by near-infrared nanosecond pulsed laser ablation in water. Applied Surface Science 2014;302:62–5. https://doi.org/10.1016/j.apsusc.2014.01.041.

[136] Menéndez-Manjón A, Chichkov BN, Barcikowski S. Influence of Water Temperature on the Hydrodynamic Diameter of Gold Nanoparticles from Laser Ablation. J. Phys. Chem. C 2010;114(6):2499–504. https://doi.org/10.1021/jp909897v.

[137] Marzun G, Nakamura J, Zhang X, Barcikowski S, Wagener P. Size control and supporting of palladium nanoparticles made by laser ablation in saline solution as a facile route to heterogeneous catalysts. Applied Surface Science 2015;348:75–84. https://doi.org/10.1016/j.apsusc.2015.01.108.

[138] Abderrafi K, García Calzada R, Gongalsky MB, Suárez I, Abarques R, Chirvony VS et al. Silicon Nanocrystals Produced by Nanosecond Laser Ablation in an Organic Liquid. J. Phys. Chem. C 2011;115(12):5147–51. https://doi.org/10.1021/jp109400v.

[139] Du X-W, Qin W-J, Lu Y-W, Han X, Fu Y-S, Hu S-L. Face-centered-cubic Si nanocrystals prepared by microsecond pulsed laser ablation. Journal of Applied Physics 2007;102(1):13518. https://doi.org/10.1063/1.2752785.

[140] Tian F, An J, Cao H, Guo S. Large scale synthesis of PbS tipped ZnS nanorods heterostructures by long-pulse-width laser ablation in liquid. Journal of Alloys and Compounds 2013;574:161–4. https://doi.org/10.1016/j.jallcom.2013.04.050.

[141] Setoura K, Okada Y, Hashimoto S. CW-laser-induced morphological changes of a single gold nanoparticle on glass: observation of surface evaporation. Phys Chem Chem Phys 2014;16(48):26938–45. https://doi.org/10.1039/c4cp03733b.

[142] Khan SZ, Liu Z, Li L. Characteristics of γ-Al2O3 nanoparticles generated by continuous-wave laser ablation in liquid. Appl. Phys. A 2010;101(4):781–7. https://doi.org/10.1007/s00339-010-5936-1.

[143] Boutinguiza M, Comesaña R, Lusquiños F, Riveiro A, Del Val J, Pou J. Palladium nanoparticles produced by CW and pulsed laser ablation in water. Applied Surface Science 2014;302:19–23. https://doi.org/10.1016/j.apsusc.2014.01.083.

[144] Tomko J, Naddeo JJ, Jimenez R, Tan Y, Steiner M, Fitz-Gerald JM et al. Size and polydispersity trends found in gold nanoparticles synthesized by laser ablation in liquids. Phys Chem Chem Phys 2015;17(25):16327–33. https://doi.org/10.1039/C5CP01965F.

[145] Lam J, Lombard J, Dujardin C, Ledoux G, Merabia S, Amans D. Dynamical study of bubble expansion following laser ablation in liquids. Appl. Phys. Lett. 2016;108(7):74104. https://doi.org/10.1063/1.4942389.

[146] Shih C-Y, Streubel R, Heberle J, Letzel A, Shugaev MV, Wu C et al. Two mechanisms of nanoparticle generation in picosecond laser ablation in liquids: the origin of the bimodal size distribution. Nanoscale 2018;10(15):6900–10. https://doi.org/10.1039/c7nr08614h.

[147] Amendola V, Meneghetti M. What controls the composition and the structure of nanomaterials generated by laser ablation in liquid solution? Phys Chem Chem Phys 2013;15(9):3027–46. https://doi.org/10.1039/c2cp42895d.

[148] Shih C-Y, Wu C, Shugaev MV, Zhigilei LV. Atomistic modeling of nanoparticle generation in short pulse laser ablation of thin metal films in water. J Colloid Interface Sci 2017;489:3–17. https://doi.org/10.1016/j.jcis.2016.10.029.

[149] Lasemi N, Pacher U, Zhigilei LV, Bomatí-Miguel O, Lahoz R, Kautek W. Pulsed laser ablation and incubation of nickel, iron and tungsten in liquids and air. Applied Surface Science 2018;433:772–9. https://doi.org/10.1016/j.apsusc.2017.10.082.

[150] Reich S, Schönfeld P, Wagener P, Letzel A, Ibrahimkutty S, Gökce B et al. Pulsed laser ablation in liquids: Impact of the bubble dynamics on particle formation. J Colloid Interface Sci 2017;489:106–13. https://doi.org/10.1016/j.jcis.2016.08.030.

[151] Tanabe R, Nguyen TT, Sugiura T, Ito Y. Bubble dynamics in metal nanoparticle formation by laser ablation in liquid studied through high-speed laser stroboscopic videography. Applied Surface Science 2015;351:327–31. https://doi.org/10.1016/j.apsusc.2015.05.030.

[152] Dabir-Moghaddam N, Liu Z, Wu B. Modeling of the shrinking process of a bubble induced by laser metal ablation in water and experimental verification. Journal of Applied Physics 2017;121(4):44908. https://doi.org/10.1063/1.4973621.

[153] Hupfeld T, Laurens G, Merabia S, Barcikowski S, Gökce B, Amans D. Dynamics of laser-induced cavitation bubbles at a solid–liquid interface in high viscosity and high capillary number regimes. Journal of Applied Physics 2020;127(4):44306. https://doi.org/10.1063/1.5116111.

[154] Lou S, Ye J, Li K, Wu A. A gold nanoparticle-based immunochromatographic assay: the influence of nanoparticulate size. Analyst 2012;137(5):1174–81. https://doi.org/10.1039/C2AN15844B.

[155] Kim DS, Kim YT, Hong SB, Kim J, Huh NS, Lee M-K et al. Development of Lateral Flow Assay Based on Size-Controlled Gold Nanoparticles for Detection of Hepatitis B Surface Antigen. Sensors 2016;16(12):2154. https://doi.org/10.3390/s16122154.

[156] Fang C, Chen Z, Li L, Xia J. Barcode lateral flow immunochromatographic strip for prostate acid phosphatase determination. Journal of Pharmaceutical and Biomedical Analysis 2011;56(5):1035–40. https://doi.org/10.1016/j.jpba.2011.08.008.

[157] Kohsakowski S, Seiser F, Wiederrecht J-P, Reichenberger S, Vinnay T, Barcikowski S et al. Effective size separation of laser-generated, surfactant-free nanoparticles by continuous centrifugation. Nanotechnology 2020;31(9):95603. https://doi.org/10.1088/1361-6528/ab55bd.

[158] Haruta M, Kobayashi T, Sano H, Yamada N. Novel Gold Catalysts for the Oxidation of Carbon Monoxide at a Temperature far Below 0 °C. Chem. Lett. 1987;16(2):405–8. https://doi.org/10.1246/cl.1987.405.

[159] Haruta M, Tsubota S, Kobayashi T, Kageyama H, Genet MJ, Delmon B. Low-Temperature Oxidation of CO over Gold Supported on TiO2, α-Fe2O3, and Co3O4. Journal of Catalysis 1993;144(1):175–92. https://doi.org/10.1006/jcat.1993.1322.

[160] Sylvestre J-P, Poulin S, Kabashin AV, Sacher E, Meunier M, Luong JHT. Surface Chemistry of Gold Nanoparticles Produced by Laser Ablation in Aqueous Media. The Journal of Physical Chemistry B 2004;108(43):16864–9. https://doi.org/10.1021/jp047134.

[161] Merk V, Rehbock C, Becker F, Hagemann U, Nienhaus H, Barcikowski S. In situ non-DLVO stabilization of surfactant-free, plasmonic gold nanoparticles: Effect of Hofmeister's anions. Langmuir 2014;30(15):4213–22. https://doi.org/10.1021/la404556a.

[162] Hermanson GT. Bioconjugation in the Study of Protein Interactions. In: Bioconjugate Techniques. Elsevier; 2013, p. 989–1016.

[163] Cárdenas M, Barauskas J, Schillén K, Brennan JL, Brust M, Nylander T. Thiol-specific and nonspecific interactions between DNA and gold nanoparticles. Langmuir 2006;22(7):3294–9. https://doi.org/10.1021/la0530438.

[164] Herne TM, Tarlov MJ. Characterization of DNA Probes Immobilized on Gold Surfaces. J Am Chem Soc 1997;119(38):8916–20. https://doi.org/10.1021/ja9719586.

[165] Burrows ND, Lin W, Hinman JG, Dennison JM, Vartanian AM, Abadeer NS et al. Surface Chemistry of Gold Nanorods. Langmuir 2016;32(39):9905–21. https://doi.org/10.1021/acs.langmuir.6b02706.

[166] Khlebtsov NG, Dykman LA. Optical properties and biomedical applications of plasmonic nanoparticles. Journal of Quantitative Spectroscopy and Radiative Transfer 2010;111(1):1–35. https://doi.org/10.1016/j.jqsrt.2009.07.012.

[167] Wang Y, Ni Y. Combination of UV-vis spectroscopy and chemometrics to understand protein-nanomaterial conjugate: a case study on human serum albumin and gold nanoparticles. Talanta 2014;119:320–30. https://doi.org/10.1016/j.talanta.2013.11.026.

[168] Miller MM, Lazarides AA. Sensitivity of metal nanoparticle surface plasmon resonance to the dielectric environment. J Phys Chem B 2005;109(46):21556–65. https://doi.org/10.1021/jp054227y.

[169] Love JC, Estroff LA, Kriebel JK, Nuzzo RG, Whitesides GM. Self-assembled monolayers of thiolates on metals as a form of nanotechnology. Chem Rev 2005;105(4):1103–69. https://doi.org/10.1021/cr0300789.

[170] Vericat C, Vela ME, Benitez G, Carro P, Salvarezza RC. Self-assembled monolayers of thiols and dithiols on gold: new challenges for a well-known system. Chem Soc Rev 2010;39(5):1805–34. https://doi.org/10.1039/b907301a.

[171] Wang L, Rangger GM, Ma Z, Li Q, Shuai Z, Zojer E et al. Is there a Au-S bond dipole in self-assembled monolayers on gold? Phys Chem Chem Phys 2010;12(17):4287–90. https://doi.org/10.1039/b924306m.

[172] Kankate L, Turchanin A, Gölzhäuser A. On the release of hydrogen from the S-H groups in the formation of self-assembled monolayers of thiols. Langmuir 2009;25(18):10435–8. https://doi.org/10.1021/la902168u.

[173] Pensa E, Cortés E, Corthey G, Carro P, Vericat C, Fonticelli MH et al. The chemistry of the sulfur-gold interface: in search of a unified model. Acc Chem Res 2012;45(8):1183–92. https://doi.org/10.1021/ar200260p.

[174] Rohloff JC, Gelinas AD, Jarvis TC, Ochsner UA, Schneider DJ, Gold L et al. Nucleic Acid Ligands With Protein-like Side Chains: Modified Aptamers and Their Use as Diagnostic and Therapeutic Agents. Mol Ther Nucleic Acids 2014;3:e201. https://doi.org/10.1038/mtna.2014.49.

[175] Hurst SJ, Lytton-Jean AKR, Mirkin CA. Maximizing DNA loading on a range of gold nanoparticle sizes. Anal Chem 2006;78(24):8313–8. https://doi.org/10.1021/ac0613582.

[176] Demers LM, Ostblom M, Zhang H, Jang N-H, Liedberg B, Mirkin CA. Thermal desorption behavior and binding properties of DNA bases and nucleosides on gold. J Am Chem Soc 2002;124(38):11248–9. https://doi.org/10.1021/ja0265355.

[177] Kimura-Suda H, Petrovykh DY, Tarlov MJ, Whitman LJ. Base-dependent competitive adsorption of single-stranded DNA on gold. J Am Chem Soc 2003;125(30):9014–5. https://doi.org/10.1021/ja035756n.

[178] Pellegrino T, Manna L, Kudera S, Liedl T, Koktysh D, Rogach AL et al. Hydrophobic Nanocrystals Coated with an Amphiphilic Polymer Shell: A General Route to Water Soluble Nanocrystals. Nano Lett. 2004;4(4):703–7. https://doi.org/10.1021/nl035172j.

[179] Kryachko ES, Remacle F. Complexes of DNA bases and Watson-Crick base pairs with small neutral gold clusters. J Phys Chem B 2005;109(48):22746–57. https://doi.org/10.1021/jp054708h.

[180] Wang W, Ding X, He M, Wang J, Lou X. Kinetic Adsorption Profile and Conformation Evolution at the DNA-Gold Nanoparticle Interface Probed by Dynamic Light Scattering. Anal. Chem. 2014;86(20):10186–92. https://doi.org/10.1021/ac502440h.

[181] Barcikowski S, Amendola V, Lau M, Marzun G, Rehbock C, Reichenberger S et al. Handbook of Laser Synthesis & Processing of Colloids. DuEPublico: Duisburg-Essen Publications online, University of Duisburg-Essen, Germany; 2019.

[182] Pfeiffer C, Rehbock C, Hühn D, Carrillo-Carrion C, Aberasturi DJ de, Merk V et al. Interaction of colloidal nanoparticles with their local environment: the (ionic) nanoenvironment around nanoparticles is different from bulk and determines the physico-chemical properties of the nanoparticles. J R Soc Interface 2014;11(96):20130931. https://doi.org/10.1098/rsif.2013.0931.

[183] Kewalramani S, Zwanikken JW, Macfarlane RJ, Leung C-Y, La Olvera de Cruz M, Mirkin CA et al. Counterion distribution surrounding spherical nucleic acid-Au nanoparticle conjugates probed by small-angle x-ray scattering. ACS Nano 2013;7(12):11301–9. https://doi.org/10.1021/nn405109z.

[184] Hill HD, Millstone JE, Banholzer MJ, Mirkin CA. The role radius of curvature plays in thiolated oligonucleotide loading on gold nanoparticles. ACS Nano 2009;3(2):418–24. https://doi.org/10.1021/nn800726e.

[185] Zhang X, Servos MR, Liu J. Instantaneous and quantitative functionalization of gold nanoparticles with thiolated DNA using a pH-assisted and surfactant-free route. J Am Chem Soc 2012;134(17):7266–9. https://doi.org/10.1021/ja3014055.

[186] Petersen S, Barchanski A, Taylor U, Klein S, Rath D, Barcikowski S. Penetratin-Conjugated Gold Nanoparticles − Design of Cell-Penetrating Nanomarkers by Femtosecond Laser Ablation. J. Phys. Chem. C 2011;115(12):5152–9. https://doi.org/10.1021/jp1093614.

[187] Krawinkel J, Richter U, Torres-Mapa ML, Westermann M, Gamrad L, Rehbock C et al. Optical and electron microscopy study of laser-based intracellular molecule delivery using peptide-conjugated photodispersible gold nanoparticle agglomerates. J Nanobiotechnology 2016;14:2. https://doi.org/10.1186/s12951-015-0155-8.

[188] Gamrad L, Rehbock C, Westendorf AM, Buer J, Barcikowski S, Hansen W. Efficient nucleic acid delivery to murine regulatory T cells by gold nanoparticle conjugates. Sci Rep 2016;6:28709. https://doi.org/10.1038/srep28709.

[189] Barchanski A, Taylor U, Sajti CL, Gamrad L, Kues WA, Rath D et al. Bioconjugated Gold Nanoparticles Penetrate Into Spermatozoa Depending on Plasma Membrane Status. j biomed nanotechnol 2015;11(9):1597–607. https://doi.org/10.1166/jbn.2015.2094.

[190] Gamrad L, Mancini R, Werner D, Tiedemann D, Taylor U, Ziefuß A et al. Triplex-hybridizing bioconjugated gold nanoparticles for specific Y-chromosome sequence targeting of bull spermatozoa. Analyst 2017;142(11):2020–8. https://doi.org/10.1039/c6an02461k.

[191] Gamrad L, Rehbock C, Krawinkel J, Tumursukh B, Heisterkamp A, Barcikowski S. Charge Balancing of Model Gold-Nanoparticle-Peptide Conjugates Controlled by the Peptide's Net Charge and the Ligand to Nanoparticle Ratio. J. Phys. Chem. C 2014;118(19):10302–13. https://doi.org/10.1021/jp501489t.

[192] Sajti CL, Petersen S, Menéndez-Manjón A, Barcikowski S. In-situ bioconjugation in stationary media and in liquid flow by femtosecond laser ablation. Appl. Phys. A 2010;101(2):259–64. https://doi.org/10.1007/s00339-010-5813-y.

[193] Sajti CL, Barchanski A, Wagener P, Klein S, Barcikowski S. Delay Time and Concentration Effects During Bioconjugation of Nanosecond Laser-Generated Nanoparticles in a Liquid Flow. J. Phys. Chem. C 2011;115(12):5094–101. https://doi.org/10.1021/jp1093405.

[194] Streich C, Akkari L, Decker C, Bormann J, Rehbock C, Müller-Schiffmann A et al. Characterizing the Effect of Multivalent Conjugates Composed of Aβ-Specific Ligands and Metal Nanoparticles on Neurotoxic Fibrillar Aggregation. ACS Nano 2016;10(8):7582–97. https://doi.org/10.1021/acsnano.6b02627.

[195] Holmberg A, Blomstergren A, Nord O, Lukacs M, Lundeberg J, Uhlén M. The biotin-streptavidin interaction can be reversibly broken using water at elevated temperatures. Electrophoresis 2005;26(3):501–10. https://doi.org/10.1002/elps.200410070.

[196] Hendrickson WA, Pähler A, Smith JL, Satow Y, Merritt EA, Phizackerley RP. Crystal structure of core streptavidin determined from multiwavelength anomalous diffraction of synchrotron radiation. Proc Natl Acad Sci U S A 1989;86(7):2190–4. https://doi.org/10.1073/pnas.86.7.2190.

[197] Berg JM, Tymoczko JL, Stryer L. Stryer Biochemie. Berlin, Heidelberg: Springer Berlin Heidelberg; 2013.

[198] Weber PC, Ohlendorf DH, Wendoloski JJ, Salemme FR. Structural origins of high-affinity biotin binding to streptavidin. Science 1989;243(4887):85–8. https://doi.org/10.1126/science.2911722.

[199] Bundesinstitut für Risikobewertung. https://www.bfr.bund.de/de/presseinformation/1997/15/bgvv_empfiehlt_hoechstmengen_fuer_ochratoxin_in_lebensmitteln-818.html: Zugriff 20.09.2018.

[200] Anfossi L, Giovannoli C, Giraudi G, Biagioli F, Passini C, Baggiani C. A lateral flow immunoassay for the rapid detection of ochratoxin A in wine and grape must. J Agric Food Chem 2012;60(46):11491–7. https://doi.org/10.1021/jf3031666.

[201] Barthelmebs L, Jonca J, Hayat A, Prieto-Simon B, Marty J-L. Enzyme-Linked Aptamer Assays (ELAAs), based on a competition format for a rapid and sensitive detection of Ochratoxin A in wine. Food Control 2011;22(5):737–43. https://doi.org/10.1016/j.foodcont.2010.11.005.

[202] Cruz-Aguado JA, Penner G. Determination of ochratoxin a with a DNA aptamer. J Agric Food Chem 2008;56(22):10456–61. https://doi.org/10.1021/jf801957h.

[203] Khoshbin Z, Verdian A, Housaindokht MR, Izadyar M, Rouhbakhsh Z. Aptasensors as the future of antibiotics test kits-a case study of the aptamer application in the chloramphenicol detection. Biosens Bioelectron 2018;122:263–83. https://doi.org/10.1016/j.bios.2018.09.060.

[204] Lai W, Fung DY, Yang X, Renrong L, Xiong Y. Development of a colloidal gold strip for rapid detection of ochratoxin A with mimotope peptide. Food Control 2009;20(9):791–5. https://doi.org/10.1016/j.foodcont.2008.10.007.

[205] Luan Y, Chen J, Li C, Xie G, Fu H, Ma Z et al. Highly Sensitive Colorimetric Detection of Ochratoxin A by a Label-Free Aptamer and Gold Nanoparticles. Toxins (Basel) 2015;7(12):5377–85. https://doi.org/10.3390/toxins7124883.

[206] McKeague M, Velu R, Hill K, Bardóczy V, Mészáros T, DeRosa MC. Selection and characterization of a novel DNA aptamer for label-free fluorescence biosensing of ochratoxin A. Toxins (Basel) 2014;6(8):2435–52. https://doi.org/10.3390/toxins6082435.

[207] Moon J, Kim G, Lee S. Development of Nanogold-Based Lateral Flow Immunoassay for the Detection of Ochratoxin A in Buffer Systems. j. nanosci. nanotech. 2013;13(11):7245–9. https://doi.org/10.1166/jnn.2013.8099.

[208] Sun Y, Xing G, Yang J, Wang F, Deng R, Zhang G et al. Development of an immunochromatographic test strip for simultaneous qualitative and quantitative detection of ochratoxin A and zearalenone in cereal. J Sci Food Agric 2016;96(11):3673–8. https://doi.org/10.1002/jsfa.7550.

[209] Yang C, Wang Y, Marty J-L, Yang X. Aptamer-based colorimetric biosensing of Ochratoxin A using unmodified gold nanoparticles indicator. Biosens Bioelectron 2011;26(5):2724–7. https://doi.org/10.1016/j.bios.2010.09.032.

[210] Yu F-Y, Chi T-F, Liu B-H, Su C-C. Development of a sensitive enzyme-linked immunosorbent assay for the determination of ochratoxin A. J Agric Food Chem 2005;53(17):6947–53. https://doi.org/10.1021/jf0513922.

[211] Zhang G, Zhu C, Huang Y, Yan J, Chen A. A Lateral Flow Strip Based Aptasensor for Detection of Ochratoxin A in Corn Samples. Molecules 2018;23(2). https://doi.org/10.3390/molecules23020291.

[212] Zhou W, Kong W, Dou X, Zhao M, Ouyang Z, Yang M. An aptamer based lateral flow strip for on-site rapid detection of ochratoxin A in Astragalus membranaceus. J Chromatogr B Analyt Technol Biomed Life Sci 2016;1022:102–8. https://doi.org/10.1016/j.jchromb.2016.04.016.

[213] Evtugyn G, Porfireva A, Stepanova V, Kutyreva M, Gataulina A, Ulakhovich N et al. Impedimetric aptasensor for ochratoxin A determination based on Au nanoparticles stabilized with hyper-branched polymer. Sensors (Basel) 2013;13(12):16129–45. https://doi.org/10.3390/s131216129.

[214] Gallagher JC, MacDougall C. Antibiotics simplified. 2nd ed. Sudbury, MA: Jones & Bartlett Learning; 2012.

[215] Nelis HJ, Vandenbranden J, Verhaeghe B, Kruif A de, Mattheeuws D, Leenheer AP de. Liquid chromatographic determination of ampicillin in bovine and dog plasma by using a tandem solid-phase extraction method. Antimicrob Agents Chemother 1992;36(8):1606–10. https://doi.org/10.1128/AAC.36.8.1606.

[216] Luo W, Ang CY, Thompson Jr HC. Rapid method for the determination of ampicillin residues in animal muscle tissues by high-performance liquid chromatography with fluorescence detection. Journal of Chromatography B: Biomedical Sciences and Applications 1997;694(2):401–7. https://doi.org/10.1016/S0378-4347(97)00171-0.

[217] Kurittu J, Lönnberg S, Virta M, Karp M. A group-specific microbiological test for the detection of tetracycline residues in raw milk. J Agric Food Chem 2000;48(8):3372–7. https://doi.org/10.1021/jf9911794.

[218] Khlebtsov B, Khlebtsov N. Enhanced solid-phase immunoassay using gold nanoshells: effect of nanoparticle optical properties. Nanotechnology 2008;19(43):435703. https://doi.org/10.1088/0957-4484/19/43/435703.

[219] Li Zhan, Guo S, Song F, Gong Y, Xu F, Boulware DR et al. The Role of Nanoparticle Design in Determining Analytical Performance of Lateral Flow Immunoassays. Nano Letters 2017;17(12):7207–12. https://doi.org/10.1021/acs.nanolett.7b02302.

[220] Reich S, Letzel A, Menzel A, Kretzschmar N, Gökce B, Barcikowski S et al. Early appearance of crystalline nanoparticles in pulsed laser ablation in liquids dynamics. Nanoscale 2019;11(14):6962–9. https://doi.org/10.1039/C9NR01203F.

[221] Ziefuß AR, Reichenberger S, Rehbock C, Chakraborty I, Gharib M, Parak WJ et al. Laser Fragmentation of Colloidal Gold Nanoparticles with High-Intensity Nanosecond Pulses is Driven by a Single-Step Fragmentation Mechanism with a Defined Educt Particle-Size Threshold. J. Phys. Chem. C 2018;122(38):22125–36. https://doi.org/10.1021/acs.jpcc.8b04374.

[222] Jendrzej S, Gökce B, Amendola V, Barcikowski S. Barrierless growth of precursor-free, ultrafast laser-fragmented noble metal nanoparticles by colloidal atom clusters - A kinetic in situ study. J Colloid Interface Sci 2016;463:299–307. https://doi.org/10.1016/j.jcis.2015.10.032.

[223] Ziefuss AR, Reich S, Reichenberger S, Levantino M, Plech A. In situ structural kinetics of picosecond laser-induced heating and fragmentation of colloidal gold spheres. Phys Chem Chem Phys 2020;22(9):4993–5001. https://doi.org/10.1039/c9cp05202j.

[224] Safenkova IV, Zherdev AV, Dzantiev BB. Correlation between the composition of multivalent antibody conjugates with colloidal gold nanoparticles and their affinity. Journal of Immunological Methods 2010;357(1-2):17–25. https://doi.org/10.1016/j.jim.2010.03.010.

[225] Liu Z, Hu J, Li A, Feng S, Qu Z, Xu F. The effect of report particle properties on lateral flow assays: A mathematical model. Sensors and Actuators B: Chemical 2017;248:699–707. https://doi.org/10.1016/j.snb.2017.04.024.

[226] Byzova NA, Safenkova IV, Slutskaya ES, Zherdev AV, Dzantiev BB. Less is More: A Comparison of Antibody-Gold Nanoparticle Conjugates of Different Ratios. Bioconjug Chem 2017;28(11):2737–46. https://doi.org/10.1021/acs.bioconjchem.7b00489.

[227] Zherdev AV, Dzantiev BB. Ways to Reach Lower Detection Limits of Lateral Flow Immunoassays. In: Anfossi L, editor. introductory Chapter: Rapid Test - Advances in Design, Formats, and Detection Strategies. [s.l.]: IntechOpen; 2018.

[228] Tereshko V, Skripkin E, Patel DJ. Encapsulating Streptomycin within a Small 40-mer RNA. Chemistry & Biology 2003;10(2):175–87. https://doi.org/10.1016/S1074-5521(03)00024-3.

[229] Chang KY, Tinoco I. Characterization of a "kissing" hairpin complex derived from the human immunodeficiency virus genome. Proc Natl Acad Sci U S A 1994;91(18):8705–9. https://doi.org/10.1073/pnas.91.18.8705.

[230] Chang KY, Tinoco I. The structure of an RNA "kissing" hairpin complex of the HIV TAR hairpin loop and its complement. J Mol Biol 1997;269(1):52–66. https://doi.org/10.1006/jmbi.1997.1021.

[231] Lee AJ, Crothers DM. The solution structure of an RNA loop–loop complex: the ColE1 inverted loop sequence. Structure 1998;6(8):993–1007. https://doi.org/10.1016/s0969-2126(98)00101-4.

[232] Gregorian RS, Crothers DM. Determinants of RNA hairpin loop-loop complex stability. J Mol Biol 1995;248(5):968–84. https://doi.org/10.1006/jmbi.1995.0275.

[233] Jossinet F, Paillart JC, Westhof E, Hermann T, Skripkin E, Lodmell JS et al. Dimerization of HIV-1 genomic RNA of subtypes A and B: RNA loop structure and magnesium binding. RNA 1999;5(9):1222–34. https://doi.org/10.1017/s1355838299990982.

[234] Ducongé F, Di Primo C, Toulme JJ. Is a closing "GA pair" a rule for stable loop-loop RNA complexes? J Biol Chem 2000;275(28):21287–94. https://doi.org/10.1074/JBC.M002694200.

[235] Beaurain F, Di Primo C, Toulmé JJ, Laguerre M. Molecular dynamics reveals the stabilizing role of loop closing residues in kissing interactions: comparison between TAR-TAR* and TAR-aptamer. Nucleic Acids Res 2003;31(14):4275–84. https://doi.org/10.1093/nar/gkg467.

[236] Ducongé F, Toulmé JJ. In vitro selection identifies key determinants for loop-loop interactions: RNA aptamers selective for the TAR RNA element of HIV-1. RNA 1999;5(12):1605–14. https://doi.org/10.1017/s1355838299991318.

[237] O'Connell D, Koenig A, Jennings S, Hicke B, Han HL, Fitzwater T et al. Calcium-dependent oligonucleotide antagonists specific for L-selectin. Proc Natl Acad Sci U S A 1996;93(12):5883–7. https://doi.org/10.1073/pnas.93.12.5883.

[238] Watson SR, Chang YF, O'Connell D, Weigand L, Ringquist S, Parma DH. Anti-L-selectin aptamers: binding characteristics, pharmacokinetic parameters, and activity against an intravascular target in vivo. Antisense Nucleic Acid Drug Dev 2000;10(2):63–75. https://doi.org/10.1089/oli.1.2000.10.63.

[239] Smestad J, Maher LJ. Ion-dependent conformational switching by a DNA aptamer that induces remyelination in a mouse model of multiple sclerosis. Nucleic Acids Res 2013;41(2):1329–42. https://doi.org/10.1093/nar/gks1093.

[240] Zu Y, Gao Z. Facile and controllable loading of single-stranded DNA on gold nanoparticles. Anal Chem 2009;81(20):8523–8. https://doi.org/10.1021/ac901459v.

[241] Zhang X, Servos MR, Liu J. Fast pH-assisted functionalization of silver nanoparticles with monothiolated DNA. Chem Commun (Camb) 2012;48(81):10114–6. https://doi.org/10.1039/c2cc35008d.

[242] Zhang X, Gouriye T, Göeken K, Servos MR, Gill R, Liu J. Toward Fast and Quantitative Modification of Large Gold Nanoparticles by Thiolated DNA: Scaling of Nanoscale Forces, Kinetics, and the Need for Thiol Reduction. J. Phys. Chem. C 2013;117(30):15677–84. https://doi.org/10.1021/jp403946x.

[243] Stein F, Schielke A, Barcikowski S, Rehbock C. Influence of Gold/Silver Ratio in Ablative Nanoparticles on Their Interaction with Aptamers and Functionality of the Obtained Conjugates. Bioconjug Chem 2021;32(11):2439–46. https://doi.org/10.1021/acs.bioconjchem.1c00468.

[244] Zhang L, Mazouzi Y, Salmain M, Liedberg B, Boujday S. Antibody-Gold Nanoparticle Bioconjugates for Biosensors: Synthesis, Characterization and Selected Applications. Biosens Bioelectron 2020;165:112370. https://doi.org/10.1016/j.bios.2020.112370.

[245] Walter J-G, Heilkenbrinker A, Austerjost J, Timur S, Stahl F, Schepe T. Aptasensors for Small Molecule Detection. Zeitschrift für Naturforschung B 2012;67(10):976–86. https://doi.org/10.5560/znb.2012-0147.

[246] Borghei Y-S, Hosseinkhani S. Aptamer-based colorimetric determination of early-stage apoptotic cells via the release of cytochrome c from mitochondria and by exploiting silver/platinum alloy nanoclusters as a peroxidase mimic. Mikrochim Acta 2019;186(12):845. https://doi.org/10.1007/s00604-019-3977-5.

[247] Ren Q, Ga L, Lu Z, Ai J, Wang T. Aptamer-functionalized nanomaterials for biological applications. Mater. Chem. Front. 2020;4(6):1569–85. https://doi.org/10.1039/C9QM00779B.

[248] Ouyang C, Zhang S, Xue C, Yu X, Xu H, Wang Z et al. Precision-Guided Missile-Like DNA Nanostructure Containing Warhead and Guidance Control for Aptamer-Based Targeted Drug Delivery into Cancer Cells in Vitro and in Vivo. J Am Chem Soc 2020;142(3):1265–77. https://doi.org/10.1021/jacs.9b09782.

[249] Chen A, Yang S. Replacing antibodies with aptamers in lateral flow immunoassay. Biosens Bioelectron 2015;71:230–42. https://doi.org/10.1016/j.bios.2015.04.041.

[250] Ni S, Zhuo Z, Pan Y, Yu Y, Li F, Liu J et al. Recent Progress in Aptamer Discoveries and Modifications for Therapeutic Applications. ACS Appl Mater Interfaces 2021;13(8):9500–19. https://doi.org/10.1021/acsami.0c05750.

[251] Tiet P, Clark KC, McNamara JO, Berlin JM. Colorimetric Detection of Staphylococcus aureus Contaminated Solutions without Purification. Bioconjug Chem 2017;28(1):183–93. https://doi.org/10.1021/acs.bioconjchem.6b00571.

[252] Chauhan DS, Prasad R, Devrukhkar J, Selvaraj K, Srivastava R. Disintegrable NIR Light Triggered Gold Nanorods Supported Liposomal Nanohybrids for Cancer Theranostics. Bioconjug Chem 2018;29(5):1510–8. https://doi.org/10.1021/acs.bioconjchem.7b00801.

[253] Huang C, Wen T, Shi F-J, Zeng X-Y, Jiao Y-J. Rapid Detection of IgM Antibodies against the SARS-CoV-2 Virus via Colloidal Gold Nanoparticle-Based Lateral-Flow Assay. ACS Omega 2020;5(21):12550–6. https://doi.org/10.1021/acsomega.0c01554.

[254] Du W, Yuan Y, Wang L, Cui Y, Wang H, Xu H et al. Multifunctional Bioconjugate for Cancer Cell-Targeted Theranostics. Bioconjug Chem 2015;26(12):2571–8. https://doi.org/10.1021/acs.bioconjchem.5b00570.

[255] Dykman LA, Khlebtsov NG. Gold Nanoparticles in Biology and Medicine: Recent Advances and Prospects. Acta Naturae 2011;3(2):34–55.

[256] Riedesel S, Kaur R, Bakshi MS. Distinguishing Nanoparticle–Nanoparticle Interactions between Gold and Silver Nanoparticles Controlled by Gemini Surfactants: Stability of Nanocolloids. J. Phys. Chem. C 2021;125(9):5399–411. https://doi.org/10.1021/acs.jpcc.1c00220.

[257] Grade S, Eberhard J, Wagener P, Winkel A, Sajti CL, Barcikowski S et al. Therapeutic Window of Ligand-Free Silver Nanoparticles in Agar-Embedded and Colloidal State: In Vitro Bactericidal Effects and Cytotoxicity. Adv. Eng. Mater. 2012;14(5):B231-B239. https://doi.org/10.1002/adem.201180016.

[258] Yin IX, Zhang J, Zhao IS, Mei ML, Li Q, Chu CH. The Antibacterial Mechanism of Silver Nanoparticles and Its Application in Dentistry. Int J Nanomedicine 2020;15:2555–62. https://doi.org/10.2147/IJN.S246764.

[259] Yadav R, Gaur MS, Bhadauria S, Berlina AN, Dzantiev BB. Efficient chemiluminescence by aptamer – reactant platform combination with activated Ag–Au alloy nanoparticles for cobalt detection. International Journal of Environmental Analytical Chemistry 2018;98(6):570–81. https://doi.org/10.1080/03067319.2018.1483500.

[260] Chen Z, Wang X, Cheng X, Yang W, Wu Y, Fu F. Specifically and Visually Detect Methyl-Mercury and Ethyl-Mercury in Fish Sample Based on DNA-Templated Alloy Ag–Au Nanoparticles. Anal. Chem. 2018;90(8):5489–95. https://doi.org/10.1021/acs.analchem.8b01100.

[261] Xu Z, He H, Zhang S, Wang B, Jin J, Li C et al. Mechanistic studies on the antibacterial behavior of Ag nanoparticles decorated with carbon dots having different oxidation degrees. Environ. Sci.: Nano 2019;6(4):1168–79. https://doi.org/10.1039/C8EN01090K.

[262] Dallaire A-M, Rioux D, Rachkov A, Patskovsky S, Meunier M. Laser-Generated Au–Ag Nanoparticles For Plasmonic Nucleic Acid Sensing. J. Phys. Chem. C 2012;116(20):11370–7. https://doi.org/10.1021/jp301735c.

[263] Link S, Wang ZL, El-Sayed MA. Alloy Formation of Gold−Silver Nanoparticles and the Dependence of the Plasmon Absorption on Their Composition. J. Phys. Chem. B 1999;103(18):3529–33. https://doi.org/10.1021/jp990387w.

[264] Grade S, Eberhard J, Jakobi J, Winkel A, Stiesch M, Barcikowski S. Alloying colloidal silver nanoparticles with gold disproportionally controls antibacterial and toxic effects. Gold Bull 2014;47(1-2):83–93. https://doi.org/10.1007/s13404-013-0125-6.

[265] Taylor U, Tiedemann D, Rehbock C, Kues WA, Barcikowski S, Rath D. Influence of gold, silver and gold-silver alloy nanoparticles on germ cell function and embryo development. Beilstein J Nanotechnol 2015;6:651–64. https://doi.org/10.3762/bjnano.6.66.

[266] Tiedemann D, Taylor U, Rehbock C, Jakobi J, Klein S, Kues WA et al. Reprotoxicity of gold, silver, and gold-silver alloy nanoparticles on mammalian gametes. Analyst 2014;139(5):931–42. https://doi.org/10.1039/c3an01463k.

[267] Pakiari AH, Jamshidi Z. Nature and strength of M-S bonds (m = Au, Ag, and Cu) in binary alloy gold clusters. J Phys Chem A 2010;114(34):9212–21. https://doi.org/10.1021/jp100423b.

[268] Zhou J, Rossi J. Aptamers as targeted therapeutics: current potential and challenges. Nat Rev Drug Discov 2017;16(6):440. https://doi.org/10.1038/nrd.2017.86.

[269] Zhou W, Saran R, Liu J. Metal Sensing by DNA. Chem Rev 2017;117(12):8272–325. https://doi.org/10.1021/acs.chemrev.7b00063.

[270] Pei H, Li F, Wan Y, Wei M, Liu H, Su Y et al. Designed diblock oligonucleotide for the synthesis of spatially isolated and highly hybridizable functionalization of DNA-gold nanoparticle nanoconjugates. J Am Chem Soc 2012;134(29):11876–9. https://doi.org/10.1021/ja304118z.

[271] Hannemann S, Grunwaldt J-D, Krumeich F, Kappen P, Baiker A. Electron microscopy and EXAFS studies on oxide-supported gold–silver nanoparticles prepared by flame spray pyrolysis. Applied Surface Science 2006;252(22):7862–73. https://doi.org/10.1016/j.apsusc.2005.09.065.

[272] Beliatis MJ, Henley SJ, Silva SRP. Engineering the plasmon resonance of large area bimetallic nanoparticle films by laser nanostructuring for chemical sensors. Opt. Lett. 2011;36(8):1362. https://doi.org/10.1364/OL.36.001362.

[273] Çıplak Z, Getiren B, Gökalp C, Yıldız A, Yıldız N. Green synthesis of reduced graphene oxide-AgAu bimetallic nanocomposite: Catalytic performance. Chemical Engineering Communications 2020;207(4):559–73. https://doi.org/10.1080/00986445.2019.1613227.

[274] Turkevich J, Stevenson PC, Hillier J. A study of the nucleation and growth processes in the synthesis of colloidal gold. Discuss. Faraday Soc. 1951;11:55. https://doi.org/10.1039/df9511100055.

[275] Blommaerts N, Vanrompay H, Nuti S, Lenaerts S, Bals S, Verbruggen SW. Unraveling Structural Information of Turkevich Synthesized Plasmonic Gold–Silver Bimetallic Nanoparticles. Small 2019;15(42):1902791. https://doi.org/10.1002/smll.201902791.

[276] Grasmik V, Rurainsky C, Loza K, Evers MV, Prymak O, Heggen M et al. Deciphering the Surface Composition and the Internal Structure of Alloyed Silver-Gold Nanoparticles. Chem. Eur. J. 2018;24(36):9051–60. https://doi.org/10.1002/chem.201800579.

[277] Neumeister A, Jakobi J, Rehbock C, Moysig J, Barcikowski S. Monophasic ligand-free alloy nanoparticle synthesis determinants during pulsed laser ablation of bulk alloy and consolidated microparticles in water. Phys Chem Chem Phys 2014;16(43):23671–8. https://doi.org/10.1039/c4cp03316g.

[278] Prymak O, Jakobi J, Rehbock C, Epple M, Barcikowski S. Crystallographic characterization of laser-generated, polymer-stabilized 4 nm silver-gold alloyed nanoparticles. Materials Chemistry and Physics 2018;207:442–50. https://doi.org/10.1016/j.matchemphys.2017.12.080.

[279] Streubel R, Barcikowski S, Gökce B. Continuous multigram nanoparticle synthesis by high-power, high-repetition-rate ultrafast laser ablation in liquids. Opt Lett 2016;41(7):1486–9. https://doi.org/10.1364/OL.41.001486.

[280] Waag F, Streubel R, Gökce B, Barcikowski S. Synthesis of gold, platinum, and gold-platinum alloy nanoparticle colloids with high-power megahertz-repetition-rate lasers: the importance of the beam guidance method. Appl Nanosci 2021;11(4):1303–12. https://doi.org/10.1007/s13204-021-01693-y.

[281] Rehbock C, Jakobi J, Gamrad L, van der Meer S, Tiedemann D, Taylor U et al. Current state of laser synthesis of metal and alloy nanoparticles as ligand-free reference materials for nano-toxicological assays. Beilstein J Nanotechnol 2014;5:1523–41. https://doi.org/10.3762/bjnano.5.165.

[282] Rehbock C, Merk V, Gamrad L, Streubel R, Barcikowski S. Size control of laser-fabricated surfactant-free gold nanoparticles with highly diluted electrolytes and their subsequent bioconjugation. Phys Chem Chem Phys 2013;15(9):3057–67. https://doi.org/10.1039/C2CP42641B.

[283] Bonaccorso F, Zerbetto M, Ferrari AC, Amendola V. Sorting Nanoparticles by Centrifugal Fields in Clean Media. J. Phys. Chem. C 2013;117(25):13217–29. https://doi.org/10.1021/jp400599g.

[284] Barcikowski S, Plech A, Suslick KS, Vogel A. Materials synthesis in a bubble. MRS Bull. 2019;44(5):382–91. https://doi.org/10.1557/mrs.2019.107.

[285] Tymoczko A, Kamp M, Rehbock C, Kienle L, Cattaruzza E, Barcikowski S et al. One-step synthesis of Fe–Au core–shell magnetic-plasmonic nanoparticles driven by interface energy minimization. Nanoscale Horiz. 2019;4(6):1326–32. https://doi.org/10.1039/C9NH00332K.

[286] Parolo C, La Escosura-Muñiz A de, Polo E, Grazú V, La Fuente JM de, Merkoçi A. Design, preparation, and evaluation of a fixed-orientation antibody/gold-nanoparticle conjugate as an immunosensing label. ACS Appl Mater Interfaces 2013;5(21):10753–9. https://doi.org/10.1021/am4029153.

[287] Cederquist KB, Keating CD. Curvature effects in DNA:Au nanoparticle conjugates. ACS Nano 2009;3(2):256–60. https://doi.org/10.1021/nn9000726.

[288] Bae CH, Nam SH, Park SM. Formation of silver nanoparticles by laser ablation of a silver target in NaCl solution. Applied Surface Science 2002;197-198:628–34. https://doi.org/10.1016/S0169-4332(02)00430-0.

[289] Grubmüller H, Heymann B, Tavan P. Ligand binding: molecular mechanics calculation of the streptavidin-biotin rupture force. Science 1996;271(5251):997–9. https://doi.org/10.1126/science.271.5251.997.

[290] Barchanski A. Design of Bi-functional Bioconjugated Gold Nanoparticles by Pulsed Laser Ablation with Minimized Degradation. JLMN 2011;6(2):124–30. https://doi.org/10.2961/jlmn.2011.02.0006.

[291] Knecht MR, Sethi M. Bio-inspired colorimetric detection of Hg2+ and Pb2+ heavy metal ions using Au nanoparticles. Anal Bioanal Chem 2009;394(1):33–46. https://doi.org/10.1007/s00216-008-2594-7.

[292] Petersen S, Barcikowski S. Conjugation Efficiency of Laser-Based Bioconjugation of Gold Nanoparticles with Nucleic Acids. J. Phys. Chem. C 2009;113(46):19830–5. https://doi.org/10.1021/jp905962f.

[293] Schade OR, Stein F, Reichenberger S, Gaur A, Saraçi E, Barcikowski S et al. Selective Aerobic Oxidation of 5-(Hydroxymethyl)furfural over Heterogeneous Silver-Gold Nanoparticle Catalysts. Adv. Synth. Catal. 2020;362(24):5681–96. https://doi.org/10.1002/adsc.202001003.

[294] Adebayo AE, Oke AM, Lateef A, Oyatokun AA, Abisoye OD, Adiji IP et al. Biosynthesis of silver, gold and silver–gold alloy nanoparticles using Persea americana fruit peel aqueous extract for

their biomedical properties. Nanotechnol. Environ. Eng. 2019;4(1). https://doi.org/10.1007/s41204-019-0060-8.

[295] Gan W, Xu B, Dai H-L. Activation of thiols at a silver nanoparticle surface. Angew Chem Int Ed Engl 2011;50(29):6622–5. https://doi.org/10.1002/anie.201101430.

[296] Puddu V, Perry CC. Peptide adsorption on silica nanoparticles: evidence of hydrophobic interactions. ACS Nano 2012;6(7):6356–63. https://doi.org/10.1021/nn301866q.

[297] Roldán-Contreras E, Salinas-Rodríguez E, Hernández-Ávila J, Cerecedo-Sáenz E, Rodríguez-Lugo V, I. Jeldres R et al. Leaching of Silver and Gold Contained in a Sedimentary Ore, Using Sodium Thiosulfate; A Preliminary Kinetic Study. Metals 2020;10(2):159. https://doi.org/10.3390/met10020159.

[298] Mukherji S, Bharti S, Shukla G, Mukherji S. Synthesis and characterization of size- and shape-controlled silver nanoparticles. Physical Sciences Reviews 2019;4(1). https://doi.org/10.1515/psr-2017-0082.

[299] Engstrom AM, Wu H, Mackiewicz MR, Harper SL. Controlling silver ion release of silver nanoparticles with hybrid lipid membranes with long-chain hydrophobic thiol anchors decreases in vivo toxicity.

[300] Schultz D, Brinson RG, Sari N, Fagan JA, Bergonzo C, Lin NJ et al. Structural insights into DNA-stabilized silver clusters. Soft Matter 2019;15(21):4284–93. https://doi.org/10.1039/c9sm00198k.

[301] Ono A, Cao S, Togashi H, Tashiro M, Fujimoto T, Machinami T et al. Specific interactions between silver(I) ions and cytosine-cytosine pairs in DNA duplexes. Chem Commun (Camb) 2008(39):4825–7. https://doi.org/10.1039/B808686A.

[302] Chen X, Lisi F, Bakthavathsalam P, Longatte G, Hoque S, Tilley RD et al. Impact of the Coverage of Aptamers on a Nanoparticle on the Binding Equilibrium and Kinetics between Aptamer and Protein. ACS Sens 2021;6(2):538–45. https://doi.org/10.1021/acssensors.0c02212.

[303] Il'ichev YV, Perry JL, Simon JD. Interaction of Ochratoxin A with Human Serum Albumin. Preferential Binding of the Dianion and pH Effects. J Phys Chem B 2002;106(2):452–9. https://doi.org/10.1021/jp012314u.

[304] Li J, Zhu B, Yao X, Zhang Y, Zhu Z, Tu S et al. Synergetic approach for simple and rapid conjugation of gold nanoparticles with oligonucleotides. ACS Appl Mater Interfaces 2014;6(19):16800–7. https://doi.org/10.1021/am504139d.

[305] Manson J, Kumar D, Meenan BJ, Dixon D. Polyethylene glycol functionalized gold nanoparticles: the influence of capping density on stability in various media. Gold Bull 2011;44(2):99–105. https://doi.org/10.1007/s13404-011-0015-8.

[306] Zhao Y, Wang Z, Zhang W, Jiang X. Adsorbed Tween 80 is unique in its ability to improve the stability of gold nanoparticles in solutions of biomolecules. Nanoscale 2010;2(10):2114–9. https://doi.org/10.1039/c0nr00309c.

[307] Held C, Neuhaus T, Sadowski G. Compatible solutes: Thermodynamic properties and biological impact of ectoines and prolines. Biophys Chem 2010;152(1-3):28–39. https://doi.org/10.1016/j.bpc.2010.07.003.

[308] Andersen HD, Wang C, Arleth L, Peters GH, Westh P. Reconciliation of opposing views on membrane-sugar interactions. Proc Natl Acad Sci U S A 2011;108(5):1874–8. https://doi.org/10.1073/pnas.1012516108.

[309] Empadinhas N, Da Costa MS. Diversity, distribution and biosynthesis of compatible solutes in prokaryotes. Contributions to Science 2009(5):95–105. https://doi.org/10.2436/20.7010.01.65.

[310] Elbein AD, Pan YT, Pastuszak I, Carroll D. New insights on trehalose: a multifunctional molecule. Glycobiology 2003;13(4):17R-27R. https://doi.org/10.1093/glycob/cwg047.

[311] Hottiger T, Virgilio C de, Hall MN, Boller T, Wiemken A. The role of trehalose synthesis for the acquisition of thermotolerance in yeast. II. Physiological concentrations of trehalose increase the thermal stability of proteins in vitro. Eur J Biochem 1994;219(1-2):187–93. https://doi.org/10.1111/j.1432-1033.1994.tb19929.x.

[312] Carpenter JF, Crowe JH. An infrared spectroscopic study of the interactions of carbohydrates with dried proteins. Biochemistry 1989;28(9):3916–22. https://doi.org/10.1021/bi00435a044.

[313] Benaroudj N, Lee DH, Goldberg AL. Trehalose accumulation during cellular stress protects cells and cellular proteins from damage by oxygen radicals. J Biol Chem 2001;276(26):24261–7. https://doi.org/10.1074/jbc.M101487200.

[314] Madin KAC, Crowe JH. Anhydrobiosis in nematodes: Carbohydrate and lipid metabolism during dehydration. J. Exp. Zool. 1975;193(3):335–42. https://doi.org/10.1002/jez.1401930309.

[315] Colaço C, Sen S, Thangavelu M, Pinder S, Roser B. Extraordinary stability of enzymes dried in trehalose: simplified molecular biology. Biotechnology (N Y) 1992;10(9):1007–11. https://doi.org/10.1038/nbt0992-1007.

[316] Iturriaga G, Suárez R, Nova-Franco B. Trehalose metabolism: from osmoprotection to signaling. Int J Mol Sci 2009;10(9):3793–810. https://doi.org/10.3390/ijms10093793.

[317] Jain NK, Roy I. Effect of trehalose on protein structure. Protein Sci 2009;18(1):24–36. https://doi.org/10.1002/pro.3.

[318] Higashiyama T. Novel functions and applications of trehalose. Pure and Applied Chemistry 2002;74(7):1263–9. https://doi.org/10.1351/pac200274071263.

[319] Song S, Liang Z, Zhang J, Wang L, Li G, Fan C. Gold-nanoparticle-based multicolor nanobeacons for sequence-specific DNA analysis. Angew Chem Int Ed Engl 2009;48(46):8670–4. https://doi.org/10.1002/anie.200901887.

[320] Kirsch F, Klähn S, Hagemann M. Salt-Regulated Accumulation of the Compatible Solutes Sucrose and Glucosylglycerol in Cyanobacteria and Its Biotechnological Potential. Front Microbiol 2019;10:2139. https://doi.org/10.3389/fmicb.2019.02139.

[321] RF739855 Dr Richard Leduc - Méd./Pharmacologie.

[322] Wu K, Ma C, Zhao H, Chen M, Deng Z. Sensitive aptamer-based fluorescene assay for ochratoxin A based on RNase H signal amplification. Food Chem 2019;277:273–8. https://doi.org/10.1016/j.foodchem.2018.10.130.

[323] Handwerker M, Wellnitz J, Marzbani H. Review of mechanical properties of and optimisation methods for continuous fibre-reinforced thermoplastic parts manufactured by fused deposition modelling. Prog Addit Manuf 2021. https://doi.org/10.1007/s40964-021-00187-1.

[324] Ballato J, Dragic PD. Glass: The carrier of light—Part II—A brief look into the future of optical fiber. Int J Appl Glass Sci 2021;12(1):3–24. https://doi.org/10.1111/ijag.15844.

[325] Heinrich M, Decker R, Reindel P, Böttcher K, Roth-Panke I, Kroll L. Effect of acoustic excitation on fiber-reinforced polypropylene and the influence on melt viscosity. Int J Adv Manuf Technol 2021. https://doi.org/10.1007/s00170-021-07158-4.

[326] Thomason JL. Glass fibre sizing: A review. Composites Part A: Applied Science and Manufacturing 2019;127:105619. https://doi.org/10.1016/j.compositesa.2019.105619.

[327] Mahmood H, Simonini L, Dorigato A, Pegoretti A. Graphene Deposition on Glass Fibers by Triboelectrification. Applied Sciences 2021;11(7):3123. https://doi.org/10.3390/app11073123.

[328] Ismail NH, Akindoyo JO, Mariatti M. Solvent mediated dispersion of carbon nanotubes for glass fibre surface modification – Suspensions stability and its effects on mechanical, interlaminar and dynamic mechanical properties of modified glass fibre reinforced epoxy laminates. Composites Part A: Applied Science and Manufacturing 2020;139:106091. https://doi.org/10.1016/j.compositesa.2020.106091.

[329] Sanz V, Conde J, Hernández Y, Baptista PV, Ibarra MR, La Fuente JM de. Effect of PEG biofunctional spacers and TAT peptide on dsRNA loading on gold nanoparticles. J Nanopart Res 2012;14(6):80. https://doi.org/10.1007/s11051-012-0917-2.

[330] Bosco A, Ambrosetti E, Mavri J, Capaldo P, Casalis L. Miniaturized Aptamer-Based Assays for Protein Detection. Chemosensors 2016;4(3):18. https://doi.org/10.3390/chemosensors4030018.

[331] Charles PT, Stubbs VR, Soto CM, Martin BD, White BJ, Taitt CR. Reduction of Non-Specific Protein Adsorption Using Poly(ethylene) Glycol (PEG) Modified Polyacrylate Hydrogels In Immunoassays for Staphylococcal Enterotoxin B Detection. Sensors 2009;9(1):645–55. https://doi.org/10.3390/s90100645.

[332] Arya SK, Solanki PR, Datta M, Malhotra BD. Recent advances in self-assembled monolayers based biomolecular electronic devices. Biosens Bioelectron 2009;24(9):2810–7. https://doi.org/10.1016/j.bios.2009.02.008.

[333] Urusov AE, Zherdev AV, Dzantiev BB. Use of gold nanoparticle-labeled secondary antibodies to improve the sensitivity of an immunochromatographic assay for aflatoxin B1. Microchim Acta 2014;181(15-16):1939–46. https://doi.org/10.1007/s00604-014-1288-4.

[334] Tarigan S. The Role of Point-of-Care Test to Control Highly Pathogenic Avian Influenza in Indonesia. WARTAZOA 2016;26(1). https://doi.org/10.14334/wartazoa.v26i1.1272.

[335] Channon RB, Yang Y, Feibelman KM, Geiss BJ, Dandy DS, Henry CS. Development of an Electrochemical Paper-Based Analytical Device for Trace Detection of Virus Particles. Anal Chem 2018;90(12):7777–83. https://doi.org/10.1021/acs.analchem.8b02042.

[336] Wu W, Zhao S, Mao Y, Fang Z, Lu X, Zeng L. A sensitive lateral flow biosensor for Escherichia coli O157:H7 detection based on aptamer mediated strand displacement amplification. Anal Chim Acta 2015;861:62–8. https://doi.org/10.1016/j.aca.2014.12.041.

[337] Wang C, Zhang L, Shen X. Development of a nucleic acid lateral flow strip for detection of hepatitis C virus (HCV) core antigen. Nucleosides Nucleotides Nucleic Acids 2013;32(2):59–68. https://doi.org/10.1080/15257770.2013.763976.

[338] Liu X, Zhao Y, Sun C, Wang X, Wang X, Zhang P et al. Rapid detection of abrin in foods with an up-converting phosphor technology-based lateral flow assay. Sci Rep 2016;6:34926. https://doi.org/10.1038/srep34926.

[339] Liu J, Zeng J, Tian Y, Zhou N. An aptamer and functionalized nanoparticle-based strip biosensor for on-site detection of kanamycin in food samples. Analyst 2017;143(1):182–9. https://doi.org/10.1039/c7an01476g.

[340] Lee B, Park J-H, Byun J-Y, Kim JH, Kim M-G. An optical fiber-based LSPR aptasensor for simple and rapid in-situ detection of ochratoxin A. Biosens Bioelectron 2018;102:504–9. https://doi.org/10.1016/j.bios.2017.11.062.

[341] Liu G, Mao X, Phillips JA, Xu H, Tan W, Zeng L. Aptamer-nanoparticle strip biosensor for sensitive detection of cancer cells. Anal Chem 2009;81(24):10013–8. https://doi.org/10.1021/ac901889s.

[342] Xu H, Mao X, Zeng Q, Wang S, Kawde A-N, Liu G. Aptamer-functionalized gold nanoparticles as probes in a dry-reagent strip biosensor for protein analysis. Anal Chem 2009;81(2):669–75. https://doi.org/10.1021/ac8020592.

[343] Wu S, Liu L, Duan N, Li Q, Zhou Y, Wang Z. Aptamer-Based Lateral Flow Test Strip for Rapid Detection of Zearalenone in Corn Samples. J Agric Food Chem 2018;66(8):1949–54. https://doi.org/10.1021/acs.jafc.7b05326.

[344] Wu Z, Shen H, Hu J, Fu Q, Yao C, Yu S et al. Aptamer-based fluorescence-quenching lateral flow strip for rapid detection of mercury (II) ion in water samples. Anal Bioanal Chem 2017;409(22):5209–16. https://doi.org/10.1007/s00216-017-0491-7.

[345] Zhu C, Zhao Y, Yan M, Huang Y, Yan J, Bai W et al. A sandwich dipstick assay for ATP detection based on split aptamer fragments. Anal Bioanal Chem 2016;408(15):4151–8. https://doi.org/10.1007/s00216-016-9506-z.

[346] Torabi S-F, Lu Y. Small-molecule diagnostics based on functional DNA nanotechnology: a dipstick test for mercury. Faraday Discuss 2011;149:125-35; discussion 137-57. https://doi.org/10.1039/c005404f.

[347] Zhu C, Zhang G, Huang Y, Yang S, Ren S, Gao Z et al. Dual-competitive lateral flow aptasensor for detection of aflatoxin B1 in food and feedstuffs. J Hazard Mater 2018;344:249–57. https://doi.org/10.1016/j.jhazmat.2017.10.026.

[348] Le TT, Chang P, Benton DJ, McCauley JW, Iqbal M, Cass AEG. Dual Recognition Element Lateral Flow Assay Toward Multiplex Strain Specific Influenza Virus Detection. Anal Chem 2017;89(12):6781–6. https://doi.org/10.1021/acs.analchem.7b01149.

[349] Zhang J, Lv X, Feng W, Li X, Li K, Deng Y. Aptamer-based fluorometric lateral flow assay for creatine kinase MB. Microchim Acta 2018;185(8):364. https://doi.org/10.1007/s00604-018-2905-4.

[350] Yan C, Zhang J, Li Yao, Xue F, Lu J, Li B et al. Aptamer-mediated colorimetric method for rapid and sensitive detection of chloramphenicol in food. Food Chem 2018;260:208–12. https://doi.org/10.1016/j.foodchem.2018.04.014.

[351] Wei X, Zhou W, Sanjay ST, Zhang J, Jin Q, Xu F et al. Multiplexed Instrument-Free Bar-Chart SpinChip Integrated with Nanoparticle-Mediated Magnetic Aptasensors for Visual Quantitative Detection of Multiple Pathogens. Anal Chem 2018;90(16):9888–96. https://doi.org/10.1021/acs.analchem.8b02055.

[352] Chen J, Fang Z, Lie P, Zeng L. Computational lateral flow biosensor for proteins and small molecules: a new class of strip logic gates. Anal Chem 2012;84(15):6321–5. https://doi.org/10.1021/ac301508b.

[353] Qin C, Gao Y, Wen W, Zhang X, Wang S. Visual multiple recognition of protein biomarkers based on an array of aptamer modified gold nanoparticles in biocomputing to strip biosensor logic operations. Biosens Bioelectron 2016;79:522–30. https://doi.org/10.1016/j.bios.2015.12.096.

[354] Deng X, Wang C, Gao Y, Li J, Wen W, Zhang X et al. Applying strand displacement amplification to quantum dots-based fluorescent lateral flow assay strips for HIV-DNA detection. Biosens Bioelectron 2018;105:211–7. https://doi.org/10.1016/j.bios.2018.01.039.

[355] Guler E, Yilmaz Sengel T, Gumus ZP, Arslan M, Coskunol H, Timur S et al. Mobile Phone Sensing of Cocaine in a Lateral Flow Assay Combined with a Biomimetic Material. Anal Chem 2017;89(18):9629–32. https://doi.org/10.1021/acs.analchem.7b03017.

[356] Keller T, Brem S, Tran V, Sritharan O, Schäfer D, Schlücker S. Rational design of thiolated polyenes as trifunctional Raman reporter molecules in surface-enhanced Raman scattering

nanotags for cytokine detection in a lateral flow assay. J Biophotonics 2020;13(6):e201960126. https://doi.org/10.1002/jbio.201960126.

[357] Lakhin AV, Tarantul VZ, Gening LV. Aptamers: Problems, Solutions and Prospects. Acta Naturae 2013;5(4):34–43. https://doi.org/10.32607/20758251-2013-5-4-34-43.

[358] Babington R, Matas S, Marco M-P, Galve R. Current bioanalytical methods for detection of penicillins. Anal Bioanal Chem 2012;403(6):1549–66. https://doi.org/10.1007/s00216-012-5960-4.

[359] Yamaki M, Berruga MI, Althaus RL, Molina MP, Molina A. Occurrence of Antibiotic Residues in Milk from Manchega Ewe Dairy Farms. J Dairy Sci 2004;87(10):3132–7. https://doi.org/10.3168/jds.S0022-0302(04)73448-7.

[360] Thavarungkul P, Dawan S, Kanatharana P, Asawatreratanakul P. Detecting penicillin G in milk with impedimetric label-free immunosensor. Biosensors and Bioelectronics 2007;23(5):688–94. https://doi.org/10.1016/j.bios.2007.08.003.

[361] Wilkowske HH, Krienke WA. Influence of Penicillin on the Lactic Acid Production of Certain Lactobacilli. J Dairy Sci 1951;34(10):1030–3. https://doi.org/10.3168/jds.S0022-0302(51)91819-X.

[362] Abouzied M, Sarzynski M, Walsh A, Wood H, Mozola M. Validation study of a receptor-based lateral flow assay for detection of beta-lactam antibiotics in milk. J AOAC Int 2009;92(3):959–74.

[363] Žvirdauskienė R, Šalomskienė J. An evaluation of different microbial and rapid tests for determining inhibitors in milk. Food Control 2007;18(5):541–7. https://doi.org/10.1016/j.foodcont.2006.01.003.

[364] Diserens JM, Beck Henzelin A, Le Breton MH, Savoy Perroud MC (2010) Current situation and compilation of commercially available screening methods for the detection of inhibitors/antibiotic residues in milk. Bulletin of the International Dairy Federation, vol 442. Int Dairy Fed; 2010.

[365] Hu Y, Li J, Zhang Z, Zhang H, Luo L, Yao S. Imprinted sol-gel electrochemical sensor for the determination of benzylpenicillin based on Fe3O4@SiO2/multi-walled carbon nanotubes-chitosans nanocomposite film modified carbon electrode. Anal Chim Acta 2011;698(1-2):61–8. https://doi.org/10.1016/j.aca.2011.04.054.

[366] Khalilzadeh MA, Khaleghi F, Gholami F, Karimi-Maleh H. Electrocatalytic Determination of Ampicillin Using Carbon-Paste Electrode Modified with Ferrocendicarboxylic Acid. Analytical Letters 2009;42(3):584–99. https://doi.org/10.1080/00032710802677126.

[367] Duan H, Liu Z, Liu S, Yi A. Resonance Rayleigh scattering, second-order scattering and frequency doubling scattering methods for the indirect determination of penicillin antibiotics based on the formation of Fe3Fe(CN)62 nanoparticles. Talanta 2008;75(5):1253–9. https://doi.org/10.1016/j.talanta.2008.01.028.

[368] Lin H, Fang F, Zang J, Su J, Tian Q, Kumar Kankala R et al. A Fluorescent Sensor-Assisted Paper-Based Competitive Lateral Flow Immunoassay for the Rapid and Sensitive Detection of Ampicillin in Hospital Wastewater. Micromachines (Basel) 2020;11(4). https://doi.org/10.3390/mi11040431.

[369] Simmons MD, Miller LM, Sundström MO, Johnson S. Aptamer-Based Detection of Ampicillin in Urine Samples. Antibiotics (Basel) 2020;9(10). https://doi.org/10.3390/antibiotics9100655.

[370] Li X, Wang X, Wang L, Yang T, Wang D. Duplex Detection of Antibiotics in Milk Powder Using Lateral-Flow Assay Based on Surface-Enhanced Raman Spectroscopy. Food Analytical Methods 2021;14(1):165–71. https://doi.org/10.1007/s12161-020-01870-9.

[371] Douglas D, Banaszewski K, Juskelis R, Al-Taher F, Chen Y, Cappozzo J et al. Validation of a rapid lateral flow test for the simultaneous determination of β-lactam drugs and flunixin in raw milk. Journal of Food Protection 2012;75(7):1270–7. https://doi.org/10.4315/0362-028X.JFP-11-570.

[372] Markovsky RJ, Douglas DW, Sullivan R, Tran AC, Legg DR, McRobbie LW et al. BL30SEC Method for Detection of Beta-Lactams in Raw Commingled Cow Milk: AOAC Performance Tested MethodSM 061902. J AOAC Int 2020;103(5):1268–76. https://doi.org/10.1093/jaoacint/qsaa022.

[373] Fan R, Tang S, Luo S, Liu H, Zhang W, Yang C et al. Duplex Surface Enhanced Raman Scattering-Based Lateral Flow Immunosensor for the Low-Level Detection of Antibiotic Residues in Milk. Molecules 2020;25(22). https://doi.org/10.3390/molecules25225249.

[374] Zhang X, Zhao F, Sun Y, Mi T, Wang L, Li Q et al. Development of a highly sensitive lateral flow immunoassay based on receptor-antibody-amorphous carbon nanoparticles to detect 22 β-lactams in milk. Sensors and Actuators B: Chemical 2020;321:128458. https://doi.org/10.1016/j.snb.2020.128458.

[375] Li X, Pan Z, Li M, Jia X, Zhang S, Lin H et al. Europium chelate-labeled lateral flow assay for rapid and multiple detection of β-lactam antibiotics by the penicillin-binding protein. Analytical Methods 2020;12(28):3645–53. https://doi.org/10.1039/d0ay01140a.

[376] Andreotti PE, Ludwig GV, Peruski AH, Tuite JJ, Morse SS, Peruski LF. Immunoassay of infectious agents. BioTechniques 2003;35(4):850–9. https://doi.org/10.2144/03354ss02.

[377] Aydindogan E, Balaban S, Evran S, Coskunol H, Timur S. A Bottom-Up Approach for Developing Aptasensors for Abused Drugs: Biosensors in Forensics. Biosensors (Basel) 2019;9(4). https://doi.org/10.3390/bios9040118.

[378] Bauer M, Strom M, Hammond DS, Shigdar S. Anything You Can Do, I Can Do Better: Can Aptamers Replace Antibodies in Clinical Diagnostic Applications? Molecules 2019;24(23). https://doi.org/10.3390/molecules24234377.

[379] Ding X, Mauk MG, Yin K, Kadimisetty K, Liu C. Interfacing Pathogen Detection with Smartphones for Point-of-Care Applications. Anal Chem 2019;91(1):655–72. https://doi.org/10.1021/acs.analchem.8b04973.

[380] Gasilova N, Girault HH. Bioanalytical methods for food allergy diagnosis, allergen detection and new allergen discovery. Bioanalysis 2015;7(9):1175–90. https://doi.org/10.4155/bio.15.49.

[381] Mazaafrianto DN, Maeki M, Ishida A, Tani H, Tokeshi M. Recent Microdevice-Based Aptamer Sensors. Micromachines (Basel) 2018;9(5). https://doi.org/10.3390/mi9050202.

[382] Olasagasti F, Ruiz de Gordoa JC. Miniaturized technology for protein and nucleic acid point-of-care testing. Transl Res 2012;160(5):332–45. https://doi.org/10.1016/j.trsl.2012.02.012.

[383] Park KS. Nucleic acid aptamer-based methods for diagnosis of infections. Biosens Bioelectron 2018;102:179–88. https://doi.org/10.1016/j.bios.2017.11.028.

[384] Pelton R. Bioactive paper provides a low-cost platform for diagnostics. Trends Analyt Chem 2009;28(8):925–42. https://doi.org/10.1016/j.trac.2009.05.005.

[385] Sajid M, Kawde A-N, Daud M. Designs, formats and applications of lateral flow assay: A literature review. Journal of Saudi Chemical Society 2015;19(6):689–705. https://doi.org/10.1016/j.jscs.2014.09.001.

[386] Selvaraj JN, ZHOU L, WANG Y, ZHAO Y, XING F, DAI X et al. Mycotoxin detection — Recent trends at global level. Journal of Integrative Agriculture 2015;14(11):2265–81. https://doi.org/10.1016/S2095-3119(15)61120-0.

[387] Sharma A, Khan R, Catanante G, Sherazi TA, Bhand S, Hayat A et al. Designed Strategies for Fluorescence-Based Biosensors for the Detection of Mycotoxins. Toxins (Basel) 2018;10(5). https://doi.org/10.3390/toxins10050197.

[388] Soh JH, Chan H-M, Ying JY. Strategies for developing sensitive and specific nanoparticle-based lateral flow assays as point-of-care diagnostic device. Nano Today 2020;30:100831. https://doi.org/10.1016/j.nantod.2019.100831.

[389] Xu L, Zhang Z, Zhang Q, Li P. Mycotoxin Determination in Foods Using Advanced Sensors Based on Antibodies or Aptamers. Toxins (Basel) 2016;8(8). https://doi.org/10.3390/toxins8080239.

[390] XU F, REN K, YANG Y, GUO J, MA G, LIU Y et al. Immunoassay of chemical contaminants in milk: A review. Journal of Integrative Agriculture 2015;14(11):2282–95. https://doi.org/10.1016/S2095-3119(15)61121-2.

[391] Zhang L, Dou X-W, Zhang C, Logrieco AF, Yang M-H. A Review of Current Methods for Analysis of Mycotoxins in Herbal Medicines. Toxins (Basel) 2018;10(2). https://doi.org/10.3390/toxins10020065.

[392] Zhou W, Huang P-JJ, Ding J, Liu J. Aptamer-based biosensors for biomedical diagnostics. Analyst 2014;139(11):2627–40. https://doi.org/10.1039/c4an00132j.

[393] Jauset-Rubio M, El-Shahawi MS, Bashammakh AS, Alyoubi AO, O'Sullivan CK. Advances in aptamers-based lateral flow assays. TrAC Trends in Analytical Chemistry 2017;97:385–98. https://doi.org/10.1016/j.trac.2017.10.010.

[394] Dhiman A, Kalra P, Bansal V, Bruno JG, Sharma TK. Aptamer-based point-of-care diagnostic platforms. Sensors and Actuators B: Chemical 2017;246:535–53. https://doi.org/10.1016/j.snb.2017.02.060.

[395] Yang T, Yang X, Guo X, Fu S, Zheng J, Chen S et al. A novel fluorometric aptasensor based on carbon nanocomposite for sensitive detection of Escherichia coli O157:H7 in milk. J Dairy Sci 2020;103(9):7879–89. https://doi.org/10.3168/jds.2020-18344.

[396] Zhang K, Li H, Wang W, Cao J, Gan N, Han H. Application of Multiplexed Aptasensors in Food Contaminants Detection. ACS Sens. 2020;5(12):3721–38. https://doi.org/10.1021/acssensors.0c01740.

[397] Rei Yan SL, Wakasuqui F, Wrenger C. Point-of-care tests for malaria: speeding up the diagnostics at the bedside and challenges in malaria cases detection. Diagn Microbiol Infect Dis 2020;98(3):115122. https://doi.org/10.1016/j.diagmicrobio.2020.115122.

[398] Phung NL, Walter JG, Jonczyk R, Seiler LK, Scheper T, Blume C. Development of an Aptamer-Based Lateral Flow Assay for the Detection of C-Reactive Protein Using Microarray Technology as a Prescreening Platform. ACS Comb Sci 2020;22(11):617–29. https://doi.org/10.1021/acscombsci.0c00080.

[399] Milchindustrie-Verband. [July 26, 2021]; Available from: https://milchindustrie.de/.

[400] Council Regulation 2377/90/EC laying down a community procedure for the establishment of maximum residue limits of veterinary medicinal products in foodstuffs of animal origin (1990) Off J Eur Communities; 2377.

[401] Khlebtsov BN, Bratashov DN, Byzova NA, Dzantiev BB, Khlebtsov NG. SERS-based lateral flow immunoassay of troponin I by using gap-enhanced Raman tags. Nano Res. 2019;12(2):413–20. https://doi.org/10.1007/s12274-018-2232-4.

[402] Adhikari M, Strych U, Kim J, Goux H, Dhamane S, Poongavanam M-V et al. Aptamer-Phage Reporters for Ultrasensitive Lateral Flow Assays. Anal Chem 2015;87(23):11660–5. https://doi.org/10.1021/acs.analchem.5b00702.

[403] Dittrich S, Streubel R, McDonnell C, Huber HP, Barcikowski S, Gökce B. Comparison of the productivity and ablation efficiency of different laser classes for laser ablation of gold in water and air. Appl. Phys. A 2019;125(6). https://doi.org/10.1007/s00339-019-2704-8.

[404] Beer. Bestimmung der Absorption des rothen Lichts in farbigen Flüssigkeiten. Ann. Phys. Chem. 1852;162(5):78–88. https://doi.org/10.1002/andp.18521620505.

[405] Stokes GG. On the Effect of the Internal Friction of Fluids on the Motion of Pendulums. In: Stokes GG, editor. Mathematical and physical papers, Volume 3. Cambridge: Cambridge University Press; 2009, p. 1–10.

[406] Resch ZT, Fautsch MP. Glaucoma-associated myocilin: a better understanding but much more to learn. Exp Eye Res 2009;88(4):704–12. https://doi.org/10.1016/j.exer.2008.08.011.

[407] Dieckmann Y, Cölfen H, Hofmann H, Petri-Fink A. Particle size distribution measurements of manganese-doped ZnS nanoparticles. Anal Chem 2009;81(10):3889–95. https://doi.org/10.1021/ac900043y.

[408] Einstein A. Über die von der molekularkinetischen Theorie der Wärme geforderte Bewegung von in ruhenden Flüssigkeiten suspendierten Teilchen. Ann. Phys. Chem. 1905;322(8):549–60. https://doi.org/10.1002/andp.19053220806.

[409] Luo D, Wang X, Zeng S, Ramamurthy G, Burda C, Basilion JP. Prostate-specific membrane antigen targeted gold nanoparticles for prostate cancer radiotherapy: does size matter for targeted particles? Chem Sci 2019;10(35):8119–28. https://doi.org/10.1039/c9sc02290b.

[410] Jimenez MS, Luque-Alled JM, Gomez T, Castillo JR. Evaluation of agarose gel electrophoresis for characterization of silver nanoparticles in industrial products. Electrophoresis 2016;37(10):1376–83. https://doi.org/10.1002/elps.201500577.

[411] Artimo P, Jonnalagedda M, Arnold K, Baratin D, Csardi G, Castro E de et al. ExPASy: SIB bioinformatics resource portal. Nucleic Acids Res 2012;40(Web Server issue):W597-603. https://doi.org/10.1093/nar/gks400.

[412] Altschul SF, Gish W, Miller W, Myers EW, Lipman DJ. Basic local alignment search tool. J Mol Biol 1990;215(3):403–10. https://doi.org/10.1016/S0022-2836(05)80360-2.

[413] Yang J, Yan R, Roy A, Xu D, Poisson J, Zhang Y. The I-TASSER Suite: protein structure and function prediction. Nat Methods 2015;12(1):7–8. https://doi.org/10.1038/nmeth.3213.

[414] Drozdetskiy A, Cole C, Procter J, Barton GJ. JPred4: a protein secondary structure prediction server. Nucleic Acids Res 2015;43(W1):W389-94. https://doi.org/10.1093/nar/gkv332.

[415] Bruno JG. Application of DNA Aptamers and Quantum Dots to Lateral Flow Test Strips for Detection of Foodborne Pathogens with Improved Sensitivity versus Colloidal Gold. Pathogens 2014;3(2):341–55. https://doi.org/10.3390/pathogens3020341.

[416] Cheng N, Liu Y, Mukama O, Han X, Huang H, Li S et al. A signal-enhanced and sensitive lateral flow aptasensor for the rapid detection of PDGF-BB. RSC Adv. 2020;10(32):18601–7. https://doi.org/10.1039/d0ra02662j.

[417] Cherkasov VR, Mochalova EN, Babenyshev AV, Vasilyeva AV, Nikitin PI, Nikitin MP. Nanoparticle Beacons: Supersensitive Smart Materials with On/Off-Switchable Affinity to Biomedical Targets. ACS Nano 2020;14(2):1792–803. https://doi.org/10.1021/acsnano.9b07569.

[418] Jin B, Yang Y, He R, Park YI, Lee A, Bai D et al. Lateral flow aptamer assay integrated smartphone-based portable device for simultaneous detection of multiple targets using upconversion nanoparticles. Sensors and Actuators B: Chemical 2018;276:48–56. https://doi.org/10.1016/j.snb.2018.08.074.

[419] Lee BH, Kim SH, Ko Y, Park JC, Ji S, Gu MB. The sensitive detection of ODAM by using sandwich-type biosensors with a cognate pair of aptamers for the early diagnosis of periodontal disease. Biosens Bioelectron 2019;126:122–8. https://doi.org/10.1016/j.bios.2018.10.040.

[420] Mukama O, Wu W, Wu J, Lu X, Liu Y, Liu Y et al. A highly sensitive and specific lateral flow aptasensor for the detection of human osteopontin. Talanta 2020;210:120624. https://doi.org/10.1016/j.talanta.2019.120624.

[421] Narayan C, Kwon J, Kim C, Kim S-J, Jang SK. Virus-based SELEX (viro-SELEX) allows development of aptamers targeting knotty proteins. Analyst 2020;145(4):1473–82. https://doi.org/10.1039/c9an01943j.

[422] Ranganathan V, Srinivasan S, Singh A, DeRosa MC. An aptamer-based colorimetric lateral flow assay for the detection of human epidermal growth factor receptor 2 (HER2). Anal Biochem 2020;588:113471. https://doi.org/10.1016/j.ab.2019.113471.

[423] Sharma R, Akshath US, Bhatt P, Raghavarao K. Fluorescent aptaswitch for chloramphenicol detection – Quantification enabled by immobilization of aptamer. Sensors and Actuators B: Chemical 2019;290:110–7. https://doi.org/10.1016/j.snb.2019.03.093.

[424] Tian R, Ji J, Zhou Y, Du Y, Bian X, Zhu F et al. Terminal-conjugated non-aggregated constraints of gold nanoparticles on lateral flow strips for mobile phone readouts of enrofloxacin. Biosens Bioelectron 2020;160:112218. https://doi.org/10.1016/j.bios.2020.112218.

[425] Wu Z, He D, Xu E, Jiao A, Chughtai MFJ, Jin Z. Rapid detection of β-conglutin with a novel lateral flow aptasensor assisted by immunomagnetic enrichment and enzyme signal amplification. Food Chem 2018;269:375–9. https://doi.org/10.1016/j.foodchem.2018.07.011.

[426] Zhu C, Li L, Wang Z, Irfan M, Qu F. Recent advances of aptasensors for exosomes detection. Biosens Bioelectron 2020;160:112213. https://doi.org/10.1016/j.bios.2020.112213.

7. Appendix

7.1 Materials and Methods

7.1.1 Materials

All utilized material´s purity throughout this thesis was of analytical grade. Chemicals were provided by Sigma Aldrich, Merck Millipore or Carl Roth, if not stated otherwise. The utilized aptamers were provided by Iba GmbH (Germany), except for the miniStrep aptamer, which was provided by Biospring GmbH (Germany). LFA test stripes were provided by either Fassisi GmbH (Germany) and Microcoat Biotechnologie GmbH (Germany). Supplier of technical devices are mentioned in the respective sections.

7.1.2 Laser Ablation in Liquids

Laser ablation in liquids has been established to generate colloidal organic-ligand-free noble metal nanoparticles [17]. Gold, silver as well as the respective alloy particles were synthesized by ablating metal sheets of 0.5 mm thickness (99.99% purity, Institute for noble metal chemistry, Schwäbisch-Gmünd, Germany) in a PTFE batch-chamber (30 mL) under constant stirring. To guarantee electrostatic stabilization, as well as required size quenching, LAL took place in low-ionic-strength electrolyte solutions (0.6 µM NaPP solution for Au NP > 10 nm, 0,1 mM NaCl for all other other colloids). Au NP > 10 nm were produced via ps Nd:YAG laser (Ekspla, Atlantic Series, 10 ps, 1064 nm, 9.6 mJ, 100 kHz, 10 min ablation time), whereas Au NP < 10 nm, Ag NP and alloy particles were produced via ns Nd:Yag laser (Rofin Powerline E, 1064 nm, 23.5 J/cm^2, 10 min ablation time). A schematic overview of the ablation chamber used during the LAL process in this work is shown in **Figure 71**.

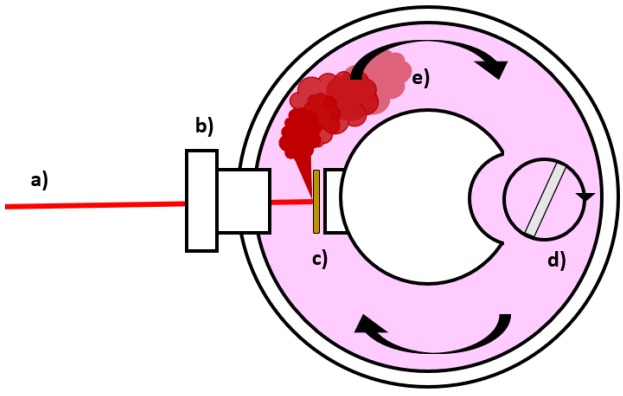

Figure 71: Schematic overview LAL a) laser beam, b) Quartz window, c) target, d) stirrer. e) is a representation of the nanoparticle fume distributed throughout the chamber by a circular flow.

To achieve a monomodal size distribution, the generated multimodal colloids were size separated via a combination of an additional maturation step (24 h incubation at high concentration after LAL) and subsequent centrifugation. Au NP < 10 nm were gained after ultracentrifugation of matured Ekspla raw colloid (Optima MAX-XP, Beckman Coulter, 17 min, 30,000 g, 7°C) according to the centrifugation protocol introduced by Krawinkel et al. [187]. The supernatants contained the desired small Au NP, whereas the pellet was further used to isolate larger Au NP. All other colloids were centrifuged according to the following centrifugation protocol:

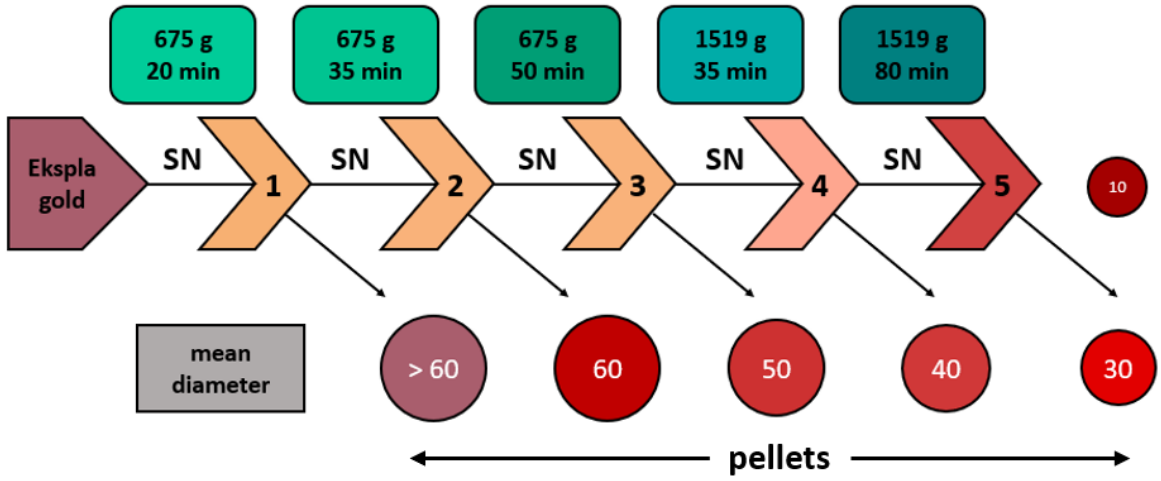

Figure 72: Centrifugation procedure for monomodal 40 nm and 30 nm Au NP. Centrifugation step 5 ultimately leads to a monomodal pellet (30 nm mean hydrodynamic diameter) and a monomodal supernatant (10 nm mean hydrodynamic diameter); (SN=supernatant, P=pellet)

If not stated otherwise, colloidal samples were diluted in MilliQ (18.2 MΩ/cm at 25°C, Merck Millipore)

7.1.3. UV-vis extinction spectroscopy

UV-vis spectroscopy allows the quantitative and qualitative analysis of UV-vis active samples. It was used throughout this work to quantify DNA and functional ligands, analyze nanoparticles with respect to their SPR-peak, as well as to assess colloidal stability. The UV-vis extinction spectroscopy represents a non-destructive analysis tool, based on Lambert-Beer´s law [404]. The sample is transferred into a quartz-glass-cuvette of known diameter and probed by a light beam of known intensity and wavelength. The light passes the cuvette and therefore the sample. Within the sample several possible interactions between analyte and light occur: scattering, absorbance, and transmission. The light passing the cuvette is detected and its remaining intensity compared with the initial intensity. In accordance with Lambert-Beer´s Law the difference of the initial and resulting intensity can be used to calculate the concentration of the sample. In addition to that, the extinction maxima of the sample can provide additional information on its very nature, e.g. gold nanoparticle feature a strong extinction at 520 nm, which is caused by their SPR.

UV-vis measurements were performed in triplicates, in 1.5 mL quartz cuvettes with 10 mm path length, using a Thermo Scientific Evolution 201 photometer. The spectral range spanned from 190 nm to 900 nm, with a step width of 1 nm. The chosen integration time was 0.05 s at a scan speed of 1200 nm/min.

7.1.4 Analytical disc centrifugation (ADC)

Analytical disc centrifugation was chosen as standard technique for analyzing colloidal samples regarding their size distribution. The measurement is based on the spatial separation of the different particle size fractions within the colloidal sample via differential centrifugal sedimentation. The analyzed colloid is injected into a spinning optically clear disc, which is filled with a saccharose density gradient for elongated sedimentation time. The nanoparticles move from the central injection spot to the outside of the disc through the gradient due to the centrifugal force. The measurement itself is based on an intensity measurement of a light source shining through the optically clear disc. Nanoparticles passing the light barrier will decrease the detected intensity. The intensity signal of a single wavelength (λ = 405 nm) is measured over time. This intensity-time-signal is used to calculate the particle diameter and provides a particle size distribution based on the work of Stokes [405], which is either weight, surface, or number weighted. It must be stressed that all resulting particle distributions are legit representations of the sample´s true nature, even though they emphasize different aspects of the sample´s size distribution. The biggest advantage of the ADC represents its ability to analyze bimodal samples due to the spatial separation of the different size modes, so that smaller particles can be detected in the presence of larger ones in contrast to measurements via dynamic light scattering. However, this measurement technique features its own drawbacks. If the analyzed particles exhibit strong back-diffusion, charge, or vary in density– like e.g. a solid gold nanoparticle carrying DNA-ligands – the resulting size distribution will be ultimately altered and distorted. [406,407]

The measurements were performed by injecting 100 µL of colloidal sample into the spinning centrifuge disc (24,000 RPM, saccharose gradient ranging from 24 wt% to 8 wt% at 2% steps, each step consisting of 1.6 mL saccharose solution). Each measurement series was preceded by an external PVC standard (0.237 µm in diameter, 1.385 g/mL, std. half width 0.15 microns, max. diameter 0.3 microns). Distributions were analyzed by applying a log normal fit onto the measured distribution and to calculate the polydispersity index (PDI), as well as the x_c-value.

7.1.5 Transmission electron microscopy (TEM)

Transmission electron microscopy was utilized to analyze the average diameter and size distribution of colloidal nanoparticles. An electron beam passes through the sample, but a fraction of the electrons is diffracted by the atomic planes of the sample. The microscopy is performed under vacuum conditions to avoid deflection of electrons by air molecules. The diffraction patterns are furthermore transformed into 2d images with elemental contrast based on the thickness of the sample and the element-dependent electron absorption. However, due to this dependence, organic samples like aptamers and hydrocarbon structures provide only very little elemental contrast whereas gold nanoparticle can be easily detected and analyzed. Due to this limitation this technique was primarily used as control measure to guarantee accurate size distributions of the analyzed colloids.

TEM samples were prepared by placing a sample droplet of 5 – 15 µL on a carbon-coated copper grid. The sample was dried under dust free conditions and the measurement finally performed on a Phillips CM12 microscope (80 – 120 kV acceleration voltage) by Dipl.-Ing. Jurij Jakobi.

7.1.6 Dynamic Light Scattering (DLS)

Dynamic light scattering represents a non-destructive, quantitative method to analyze colloidal samples with regard on their size distribution. A laser beam probes the sample colloid and the nanoparticles within the sample scatter the laser light, when passing the laser-beam due to Brownian motion. The scatter intensity is detected, and its fluctuation observed over time. The resulting intensity signals are analyzed and transformed into diffusion coefficients via autocorrelation, which can be further transformed into the hydrodynamic size via Stokes-Einstein relation [405,408]. The method allows to analyze monomodal samples with high accuracy but is prone to errors if bimodal distributions are analyzed, since larger particles have a much higher scatter intensity which scales with the sixth power of the nanoparticle diameter, and therefore, tend to outshine smaller particles [409]. At the same time, Brownian movement is strictly temperature and viscosity dependent.

DLS measurements were performed in triplicates via the Nicomp 3800-DLS-ZLS, at 25°C using a 1 mL quartz glass cell. The cell was preincubated in the device until a constant fluctuation was achieved before. Ten measurement repetitions were performed for each sample.

7.1.7 Zeta Potential

The zeta potential provides a measure for colloidal stability. Highly positive and negative zeta potentials of ± 40 mV are considered long-term stable. The measurement of the zeta potential is based on light scattering. The colloidal particles are exposed to an external electric field, which leads to particle movements. A laser probes the sample, and a detector observes the scattering signals and

Doppler frequency shifts. Those raw data can be converted into the particle electrophoretic velocities. According to either the Smoluchoski (larger particles, high ionic strength) or the Hückel (smaller particles, low ionic strength) model the electrophoretic velocities are used to calculate the zeta potential of the particles. The zeta potential describes the potential required to cause the slipping to shear off from the stern layer. Thus, it correlates with the colloidal stability, which is based on electrostatic repulsion. Anyway, due to the strong scattering intensity differences for small and large particles, large particles may always dominate the outcome of these measurements.

Zeta potential measurements were performed in triplicates via the Nicomp 3800-DLS-ZLS. A quartz glass cell with a sample volume of 1 mL was used. The Hückel model was utilized for the calculations of the potentials. All samples could equilibrate their temperature prior to the measurement.

7.2 Bioconjugation, quantification and bioconjugate analysis

The generation of nano-bio-conjugates represents the very heart of this work. The following sections provide detailed information on the conjugation procedures, conjugation quantification and functional analysis of conjugates. However, in some cases these conjugation procedures were adjusted to the requirements of the experimental design of previously described experiments. Such alterations are separately marked in the respective sections.

7.2.1 Bioconjugation and quantification

Bioconjugation describes the functionalization of a suitable surfaces (flat, curved, or spherical) with biomolecules. Here, it must be stressed that those biomolecules must not be of biological origin, but belong to the main types of molecules, which can be found in nature: peptides and proteins (including antibodies and enzymes), DNA and RNA, and combinations of all those molecules, featuring various modifications like fluorescence markers, thiol-, or amino-groups, etc. This work focusses mainly on the conjugation of laser-generated noble-metal nanoparticles with thiolated aptamers. Throughout this work a large variation of conjugation procedures was tested. Therefore, this section will provide the final core conjugation protocol, which has been modified for the different aptamers, nanoparticles, etc.

Salt solutions, colloids and surfactants were stored at 4°C prior to experiments. DNA aliquots were stored at -20°C and thawed on ice directly before the conjugation procedure. The generated conjugates were subsequently heat-treated at 95°C for 5 min in accordance to Song et al. [36]. All conjugations were performed in triplicates.

Each colloid was diluted to the desired concentration (final concentration 50 – 100 µg/mL). The colloids were subsequently mixed with a ready to use aptamer solution (working concentration 10 µM; final concentration: 0.1 µM – 5 µM). The solutions were mixed thoroughly and incubated for 10 min at RT. The respective salt (1 M $MgCl_2$: final concentration 200 µM; 1 M NaCl: final concentration 0.3 mM), was added within 3 – 7 steps until the desired final concentration was achieved. In between each salt aging step, the samples were incubated for 10 min. The last step consisted of the addition of 0.1 % Tween 20 and 0.01 % SDS in accordance with the conjugation protocol presented by Hurst et al. [175] Afterwards, samples were incubated at 4°C overnight. Excess unbound DNA molecules were separated from the conjugates via centrifugation (1. conjugate extraction: 2x 1180 g, 7°C, 1 h; 2. DNA quantification: 100.000 g, 7°C, 1 h). The conjugate was resuspended in resuspension buffer (0.01 M PBS, 0.5% PEG250, 2% saccharose, 0.1 % Tween20; according to Song et al. [319]). The supernatant containing unbound DNA was further analyzed via UV-vis analysis. This indirect technique to determine the conjugation efficiency has been previously described by Petersen & Barcikowski in 2009 and was shown to be able to quantify the surface coverage and conjugation efficiency of the generated conjugates without significant difference to the previously established direct method based on fluorescence measurement of the bound DNA molecules. [25]

7.2.2 96-well plate conjugation and optical evaluation

Decreasing the conjugation volume drastically decreases the required material demand. Therefore, it is possible to evaluate the conjugation behavior of nanoparticles exposed to drastic DNA excess concentrations. In addition to that, it is possible to analyze more parameters at the same time, in comparison to the conjugation of 1.5 mL samples, which limited the testing to twelve 1 mL samples per run due to the limitations of centrifuges, etc. Here, 96-well-plates, or microplates, by Eppendorf (96/F-PP, clear wells, PCR clean) were utilized to systematically analyze the conjugation behavior of 96 samples at the same time. The sample volume was kept at 200 µL to allow the subsequent analysis of samples via the TECAN Spark 20 M multimode microplate reader. The conjugation procedure itself was performed in accordance with 8.2.1. Conjugate stability was analyzed via the rapid red determination (RR-value, see following section for details).

7.2.3 Rapid Red (RR) – conjugate stability evaluation based on digital images

Conjugate stability plays a major role in the successful utilization of nano-bio-conjugates in POC devices. Without sufficient stability there is no functionality. However, when it comes to determining the colloidal stability of DNA functionalized nano-bio-conjugates, the established techniques like zeta-potential analysis and UV-vis spectroscopy turned out to be too time-consuming. The Rapid Red (RR) value was invented to quickly evaluate the reddishness of a sample featuring laser-generated gold

nanoparticles. Stable gold nanoparticles feature a strong SPR-peak at around 520 nm, resulting in an intense red color. A destabilization of the nanoparticles will always lead to a color shift towards longer wavelengths, thus leading to a purple-bluish color. Since the human color vision is based on additive color signal analysis of red, blue and green, the RGB color code system was used to analyze digital photos of conjugate samples, according to the following formula:

$$\boldsymbol{RR}: \quad X = \frac{R}{1 + G + B}$$

To allow the comparability of pictures and the respective RR-values of conjugates, all digital images were acquired using standardized conditions. 96-well-plates, as well as 1.5 mL reaction tubes were placed on the Phototherapy Unit TL 30 (Beurer GmbH, Germany) after a pre-warm phase of 10 min. Pictures were taken with a Huawei Y6 (2019) and further analyzed via FIJI (version 1.53 g December 2020). Long-term observation of samples revealed that samples, featuring a RR-value of at least 1 can be considered stable. However, it has to be stressed, that the opaqueness of the analyzed material can influence the RR-value determination and that it has been designed to match the color palette of laser-generated gold nanoparticles. Color outside of this range, e.g., orange, brown, green, might generate misleading RR-values and should not be analyzed via this method.

7.2.4 Functionality Assay – streptavidin binding

Conjugates featuring the miniStrep-aptamer can bind streptavidin. To quantify their binding ability the two-times purified conjugates were mixed with a streptavidin solution (final concentration 25 µg/mL) and incubated overnight (4°C). The mixture was subsequently centrifuged (100.000 g, 7°C, 1 h) to separate the conjugate and its bound streptavidin (pellet) and the unbound streptavidin (supernatant). UV-vis extinction spectroscopy was ultimately used to analyze the amount of unbound streptavidin.

7.2.5 Gel electrophoresis and polyacrylamide gel electrophoresis

Agarose gel electrophoresis was used to analyze conjugates, aptamers, oligonucleotides as well as possible aptamer fragments. Casted gels contained 0.2 – 0.3 % (w/v) agarose (Carl Roth) dissolved in 0.5 x TAE buffer (20 mM acetic acid, 20 mM Tris, 0.5 mM ethylenediaminetetraacetic acid (EDTA), pH 8.5). Varying volumes of conjugate samples were provided with loading buffer (30w% Glycerin + 0.001 v% Tween80 + 0.5 x Tris, Borate, EDTA (TBE) buffer) in a 1-to-1-ratio [410]. Electrophoresis was performed for 1 h at 100 V using the peqPOWER300 power supply by peqlab. Gels were stained via ethidium-bromide and documented using the BIORAD *ChemiDoc* MP (302 nm for ethidium-bromide: 625 – 650 nm for Cy5).

7.2.6 Native PAGE

Native PAGE was utilized to analyze the successful hybridization of aptamers and their respective complementary oligonucleotides. A native gel (10 – 15 %wt; 1.5 mm thickness) was used to analyze the DNA samples (0.1 µM – 1.0 µM), which were beforehand diluted with 6xDNA-loading dye by Thermo Scientific (up to a total volume of 24 µL). The electrophoresis was performed at 120 V for 60 min in 1x TBE buffer, after a pre-running of time of 30 min at 120 V without any samples to allow for sharper bands. Samples were subsequently stained with 1: 10.000 ethidium bromide in 1x TBE buffer for 15 min.

7.3 Lateral Flow Assay Development and Functionality Assays

The goal of this project was to develop LFAs for different target systems, including OtA and ampicillin. In this regard, LFA systems by Fassisi GmbH and Microcoat Biotechnologie GmbH were tested. The optimization of the LFA conditions were purely done for Microcoat test stripes (backing with a total length of 72 mm, fast nitrocellulose membrane of 25 mm (CN95), test line: polymerized streptavidin (1 mg/mL), control line: FITC labelled unspecific IgG, standard waste and conjugate pad, 5 mm width). The test stripes were either equipped with conjugate dried onto a glass fiber membrane (10 µL – 50 µL conjugate, dried at 40°C for 2 h), 10 µL – 50 µL conjugate (applied via Eppendorf pipette onto the test stripe, or via dipping into the respective conjugate (dip stick assay). In addition to that 40 µL of running buffer (100 mM Tris (pH 8), 0.05 % Tween20, 1 % BSA) were applied onto the test stripe, respectively dipstick tests were transferred into wells containing running buffer. The test stripes were incubated for 15 min at RT and further analyzed via digital photography.

7.4 Bioinformatics

7.4.1 Apta-Index™

The Apta-Index™ by AptaGen, LLC, is an aptamer database, which was used to identify aptamer sequences for the respective target substances featured throughout this work. It features 594 aptamer sequences, which have been described in literature and lists the aptamer chemistry (DNA, RNA, protein), antigen/target category, base-length, as well as, affinity given in K_d.

https://www.aptagen.com/apta-index/ (last access: 23.06.2021)

7.4.2 ExPASy

The Expert Protein Analysis System (ExPASy) covers a wide range of information regarding proteins as well as antibodies. In addition to that, it contains the molecular weight calculator, which allows to

estimate the molecular weight of a protein and peptide, based on its amino acid sequence. ExPASy is operated by the SIB [411].

https://www.expasy.org/ (last access: 21.06.2021)

7.4.3 BLAST®

The Basic Local Alignment Search Tool represents a logarithm to compare biological sequences, such as nucleotide and protein sequences with a large database of known sequences [412]. It was used for sequence alignments of aptamers and complementary oligonucleotides.

https://blast.ncbi.nlm.nih.gov/Blast.cgi (last access: 19.06.2021)

7.4.4 I-TASSER

The Iterative Threading Assembly Refinement (I-TASSER) represents a bioinformatic tool for protein structure and function prediction. It can be used to predict three – dimensional models of proteins and peptides, based only on their amino acid sequence [413]. User can access the server of the Yang Zhang Lab of the University of Michigan to use I-TASSER for academic purposes.

http://zhanglab.ccmb.med.umich.edu/I-TASSER/ (last access: 03.06.2021)

7.4.5 JPred – A Protein Secondary Structure Prediction Server

Jpred v.4 represents an accurate secondary structure prediction tool that is available since 1998 [414]. It is based on the JNet algorithm and was used to predict the secondary structure of peptide sequences in silico.

http://www.compbio.dundee.ac.uk/jpred/ (last access: 23.06.2021)

7.5 Calibration curves

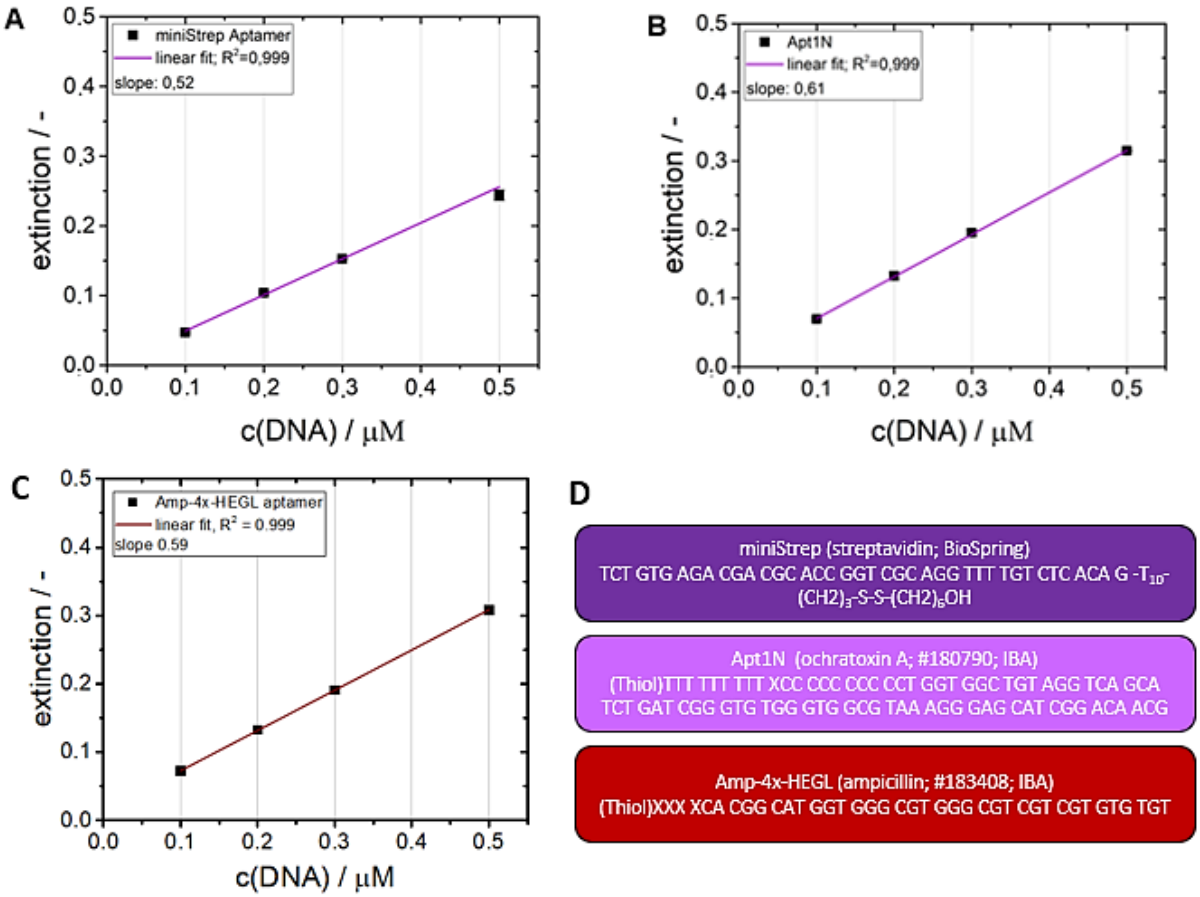

Figure 73: UV-vis extinction spectroscopy-based calibrations for A) miniStrep, B) Apt1N, and C) Amp-4x-HEGL aptamers. The respective sequences are provided in section D). Measurements were performed in triplicates. Error bars are included but too small to be seen.

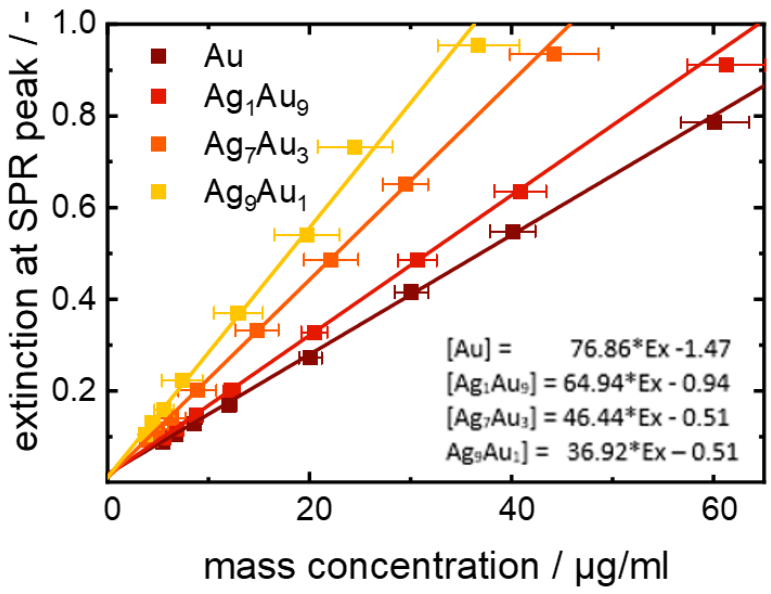

Figure 74: UV-vis extinction spectroscopic calibration of colloids of different elemental nanoparticle compositions.

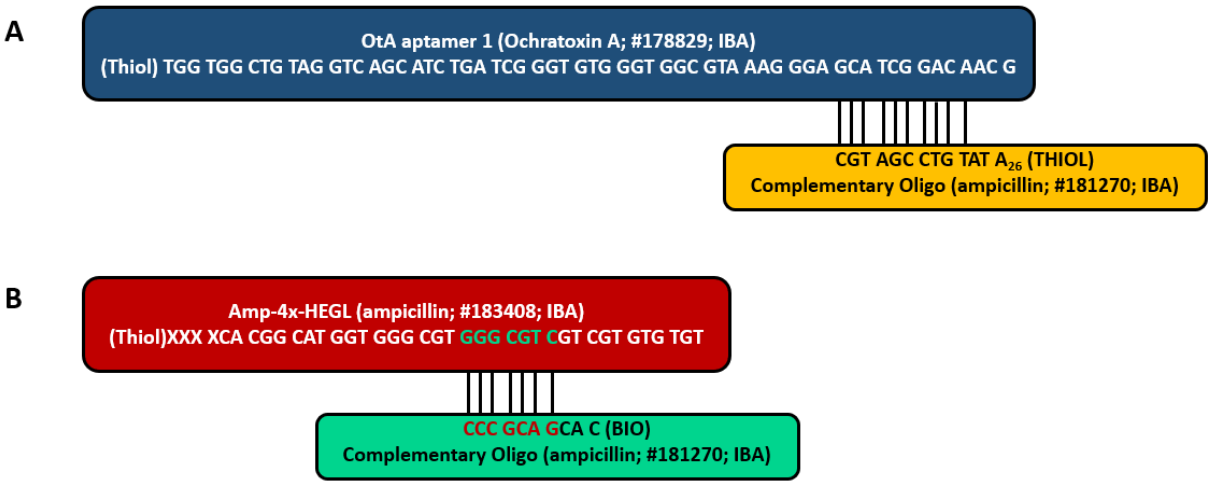

Figure 75: Aptamers and their complementary oligonucleotide sequences; A) ochratoxin A aptamer; B) ampicillin aptamer. BIO = biotin group; Thiol = thiol group.

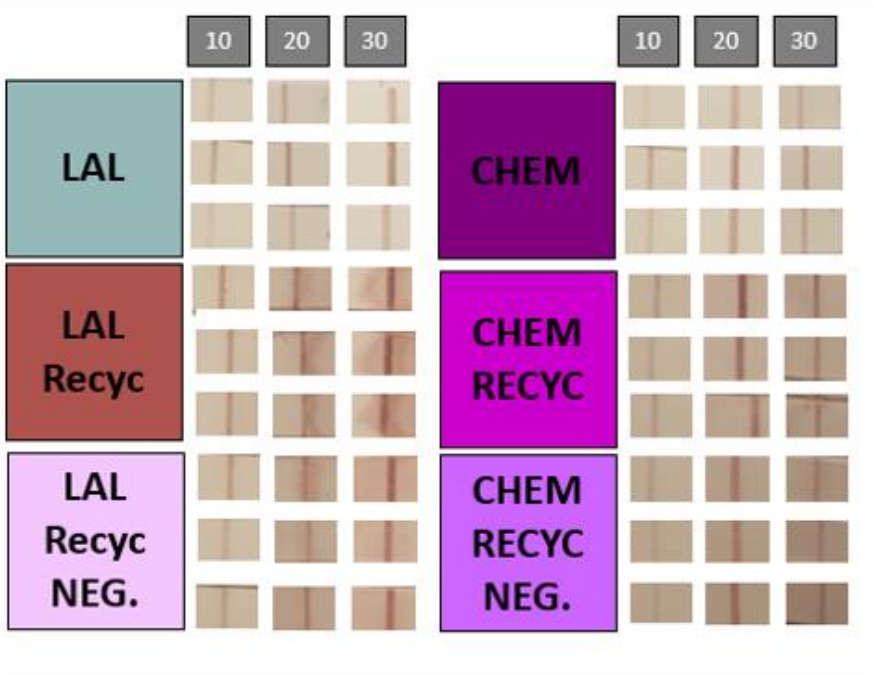

Figure 76: LFAs featuring LAL-Au NP-nano-bio-conjugates (LAL) and chemically-synthesized-Au NP – conjugates at varying volumes (10 µL – 30 µL). RECYC = recycled aptamer; NEG. = negative control without salt-aging.

8. Contributions

Jurij Jakobi

Mr. Jakobi was responsible for generating the TEM images, that were used throughout this Thesis.

Jana Heiden

Mrs. Heiden researched the conjugation of 40 nm Au NP with OtA aptamer at varying ionic strength and varying pH during her bachelor thesis.

Rosa van Vlodrop

Mrs. van Vlodrop developed the optimized Au NP centrifugation procedure for monomodal 30 nm Au NP, provided detailed insights into the conjugation and functionality of the OtA aptamer to a variation of different Au NP during her master thesis.

Jarno Banas

Mr. Banas provided TEM analysis of colloidal nanoparticles as well as data regarding the conjugation of LAL particles with Amp aptamer.

Farbod Riahi, Farbod Ebrahimi, Shayan Shoja

Mr. Riahi, Mr. Ebrahimi, and Mr. Shoja contributed data regarding the application and drying of nano-bio-conjugates onto glass fiber membrane.

Dana Krenz

Mrs. Krenz analyzed the effect of different buffers on conjugate stability and the conjugate´s functionality during her bachelor thesis.

Sem Klunder

Mr. Klunder helped to develop the rapid red quantification method for conjugates immobilized on glass fiber during his practical course.

Frederic Stein

Mr. Stein and I contributed equally to our manuscript “Influence of the gold/silver ratio on the conjugation and functionality of gold-silver alloy nanoparticle aptamer bioconjugates”.

Sections of the introduction featuring alloy nanoparticles and results regarding alloy nanoparticles and their functionality were written by Frederic Stein. Introduction and discussion of aptamer functionality were mainly written by Andreas Schielke.

Frederic Stein performed all experiments featuring AgAu NP, whereas Andreas Schielke developed the functionality assay and performed the functionality experiments featuring Au NP.

Microcoat Biotechnologie GmbH

The team around Martin Kind at Microcoat assisted in the design of the final functional LFA test stripe and manufactured the test stripes used throughout the chapters 4.3 and 4.4.

Fassisi

The Fassisi team assisted in the design of the original OtA LFA and manufactured the initial test stripes.

Iba

The team around Joachim Bertram provided insights into aptamer design and helped to develop the improved OtA-Apt1N-seqeuence, as well as the final HEGL-4x-Amp-aptamer.

9. Curriculum Vitae

Der Lebenslauf ist in der Online-Version aus Gründen des Datenschutzes nicht enthalten.

10. Acknowledgements

Project ALFA has been an exciting ride. Friends were made along the way; almost lost on late-night strolls through foreign cities. Experiments did not work, or unexpected findings were made. The ADC tried to drive me insane, and almost succeeded. We played a lot of werewolf and went on amazing trips. In short, it had everything: tears, sweat, and joy.

The ZIM project ZF 4044505AJ7 was funded by the Zentrales Innovationsprogramm Mittelstand by the Bundesministerium für Wirtschaft und Energie based on a decision by the German Bundestag. We would like to thank the institutions mentioned for providing the financial means.

I thank Prof. Dr. Stephan Barcikowski for welcoming me in his working group and the knowledge and experience he shared with me as my supervisor. I will always have fond memories of Nizza. My gratitude also goes to Prof. Dr. Sebastian Schlücker as my second supervisor.

In addition to that, I want to show my gratitude to Dr. Christoph Rehbock, my group leader. He always listened to all my complaints and guided me. He may have forgotten at times that I served as his vice-vice-group leader, but I will never forget the great nerd-talks we had. May the force be with you! Live long and prosper!

Many partners were involved in project ALFA. I want to say thank you to my project coordinator Joachim Bertram and the team of Iba, Kristine Knipper, Stephan Sanders and the team of Fassisi, and last but not least, Johanna Walter, Alina Eilers and Torsten Schüling of the Leibniz Universität Hannover. In addition to that a heartly thank you goes to Martin Kind and his team.

Before I thank the team of the TC 1, I want to especially mention Anna Ziefuß, who served as my supervisor during my research practical and turned a molecular biologist into a proper nanoparticle scientist within three weeks. She has always been a great mentor and has become a good friend of mine. I wish you the very best for your career and your new group!

In addition to that I want to highlight how much I learned from Frederic Stein during our work on the AgAu paper. He is an inspiring researcher and a highly supportive colleague. I really enjoyed our collaboration and are grateful for all your hard work, support and great ideas, my friend. Thank you!

With that out of the way it’s about time to thank my team. I enjoyed having you around and will miss our activities and your company. Thank you, my dear friend Dr. Sarah Dittrich, Dr. Carlos Donate-Buendia, Gaétan Laurens, Tim Hupfeld, Galina Marzun, Alexander Heinemann, Jacob Johny, Hanna

Martin, Dominik Wäsche, Mark Kalus, Sebastian Kohsakowski, Ruksan Nadarajah, Simon Siebeneicher, Friedrich Waag, Carmen Streich, Yaya Li, Jurij Jacobi, Florian de Kock, René Streubel, Dario Becker, Olga Gridina, Lisa Gamrad, Elisabeth Mühlhausen, Ina Haxhiaj, Marcus Lau, and all other team members. I also want to show my gratitude to the team behind the team: Nina Stockem and Claudine Florian. Thank you! Last but not least: Thank you Dieter! You were the heart of the group and I feel thankful and honored that you were still around when I started. You will be missed.

Project ALFA wouldn´t have been possible without a strong team. I heartfully thank all my ALFA students: my dear friend Rosa van Vlodrop, Jana Heiden, Farbod Ebrahimi, Farbod Riahi, Shayan Shoja, Jarno Banas, Sem Klunder, and Dana Krenz. I am grateful for all your work, brilliant ideas, and the fun we had. I am proud to have served as your supervisor.

I also want to thank my friends from my old department, namely Sabine Dietl, Christina Stracke, Thomas Knura, and Agathe Materla. It was always great coming back to you for a chat and a coffee. Thank you for keeping me sane and for your support.

Speaking of coffee, how can one thank his best friends for being always around, cheering me up, all the laughing, and the great time we had. Thank you! I can hardly imagine having such amazing breaks with my future teams. We may not meet again in our cozy little coffee kitchen, but I am happy to have found friends in you for life. You are the best.

With that said, I want to thank my family. Thank you for supporting me, cheering me up, and just being like you are. A heartly thank you to Marlies, Hartmut, Anika and Kathrin. Speaking of family this also includes my close friends Martin, Björn, Kathi & Leo, Gretlies & Tim, Sven, and Matin.

Finally, I need to thank my beloved companion. Thank you, Amelie, for everything you do. You keep me sane, healthy, and ground me. You support me whatever I do and encourage me to follow my dreams. Everything is easier when you are around. Thank you for all the laughs, the happiness, and great time we have. I love you.